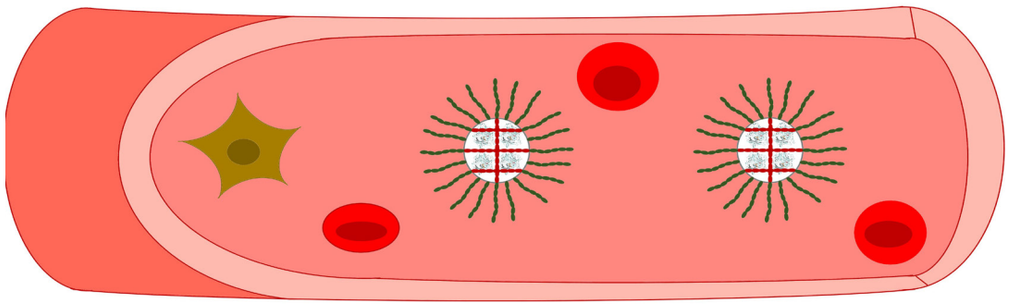

Stuck inside- Strategies for improving the stability of enzyme-containing complex coacervate core micelles Riahna Kembaren 2022

Stuck inside-

Strategies for improving the stability of enzyme-containing complex coacervate core micelles

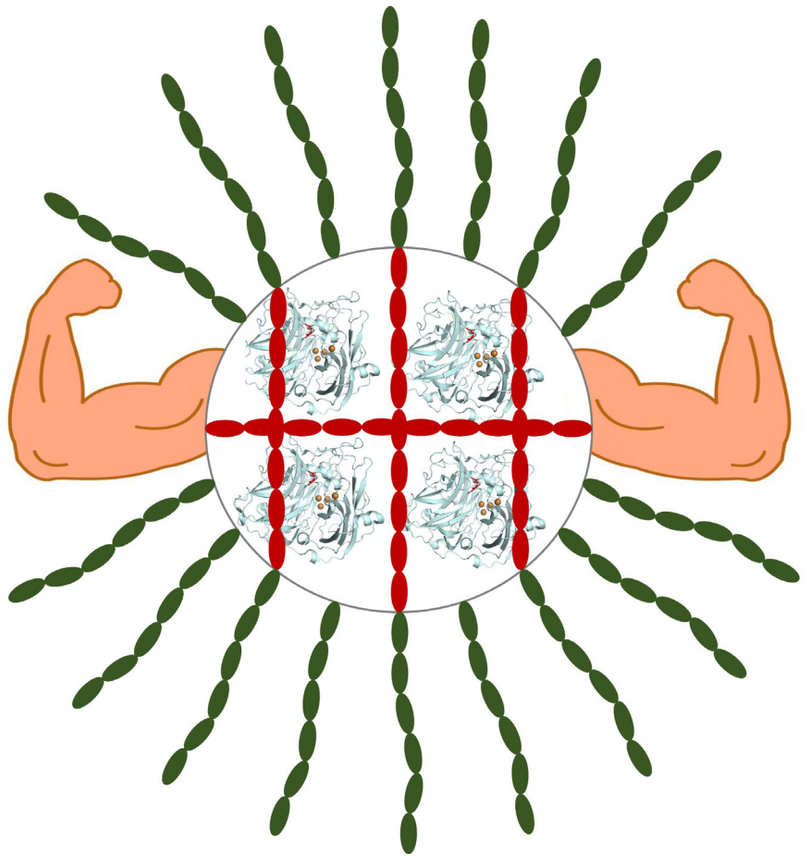

Riahna Kembaren

Propositions

1. Increasing the net charge of a protein can be done more effectively by following a genetic engineering strategy than by bioconjugation (This thesis).
2. For keeping enzymes inside complex coacervate core micelles, crosslinking of the core is by far the most effective strategy (This thesis).
3. Regular or non-organic foods are just as healthy and nutritious as organic foods.
4. Lack of industrial and business perspectives make many research results dormant.
5. The Covid19 pandemic has been a powerful stimulus for the rapid growth of science and technology.
6. To see the truth clearly, we need to see and learn from many perspectives.
7. Like Förster Resonance Energy Transfer (FRET) efficiency, human relationships are also highly affected by distance, overlap of spectral/interests, and orientation.
8. A scientist is also an artist that has ability to conceptualize and create original works.

Proposition belonging to the thesis, entitled:
"Stuck inside - Strategies for improving the stability of enzyme-containing complex coacervate core micelles"

Riahna Kembaren
Wageningen, 31 August 2022

Stuck inside-
Strategies for improving the stability of enzyme-containing complex coacervate core micelles

Riahna Kembaren

Thesis Committee

Promotor

Prof. Dr Jasper van der Gucht
Professor of Physical Chemistry and Soft Matter
Wageningen University and Research

Co-promotors

Dr Jan Willem Borst
Assistant Professor, Laboratory of Biochemistry
Wageningen University and Research.

Dr J. Mieke Kleijn
Assistant Professor, Physical Chemistry and Soft Matter
Wageningen University and Research

Prof. Dr Marleen Kamperman
Professor of Polymer Science at the Zernike Institute for Advance Materials
University of Groningen

Other members

Prof. Dr C.G.P.H. Schroën, Wageningen University and Research
Dr M.A. Hink, University of Amsterdam
Prof. Dr Mireille M.A.E. Claessens, University of Twente
Dr Evan Spruijt, Radboud University

This research was conducted under the auspices of Graduate School VLAG (Advanced Studies in Food Technology, Agrobiotechnology, Nutrition, and Health Sciences).

Stuck inside-
Strategies for improving the stability of enzyme-containing complex coacervate core micelles

Riahna Kembaren

Thesis

Submitted in fulfilment of the requirements for the degree of doctor
at Wageningen University
by the authority of the Rector Magnificus,
Prof. Dr A.P.J. Mol,
in the presence of the
Thesis Committee appointed by Academic Board
To be defended in public
On Wednesday 31 August 2022
At 16:00 in the Omnia Auditorium.

Riahna Kembaren
Stuck inside- Strategies for improving the stability of enzyme-containing complex coacervate core micelles
236 pages

PhD thesis, Wageningen University, Wageningen, the Netherlands (2022)
With references, with summary in English.

ISBN: 978-94-6447-249-3
DOI: https://doi.org/10.18174/570654

Table of Contents

Chapter 1 :
General introduction

Encapsulation of proteins is important in many applications, such as controlled delivery of functional ingredients in foods and medical formulations. Amongst many other methods, encapsulation of proteins can be realized by generating micelles composed of polyelectrolyte complexes, so-called complex coacervate core micelles (C3Ms).[1] Protein-containing C3Ms are simple to prepare by just mixing a charged protein solution with an oppositely charged neutral-ionic diblock copolymer solution at stoichiometric charge ratio. Micellar structures are spontaneously formed and remain in solution. Furthermore, C3Ms typically have a high loading capacity: many protein molecules can be incorporated into one micelle.[2,3] The micellar core provides a relatively water-rich environment,[4,5] thereby shielding protein molecules from the bulk solution, while the protein structure is preserved.[2,6,7]

Despite all these advantages, practical application of protein-containing C3Ms is hampered by their low salt stability (salt-induced disintegration)[8–10] and the high exchange dynamics between protein and diblock copolymer in the micelles and free in solution.[10–12] The salt stability of C3Ms and their exchange dynamics determine the level of protection and controlled delivery offered by C3Ms as protein carriers. This thesis describes several strategies to address these challenges and aims to contribute to the design of C3M protein carriers of which the stability and dynamics can be tuned to specific applications.

This chapter serves as an introduction to protein encapsulation in general, polyelectrolyte complexes, C3Ms as protein carriers, and the properties of the model proteins used in our study: the spore coat protein A (CotA) laccase and fluorescent protein. Furthermore, we discuss the strategies followed in this thesis to face the challenges related to salt-induced disintegration of C3Ms and C3Ms exchange dynamics: adding a charged homopolymer to form three-component C3Ms, increasing the total charge on the protein molecules (either by bioconjugation or by genetic engineering techniques), and crosslinking the core of C3Ms. We also describe the main techniques that we have used to investigate the formation, size and shape, salt stability and exchange dynamics of protein-containing C3Ms, as well as the effect of encapsulation in C3Ms on the structure and activity of CotA. This chapter is concluded by providing an outline of the thesis.

1.1. Protein encapsulation

Proteins are biomolecules consisting of a variation of 20 amino acids as building blocks, covalently linked by peptide bonds. The amino acid sequence of a protein determines its structure and function. In living organisms proteins have many functions that can be divided into different classes such as enzymes, transport proteins, carriers (e.g., for ligands and nucleic acids), structural proteins, storage proteins, and motor proteins.[13] Enzymes catalyze biochemical reactions by accelerating conversion of substrates into products in their active site.[14]

Proteins are used in many applications such as food and beverage production, personal care products formulations, manufacture of commodities such as pulp and paper, leather, and textile, and also as therapeutic agents such as insulin and monoclonal antibodies.[15,16] Generally, proteins are sensitive to (potentially detrimental) environmental conditions such as temperature and pH; their activity can be suppressed by substances that act as inhibitors; and they can be broken down by proteases. When a protein is denatured or degraded, it has lost its conformation and biological function. Immobilization of proteins may reduce protein unfolding and improve their stability against denaturing and degrading conditions.[17–19] Besides protection, protein immobilization can facilitate protein reutilization and recovery. In addition, particular protein immobilization and encapsulation techniques show potential for controlled protein release, which is beneficial for many applications especially therapeutic protein delivery.

Protein immobilization is a physical or chemical confinement of proteins onto a solid surface or into a polymeric matrix or a polymeric membrane, which can be reversible or irreversible. There are several methods for protein immobilization such as adsorption, covalent bonding, entrapment, crosslinking, and encapsulation.[17,19] The most important method of protein immobilization is encapsulation. For protein encapsulation many (micro)structures can be used, such as complex coacervates, emulsions, nanogels, (hollow) polymeric microspheres, liposomes and polymeric vesicles (Figure 1.1).

Several methods exist for protein encapsulation in emulsions. For example, a single water-in-oil (W/O) emulsion can be produced by dispersion of a protein solution in an organic solvent. A double emulsion, i.e. a water-in-oil-in-water (W/O/W) emulsion can be prepared in a further step by dispersing the W/O emulsion in an external aqueous phase using an emulsifier.[21] However, emulsion preparation often involves high shear stresses that can denature the protein.[21] Moreover, some proteins unfold at the W/O interface and generally emulsions have

a low encapsulation efficiency (implying that a large fraction of protein is lost during the manufacturing process).[22,21]

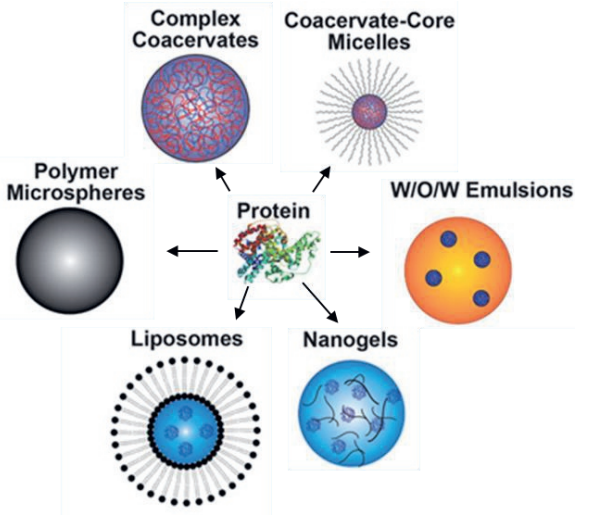

Figure 1.1. Methods for protein encapsulation.[20] Reprinted with permission. Copyright 2020 John Wiley and Sons, Inc.

The use of liposomes (lipid vesicles) or polymersomes (polymeric vesicles) involves capturing the protein inside a bilayer system.[23,24] This bilayer structure serves as a compartment. The bilayer structure of liposomes and polymersomes is formed by lipids and amphiphilic polymers, respectively. The internal volume for polymersomes is dependent on the membrane thickness and vesicular size and affects the encapsulation efficiency. Vesicle preparation usually involves organic solvents to promote the self-assembly of the amphiphiles, after which the organic phase is removed by the aqueous phase (solvent displacement). However, residual organic solvent may remain in the system, trapped in the hydrophobic bilayer or dissolved in the aqueous phase, causing exposure of protein to this solvent.[23]

Nanogels are nanoparticles consisting of crosslinked swellable polymer networks that can hold a lot of water without dissolving in the aqueous media. This method allows for the incorporation of proteins into the nanoscale size hydrogels.[25,26] Although nanogels can transport and protect proteins from denaturation, their structural and colloidal stability is determined by many parameters like size, shape, charge, pH, temperature, composition, and surface composition.[25,27–29]

The most frequently used (hollow) polymeric microspheres for protein encapsulation have shells composed of poly(lactide-co-glycolide) (PLGA) and poly(lactic acid) (PLA).[30–32] The

most common process to encapsulate protein in such microspheres is forming a double emulsion of water-in-oil-in-water (W/O/W) followed by solvent removal. The PLGA/ PLA is first dissolved in the organic solvent. An aqueous solution of the protein is then added to the polymer solution. Subsequently, a water-in-oil (W/O) emulsion is formed through stirring or homogenizing with or without addition of emulsifier. This W/O emulsion is then added to an aqueous solution of poly(ethylene glycol) (PEG) or poly(vinyl alcohol) (PVA) as a stabilizer resulting into a W/O/W emulsion. The solvent is then eliminated by extraction or evaporation.[31,32] However, in the process, the organic solvents used can lead to enzyme denaturation. Moreover, in the W/O/W solvent extraction, protein aggregation and protein activity loss can occur. A limitation of PLGA/ PLA microspheres for protein delivery is the inconstant protein release in which an initial burst is followed by a prolonged and incomplete release.[32]

Protein encapsulation using complex coacervates is based on the attractive interactions between oppositely charged macromolecules in aqueous solution resulting in a liquid-liquid phase separation. The formation of complex coacervates is a spontaneous process that does not require organic solvent, heat, or additional chemical reagents.[1,33] Moreover, a high encapsulation efficiency can be achieved in complex coacervates.[2,34] Besides encapsulation of proteins in macroscopic complex coacervates phases, it is also possible to form complex coacervate core micelles (C3Ms) in aqueous solution.[1,2,8] The key of protein encapsulation in such micelles is using a diblock copolymer with a neutral hydrophilic part and a part with a charge opposite to the protein. Since this thesis deals with protein encapsulation in C3Ms we will describe the formation and properties of complex coacervates and C3Ms in more detail in the next sections.

1.2. Polyelectrolyte complexes

A polymer is a long molecule that consists of many repeating subunits or monomers that are covalently bound. The skeletal structures of polymers can be linear or branched. Polymers can be classified into natural polymers (biopolymers) and synthetic polymers. Synthetic polymers can be furthermore divided into homopolymers and copolymers. A homopolymer consists of one type of monomer, while a copolymer is derived from more than one type of monomer. Copolymers that consist of two blocks (long sequences) of different types of monomers, are known as diblock copolymers, and polymers with three blocks of different compositions are known as tri-block copolymers. A particular class of polymers encompasses polymers with

charged groups, known as polyelectrolytes. This charge gives polyelectrolytes different physical, mechanical, and chemical properties compared to non-ionic polymers.[35,36] The charge of a polyelectrolyte can be positive (cationic) or negative (anionic). Polyelectrolytes with a pH-dependent charge are weak polyelectrolytes, and polyelectrolytes with a pH-independent charge are strong polyelectrolytes.

When charged macromolecules such as proteins, DNA or synthetic polymers (polyelectrolytes) are dissolved in an aqueous solution, they are surrounded by a diffuse electric double layer of small counterions. Oppositely charged polymers tend to bind to each other by electrostatic interaction, which induces the release of counterions from both polyelectrolytes. Under the right conditions this results in the formation of polyelectrolyte complexes and a liquid-liquid phase separation: the solution phase separates into a polymer-rich coacervate phase and a polymer-poor phase that mainly contains water and released counterions (Figure 1.2).

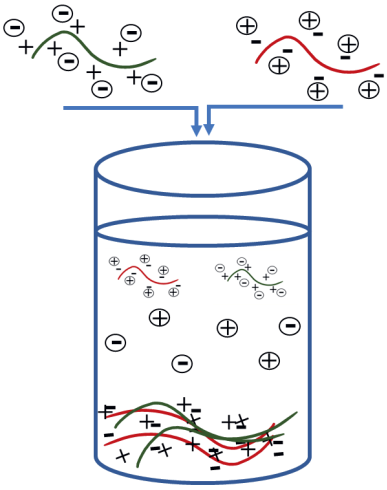

Figure 1.2. Complex coacervate formation by mixing two oppositely charged polyelectrolytes.

The formation of complex coacervates depends on many factors, such as the length of the polyelectrolytes, their charge densities, concentrations, the charge mixing ratio, ionic strength, pH, and temperature.[33,37–40] The charge of weak polyelectrolytes varies with pH, which influences the charge balance between oppositely charged polyelectrolytes and influences electrostatic forces in the complex formation.

The energy (enthalpy) and the entropy of the system of two opposite polyelectrolytes in solution change when they are mixed. This change is strongly affected by the salt concentration

(ionic strength) (Figure 1.3). The salt concentration also influences the enthalpy of complexation, which can be either exothermic or endothermic. At low ionic strength the two separate polyelectrolytes have a large Debye screening length and dilute counterion clouds. However, after mixing and complex formation, dense and tight ion-pairing between oppositely charged groups occurs. In this condition, the complexation is exothermic because the Coulomb energy of the system decreases. However, as the salt concentration increases, complexation becomes endothermic: the counterion clouds around the separate polyelectrolytes are compact, and the increase in electrostatic energy of the released ions is not compensated for by the decrease in energy due to the inter-polyelectrolyte ion pairs formation. Furthermore, the entropic gain due to counterion release steadily decreases with increasing salt concentration.[1,41,42] Above a certain salt concentration phase separation is completely suppressed, which is known as the critical salt concentration (CSC). The salt concentration where exothermic complexation, endothermic complexation, and no complexes occur varies depending on charge density of polyelectrolytes.[6,41] Polyelectrolytes with low charge densities have lower critical salt concentration than polyelectrolytes with high charge densities.

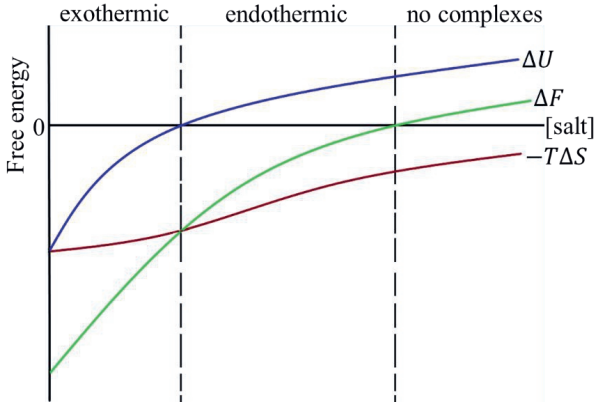

Figure 1.3. Schematic representation of the effect of salt concentration on the change in electrostatic energy (*ΔU)* upon polyelectrolyte complex formation, the counterion release entropy (-*T*Δ*S*), and the total free energy of complexation (Δ*F*).[41]

The relation between the phase separation and salt concentration is represented by a coacervation phase diagram. This is a binodal phase boundary diagram as a function of the salt and polymer concentration (Figure 1.4). In the two-phase region the mixing composition of polymer concentration and salt concentration results into a liquid-liquid phase separation. The samples prepared with mixing combination above the binodal result in the single-phase region.

The binodal's critical point corresponds to the critical salt concentration beyond which no phase separation occurs.

Complex coacervates can be formed between charged biopolymers; between charged biopolymers and synthetic polyelectrolytes; and between synthetic polyelectrolytes. Complexes of synthetic polyelectrolytes with biopolymers such as proteins are much weaker than complexes between synthetic polyelectrolytes due to their relatively low charge density.[41] Nevertheless, in nature complex coacervation is a frequently observed and important phenomenon. For example, DNA is compacted by positively charged histone proteins into chromatin fibers,[44] complex coacervation plays a role in blood clothing,[45] and organisms use complex coacervates as a natural underwater glue.[46]

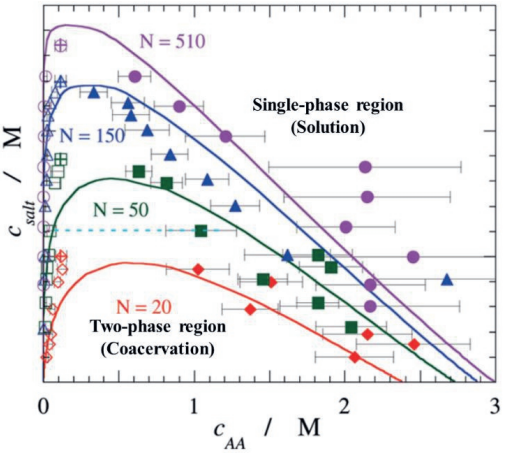

Figure 1.4. Coacervation phase diagram as a function of salt concentration (c_{salt}) and polymer concentration (c_{AA}) with different length of polymer poly(acrylic acid) (PAA) (N).[4] Reprinted with permission. Copyright 2010 American Chemical Society.

1.3. Complex coacervate core micelles for protein encapsulation

Polyelectrolytes can also form complexes with diblock copolymers which have an oppositely charged part and a neutral-hydrophilic part. When these two components are mixed in water, the oppositely charged parts bind electrostatically and form small soluble complexes (SCs). Above a certain concentration, known as the critical micellar concentration (CMC), these SCs start to aggregate and form an almost electroneutral complex coacervate core that grows spontaneously. The growth is limited by the hydrophilic neutral chains of the diblock copolymer. The neutral hydrophilic of diblock copolymer form a stabilizing corona prohibiting the growth of the complex coacervate droplets to macroscopic sizes and thus preventing

macroscopic phase separation, and protecting the micelles against aggregation by steric repulsion.[1,10,47,48] These core-shell coacervate micelles (Figure 1.5) are known as C3Ms[1,48] or block ionomer complexes[49] or polyion complex micelles.[50]

The formation of C3Ms depends on the charge mixing composition. When the total charge on the cationic and anionic polyelectrolytes is about equal, the number of micelles formed is highest and this composition is known as the preferred micellar composition (PMC). A deviation of the PMC from the charge balance may happen if additional driving forces (not only by electrostatic interactions and entropy gain from the counterion release) such as hydrophobic interactions are at play. Proteins have several hydrophobic amino acid residues on their surfaces with different exposure levels. Moreover, some polyelectrolytes also contain hydrophobic groups such as alkyls or phenyls.[1,2,7] The shape of C3Ms is generally spherical because in thermodynamic equilibrium such structures possess the lowest free energy.[51] However, other shapes such as rods and wormlike micelles can be found depending on the polymer chain composition, the strengths of interactions and additional driving or destabilizing forces, such as hydrophobic interactions, or for non-stoichiometric conditions.[1] Van der Kooij et al. reported the transition from spherical to worm-like micelles after addition of salt into C3Ms solutions.[52]

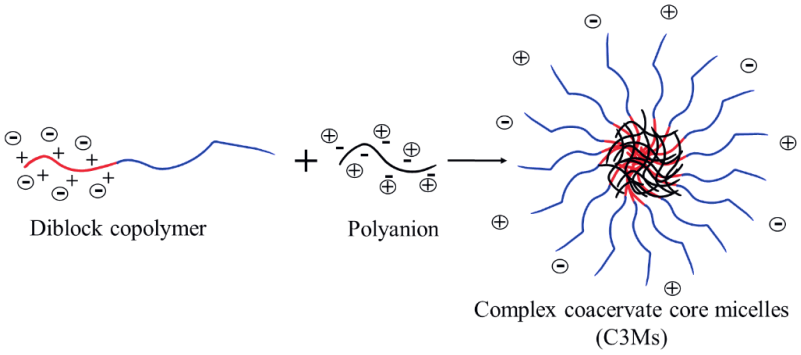

Figure 1.5. Complex coacervate core micelle formation between a charged-neutral hydrophilic diblock copolymer and an oppositely charged polyelectrolyte.

C3Ms can be used as carriers of biomolecules such as proteins and DNA. Previous research has shown that proteins can be easily encapsulated into C3Ms.[2,8,7] These protein-containing C3Ms are soluble in aqueous solution and can contain many (up to hundreds) protein molecules in one micelle.[2] Protein-containing C3Ms are formed by mixing a protein solution with an oppositely charged-neutral diblock copolymer solution (Figure 1.6). Because proteins also contain hydrophobic amino acid residues, the formation of protein-containing C3Ms may be

partly driven by hydrophobic interactions.[1,2,53] For protein encapsulation in C3Ms, the pH of the system is important since this influences the net charge of the protein molecules. At solution pH conditions below the isoelectric point (pI) of the protein, it has a net positive charge, while above the pI, it has a net negative charge. Moreover, clustering of charges on the outside of globular proteins (charge anisotropy) significantly impacts coacervation. Next to the advantages of C3Ms as packing systems for proteins, i.e. solubility in aqueous solution and high packing capacity, C3Ms offer the possibility of controlled release.[54,55] For example, C3Ms that dissociate in response to decreased pH levels have been designed to free their incorporated drug molecules upon accumulation at a tumor site.[54] Enzyme-containing C3Ms can also be used as microreactors, for example to overcome incompatibility problems between polar enzymes and non-polar substrates.[56]

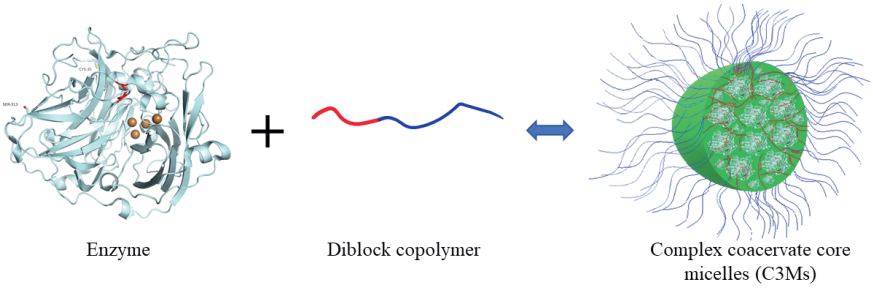

Figure 1.6. Scheme of the formation of protein-containing complex coacervate core micelles.

Despite the many advantages, application of C3Ms to encapsulate proteins still has some significant challenges: the micelles can swiftly disintegrate with increasing salt concentration[8,10] and furthermore they are in dynamic equilibrium with protein and diblock copolymer free in solution.[10] Increasing the salt concentration lowers the entropic gain of complex formation and screens the charged parts of the diblock copolymer and protein, resulting in weaker electrostatic interactions, leading to disintegration of the micelles. Protein-containing C3Ms are very sensitive to this salt-induced disintegration due to the low charge density of proteins[3,10,57] Nolles et al. reported that C3Ms containing green fluorescent protein (GFP) already fall apart at NaCl concentrations less than 40 mM.[10] When the micelles are undesirably disintegrated, the protein is undesirably released and no longer protected. Moreover, the CMC of C3Ms increases almost exponentially with the square root of salt concentration.[58,59]

After mixing a diblock copolymer with an oppositely charged protein, complexes are obtained and rearranged into micelles quickly, within milliseconds to seconds timescales.[10]

Zhang et al. observed that the complexation process between poly(ethylene oxide)-*b*-poly(quaternized 2-(dimethyl amino)ethyl methacrylate) (PEO-*b*-PQDMA) and poly(ethylene oxide)-*block*-poly(sodium 4-styrene sulfonate) (PEO-*b*-PSSNa) was fast and could finish within seconds.[60] These protein-containing C3Ms are dynamic complexes.[1,10] There is an exchange between encapsulated protein inside the C3Ms and free protein in solution. It is necessary to minimize their exchange dynamics to limit the undesired exposure of the protein to the environment and to protect and deliver the protein. Some models describe the exchange dynamics of amphiphilic diblock copolymer micelles based on theoretical frameworks and experimental studies. Dormidontova presented two kinetic theories for micelles formed by polymeric surfactants (hydrophilic-hydrophobic block copolymers): the unimer exchange, and micelle fusion/ fission.[61] Holappa et al. observed the exchange dynamic of C3Ms composed of diblock copolymer poly(ethylene oxide)-*block*-poly(sodiummethacrylate) (PEO-*b*-(PMA)Na) and homopolymer poly((methacryloyloxyethyl) trimethylammonium chloride) (PMOTAC) using fluorescence spectroscopy. They concluded that there are two processes involved in micellization kinetics, i.e., merging/ splitting of micelles and insertion/ expulsion of single chains. They found that the exchange mechanism via insertion/ expulsion of single chains is faster than merging/ splitting of C3Ms.[62] The rate of exchange kinetics of C3Ms strongly depends on the salt concentration. Increasing the ionic strength will lead to a higher rate of exchange.[1]

Nolles et al. observed the exchange of protein and relaxation of protein-containing C3Ms using Förster resonance energy transfer (FRET). On the basis of their results they proposed that addition of diblock copolymer into the protein solution rapidly leads to formation of small soluble protein-polymer complexes (SCs).[10] Above the CMC, these SCs will aggregate to form C3Ms. These C3Ms then relax by association and dissociation of SCs and micelles. The easy dissociation and association of the near-neutral SCs also results in a rapid exchange of protein between the micelle core and the bulk solution. Bos and Sprakel (2019) studied the exchange dynamics of C3Ms during the initial micellization in Langevin dynamics simulations.[63] This confirmed the proposed model of Nolles et al. that small charge-neutral complexes are the primary mediator for exchange. They demonstrated that the kinetic stability of C3Ms can be tuned not only by electrostatic interaction but also by non-electrostatic attraction between the polyelectrolytes, the polyelectrolyte length ratio, and the overall polyelectrolyte length. The salt-induced disintegration and the generally high exchange dynamics between micelles and solution determine the packing stability of the protein in the core of C3Ms and the level of protection offered by C3Ms as carriers for protein encapsulation.

1.4. Model proteins to study protein encapsulation

1.4.1. The spore coat protein A (CotA) laccase as a model enzyme

A number of proteins has already been used as model protein to study protein encapsulation in complex coacervate core micelles, such as GFP and other fluorescent proteins[2,7] and the enzymes: lysozyme, lipase and organophosphate hydrolase.[8,57,64,65] Using fluorescent proteins enables observation of the formation of C3M and their dynamic behavior with fluorescence techniques like fluorescence spectroscopy and FRET without an extra fluorescent labeling step. However, using an enzyme as a model protein allows to study preservation of enzyme activity after encapsulation and release, which is important for delivery and application purposes. For a model protein, it is convenient to use a well-studied enzyme, which is already used in many applications.

In this study, we have chosen the recombinant spore coat protein A (CotA) laccase as a model enzyme. Some laccases have already been used to study protein immobilization. Pich et al. used fungus laccase to study composite magnetic particles as enzyme carriers.[66] Bryjak et al. immobilized fungus laccase by covalently binding it to a copolymer of butyl acrylate and ethylene glycol dimethacrylate.[67] Here, we use recombinant CotA laccase to study protein encapsulation in complex coacervate core micelles because this enzyme has already been well-characterized, is relatively stable, easy to handle (CotA is high temperature and high pH resistant), can be efficiently overexpressed in *Escherichia coli* bacteria,[68] and is also relatively easy to purify.

Laccases belong to the family of multicopper oxidases (MCOs), together with, for example, ascorbate oxidase, ferroxidase, nitrite reductase, and ceruloplasmin.[69] Multicopper oxidases (MCOs) are a group of oxidoreductases that can oxidize a wide range of substrates and use copper ions as the initial electron acceptor. Laccases can be found in plants, insects, fungi, and bacteria. Based on their redox potential, laccases are divided into two main groups: low redox potential laccases and high redox potential laccases. The first group is found in bacteria, plants, and insects. In contrast, high redox potential laccases are found in fungi.[70]

The most well-known bacterial laccase is spore coat protein A (CotA) laccase that is present in *Bacillus subtilis*. This enzyme is located at the outer coat of the endospore of *B. subtilis.* Its function is to protect endospores from an unfavorable environment such as high temperature. The CotA gene also participates in the biosynthesis of a brown spore pigment that is responsible for protection against UV radiation. CotA is highly thermostable and high pH resistant.

CotA has a molecular weight of 65 kDa and an isoelectric point at pH 5.84. The crystal structure of CotA (Figure 1.7) shows a larger, putatively substrate-binding, cavity in CotA compared to fungal or plant laccases.[71] CotA has three domains, and there is a positively charged patch on its surface at the interface between domains 1, 2, and 3. The positive patch in the CotA structure is composed of ten lysine and five arginine amino acid residues and has a biological function in the assembly of CotA into the spore outer coat layer.

Like other MCOs, CotA is characterized by four copper (Cu) ions, which are commonly classified into three classes based on their absorption in the UV/ visible region and their electronic paramagnetic resonance (EPR) spectra. The classes are type 1 (T1), type 2 (T2), and type 3 (T3).[72,73] The T1 Cu is located in the cavity close to the enzyme's surface, whereas T2 and T3 Cu are buried in the center of the enzyme.[74] The T1 Cu contributes to the enzyme's intense blue color, and its absorbance can be detected around 600 nm and is also EPR detectable. T2 Cu does not absorb in the UV/ visible spectrum but is EPR detectable. T3 Cu contains a pair of Cu ions in a binuclear conformation and has a weak absorbance at 330 nm but is undetected using EPR.[72] In the protein structure, the Cu ion from T2 and the two Cu ions from T3 together form the trinuclear center (TNC).[75] T1 Cu is bound to CotA by one cysteine, one methionine and two histidine ligands. The T2 Cu is bound by two histidine ligands, while the two T3 Cu are bound by six histidine ligands.[69]

Figure 1.7. The spore coat protein A (CotA) laccase structure. Copper ions are represented as yellow spheres. The red spheres at the top represent the channels within CotA that provide access to the trinuclear center for dioxygen. The red spheres at the bottom represent the release of water molecules into the outlet channel from the reduction of dioxygen molecules.[76,80,81] Reprinted with permission. Copyright 2005 Royal Society of Chemistry.

CotA can catalyze the oxidation of various kinds of substrates. Substrate oxidation occurs at T1 Cu (binding pocket of the substrate), and four electrons from four laccase substrates are transferred to the TNC, in which the reduction of dioxygen to water occurs.[76,77] The reduction of T1 Cu is the rate-limiting step in the reactions catalyzed by laccase.[69] Mutation of ligands in the T1 Cu site impairs copper coordination, which alters the CotA biochemical properties drastically. CotA laccase can oxidize phenolic compounds that has been used in the pulp and paper industry[78] and bioremediation.[79]

1.4.2. Fluorescent proteins (FP) as model proteins to study exchange dynamics

Next to CotA, in this study we also used a FRET pair of fluorescent proteins: mTurquoise2 (a cyan FP) and SYFP2 (a strong enhanced yellow FP) to study exchange dynamics of C3Ms. Nolles et al. have used these proteins to study the protein-containing C3Ms.[2,7,10] mTurquoise2 has monomeric behavior, high photostability and high quantum yield, that make this protein as a preferable donor for resonance energy transfer to SYFP2 (Figure 1.8).[82,83]

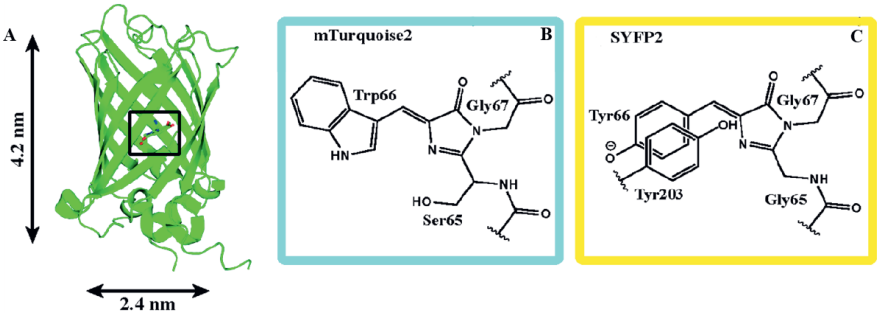

Figure 1.8. (A) Fluorescent protein structure with its chromophore in the center of the barrel. (B) Chromophore of mTurquoise2. (C) Chromophore of SYFP2.[7]

1.5. Strategies to improve the stability of protein-containing C3Ms

This thesis describes some strategies to improve salt stability and decrease the exchange dynamics of protein-containing C3Ms. Since the low charge density on protein molecules is an important cause for the low salt stability of protein-containing C3Ms, we will include homopolymers (polyelectrolytes) of the same charge sign as the enzyme (three-component C3Ms), and add extra charge to the enzyme by bioconjugation and by genetic engineering. Furthermore, we investigate covalent crosslinking of the core of the C3Ms. Below we outline these strategies in more detail.

1.5.1. Three-component C3Ms

Three-component C3Ms are formed by adding a homopolymer that has the same charge sign as the enzyme into the enzyme solution before the diblock copolymer is added. Such three-component C3Ms have already been used to encapsulate enzymes. For example, Mills et al. packed organophosphate hydrolase (OPH) into three component micelles by mixing OPH with poly(acrylic acid) (PAA) and poly(oligo(ethylene glycol) methacrylate)-*block*-poly(4-vinyl *N*-methylpyridyl iodide) (POEGMA-*b*-qP4VP).[64] Moreover, Lindhoud et al. also encapsulated lysozyme into three component micelles by mixing lysozyme with poly(acrylic acid)-*block*-poly(acryl amide) (PAA-*b*-PAAm) and poly(*N*,*N* dimethylaminoethyl methacrylate) (PDMAEMA).[8] These previous studies showed that the addition of a homopolymer with the same charge sign as the protein improved the stability of protein-containing C3Ms. However, it is still unclear how exactly such a three-component system affects the encapsulation efficiency and salt stability of the micelles. To investigate these aspects, we added the negatively charged homopolymer poly(4-styrenesulfonate)$_{215}$ (PSS_{215}) to the CotA/ $PM2VP_{128}$-*b*-PEO_{477} system, with varying ratios of homopolymer and enzyme.

1.5.2. Adding extra charge to the enzyme

Previously, Obermeyer et al. increased the net charge of several proteins by converting lysine residues by chemical modification using succinic anhydride to improve the stability of C3Ms. This modification results to higher negatively charged proteins.[84] They indeed found an improvement in salt stability of C3Ms although the effect was limited: the micelles were stable up to maximally 50 mM NaCl. The micelles were also stable to dehydration and elevated temperatures. In this study we added extra charges to the enzyme in two different ways, by a chemical approach (bioconjugation) and a biological approach (genetic engineering).

1.5.2.1. Bioconjugation

Bioconjugation is a technique to form a stable covalent link between two molecules, at least one of which is a biomolecule.[85,86] The bioconjugation process can be controlled by choosing an appropriate target reactive/ functional group, linker agents, and reaction conditions. Bioconjugation has already been used for many applications, such as fluorescent labelling of antibodies and to biotinylate enzymes. Bioconjugation techniques can be used for biosensing, bioimaging, and targeted drug delivery.[87] In this study, we use the bioconjugation technique to increase the protein's charge by coupling it to a charged polymer.

Bioconjugation is carried out by using a reactive linker agent. This reactive linker agent binds one reactive group to another reactive group. In addition, a secondary linker agent may be used to create a more stable intermediate of one of the components to be conjugated. The nucleophilicity of the functional group is essential for bioconjugation because it determines how reactive this group is. Based on nucleophilicity, there are three important reactive groups for bioconjugation, for which the order of this reactivity is R-S^- (thiol or sulfhydryl groups) > R-NH_2 (amine groups) > R-COO^- (carboxylate groups).[88–90]

1.5.2.1.i. Thiol reactions

Some reactive groups can react with sulfhydryl-containing biomolecules. The coupling reaction for sulfhydryl is proceeded by alkylation to form a thioether bond or disulfide exchange reaction with another thiol to form a new disulfide bond (also called disulfide interchange). Maleimides are often used for coupling thiol. Maleimide reacts with sulfhydryl to form a stable thioether bond (Figure 1.9). This reaction is popular for protein labeling. Some fluorescent probes have maleimide derivates that can react with cysteine residues.

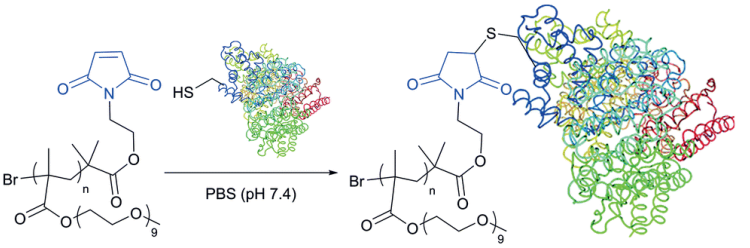

Figure 1.9. Bioconjugation of a maleimide reactive group with protein using the thiol reaction.[88,91] Reproduced from Koniev and Wagner[88] with permission from the Royal Society of Chemistry.

1.5.2.1.ii. Amine reactions

For amine-containing biomolecules the amine can be targeted as functional group for bioconjugation. For primary amines the coupling reaction can be conducted in two ways, by acylation or alkylation. In alkylation, an activated alkyl group is coupled to the amine nucleophile under release of one hydrogen. In acylation, an activated carbonyl group is linked to the amine (Figure 1.10). Amine reactions are commonly used in bioconjugation because the amine functional group can react with many different reactive groups, such as isothiocyanate, isocyanate, acyl azide, *N*-hydroxysuccinimide (NHS), sulfonyl chloride, imido, carbodiimide, and aldehyde groups.[86,88,90,92–94]

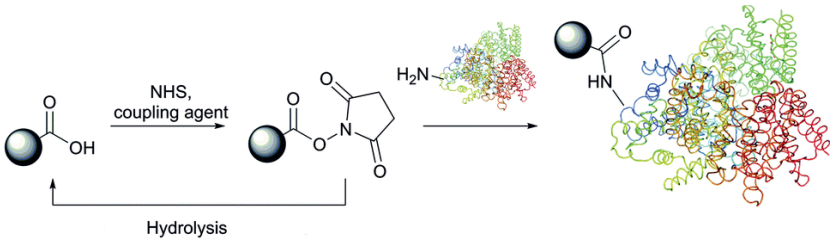

Figure 1.10. Bioconjugation of NHS reactive group with protein using the amine reaction.[88] Reproduced from Koniev and Wagner[88] with permission from the Royal Society of Chemistry.

1.5.2.1.iii. Carboxylate reactions

The carboxylate group has a low nucleophilicity, which limits the range of functional groups that react with carboxylic acids. Some groups that can react with the carboxylate group are diazoalkanes, and carbodiimides (Figure 1.11).

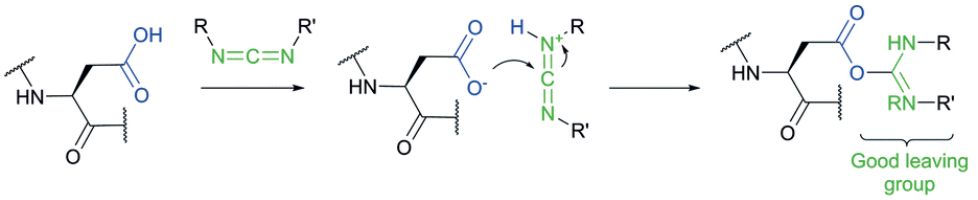

Figure 1.11. Reaction of a carbodiimide group with the carboxylic acid side chain of glutamate using the carboxylate reaction.[88] Reproduced from Koniev and Wagner[88] with permission from the Royal Society of Chemistry.

Proteins can be modified to perform a variety of functions, including cellular tracking, imaging biomarkers, and target drug delivery. In addition, protein-polymer bioconjugation improves the stability and the potential storage capacity of proteins.[95] Nucleophilic amino acid side chains such as aspartic acid, glutamic acid, lysine, and cysteine are the most used targets for bioconjugation. The sulfhydryl group of cysteine is the strongest nucleophile in the protein. The second most nucleophilic targets in proteins are the amine groups (e.g., the α-amines at the N-terminus, and the amine in the lysine side chain). Finally, the least nucleophilic groups in proteins are the oxygen-containing ionizable groups (e.g., the α-carboxylate at the C-terminus, and the carboxyl in the aspartic acid and glutamic acid side chains). However, lysine is the most accessible amino acid at the surface of proteins, while cysteine is the least exposed amino acid and is naturally buried inside the protein conformation. These features make lysine a more popular amino acid residue for bioconjugation. Moreover, using lysine increases the efficiency

of bioconjugation.[85] Moreover, the abundance of lysine in the protein surface result in a less specific bioconjugation site and can result in multiple polymer chains that are covalently bound to proteins/ peptides.[85] For protein bioconjugation in general, lysine is targeted with electrophilic reagents such as activated carboxylic acids, and by using a carbodiimide linker, an amide bond is formed.[96]

For bioconjugation protein in this study, we used lysine as a target amino acid because it has possibility to couple more charged polymer chain to protein, so that the protein can has higher net charged and strongly bound in the core of C3Ms. We bioconjugated lysine residues of CotA laccase to poly(acrylic acid) (PAA) (with several length and concentration ratio of PAA) using 1-ethyl-3-(3-dimethyl aminopropyl) carbodiimide hydrochloride (EDC) and *N*-hydroxy succinimide (NHS) linker.

1.5.2.2. Genetic engineering

Genetic engineering is a modification of genes by inserting genes, removing some parts of genes, or changing genes. This modification can be random or targeted to a specific part of the gene. A protein generated from a gene that has been cloned into a host using genetic engineering is known as a recombinant protein.[97,98] Genetic engineering is used in many fields, such as medicine, industrial biotechnology, and agriculture.[97] Modifying DNA and transferring it to another organism such as *Escherichia coli* bacteria facilitates the bulk manufacturing of various substances such as enzymes, monoclonal antibodies, hormones, and vaccines. In this study we used genetic engineering to modify the genetic code of CotA by adding a sequence that encodes for a string of charged amino acids (glutamic acid residues) of varying length (10, 20, 30, and 40 additional glutamic acids) to the C-terminus of protein. The length of this glutamic acid chains can be used to tune the salt stability properties. Expression in *E. coli* results in the recombinant protein with extra charges in its structure.

Cloning is essential in genetic engineering. The first step in cloning is to isolate and modify DNA. In conventional cloning strategy, restriction enzymes are used to isolate targeted DNA fragments. Restriction enzymes cut the DNA at specific sites and generate a DNA fragment with blunt or sticky ends. This gene is then ligated into a plasmid as vector using DNA ligase. For ligation, the ends of this gene should be compatible to the ends of the plasmid. The procedure of using restriction enzymes has many limitations: it depends on the presence of appropriate restriction sites to generate both vector and inserted DNA and often leaves unwanted sequences at the junction sites. Moreover, it requires restriction enzymes and ligase that are expensive, which makes this procedure highly costly. To overcome these limitations,

in this study, we have used SLiCE (Seamless Ligation Cloning Extract). SLiCE is a new cloning method that does not require restriction sites and ligase. It is based on *in vitro* recombination of short regions of homologies (about 15–52 base pairs overlap sequences between target DNA fragment and vector) in bacterial cell extracts.[99] Moreover, SLiCE allows the assembly of several DNA fragments in one cloning step, making this method ideal for assembling multiple DNA fragments during gene synthesis.

1.5.3. Crosslinking the core of C3Ms

Crosslinking is the general term for the process of forming bonds between polymer chains, in that way creating a polymer network. Crosslinking strategies are usually implemented to functionally modify the mechanical, biological, or degradation properties of materials.[100] Crosslinks can be formed by chemical reactions (chemical crosslinks, covalent bonds) or by physical interactions (physical crosslinks). Chemical crosslinks can be induced by irradiation (photo-polymerization), a pH change, enzymes, or by using "click" chemistry. Physical crosslinks are resulting from weak interactions such as ionic/ electrostatic interactions, hydrogen bonding, metal coordination, or hydrophobic interactions.[101]

Chemical crosslinking gives a stable network. For chemical crosslinking at room temperature various reactive functional groups can be used such as carboxylic acids, primary amines, acetoacetyl groups, acetal groups, acrylamide derivates, and carbonyl groups (aldehydes, ketones).[102] Amines are a highly nucleophilic functional groups compared to carboxylic acid groups.[102] For chemical crosslinks using an amine group, a number of crosslinking agents are available such as isothiocyanate, NHS ester, imidoester, and glutaraldehyde. For chemical crosslinks using the carboxylic acid group the two main crosslinking agents are carbodiimides and diazoalkanes. Regarding the crosslinkers one can discriminate between zero-length crosslinkers, homobifunctional crosslinkers, and heterobifunctional crosslinkers.[25,100,103] A zero-length crosslinker connects two molecules by forming covalent bonds without an additional spacer. Homobifunctional crosslinkers conjugate two molecules with the same type of functional group. Heterobifunctional crosslinkers couple two molecules with different functional groups.

In this study, we crosslinked the core of C3Ms using a chemical crosslinker. With the core-crosslink C3M strategy, it entrapped the protein in the core of micelles that result in higher salt stability and reduce its exchange dynamics. It is necessary to have a reactive functional group on diblock copolymer to be able to couple the core of C3Ms. Through quaternization, we functionalized diblock copolymer with primary amine group. We investigated two types of

crosslinkers to crosslink the core of C3Ms: 1-ethyl-3-(3'-dimethylaminopropyl)carbodiimide hydrochloride (EDC) and dimethyl 3,3′-dithiopropionimidate dihydrochloride (DTBP). EDC is a zero-length crosslinker that creates irreversible crosslinks between carboxylate and amine groups. DTBP is a homobifunctional crosslinker that joins two amine groups. Additionally, because DTBP crosslinks contain disulfide bridges, they can be broken again by adding a reducing agent.

1.6. The properties of C3Ms and the effect of encapsulation on the structure and activity of CotA

In this thesis, we will discuss several techniques that have been used to observe properties of the enzyme-containing C3Ms. These properties include the preferred micellar composition (PMC) and micellar morphology (size and shape), the protein loading, salt stability and, when relevant, the exchange dynamics. We also investigated the effect of encapsulation (and release) on the properties of CotA: secondary structure and activity.

1.6.1. Formation, size, and shape of protein-containing C3Ms

The formation of C3Ms and their properties (i.e., size and shape) has been investigated by dynamic light scattering (DLS) and fluorescence correlation spectroscopy (FCS). In DLS, the Brownian motion of light scattering particles is monitored by recording the real-time fluctuations of scattered light intensities.[104,105] From the autocorrelation function of these fluctuations, the diffusion coefficient can be determined, enabling to calculate the size of molecules by using the Stokes-Einstein equation.

In DLS a laser is used as the source for light scattering measurements, for example a Helium-Neon laser, Argon laser, or diode-pumped solid-state laser (DPSS) laser. Detection of the scattered light can be done at a fixed scattering angle or at multiple scattering angles. We used a fixed angle of 90° to follow the formation of C3Ms and to determine the PMC, hydrodynamic radius, and polydispersity index (PDI). On the other hand, multi-angle DLS has been used to determine the shape of the protein-containing C3Ms by plotting the correlation decay rate (Γ) against the squared scattering wave vector (q^2). The diffusion coefficient D can be estimated from the linear fit of this plotting function:

$$\Gamma = -Dq^2 \tag{1.1}$$

$$q = \left(\frac{4\pi n}{\lambda}\right)\sin\left(\frac{\theta}{2}\right) \tag{1.2}$$

where θ is the detection angle, n is refractive index of solvent, and λ is the wavelength of the laser light.[106,107]

In FCS, the Brownian motion of fluorescent particles or molecules is monitored by recording the real-time fluctuations of the fluorescence intensity in the confocal volume (the detection volume depending on the confocal optics of the FCS instrument). Several lasers are available to excite the fluorescent molecules in the confocal volume, such as an Argon laser or a white light laser. The fluorescence emission passes through a pinhole and is detected by a highly sensitive detector. Non-fluorescent particles or molecules should be labeled with a fluorescent dye first to be able to observe them by FCS. FCS can be used to measure diffusion coefficients; like in DLS these follow from the autocorrelation functions of the fluctuations of the emitted light and from these hydrodynamic radii can be derived. In addition to this, for protein-containing C3Ms, FCS can be used to determine the distribution of protein molecules over micelles and solution as well as the number of protein molecules incorporated per micelle.[2]

1.6.2. C3M stability

The salt stability of enzyme-containing C3Ms was observed using DLS and FCS. In DLS, disintegration of the protein-containing C3Ms upon addition of salt to the system is observed as a decrease in light scattering intensity. In FCS this process can be followed by monitoring the number of fluorescent particles (N) detected in the confocal volume: this number increases as disintegration of the micelles leads to release of the (fluorescently labelled) enzyme molecules. Moreover, with FCS, we can follow the changes in the fractions of enzyme free in solution and of encapsulated enzyme during the addition of salt.

1.6.3. Exchange dynamics

Exchange dynamics of proteins between the C3Ms and the bulk solution is studied using FRET analysis. FRET is a photophysical phenomenon in which a fluorophore (the donor) in an excited state transfers its energy non-radiatively to a neighboring fluorophore (the acceptor) in the ground state by weak dipole-dipole interaction.[108–110] FRET occurs when two fluorophores (donor and acceptor) have a spectral overlap, a favorable dipole-dipole orientation, and are in close proximity of each other (< 10 nm) (Figure 1.12). As a result of the energy transfer, the donor fluorescence is quenched and its fluorescence lifetime is decreased, while the fluorescence intensity of the acceptor increases.[111]

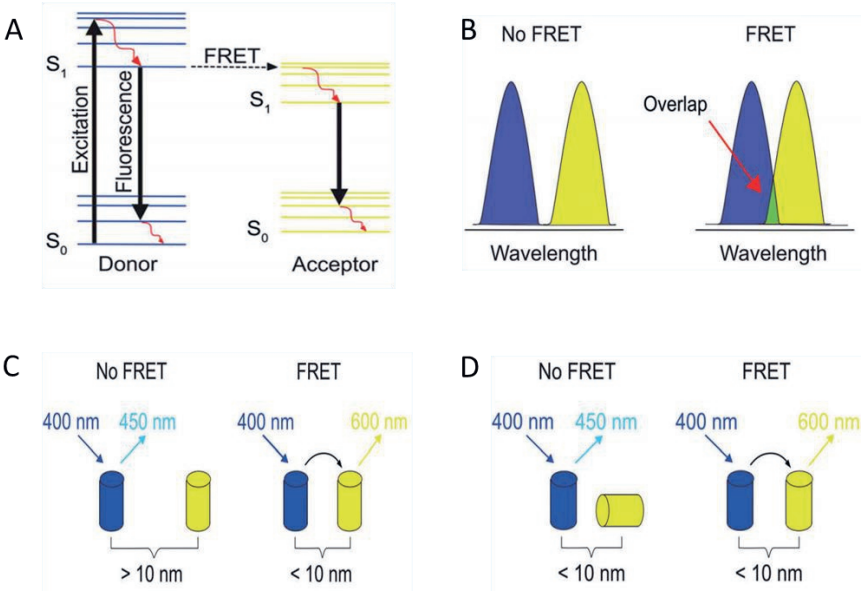

Figure 1.12. FRET (A) Energy transfer from donor to acceptor. (B) FRET depends on spectral overlap. (C) FRET depends on distance. (D) FRET depends on orientation.[109] Reproduced from Teunissen et al.[109] with permission from the Royal Society of Chemistry.

The FRET efficiency (E_{FRET}) can be calculated with the Förster equation below:

$$E_{FRET} = 1/[1 + (R/R_0)^6] \tag{1.3}$$

where R is the distance between donor and acceptor molecules, and R_0 is the distance where the FRET efficiency is 50 percent. R_0 can be calculated using the equation:

$$R_0 = 0.02108\,[k^2 Q_D\,\eta^{-4} J(\lambda)]^{1/6} \tag{1.4}$$

where k^2 is the orientation factor, Q_D is the quantum yield of donor fluorescence (without acceptor), η is the refractive index of the medium surrounding the fluorophore, and $J(\lambda)$ is the degree of spectral overlap between the donor fluorescence spectrum and acceptor absorption spectrum, that is given by:

$$J(\lambda) = \int f_D(\lambda)\,\varepsilon_A(\lambda)\,\lambda^4\,d\lambda \tag{1.5}$$

Where $f_D(\lambda)$ is the donor fluorescence intensity at wavelength λ and ε_A is the (wavelength dependent) extinction coefficient of the acceptor. FRET efficiency (E_{FRET}) can also be measured as the relative fluorescence intensity of the donor in the presence (I_{DA}) and absence (I_D) of the acceptor.[110,111]

$$E_{FRET} = 1 - \frac{I_{DA}}{I_D} \quad (1.6)$$

Quantification of FRET can be done based either on donor fluorescence lifetime or fluorescence intensity. The first approach is more straightforward because it is concentration-independent while fluorescence intensity is a concentration-dependent quantity.[108] FRET analysis allows determining the kinetics of C3M formation and protein exchange between C3Ms.[10] The kinetics of C3M formation can be studied by fluorescent labeling one batch of the protein with a donor label and another with an acceptor label, mixing these first, then add the diblock copolymer to form C3Ms and immediately start observing FRET over time. To determine the dynamics of protein exchange between C3Ms, one needs to prepare separate C3Ms of donor and acceptor (fluorescent) protein, then mix the two C3Ms solutions and immediately follow the changes in fluorescence intensity or fluorescence lifetimes over time.

1.6.4. Protein secondary structure

The secondary structure of proteins is the way in which its amino acid chains are locally folded in a three-dimensional structure. Secondary structure elements typically spontaneously form as an intermediate before the protein folds into its three-dimensional tertiary structure. The most common structural elements are α-helices and β-sheets. The secondary structure can be observed using circular dichroism (CD).[112] Circular dichroism is the differential absorption of the left and right circularly polarized components of plane-polarized radiation.

Circular dichroism is divided into far-UV CD and near-UV CD. From far-UV CD, the proportions of α-helix, β-sheet, β-turns and random coil in a protein can be reliably estimated based on absorption by the peptide bonds.[112] The α-helix structures will appear as two intense negative bands at about 222 nm and at 208 nm, and a positive band at 193 nm (Figure 1.13). Moreover, well-defined antiparallel β-pleated sheets (β-helices) will appear as negative bands at 218 nm and positive bands at 195 nm. A disordered structure (random coil) in the protein will have very low ellipticity above 210 nm and negative bands near 195 nm (Figure 1.13).[113,114] The CD spectrum of a protein is a linear combination of the CD responses of the different structural elements in its secondary structure. Moreover, near-UV CD provides information on the tertiary folding of the protein: if a disulfide bond is present, it is manifested in the CD spectrum in the 240 to 290 nm region. We applied CD to investigate whether chemical or genetic modification of CotA and/ or encapsulation in C3Ms results into structural changes.

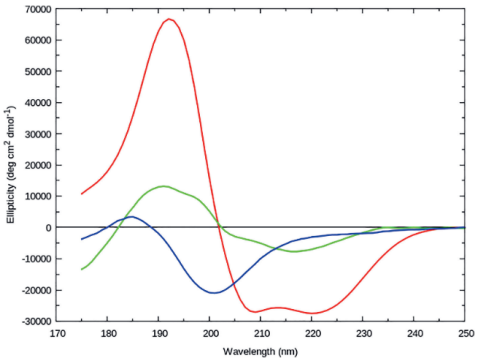

Figure 1.13. Far-UV CD spectra from various types of secondary structure. The red line represents the α-helix; the green line represent the β-sheet; blue line represent the disordered structure or random coil.[114,115] Reproduced from Rogers et al.[115] with permission from Elsevier.

1.6.5. Enzyme activity

The activity of enzymes is an important feature and we measured the activity of CotA in this study to see how it changes after chemical or genetic modification as well as after encapsulation and release. The activity test that we used is based on conversion of a substrate to a colored oxidation product which can be detected using UV VIS spectrometry. The substrate chosen is azino-bis-(3-ethylbenzothiazoline-6-sulphonic acid) (ABTS) which is converted to the stable blue-green radical cation ($ABTS^{\bullet+}$) after the loss of one electron during the oxidation.[116] One unit (U) of laccase activity is defined as the enzyme amount that is able to oxidize one µmol of substrate per minute.

1.7. Outline of this thesis

In **Chapter 2,** we report on the encapsulation of the spore coat protein A (CotA) laccase into complex coacervate core micelles (C3Ms). First, we describe the production and purification of CotA laccase from *Escherichia coli* Rosetta cells. Then, we present the stability of CotA as a function of pH as measured by activity measurements and circular dichroism (CD). Enzyme containing two-component C3Ms were prepared by mixing solutions of CotA laccase and the positive diblock copolymer, poly(*N*-methyl-2-vinyl-pyridinium)$_{128}$-*block*-poly(ethylene oxide)$_{477}$ ($P2MVP_{128}$-*b*-PEO_{477}), at pH 10.8. Enzyme-containing three-component C3Ms were prepared by adding the negatively charged homopolymer poly(4-styrene sulfonate)$_{215}$ (PSS_{215}) into the CotA solution (we used different ratios CotA/ homopolymer) before adding $P2MVP_{128}$-*b*-PEO_{477}. Subsequently, we observed the formation and salt stability of enzyme-containing

C3Ms by using fluorescence correlation spectroscopy (FCS) and dynamic light scattering (DLS). DLS showed improved stability of the three-component C3M system against salt addition compared to the two-component system. However, FCS showed that CotA is excluded from the C3Ms already at ionic strengths much lower than that at which the micelles actually disintegrate, because the homopolymer acts as a competitor of the enzyme for encapsulation.

In **Chapter 3**, based on the results described in Chapter 2, we investigate the bioconjugation technique to increase the enzyme's net charge to achieve more stable enzyme-containing complex coacervate core micelles. In this chapter, we couple poly(acrylic acid) (PAA) to lysine residue of CotA using 1-ethyl-3-(3'-dimethylaminopropyl)carbodiimide hydrochloride (EDC) and *N*-hydroxy succinimide (NHS) linker. The effect of the length and the concentration ratio of the PAA chain and the average number of PAA chains per CotA molecule was investigated. Successful bioconjugation was confirmed by native agarose gel electrophoresis, SDS PAGE, and zeta potential measurements that showed the increase of negative charge in the conjugate CotA-PAA. Enzyme-containing C3Ms were prepared at pH 10.8 by titrating the diblock copolymer $PM2VP_{128}$-*b*-PEO_{477} solution into to the CotA-PAA solution and micelle formation was observed with DLS. The stability of enzyme-containing C3Ms was observed by using DLS and FCS. From the results, we conclude that bioconjugation of PAA to CotA is a successful strategy to improve the salt-stability of the enzyme-containing C3Ms.

In **Chapter 4**, we explore a biological approach to increase the charge density of the enzyme. We used genetic engineering to increase the negative charge of CotA by adding some glutamic acid residues to the C-terminus of CotA. First, we describe the CotA gene's modification by using PCR and SLiCE (Seamless Ligation Cloning Extract) cloning methods. Then, we discuss the production and purification of genetically modified CotA laccase from *Escherichia coli* Rosetta cells. We investigated the effect of different numbers of glutamic acid added to the stability of CotA by activity measurements. Enzyme-containing C3Ms were prepared by mixing the genetically modified CotA laccase with the diblock copolymer $P2MVP_{128}$-*b*-PEO_{477}, at pH 10.8. The stability of the C3Ms was observed by DLS and FCS. The results show a significant improvement of the enzyme-containing C3Ms' stability against high salt conditions.

In **Chapter 5**, we investigate a chemical crosslinking approach to achieve stable C3Ms between homopolymer and diblock copolymer. We discuss quaternizing of diblock copolymers with amine-protected quaternization reagents in this chapter. After deprotection, the diblock copolymer has positive charges and primary amine functional groups. The C3Ms were prepared

by mixing the PAA with the modified diblock copolymer. Crosslinking of the micellar core was achieved by two type of crosslinkers; 1-ethyl-3-(3'-dimethylaminopropyl)carbodiimide hydrochloride (EDC) and dimethyl 3,3′-dithiopropionimidate dihydrochloride (DTBP). The stability of the C3Ms was observed by DLS. The results show a significant improvement of the C3Ms' stability against high salt conditions and pH changes. In addition, when the disulfide bridges in the DTBP of core-crosslinked micelles were reduced at pH 7.4, the original salt-stability profile was largely restored.

In **Chapter 6**, we continue our study on core-crosslink strategies of C3Ms composed of CotA laccase and amine-functionalized diblock copolymer. For the core-crosslinking of enzyme-containing C3Ms, we used DTBP crosslinker. Then, we present the effect of crosslinking on the activity of CotA. The formation and the salt stability of core-crosslinked C3Ms were observed by DLS and FCS. The results reveal that the C3Ms' resilience against high salt environments has significantly improved.

In **Chapter 7**, we examine the effect of the additional charges by genetic engineering and micellar core-crosslinking on the exchange dynamics of micelles by using the Förster resonance energy transfer method (FRET). For genetic engineering strategy, we used CotA laccase that were labeled with a FRET pair, Alexa Fluor 488 (donor) and Alexa Fluor 568 (acceptor). For core-crosslink strategy, we used the FRET pair of fluorescent proteins mTurquoise2 and SYFP2. The micelles composed of donor and acceptor proteins were mixed and the emission at donor excitation at donor and acceptor channel was recorded over time. Fitting the FRET efficiency data with an analytical model for FRET-based micelle exchange using two exchange rates (k_1 and k_2), we found that core-crosslink strategy decreases the exchange dynamics significantly which makes this strategy the most effective strategy to increase the salt stability and limiting protein exchange between C3Ms.

In **Chapter 8** we present a general discussion on the most critical findings from this study. From this work, we show that C3Ms are promising to encapsulate CotA. Our chemical and biological approaches (bioconjugation and genetic engineering) to increase the number of charges on the enzyme can be used to improve the stability of enzyme-containing C3Ms against the high salt environment. The core-crosslink strategy is the most effective strategy to increasing the salt stability and decreasing the exchange dynamic of the protein between micelles. Here we also discuss some recommendations that can be done to optimize the proposed strategies and some possible alternative strategies for future study. Finally, we described the implementation of strategies for potential applications of enzyme-containing C3Ms.

References

1. Voets, I. K., de Keizer, A. and Cohen Stuart, M. A. Complex coacervate core micelles. *Adv. Colloid Interface Sci.* **147**–**148**, 300–318 (2009).
2. Nolles, A., Westphal, A. H., de Hoop, J. A., Fokkink, R. G., Kleijn, J. M., van Berkel, W. J. H., and Borst, J. W. Encapsulation of GFP in complex coacervate core micelles. *Biomacromolecules* **16**, 1542–1549 (2015).
3. Lindhoud, S. and Claessens, M. M. A. E. Accumulation of small protein molecules in a macroscopic complex coacervate. *Soft Matter* **12**, 408–413 (2015).
4. Spruijt, E., Westphal, A. H., Borst, J. W., Cohen Stuart, M. A. and Van Der Gucht, J. Binodal compositions of polyelectrolyte complexes. *Macromolecules* **43**, 6476–6484 (2010).
5. Schaaf, P. and Schlenoff, J. B. Saloplastics: Processing compact polyelectrolyte complexes. *Adv. Mater.* **27**, 2420–2432 (2015).
6. Kembaren, R., Fokkink, R., Westphal, A. H., Kamperman, M., Kleijn, J. M., Borst, J. W. Balancing Enzyme Encapsulation Efficiency and Stability in Complex Coacervate Core Micelles. *Langmuir* **36**, 8494–8502 (2020).
7. Nolles, A., Westphal, A. H., Kleijn, J. M., van Berkel, W. J. H. and Borst, J. W. Colorful packages: Encapsulation of fluorescent proteins in complex coacervate core micelles. *Int. J. Mol. Sci.* **18**, (2017).
8. Lindhoud, S., de Vries, R., Norde, W. and Cohen Stuart, M. A. Structure and stability of complex coacervate core micelles with lysozyme. *Biomacromolecules* **8**, 2219–2227 (2007).
9. Water, J. J., Schack, M. M., Velazquez-Campoy, A., Maltesen, M.J., van de Weert, M., and Jorgensen, L. Complex coacervates of hyaluronic acid and lysozyme: Effect on protein structure and physical stability. *Eur. J. Pharm. Biopharm.* **88**, 325–331 (2014).
10. Nolles, A., Hooiveld, E., Westphal, A. H., van Berkel, W. J. H., Kleijn, J. M., and Borst, J. W. FRET Reveals the Formation and Exchange Dynamics of Protein-Containing Complex Coacervate Core Micelles. *Langmuir* **34**, 12083–12092 (2018).
11. Bos, I., Timmerman, M. and Sprakel, J. FRET-based determination of the exchange dynamics of complex coacervate core micelles. *Macromolecules* **54**, 398–411 (2021).
12. Heo, T. Y., Kim, S., Chen, L., Sokolova, A., Lee, S., and Choi, S.H. Molecular Exchange Kinetics in Complex Coacervate Core Micelles: Role of Associative Interaction. *ACS Macro Lett.* **10**, 1138–1144 (2021).
13. Ouzounis, C. A., Coulson, R. M. R., Enright, A. J., Kunin, V. and Pereira-Leal, J. B. Classification schemes for protein structure and function. *Nat. Rev. Genet.* **4**, 508–519 (2003).
14. Rahman, S. A., Furnham, N., Thornton, J. M. and Martı, S. Biophysical Perspective The Classification and Evolution of Enzyme Function. **109**, 1082–1086 (2015).
15. Kirk, O., Borchert, T. V. and Fuglsang, C. C. Industrial enzyme applications. *Curr. Opin. Biotechnol.* **13**, 345–351 (2002).
16. Carter, P. J. Introduction to current and future protein therapeutics: A protein engineering perspective. *Exp. Cell Res.* **317**, 1261–1269 (2011).
17. Nguyen, H. H. and Kim, M. An Overview of Techniques in Enzyme Immobilization. *Appl. Sci. Converg. Technol.* **26**, 157–163 (2017).
18. Bilal, M., Iqbal, H.M.N., Guo, S., Hu, H., Wang, W., and Zhang, X. State-of-the-art protein engineering approaches using biological macromolecules: A review from immobilization to implementation view point. *Int. J. Biol. Macromol.* **108**, 893–901 (2018).
19. Thangaraj, B. and Solomon, P. R. Immobilization of Lipases – A Review. Part I: Enzyme Immobilization. *ChemBioEng Rev.* **6**, 157–166 (2019).
20. Blocher McTigue, W. C. and Perry, S. L. Protein Encapsulation Using Complex Coacervates: What Nature Has to Teach Us. *Small* **16**, 1–17 (2020).
21. Tan, M. X. L. and Danquah, M. K. Drug and Protein Encapsulation by Emulsification: Technology Enhancement Using Foam Formulations. *Chem. Eng. Technol.* **35**, 618–626 (2012).
22. Mcclements, D. J. Encapsulation , protection , and delivery of bioactive proteins and peptides using nanoparticle and microparticle systems : A review. *Adv. Colloid Interface Sci.* **253**, 1–22 (2018).
23. Rideau, E., Dimova, R., Schwille, P., Wurm, F. R. and Landfester, K. Liposomes and polymersomes: a comparative review towards cell mimicking. *Chem. Soc. Rev.* **47**, 8572–8610 (2018).
24. Pisal, D. S., Kosloski, M. P. and Balu-iyer, S. V. Delivery of Therapeutic Proteins. *J. Pharm. Sci.* **99**, 2557–2575 (2010).
25. Soni, K. S., Desale, S. S. and Bronich, T. K. Nanogels: An overview of properties, biomedical applications and obstacles to clinical translation. *J. Control. Release* **240**, 109–126 (2016).
26. Ghimire, A., Zore, O. V., Thilakarathne, V. K., Briand, V. A., Lenehan, P. J., Lei, Y., Kasi, R. M., and Kumar, C. V. 'Stable-on-the-Table' Biosensors: Hemoglobin-Poly (Acrylic Acid) Nanogel BioElectrodes

with High Thermal Stability and Enhanced Electroactivity. *Sensors (Basel)*. **15**, 23868–23885 (2015).
27. Nguyen, D. H., Choi, J. H., Joung, Y. K. and Park, K. D. Disulfide-crosslinked heparin-pluronic nanogels as a redox-sensitive nanocarrier for intracellular protein delivery. *J. Bioact. Compat. Polym.* **26**, 287–300 (2011).
28. Yin, Y., Hu, B., Yuan, X., Cai, L. and Gao, H. Nanogel : A Versatile Nano-Delivery System for Biomedical Applications. *Pharmaceutics* **12**,1-25 (2020).
29. Yusa, S. I., Sugahara, M., Endo, T. and Morishima, Y. Preparation and characterization of a pH-responsive nanogel based on a photo-cross-linked micelle formed from block copolymers with controlled structure. *Langmuir* **25**, 5258–5265 (2009).
30. De Alteriis, R., Vecchione, R., Attanasio, C., De Gregorio, M., Porzio, M., Battista, E., and Netti, P. A. A method to tune the shape of protein-encapsulated polymeric microspheres. *Sci. Rep.* **5**, 1–9 (2015).
31. Chandy, T., Das, G. S., Wilson, R. F. and Rao, G. H. R. Development of polylactide microspheres for protein encapsulation and delivery. *J. Appl. Polym. Sci.* **86**, 1285–1295 (2002).
32. Blanco, D. and Alonso, M. J. Protein encapsulation and release from poly(lactide-co-glycolide) microspheres: Effect of the protein and polymer properties and of the co- encapsulation of surfactants. *Eur. J. Pharm. Biopharm.* **45**, 285–294 (1998).
33. Sing, C. E. and Perry, S. L. Recent progress in the science of complex coacervation. *Soft Matter* **16**, 2885–2914 (2020).
34. Black, K. A., Priftis, D., Perry, S. L., Yip, J., Byun, W. Y., and Tirrell, M. Protein encapsulation via polypeptide complex coacervation. *ACS Macro Lett.* **3**, 1088–1091 (2014).
35. Salamone, J. C., Mahmud, N. A., Mahmud, M. U., Nagabhushanam, T. and Watterson, A. C. Acrylic ampholytic ionomers. *Polymer (Guildf).* **23**, 843–848 (1982).
36. Rosso, F., Barbarisi, A., Barbarisi, M., Petillo, O., Margarucci, S., Calarco, A., and Peluso, G. New polyelectrolite hydrogels for biomedical applications. *Mater. Sci. Eng. C* **23**, 371–376 (2003).
37. Zhou, L., Shi, H., Li, Z. and He, C. Recent Advances in Complex Coacervation Design from Macromolecular Assemblies and Emerging Applications. *Macromol. Rapid Commun.* **41**, 1–20 (2020).
38. Rumyantsev, A. M., Jackson, N. E. and de Pablo, J. J. Polyelectrolyte Complex Coacervates: Recent Developments and New Frontiers. *Annu. Rev. Condens. Matter Phys.* **12**, 155–176 (2021).
39. Rumyantsev, A. M., Zhulina, E. B. and Borisov, O. V. Scaling Theory of Complex Coacervate Core Micelles. *ACS Macro Lett.* **7**, 811–816 (2018).
40. Wang, J., Cohen Stuart, M. A. and Van Der Gucht, J. Phase diagram of coacervate complexes containing reversible coordination structures. *Macromolecules* **45**, 8903–8909 (2012).
41. Gucht, J. van der, Spruijt, E., Lemmers, M. and Cohen Stuart, M. A. Polyelectrolyte complexes: Bulk phases and colloidal systems. *J. Colloid Interface Sci.* **361**, 407–422 (2011).
42. Perry, S. L., Li, Y., Priftis, D., Leon, L. and Tirrell, M. The effect of salt on the complex coacervation of vinyl polyelectrolytes. *Polymers (Basel).* **6**, 1756–1772 (2014).
43. Blocher, W. C. and Perry, S. L. Complex coacervate-based materials for biomedicine. *Wiley Interdiscip. Rev. Nanomedicine Nanobiotechnology* **9**, 76–78 (2017).
44. Lawrence, M., Daujat, S. and Schneider, R. Lateral Thinking: How Histone Modifications Regulate Gene Expression. *Trends Genet.* **32**, 42–56 (2016).
45. Tavoosi, N., Davis-Harrison, R. L., Pogorelov, T.V., Ohkubo, Y. Z., Arcario, M. J., Clay, M. C., Rienstra, C. M., Tajkhorshid, E., and Morrissey, J. H. Molecular determinants of phospholipid synergy in blood clotting. *J. Biol. Chem.* **286**, 23247–23253 (2011).
46. Dompé, M., Cedano-Serrano, F. J., Vahdati, M., van Westerveld, L., Hourdet, D., Creton, C., van der Gucht, J., Kodger, T., and Kamperman, M. Underwater Adhesion of Multiresponsive Complex Coacervates. *Adv. Mater. Interfaces* **7**, (2020).
47. Amann, M., Diget, J. S., Lyngsø, J., Pedersen, J.S., Narayanan, T., and Lund, R. Kinetic Pathways for Polyelectrolyte Coacervate Micelle Formation Revealed by Time-Resolved Synchrotron SAXS. *Macromolecules* **52**, 8227–8237 (2019).
48. Cohen Stuart, M. A., Besseling, N. A. M. and Fokkink, R. G. Formation of micelles with complex coacervate cores. *Langmuir* **14**, 6846–6849 (1998).
49. Bronich, T. K., Kabanov, A. V and Kabanov, V. A. Soluble Complexes from Poly(ethylene oxide) - block -polymethacrylate Anions and N -Alkylpyridinium Cations. *Macromolecules* **30**, 3519–3525 (1997).
50. Harada, A. and Kataoka, K. Formation of Polyion Complex Micelles in an Aqueous Milieu from a Pair of Oppositely-Charged Block Copolymers with Poly(ethylene glycol) Segments. *Macromolecules* **28**, 5294–5299 (1995).
51. Mayes, A. M., Olvera, M. and Cruz, D. Micelle Formation in Block Copolymer/ Homopolymer. *Macromolecules* **21**, 2543–2547 (1988).
52. Van Der Kooij, H. M., Spruijt, E., Voets, I. K., Fokkink, R., Cohen Stuart, M. A., and Van Der Gucht, J. On the stability and morphology of complex coacervate core micelles: From spherical to wormlike

micelles. *Langmuir* **28**, 14180–14191 (2012).
53. Cooper, C. L., Dubin, P. L., Kayitmazer, A. B. and Turksen, S. Polyelectrolyte-protein complexes. *Curr. Opin. Colloid Interface Sci.* **10**, 52–78 (2005).
54. Gaucher, G., Dufresne, M. H., Sant, V. P., Kang, N., Maysinger, D., and Leroux, J. C. Block copolymer micelles: Preparation, characterization and application in drug delivery. *J. Control. Release* **109**, 169–188 (2005).
55. Sproncken, C. C. M., Magana, J. R. and Voets, I. K. 100th Anniversary of Macromolecular Science Viewpoint: Attractive Soft Matter: Association Kinetics, Dynamics, and Pathway Complexity in Electrostatically Coassembled Micelles. *ACS Macro Lett.* **10**, 167–179 (2021).
56. Kötz, J., Kosmella, S. and Beitz, T. Self-assembled polyelectrolyte systems. *Prog. Polym. Sci.* **26**, 1199–1232 (2001).
57. Lindhoud, S., De Vries, R., Schweins, R., Cohen Stuart, M. A. and Norde, W. Salt-induced release of lipase from polyelectrolyte complex micelles. *Soft Matter* **5**, 242–250 (2009).
58. Yan, Y., De Keizer, A., Cohen Stuart, M. A., Drechsler, M. and Besseling, N. A. M. Stability of complex coacervate core micelles containing metal coordination polymer. *J. Phys. Chem. B* **112**, 10908–10914 (2008).
59. Wang, J., De Keizer, A., Fokkink, R., Yan, Y., Cohen Stuart, M. A., Van Der Gucht, J. Complex coacervate core micelles from iron-based coordination polymers. *J. Phys. Chem. B* **114**, 8313–8319 (2010).
60. Zhang, J., Chen, S., Zhu, Z. and Liu, S. Stopped-flow kinetic studies of the formation and disintegration of polyion complex micelles in aqueous solution. *Phys. Chem. Chem. Phys.* **16**, 117–127 (2014).
61. Dormidontova, E. E. Micellization kinetics in block copolymer solutions: scaling model. *Macromolecules* **32**, 7630–7644 (1999).
62. Holappa, S., Kantonen, L., Andersson, T., Winnik, F. and Tenhu, H. Overcharging of polyelectrolyte complexes by the guest polyelectrolyte studied by fluorescence spectroscopy. *Langmuir* **21**, 11431–11438 (2005).
63. Bos, I. and Sprakel, J. Langevin Dynamics Simulations of the Exchange of Complex Coacervate Core Micelles: The Role of Nonelectrostatic Attraction and Polyelectrolyte Length. *Macromolecules* **52**, 8923−8931 (2019).
64. Mills, C. E., Obermeyer, A., Dong, X., Walker, J. and Olsen, B. D. Complex Coacervate Core Micelles for the Dispersion and Stabilization of Organophosphate Hydrolase in Organic Solvents. *Langmuir* **32**, 13367–13376 (2016).
65. Olsen, B. D., Mills, C. E., Dong, X. and Obermeyer, A. C. Block copolymer complex coacervate core micelles for enzymatic catalysis in organic solvent. *PCT Int. Appl.* **1**, 1–32 (2016).
66. Pich, A., Bhattacharya, S., Adler, H. J. P., Wage, T., Taubenberger, A., Li, Z., Van Pee, K. H., Böhmer, U., and Bley, T. Composite magnetic particles as carriers for laccase from Trametes versicolor. *Macromol. Biosci.* **6**, 301–310 (2006).
67. Bryjak, J., Kruczkiewicz, P., Reku, A. and Peczy, W. Laccase immobilization on copolymer of butyl acrylate and ethylene glycol dimethacrylate. **35**, 325–332 (2007).
68. Martins, L. O., Soares, C. M., Pereira, M.M., Teixeira, M., Costa, T., Jones, G. H., and Henriques, A. O. Molecular and biochemical characterization of a highly stable bacterial laccase that occurs as a structural component of the Bacillus subtilis endospore coat. *J. Biol. Chem.* **277**, 18849–18859 (2002).
69. Reiss, R., Ihssen, J., Richter, M., Eichhorn, E., Schilling, B., and Thöny-Meyer, L. Laccase versus Laccase-Like Multi-Copper Oxidase: A Comparative Study of Similar Enzymes with Diverse Substrate Spectra. *PLoS One* **8**, 65633–65634 (2013).
70. Mate, D. M. and Alcalde, M. Minireview Laccase : a multi-purpose biocatalyst at the forefront of biotechnology. *Microb. Biotechnol.* **10**, 1457–1467 (2016).
71. Hakulinen, N. and Rouvinen, J. Three-dimensional structures of laccases. *Cell. Mol. Life Sci.* **72**, 857–868 (2015).
72. Shraddha, Shekher, R., Sehgal, S., Kamthania, M. and Kumar, A. Laccase: Microbial sources, production, purification, and potential biotechnological applications. *Enzyme Res.* **2011**, 1-11 (2011).
73. Guzik, U., Hupert-Kocurek, K. and Wojcieszynska, D. Immobilization as a strategy for improving enzyme properties- Application to oxidoreductases. *Molecules* **19**, 8995–9018 (2014).
74. Janusz, G., Pawlik, A., Świderska-Burek, U., Polak, J.,Sulej, J., Jarosz-Wilkołazka, A., and Paszczyński, A. Laccase properties, physiological functions, and evolution. *Int. J. Mol. Sci.* **21**, 1-25 (2020).
75. Fernandes, A. T., Lopes, C., Martins, L. O. and Melo, E. P. Unfolding pathway of CotA-laccase and the role of copper on the prevention of refolding through aggregation of the unfolded state. *Biochem. Biophys. Res. Commun.* **422**, 442–446 (2012).
76. Enguita, F. J., Martins, L. O., Henriques, A. O. and Carrondo, M. A. Crystal structure of a bacterial endospore coat component: A laccase with enhanced thermostability properties. *J. Biol. Chem.* **278**, 19416–19425 (2003).

77. Beneyton, T., Beyl, Y., Guschin, D. A., Griffiths, A. D., Taly, V., and Schuhmann, W. The Thermophilic CotA Laccase from Bacillus subtilis: Bioelectrocatalytic Evaluation of O2 Reduction in the Direct and Mediated Electron Transfer Regime. *Electroanalysis* **23**, 1781–1789 (2011).
78. Virk, A. P., Sharma, P. and Capalash, N. Use of laccase in pulp and paper industry. *Biotechnol. Prog.* **28**, 21–32 (2012).
79. Viswanath, B., Rajesh, B., Janardhan, A., Kumar, A. P. and Narasimha, G. Fungal laccases and their applications in bioremediation. *Enzyme Res.* **2014**, 1–21 (2014).
80. Bento, I., Martins, L. O., Lopes, G. G., Carrondo, M. A. and Lindley, P. F. Dioxygen reduction by multi-copper oxidases; a structural perspective. *Dalt. Trans.* **4**, 3507–3513 (2005).
81. Christopher, L. P., Yao, B. and Ji, Y. Lignin biodegradation with laccase-mediator systems. *Front. Energy Res.* **2**, 1–13 (2014).
82. Mastop, M., Bindels, D. S., Shaner, N. C., Postma, M., Gadella, Theodorus W.J., and Goedhart, J. Characterization of a spectrally diverse set of fluorescent proteins as FRET acceptors for mTurquoise2. *Sci. Rep.* **7**, 1–18 (2017).
83. Goedhart, J., Von Stetten, D., Noirclerc-Savoye, M., Lelimousin, M., Joosen, L., Hink, M. A., Van Weeren, L., Gadella, T. W.J., and Royant, A. Structure-guided evolution of cyan fluorescent proteins towards a quantum yield of 93%. *Nat. Commun.* **3**, 1–9 (2012).
84. Obermeyer, A. C., Mills, C. E., Dong, X. H., Flores, R. J. and Olsen, B. D. Complex coacervation of supercharged proteins with polyelectrolytes. *Soft Matter* **12**, 3570–3581 (2016).
85. Wilson, P. Synthesis and Applications of Protein/Peptide-Polymer Conjugates. *Macromol. Chem. Phys.* **218**, 1–15 (2017).
86. Baslé, E., Joubert, N. and Pucheault, M. Protein Chemical Modification on Endogenous Amino Acids. *Chem. Biol.* **17**, 213–227 (2010).
87. West, J. L. and Halas, N. J. A gold nanoparticle bioconjugate-based colorimetric assay. *Curr. Opin. Biotechnol.* **11**, 215–217 (2000).
88. Koniev, O. and Wagner, A. Developments and recent advancements in the field of endogenous amino acid selective bond forming reactions for bioconjugation. *Chem. Soc. Rev.* **44**, 5495–5551 (2015).
89. Li, Y., Gabriele, E., Samain, F., Favalli, N., Sladojevich, F., Scheuermann, J., and Neri, D. Optimized reaction conditions for amide bond formation in DNA- encoded combinatorial libraries. *ACS Comb Sci.* **18**, 438–443 (2017).
90. Rosen, C. B. and Francis, M. B. Targeting the N terminus for site-selective protein modification. *Nat. Chem. Biol.* **13**, 697–705 (2017).
91. Mantovani, G., Lecolley, F., Tao, L., Haddleton, D. M., Clerx, J., Cornelissen, J. J.L.M., and Velonia, K. Design and synthesis of N-maleimido-functionalized hydrophilic polymers via copper-mediated living radical polymerization: A suitable alternative to pegylation chemistry. *J. Am. Chem. Soc.* **127**, 2966–2973 (2005).
92. Totaro, K. A., Liao, X., Bhattacharya, K., Finneman, J. I., Sperry, J. B., Massa, M. A., Thorn, J., Ho, S. V. and Pentelute, B. L. Systematic Investigation of EDC/sNHS-Mediated Bioconjugation Reactions for Carboxylated Peptide Substrates. *Bioconjug. Chem.* **27**, 994–1004 (2016).
93. Riccardi, C. M., Mistri, D., Hart, O., Anuganti, M., Lin, Y., Kasi, R. M., and Kumar, C. V. Covalent interlocking of glucose oxidase and peroxidase in the voids of paper: Enzyme-polymer "spider webs. *Chem. Commun.* **52**, 2593–2596 (2016).
94. Hong, J., Gong, P. J., Yu, J. H., Xu, D. M., Sun, H. W., and Yao, S. Conjugation of α-chymotrypsin on a polymeric hydrophilic nanolayer covering magnetic nanoparticles. *J. Mol. Catal. B Enzym.* **42**, 99–105 (2006).
95. Collins, J., Tanaka, J., Wilson, P., Kempe, K., Davis, T. P., Mcintosh, M. P., Whittaker, M. R., and Haddleton, D. M. In situ conjugation of dithiophenol maleimide polymers and oxytocin for stable and reversible polymer-peptide conjugates. *Bioconjug. Chem.* **26**, 633–638 (2015).
96. Gauthier, M. A. and Klok, H. A. Peptide/protein-polymer conjugates: Synthetic strategies and design concepts. *Chemical Communications* 2591–2611 (2008).
97. Uzogara, S. G. The impact of genetic modification of human foods in the 21st century: A review. *Biotechnol. Adv.* **18**, 179–206 (2000).
98. Court, D. L., Sawitzke, J. A. and Thomason, L. C. Genetic engineering using homologous recombination. *Annu. Rev. Genet.* **36**, 361–388 (2002).
99. Zhang, Y., Werling, U. and Edelmann, W. SLiCE: A novel bacterial cell extract-based DNA cloning method. *Nucleic Acids Res.* **40**, 1–10 (2012).
100. Krishnakumar, G. S., Sampath, S., Muthusamy, S. and John, M. A. Importance of crosslinking strategies in designing smart biomaterials for bone tissue engineering: A systematic review. *Materials Science and Engineering C* **96**, 941–954 (2019).
101. Hennink, W. E. and van Nostrum, C. F. Novel crosslinking methods to design hydrogels. *Advanced Drug*

Delivery Reviews **64**, 223–236 (2012).
102. Tillet, G., Boutevin, B. and Ameduri, B. Chemical reactions of polymer crosslinking and post-crosslinking at room and medium temperature. *Progress in Polymer Science* **36**,191–217 (2011).
103. Reddy, N., Reddy, R. and Jiang, Q. Crosslinking biopolymers for biomedical applications. *Trends Biotechnol.* **33**, 362–369 (2015).
104. Xu, R. Particuology Light scattering : A review of particle characterization applications. *Particuology* **18**, 11–21 (2015).
105. Villari, V. and Micali, N. Light Scattering as Spectroscopic Tool for the Study of Disperse Systems Useful in Pharmaceutical Sciences. *J. Pharm. Sci.* **97**, 1703–1730 (2008).
106. Harding, S. E. *Chapter 7 Protein hydrodynamics*. vol. 2 (1999).
107. Stetefeld, J., McKenna, S. A. and Patel, T. R. Dynamic light scattering: a practical guide and applications in biomedical sciences. *Biophys. Rev.* **8**, 409–427 (2016).
108. Willem Borst, J. and Visser, A. J. W. G. Fluorescence lifetime imaging microscopy in life sciences. *Meas. Sci. Technol.* **21**, 1–21 (2010).
109. Teunissen, A. J. P., Pérez-Medina, C., Meijerink, A. and Mulder, W. J. M. Investigating supramolecular systems using Förster resonance energy transfer. *Chem. Soc. Rev.* **47**, 7027–7044 (2018).
110. Berney, C. and Danuser, G. FRET or no FRET: A quantitative comparison. *Biophys. J.* **84**, 3992–4010 (2003).
111. Wallrabe, H. and Periasamy, A. Imaging protein molecules using FRET and FLIM microscopy. *Curr. Opin. Biotechnol. 2005,* **16**, 19–27 (2005).
112. Kelly, S. and Price, N. The Use of Circular Dichroism in the Investigation of Protein Structure and Function. *Curr. Protein Pept. Sci.* **1**, 349–384 (2005).
113. Greenfield, N. J. Using circular dichroism spectra to estimate protein secondary structure. *Nat. Protoc.* **1**, 2876–2890 (2007).
114. Johnson, W. C. Protein secondary structure and circular dichroism: A practical guide. *Proteins Struct. Funct. Bioinforma.* **7**, 205–214 (1990).
115. Rogers, D. M., Jasim, S. B., Dyer, N. T., Auvray, F., Réfrégiers, M., and Hirst, J. D. Electronic Circular Dichroism Spectroscopy of Proteins. *Chem* **5**, 2751–2774 (2019).
116. Johannes, C. and Majcherczyk, A. Laccase activity tests and laccase inhibitors. *J. Biotechnol.* **78**, 193–199 (2000).

Chapter 2 :
Balancing enzyme encapsulation efficiency and stability in complex coacervate core micelles

Published as:

Kembaren, R., Fokkink, R., Westphal, A. H., Kamperman, M., Kleijn, J. M., and Borst, J. W. Balancing enzyme encapsulation efficiency and stability in complex coacervate core micelles. *Langmuir* **36**, 8494-8502 (2020).

Abstract

Encapsulation of charged proteins into complex coacervate core micelles (C3Ms) can be accomplished by mixing them with oppositely charged diblock copolymers. However, these micelles tend to disintegrate at high ionic strength. Previous research showed that the addition of a homopolymer with the same charge sign as the protein improved the stability of protein-containing C3Ms. In this research, we used fluorescence correlation spectroscopy (FCS) and dynamic light scattering (DLS) to study how the addition of the homopolymer affects the encapsulation efficiency and salt stability of the micelles. We studied the encapsulation of laccase spore coat protein A (CotA), a multicopper oxidase, using a strong cationic-neutral diblock copolymer, poly(*N*-methyl-2-vinyl-pyridinium)-*block*-poly(ethylene oxide) ($PM2VP_{128}$-*b*-PEO_{477}), and a negatively charged homopolymer, poly(4-styrenesulfonate) (PSS_{215}). DLS indeed showed an improved stability of this three-component C3M system against the addition of salt compared to a two-component system. Remarkably, FCS showed that the release of CotA from a three-component C3M system occurred at a lower salt concentration and over a narrower concentration range than the dissociation of C3Ms. In conclusion, although the addition of the homopolymer to the system leads to micelles with a higher salt stability, CotA is excluded from the C3Ms already at lower ionic strengths because the homopolymer acts as a competitor of the enzyme for encapsulation.

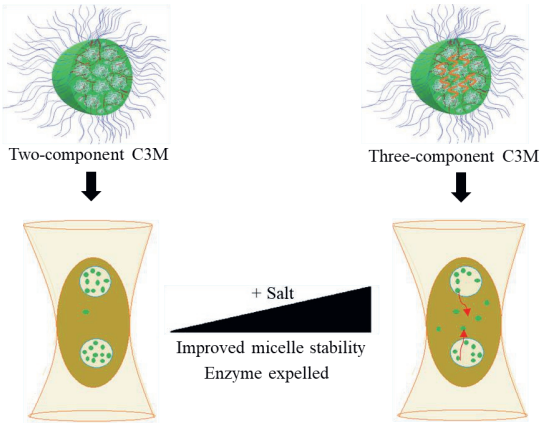

2.1. Introduction

Complex coacervate core micelles (C3Ms) can be formed by mixing a diblock copolymer composed of a neutral block and a charged block with an oppositely charged polyelectrolyte or a charged biomolecule such as DNA,[1] RNA,[2] or protein.[3–5] The oppositely charged parts bind electrostatically to form an almost electroneutral coacervate.[6] This coacervate forms the core of the micelle, surrounded by a corona consisting of the neutral hydrophilic parts of the diblock copolymer, which keeps the micelles in solution.[7] C3Ms can be used for a wide variety of applications, for example, as nanoreactors,[8] diffusional nanoprobes,[9] anti-biofouling coatings,[10] and drug delivery systems.[11] Advantages of C3Ms as packing system for proteins are their solubility in aqueous solution, that many protein molecules can be encapsulated in one micelle,[3] and that they offer opportunities for controlled release.[12] Encapsulation of proteins can protect them against detrimental environmental effects and protease activity, and enzyme-containing C3Ms can be used as a microreactor to overcome incompatibility problems between polar enzymes and non-polar substrates.[13]

For the encapsulation of a protein in C3Ms, the total protein charge and charge distribution over its surface are very important and are dependent on amino acid composition, structure, and pH of the surrounding solution.[4] In addition, because of the hydrophobic nature of various amino acid residues, the formation of protein-containing C3Ms may not only be driven by electrostatic interactions and entropy gain due to counterion release,[14] but hydrophobic interactions may also contribute significantly.[15]

One of the most significant challenges regarding the use of C3Ms as packing systems for proteins is that they easily disintegrate, often due to the low charge density of proteins. Lindhoud et al. showed, using dynamic light scattering (DLS), that the most stable enzyme-containing C3Ms could be obtained by adding homopolymer with the same charge sign as the protein to the two-component system, in excess over the protein concentration.[16] Research from Black et al. showed that bovine serum albumin (BSA) could be encapsulated in coacervate droplets of two oppositely charged polypeptides. However, increasing the ratio of BSA to the total amount of polypeptides in the system led to a less than linear increase of BSA in the coacervate, as observed using a Bradford colorimetric assay.[17] This illustrates the need for further investigation of three-component coacervate systems for protein encapsulation, studied using additional techniques, as already suggested by Blocher and Perry (2016).[18]

In 2010, Gapinski et al. showed that the relatively novel technique of fluorescence correlation spectroscopy (FCS) could be used to measure micellar sizes and shapes.[19] Research

of Nolles et al. showed that DLS and FCS provided similar results concerning the hydrodynamic radius and preferred micellar composition (PMC) of two-component C3Ms that contained green fluorescent protein (GFP).[3,5] In addition, FCS enabled them to obtain the distribution of protein over micelles and solution and the number of protein molecules incorporated per micelle.[3] Compared to DLS, FCS has a relative low background noise due to the Stokes shift of the fluorescence emission, and measurements can be conducted at very low (nanomolar) concentrations. Furthermore, FCS has a selectivity that allows for the measurement of specific fluorescent molecules in systems.[20] On the other hand, FCS experiments and analysis are more labor-intensive than DLS measurements, and often fluorescence labelling of biomolecules is required.

The spore coat protein A (CotA) laccase is the model enzyme of the present study. CotA is originally found in the outer coat layer of the *Bacillus subtilis* endospore.[21] CotA has an isoelectric point (pI) at pH 5.84 and a molar weight of 65 kDa. It is a multicopper oxidase (MCO), characterized by the presence of four copper ions[22] (Figure 2.1). These four copper ions are classified into three categories based on the ultraviolet/ visible (UV/ vis) and electronic paramagnetic resonance (EPR) spectra, denoted as type 1 (T1), type 2 (T2) a type 3 (T3).[23] The T1 Cu ion is responsible for the intense blue color of the enzyme, and its absorption can be detected around 600 nm. The T2 and two T3 Cu ions form the trinuclear center (TNC) in the protein structure.[24] CotA can catalyze the oxidation of a wide variety of substrates using dioxygen as an electron acceptor. Substrate oxidation occurs at the T1 binding pocket, and the electrons are then transferred to the TNC, where the reduction of dioxygen occurs.[25–27] CotA has a region of positive charge on its surface at the interface between domains 1, 2 and 3, including ten lysine and five arginine amino acid residues. The biological function of this positively charged patch is its involvement in the assembly of CotA into the spore outer coat layer.[8, 27]

Some types of laccases have already been used as a model to study enzyme immobilization. For example, Pich et al. used laccase from fungus in their study of composite magnetic particles as enzyme carriers,[28] while Bryjak et al. immobilized laccase from fungus by covalently binding it to a copolymer of butyl acrylate and ethylene glycol dimethacrylate.[29] However, so far laccases have not been used to study encapsulation in complex coacervate core micelles. In this research, we studied the stability and encapsulation efficiency of CotA containing C3Ms. We show that a combination of DLS and fluorescence correlation spectroscopy (FCS) data is necessary to optimize the balance between micelle stability and encapsulation efficiency.

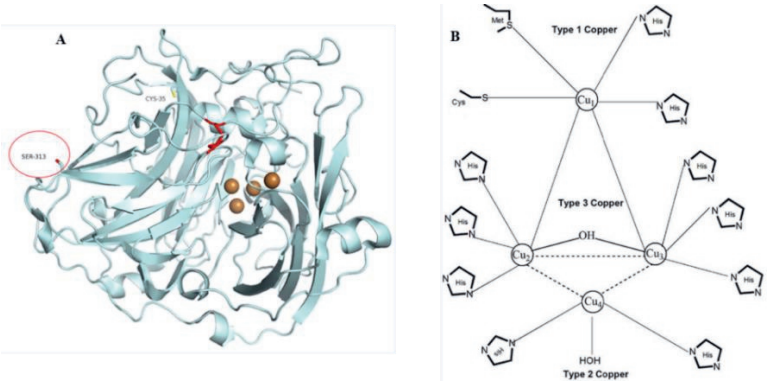

Figure 2.1. (A) native CotA structure. Cu atoms are represented as spheres colored in brown. The protein contains one disulfide bridge, which is represented as a red line. (B) Copper coordination in CotA laccase structure.[25,30]

2.2. Experimental section

2.2.1. Materials

2,2'-Azino-bis(3-ethylbenzothiazoline-6-sulfonic acid) diammonium salt (ABTS) was purchased from Sigma-Aldrich. The probe Alexa Fluor C5 maleimide (Alexa 488) was purchased from Thermo Fisher Scientific. The diblock copolymer poly(2-vinyl pyridine)$_{128}$-*block*-poly(ethylene oxide)$_{477}$ (M_n = 34.5 kg/ mol, M_w/ M_n = 1.1) was obtained from Polymer Source Inc. This diblock copolymer then was quaternized with iodomethane following the procedure described by Lindhoud et al.[31] The quaternization degree was about 70 % as measured by ^{1}H-NMR (Figure S2.1., Supplementary information).[32] The homopolymer poly(4-styrenesulfonate)$_{215}$ (M_n = 43 kg/ mol, M_w/ M_n =1.03, degree of sulfonation about 90 %) was purchased from Polymer Source Inc.

2.2.2. CotA production

The production and purification of CotA were done following the procedure described by Martins et al.[21] The CotA gene was cloned into a pLOM 10 vector and heterologously expressed in *Escherichia coli* Rosetta cells. The induction of CotA laccase expression was done by adding 0.1 mM isopropyl *β*-D-1- thiogalactopyranoside (IPTG) and 0.25 mM $CuSO_4$ at 25 ºC. The purification of CotA laccase was performed using cation exchange chromatography (cIEX using a SP-Sepharose FF column from GE Healthcare) and gel filtration chromatography (Superdex 200 column from GE Healthcare).

A variant of CotA was obtained by replacing a serine at position 313 in the amino acid sequence by a cysteine (CotA S313C). Copper is an oxidation catalyst that can promote the oxidation of free sulfhydryl in cysteine of CotA S313C. Because of that reason, for this variant, apoenzyme was produced, i.e. without the addition of 0.25 mM $CuSO_4$ during induction.[33] The CotA containing fractions from cIEX were pooled and subsequently labeled with Alexa Fluor 488 C5 maleimide with a molar ratio of 1:10 at 4 ºC by incubation in the dark for 16 h. Next, the mixture was loaded to a Biogel-P6DG gel filtration column (BioRad) to separate the labeled protein from the unreacted label. The fractions that showed fluorescence and contained protein were pooled and concentrated by using an Amicon concentrator (cutoff of 10 kDa). The pooled concentrated enzyme was then loaded to a gel filtration column (Superdex 200 column). The fractions that showed absorptions both at 280 nm and 490 nm were collected and concentrated. The purity of labeled CotA was analyzed using SDS-PAGE analysis (Figure S2.2., Supplementary information).

2.2.3. pH stability of CotA: enzyme activity test and Circular Dichroism (CD)

For the activity assay (standard assay), we used 1.0 mM ABTS as a substrate for CotA. The assay was done in 0.1 M sodium acetate buffer at pH 4.4. The oxidation product, the green-colored cationic radical ($ABTS^{\bullet+}$), was measured spectrophotometrically at 420 nm (ε = 36 000 M^{-1} cm^{-1}). One unit of laccase activity was defined as the amount of laccase that oxidized one µmol of ABTS per minute at 25 ºC.

To determine the stability of CotA at different pH values, the buffer of the enzyme solution was exchanged with buffers of pH 7.6, 9.0, and 10.8 at 4 ºC. The enzyme solutions were incubated at the three-pH values room temperature and sampled every five minutes up to a total of 1 h. The samples were assayed using the standard assay. Next to the activity measurements, we also performed Circular Dichroism (CD) spectroscopy at the three pH values, after incubation for one hour, to determine any secondary structure changes of CotA. CD experiments were performed on a JASCO J-715 spectropolarimeter with a Jasco PTC 348 WI temperature controller. The far-UV CD spectra were recorded from 200 to 260 nm at 25 ºC. The sample was a load to quartz cuvette with an optical path length of 1 mm. Twenty spectra, each recorded with a resolution of 1 nm and a scan speed of 50 nm/ min were accumulated and averaged.

2.2.4. Preparation of protein-containing C3Ms

Enzyme and polymer solutions containing 10 mM sodium carbonate buffer were prepared, with a final pH of 10.8. All of the solutions were filtered using a 0.2 μm poly(ether-sulfone) membrane syringe filters (Advanced Microdevices Pvt. Ltd.). The PMC of the two-component C3Ms was determined by mixing a constant concentration of CotA with different concentrations of PM2PV-*b*-PEO. DLS measurements were performed to determine at which charge composition optimal micelle formation took place.

The amino acid sequence of CotA and the pH value of the buffer determines to a great extent the net charge of the enzyme. The pH-charge profile can be calculated from the protein's three-dimensional structure using the PROPKA 3.1 software package.[3,34] Using this approach, we determined a net charge for CotA of about −41 at pH 10.8 (Figure S2.3., Supplementary information). PM2PV-*b*-PEO has a pH-independent charge of about +90. To form three-component micelles, the homopolymer PSS, which has a charge of about −188, was added to CotA solutions with a charge concentration two, four, or six times higher than that of CotA. To find the PMC for each of these cases, different concentrations of PM2PV-*b*-PEO were added to the CotA-PSS mixtures and, using DLS, the charge composition at which optimal micelle formation took place was determined. The order of mixing for creating three-component C3Ms does not affect micelle formation to a great extent (Figure S2.4 and S2.5., Supplementary information).

Two- and three-component C3M solutions were prepared at their PMCs and stored at room temperature overnight before measurements. To monitor the salt stability of the C3Ms, a 4 M solution of NaCl was titrated to enzyme-containing micelles at their PMCs and observed by both DLS and FCS.

2.2.5. Dynamic light scattering (DLS)

Dynamic light scattering (DLS) was performed with an ALV instrument equipped with a DPSS laser operating at 660 nm. All measurements to determine the preferred micellar composition (PMC), hydrodynamic radius, and polydispersity index (PDI) were performed at a scattering angle of 90º. Multi-angle DLS was performed to determine the shape of the protein-containing C3Ms. The laser power used was 100 mW. The hydrodynamic radius R_h was calculated from the diffusion coefficient D,[35] obtained from the autocorrelation function by cumulants analysis, and using the Stoke-Einstein equation, assuming spherical particles:

$$D = \frac{k_B T}{6\pi\eta R_h} \tag{2.1}$$

where k_B is the Boltzmann constant, T is the absolute temperature, and η is the viscosity of the solution.

2.2.6. Fluorescence correlation spectroscopy (FCS)

Fluorescence correlation spectroscopy (FCS) was performed using a Leica TCS SP8 X system equipped with a 63× 1.20 NA water immersion objective and a supercontinuum laser. CotA labeled with Alexa Fluor 488 was excited by selecting the 488 nm laser line with a pulse frequency of 40 MHz. Fluorescence was collected through a size-adjustable pinhole, set at 1 Airy unit, and filtered using a 495−525 nm spectral filter using a hybrid detector coupled to a PicoHard 300 TCSPC module (PicoQuant). FCS data were analyzed with software FFS data processor version 2.3 (Scientific Software Technologies Software Centre, Belarus), using a two-component 3D diffusion model including triplet state.[36,37] Rhodamine 110, which has a diffusion coefficient of 4.3 x 10^{-10} m^2s^{-1}, was used to determine the confocal structure parameter ($a = \omega_z/\omega_{xy}$ with ω_{xy} and ω_z the equatorial and axial radii of the detection volume, respectively).

In FCS, fluorescent particles move in and out of the confocal volume, causing intensity fluctuations. These intensity fluctuations can be correlated with an autocorrelation function as follows:

$$G(t) = \frac{\langle I\rangle^2 + \langle \Delta I\,(t)\;\Delta I\,(t+\tau)\rangle}{\langle I\rangle^2} \tag{2.2}$$

where $G(t)$ is the normalized fluorescence fluctuation autocorrelation function, I is the fluorescence intensity, and $\Delta I(t)$ is the deviation of the average signal intensity at time t.

After excitation, intersystem crossing may occur, i.e., the transition of a fluorophore from the singlet state to the triplet state. Relaxation from the triplet state to the ground state can occur without emission of photons, and as a result, the fluorophore appears to be dark for a short interval. For autocorrelation analysis, this phenomenon needs to be considered because intersystem crossing to the triplet state may lead to an additional shoulder on the microsecond time scale.[37] For autocorrelation analysis, including the triplet state, the following equation applies:

$$G(t) = 1 + \frac{1}{\langle N\rangle} \cdot \left(1 + \frac{F_{trip}}{1-F_{trip}}\right) e^{-t/\,T_{trip}} \cdot \sum_{i=1}^{n} \frac{F_i}{\left(1+\frac{t}{\tau_{dif,i}}\right) \cdot \sqrt{1 + \left(\frac{\omega_{xy}}{\omega_z}\right)^2 \cdot \frac{t}{\tau_{dif,i}}}} \tag{2.3}$$

where $\langle N\rangle$ is the average number of fluorescent particles in the confocal volume, F_{trip} is the fraction of molecules in the triplet state, T_{trip} is the average time a fluorophore resides in the

triplet state, F_i is the fraction of species i, and τ_{dif} is the diffusion time of the fluorophore in the confocal volume. From the diffusion time, the diffusion coefficient D can be calculated using this equation:

$$D = \frac{\omega_{xy}^2}{4\tau_{dif}} \quad (2.4)$$

2.2.7. Activity and secondary structure of encapsulated enzyme

The activity of CotA-containing C3Ms was measured by using the ABTS assay, and the protein secondary structure was determined using far-UV CD as described above. During measurements, the temperature was kept to 25 ºC. For each sample, the far-UV CD spectrum was recorded between 200 and 260 nm.

2.3. Results and discussion

2.3.1. pH stability of CotA: enzyme activity and secondary structure

To encapsulate CotA in C3Ms using a positively charged diblock copolymer, a high pH of 10.8 was chosen to establish a sufficient negative charge on the enzyme and to eliminate the effect of the positively charged patch on its surface.

The activity of CotA as a function of incubation time at different pH values is presented in Figure 2.2. It shows that CotA laccase activity does not depend on the time of incubation and is an alkali-resistant enzyme. As described in the introduction, the active site of CotA involves Cu ions; incubation of the enzyme at high pH results in an increase of the redox potential of CotA, where the T1 Cu in the enzyme will have a higher tendency to gain electrons from the substrate, speeding up the catalytic cycle.[38,39,40]

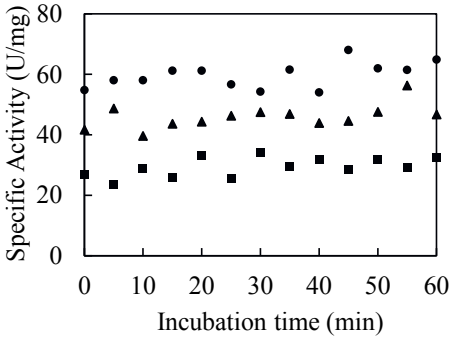

Figure 2.2. Specific activity of CotA measured at pH 4.4 after incubation of enzyme at different pH values (●, pH 10.8; ▲,pH 9.0; and ■, pH 7.6) as a function of incubation time at 25 ºC .

The CD spectra presented in Figure 2.3 show that the secondary structure of CotA laccase is not significantly affected by incubation at high pH: the functional conformation of the enzyme is maintained despite of the deprotonation of amino acid residues at alkaline pH.

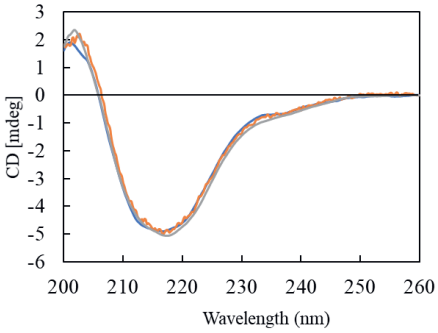

Figure 2.3. CD spectra of CotA measured after incubation for 1 hour at different pH values measured at the pH of incubation (at pH 10.8 (orange), pH 9.0 (grey), and pH 7.6 (blue)).

2.3.2. Complex coacervate core micelles: two-component micelles

Two-component complex coacervates core micelles were obtained by mixing CotA with $PM2PV_{128}$-*b*-PEO_{477}. At neutral pH, CotA has a highly positive patch on its surface due to ten lysines and five arginines that are located at the interface between domains 1, 2, and 3,[25,27] while the net charge of the CotA molecules is negative (–10). Adding the diblock copolymer PM2PV-*b*-PEO to the protein solution at neutral pH led to the formation of heterogeneous large aggregates and precipitation (data not shown). For the formation of C3Ms it is therefore essential to decrease the protein's charge anisotropy by neutralization of the lysine residues in the protein by increasing the pH.[15]

At pH 10.8 the formation of C3Ms consisting of CotA and PM2PV-*b*-PEO was successful. At this pH, the net charge on the protein amounts to –41. The charge composition of the system can be described by partition coefficient F^- according to the equation:

$$F^- = \frac{n^-}{n^- + n^+} \tag{2.5}$$

where $n^- = c^- N^-$ and $n^+ = c^+ N^+$, i.e., the total concentration of negative charges and the total concentration of positive charges on the two types of macromolecules, respectively, with c their molar concentrations and N the number of charged groups per molecule.

To determine the preferred micellar composition (PMC) usually a solution with a constant amount of polyelectrolyte or charged biomolecule is mixed with increasing amounts of diblock copolymer. At the PMC, the concentration of micelles reaches a maximum and using DLS this can be detected as a maximum in light scattering intensity.[10] When F^- is far from the PMC, the interaction between polyelectrolyte (biomolecule) and oppositely charged diblock would only produce a limited number of small soluble complexes resulting in low light scattering intensities.[3,10]

DLS measurements on solutions with varying charge compositions (mixing ratios) show the highest intensity at $F^- = 0.5$ (Figure 2.4A), implying that the PMC corresponds to equal concentrations of positive and negative charges on the diblock and the protein. At the PMC, the scattering objects have a hydrodynamic radius of 34.0 ± 0.8 nm (Figure 2.4B). At the PMC, a minimum in the polydispersity index (PDI) is found (Figure 2.4C), indicating a narrow size distribution of the formed micelles.

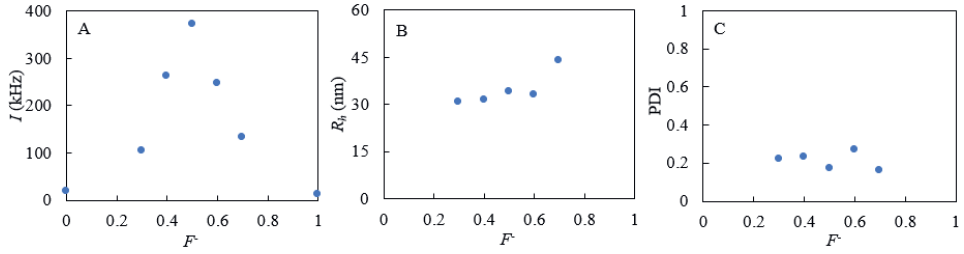

Figure 2.4. DLS results for mixtures of CotA and PM2PV$_{128}$-*b*-PEO$_{477}$ as a function of charge composition F^-. (A) Scattering intensity (I), (B) hydrodynamic radius (R_h), and (C) polydispersity index (PDI).

The shape of the micelles can be determined using multi-angle DLS. At each detection angle, the decay rate Γ of the DLS correlation function is determined by means of cumulant fits. From Figure 2.5 it can be seen that Γ fitted with the first, second, and third cumulant as a function of the squared wave vector (q^2) gives three overlapping straight lines, showing that the C3Ms are spherical and monodisperse.[41] The slope of the lines equals the diffusion coefficient.

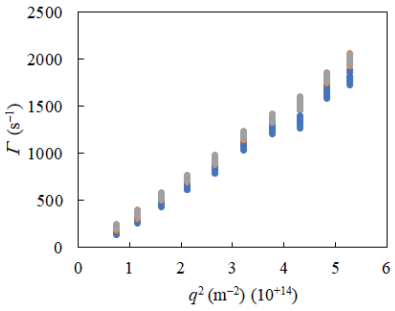

Figure 2.5. Multi-angle DLS results for two-component enzyme-containing C3Ms. Decay rate $\Gamma(q)$ obtained from the DLS correlation curves by a first (blue), second (orange), and third (grey) cumulant fit.

Activity measurements were performed for samples with various mixing ratios of CotA and diblock copolymer, where $F^- = 0$ is only polymer, and $F^- = 1$ is only enzyme. Except for $F^- = 0$, all samples had the same enzyme concentration. The activity of CotA was found to be constant (Figure 2.6) and similar to the activity of free enzyme incubated at pH 10.8 (Figure 2.2). It should be noted that the mixed samples were prepared at pH 10.8, but the ABTS test was carried out at the pH 4.4. At this lower pH, CotA will be released from the micelles and then oxidize the substrate ABTS. Packing and subsequent release from the C3Ms apparently did not affect the activity of the enzyme significantly. The CD results (Figure 2.7) confirmed that the secondary structure of the enzyme was maintained when the enzyme was encapsulated in C3Ms.

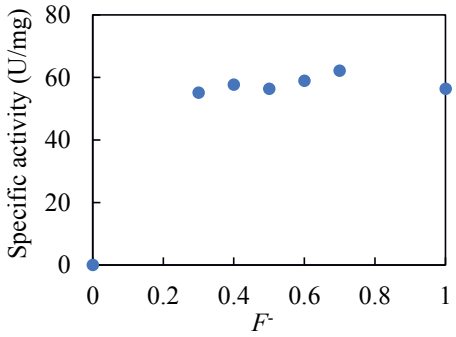

Figure 2.6. Specific activity of CotA measured after being encapsulated in different charge ratios with diblock copolymer.

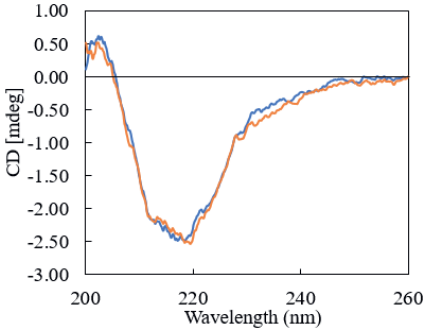

Figure 2.7. CD spectra of two component enzyme-containing C3Ms (orange lines) and the free enzyme (blue lines).

2.3.3. Complex coacervate core micelles: three-component micelles

To obtain three-component micelles, the negatively charged homopolymer PSS_{215} was added to mixtures of CotA and $PM2PV_{128}$-*b*-PEO_{477} with a charge concentration two, four or six times higher than that of CotA. DLS measurements showed that for all PSS/ CotA charge concentration ratios, a maximum in light scattering intensity was observed at an overall charge composition of $F^- = 0.6$ (Figure 2.8A), indicating that micelles are mostly formed at this mixing composition. The deviation of the PMC from 0.5 suggests that micelle formation is not only due to electrostatic interactions and counterion release, but that other interactions also play a role, most probably hydrophobic interactions. CotA has several hydrophobic residues at its surface with different levels of exposure. The polyelectrolytes used in this study also have hydrophobic parts, i.e., the vinyl backbone of PM2PV-*b*-PEO and the styrene group of PSS, and these could be involved in protein-polyelectrolyte interactions.[15] It seems that hydrophobic interactions are more important in the three-component micelles than in the two-component ones (PMC at $F^- = 0.5$).

At the PMC of the three-component C3Ms, the lowest PDI was found compared to other mixing ratios (Figure 2.8C). The hydrodynamic radii of the three-component micelles are about 26.6 ± 0.5 nm, 24.2 ± 0.2 nm, and 23.6 ± 0.5 nm for two, four, six times higher of charge concentration to CotA, respectively (Figure 2.8B). This is smaller than the size of two-component C3Ms, which suggests that the amount of encapsulated enzyme molecules per micelle is less in the three-component C3Ms. As shown in Figure 2.9, multi-angle DLS results indicate that three-component C3Ms also have a spherical shape and are fairly monodisperse, similar to the two-component C3Ms.

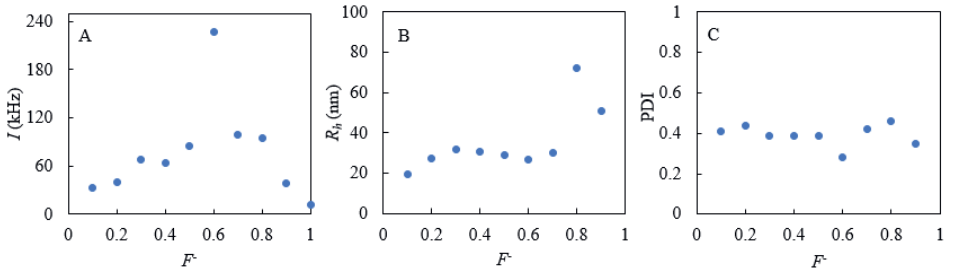

Figure 2.8. DLS results for three-component C3Ms (with a PSS/ CotA charge ratio of 2:1) as function of charge composition F^-. (A) Scattering intensity (I), (B) hydrodynamic radius (R_h) and (C) polydispersity index (PDI).

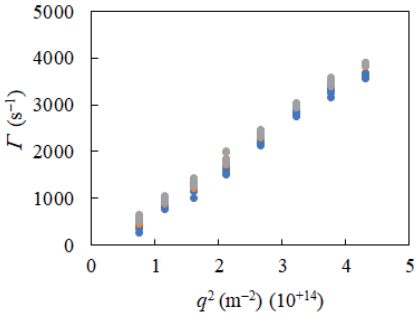

Figure 2.9. Multi-angle DLS results for three-component C3Ms with a PSS/ CotA charge ratio of 2. Decay rate $\Gamma(q)$ obtained from the DLS correlation curves by a first (blue), second (orange), and third (grey) cumulant fit. Similar trend lines were also observed for the PSS/ CotA charge ratio of 4 and 6.

2.3.4. FCS analysis of two- and three component C3Ms

Native CotA is not fluorescent in the visible spectrum, therefore the CotA S313C variant was used for labeling with the fluorescent dye Alexa Fluor 488 via a maleimide reaction and after purification (Figure S2.2, Supplementary information), applied in FCS experiments.[42]

The two- and three-component C3Ms were prepared using labeled CotA at their PMCs obtained from the DLS measurements. FCS analysis allows to discriminate between CotA free in solution (small particles) and incorporated into micelles (large particles) based on their different diffusion times. In addition, the enzyme-containing C3Ms are much brighter than the free enzyme molecules. The fluorescence intensity of the C3Ms is expected to be proportional to the number of encapsulated proteins.

The normalized autocorrelation curves in Figure 2.10 show a faster decay, and thus a larger diffusion coefficient for the solution that contained only fluorescently labeled CotA than for the mixture of CotA and the diblock copolymer. In addition, the number of fluorescent particles detected in the confocal volume (N) was much higher for the solution without the diblock copolymer (87 versus 3 particles, data not shown), with a much lower fluorescence intensity. These results confirm the encapsulation of labeled CotA in C3Ms upon mixing with PM2PV-*b*-PEO and show that a large amount of CotA can be entrapped in the core of the two-component C3Ms.

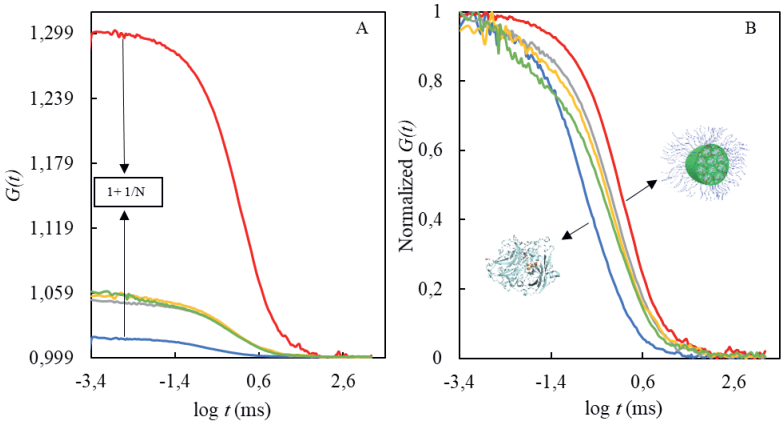

Figure 2.10. Autocorrelation curves obtained with FCS. (A) Not normalized $G(t)$. (B) Normalized $G(t)$. Blue curves represent free labeled CotA, and red curves represent the two-component C3Ms. Grey, yellow, and green curves represent the three-component C3Ms made using two, four, and six-fold charge excess of PSS over CotA, respectively. The total CotA concentration was identical in all samples.

The three-component systems also show a decrease in diffusion coefficients compared to the free CotA, while N decreased from 87 to 20, 19, and 30 for PSS charge concentrations of two, four, and six times that of CotA, respectively. The amplitude of the autocorrelation curve of the particles in the three-component systems is in between the amplitude of the free labeled CotA and that of the two-component C3Ms. These results show that CotA is also encapsulated in the three-component C3Ms, with a lower amount of encapsulated enzyme molecules per micelle than in the two-component system.

Further analysis of the FCS results revealed that free labeled CotA has R_h of about 2.4 ± 0.2 nm. In the two-component system, about 84 % of the enzyme was present in micelles with an R_h of about 38 nm. The three-component C3Ms appeared smaller, having a size of about 24

nm, and here about 80 % of the CotA is encapsulated in the core of micelles. Apparently, there is no significant difference in encapsulation efficiency among the three-component micelles made with different charge ratios of CotA and PSS. This is probably because for the samples with different CotA/ PSS ratios, the total CotA concentration was kept constant, while the concentration of the diblock copolymer PM2PV-*b*-PEO was increased with the concentration of PSS to keep F^- at –0.6 (the PMC). As a result, more micelles are formed but with a lower amount of CotA per micelle. The hydrodynamic radii found with FCS are similar to those obtained with DLS.

2.3.5. Stability of two- and three component C3Ms against salt

FCS can provide information on the fractions of CotA encapsulated in C3Ms and free in solution, data which is not provided by DLS. We used both techniques to monitor the change in stability of the enzyme-containing C3Ms upon the addition of salt (NaCl). From the DLS results in Figure 2.11 it can be seen that by stepwise adding salt to the two-component C3M system, the scattering intensity as well as the R_h of the micelles gradually decreases. These phenomena occur because upon increasing the salt concentration, the electrostatic interactions become weaker and the entropy gain from counter ion release becomes smaller, leading to a lower stability constant for C3M formation.[43] As a result, the micelles start to disintegrate.[44–50]

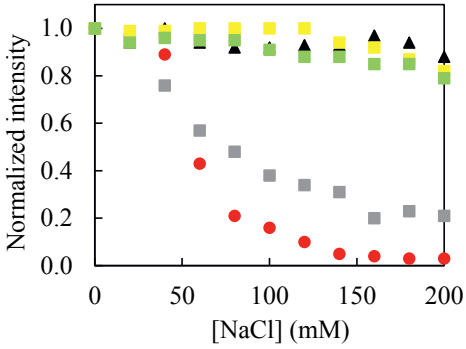

Figure 2.11. Normalized DLS scattering intensity for salt titration (NaCl) of C3M solutions. Circles (red) represent the two-component C3MS of CotA and diblock copolymer. Triangles (black) represent micelles formed only by homopolymer and diblock copolymer. Squares represent three-component C3Ms made with 2 (grey), 4 (yellow), and 6 (green) -time charge excess of PSS over CotA.

The DLS data clearly shows that addition of homopolymer improved the salt stability of the protein-containing C3Ms. The more PSS is present in the system, the more resistant it is

towards salt addition. We found that in the limiting case of an infinite ratio PSS/ CotA, i.e., for micelles consisting of only homopolymer PSS and diblock copolymer PM2VP-*b*-PEO, the system was still stable at 1 M NaCl (data not shown). This is in line with the observation of Van der Gucht et al. that for mixtures of the polyelectrolytes $PM2VP_{88}$ and PSS_{165} the critical salt concentration, i.e., the salt concentration above which no coacervate phase is formed, amounts to about 2 M (KCl).[6] We assume the limit of the salt stability of the C3Ms with increasing the PSS content is also well above 1.5 M salt.

DLS data cannot provide changes in the number of CotA encapsulated in C3Ms upon increasing the ionic strength. Therefore, we used FCS as a read-out as this technique allows for distinguishing between the fraction of free enzyme (fraction 1) and the fraction of enzyme encapsulated in C3Ms in the confocal volume (fraction 2). By adding salt, fraction 2 decreased, corresponding to an increase in fraction 1. As shown in Figure 2.12, the total number of fluorescent particles detected in the confocal volume (*N*) also increased upon stepwise addition of salt, indicating the release of CotA as well. These results clearly show that CotA was released from the three-component C3Ms at a significantly lower salt concentration and over a narrower salt concentration range than from the two-component C3Ms. Evidently, the presence of PSS caused CotA to be expelled from the micelles upon addition of salt, even though the DLS results showed that the micelles become more salt resistant with the presence of PSS. Therefore, addition of homopolymer with the same charge sign as the enzyme is not an appropriate strategy for improving the stability of enzyme-containing C3Ms in high salt environment.

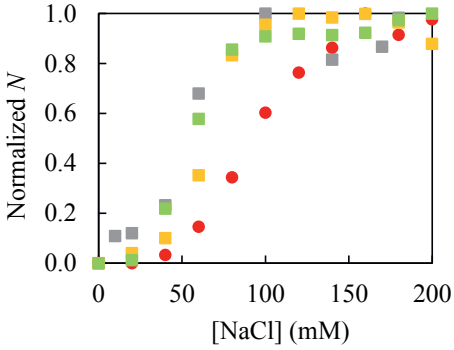

Figure 2.12. FCS analysis for salt titration of two-component and three-component C3Ms: normalized number of particles *N* in the confocal volume. Circles (red) represent the two-component C3MS of CotA and diblock copolymer. Squares represent three-component C3Ms made with 2 (grey), 4 (yellow), and 6 (green) -time charge excess of PSS over CotA.

An explanation for the FCS results is that the attraction between PM2PV-*b*-PEO and PSS is stronger than between PM2PV-*b*-PEO and CotA, because PSS has a much higher charge density than CotA. Therefore, the homopolymer is preferably taken up in the micelles, and only a relatively small amount of negatively charged CotA contributes to the stoichiometry. When salt is added to the micellar solution, the electrostatic interactions decrease and especially the attraction between protein and diblock copolymer becomes very weak. Moreover, the enzyme is a bulky molecule with only a few charges and by adding small ions it becomes entropically no longer favorable to incorporate the enzyme in the C3Ms.[45] As a result, the enzyme is expelled from the complex coacervate core and replaced by homopolymer.[46]

Adding salt to C3Ms solutions also affects the micellar dynamics. With increasing ionic strength, intermolecular exchange processes will be faster, as well as rearrangements in the micellar core.[3,51] This facilitates the replacement of CotA by PSS.

2.4. Conclusions

Using DLS and FCS, we showed that at high pH (10.8) the enzyme CotA can be encapsulated with the diblock copolymer PM2PV-*b*-PEO into complex coacervate core micelles. At neutral pH micelle formation does not take place, most probably because of the low net negative charge of the enzyme and the presence of a positively charged patch on its surface. To improve the salt stability of the micelles the negatively charged homopolymer PSS was added to create three-component C3Ms. The three-component C3Ms are smaller (hydrodynamic radius 24 nm versus 32 nm for the two-component system) and FCS measurements showed that per micelle less CotA is encapsulated, although the fraction of enzyme that is encapsulated is still high (80 % versus 84 %). DLS measurements confirmed that the three-component C3Ms are indeed more salt resistant than the two-component C3Ms. However, FCS analysis revealed that CotA is expelled from the three-component C3Ms already at relatively low salt concentrations.

From our results it is clear that FCS experiments are vital to get insight into the composition and salt stability of the three-component C3Ms, since this technique enables to discriminate between free CotA and encapsulated CotA. From these analyses it can be concluded that adding homopolymer with the same charge sign as the protein is not a good strategy to improve the salt stability of protein-containing C3Ms. We suggest that it is important to increase the charge density of enzyme by bioconjugation technique then enzyme-containing C3Ms more salt resistant.

References

1. Agarwal, N. P., Matthies, M., Gür, F. N., Osada, K. and Schmidt, T. L. Block copolymer micellization as a protection strategy for dna origami. *Angew. Chemie - Int. Ed.* **56**, 5460–5464 (2017).
2. Itaka, K., Kanayama, N., Nishiyama, N., Jang, W.D., Yamasaki, Y., Nakamura, K., Kawaguchi, H., and Kataoka, K. Supramolecular nanocarrier of siRNA from PEG-based block catiomer carrying diamine side chain with distinctive pKa directed to enhance intracellular gene silencing. *J. Am. Chem. Soc.* **126**, 13612–13613 (2004).
3. Nolles, A., Westphal, A. H., de Hoop, J. A., Fokkink, R. G., Kleijn, J. M., van Berkel, W. J. H., and Borst, J. W. Encapsulation of GFP in complex coacervate core micelles. *Biomacromolecules* **16**, 1542–1549 (2015).
4. Mills, C. E., Obermeyer, A., Dong, X., Walker, J. and Olsen, B. D. Complex coacervate core micelles for the dispersion and stabilization of organophosphate hydrolase in organic solvents. *Langmuir* **32**, 13367–13376 (2016).
5. Nolles, A., Westphal, A. H., Kleijn, J. M., van Berkel, W. J. H. and Borst, J. W. Colorful packages: Encapsulation of fluorescent proteins in complex coacervate core micelles. *Int. J. Mol. Sci.* **18**, 1-19 (2017).
6. Gucht, J. van der, Spruijt, E., Lemmers, M. and Cohen Stuart, M. A. Polyelectrolyte complexes: Bulk phases and colloidal systems. *J. Colloid Interface Sci.* **361**, 407–422 (2011).
7. Voets, I. K., de Keizer, A. and Cohen Stuart, M. A. Complex coacervate core micelles. *Adv. Colloid Interface Sci.* **147**–**148**, 300–318 (2009).
8. Kaur, R. and Khullar, P. Block copolymer micelles as nanoreactors for the synthesis of gold nanoparticles. *Mater. Biomed. Eng. Inorg. Micro- Nanostructures* 177–210 (2019).
9. Bourouina, N., Cohen Stuart, M. A. and Mieke Kleijn, J. Complex coacervate core micelles as diffusional nanoprobes. *Soft Matter* **10**, 320–331 (2014).
10. van der Burgh, S., Fokkink, R., de Keizer, A., and Cohen Stuart, M.A. Complex coacervation core micelles as anti-fouling agents on silica and polystyrene surfaces. *Colloids Surfaces A Physicochem. Eng. Asp.* **242**, 167–174 (2004).
11. Mathot, F., Van Beijsterveldt, L., Préat, V., Brewster, M. and Ariën, A. Intestinal uptake and biodistribution of novel polymeric micelles after oral administration. *J. Control. Release* **111**, 47–55 (2006).
12. Sant, V. P., Smith, D. and Leroux, J. C. Enhancement of oral bioavailability of poorly water-soluble drugs by poly(ethylene glycol)-block-poly(alkyl acrylate-co-methacrylic acid) self-assemblies. *J. Control. Release* **104**, 289–300 (2005).
13. Kötz, J., Kosmella, S. and Beitz, T. Self-assembled polyelectrolyte systems. *Prog. Polym. Sci.* **26**, 1199–1232 (2001).
14. Hofs, B., Voets, I. K., De Keizer, A. and Cohen Stuart, M. A. Comparison of complex coacervate core micelles from two diblock copolymers or a single diblock copolymer with a polyelectrolyte. *Phys. Chem. Chem. Phys.* **8**, 4242–4251 (2006).
15. Cooper, C. L., Dubin, P. L., Kayitmazer, A. B. and Turksen, S. Polyelectrolyte-protein complexes. *Curr. Opin. Colloid Interface Sci.* **10**, 52–78 (2005).
16. Lindhoud, S., de Vries, R., Norde, W. and Stuart, M. A. C. Structure and stability of complex coacervate core micelles with lysozyme. *Biomacromolecules* **8**, 2219–2227 (2007).
17. Black, K. A., Priftis, D., Perry, S. L., Yip, J., Byun, W. Y., and Tirrell, M. Protein encapsulation via polypeptide complex coacervation. *ACS Macro Lett.* **3**, 1088–1091 (2014).
18. Blocher, W. C. and Perry, S. L. Complex coacervate-based materials for biomedicine. *Wiley Interdiscip. Rev. Nanomedicine Nanobiotechnology* **9**, 76–78 (2017).
19. Gapiński, J., Szymański, J., Wilk, A., Kohlbrecher, J., Patkowski, A., and Hołyst, R. Size and shape of micelles studied by means of SANS, PCS, and FCS. *Langmuir* **26**, 9304–9314 (2010).
20. Elson, E. L. Fluorescence correlation spectroscopy: Past, present, future. *Biophys. J.* **101**, 2855–2870 (2011).
21. Martins, L. O., Soares, C. M., Pereira, M. M., Teixeira, M., Costa, T., Jones, G. H., and Henriques, A. O. Molecular and biochemical characterization of a highly stable bacterial laccase that occurs as a structural component of the *Bacillus subtilis* endospore coat. *J. Biol. Chem.* **277**, 18849–18859 (2002).
22. Guzik, U., Hupert-Kocurek, K. and Wojcieszynska, D. Immobilization as a strategy for improving enzyme properties- Application to oxidoreductases. *Molecules* **19**, 8995–9018 (2014).
23. Shraddha, Shekher, R., Sehgal, S., Kamthania, M. and Kumar, A. Laccase: Microbial sources, production, purification, and potential biotechnological applications. *Enzyme Res.* **2011**, 1-11 (2011).
24. Fernandes, A. T., Lopes, C., Martins, L. O. and Melo, E. P. Unfolding pathway of CotA-laccase and the role of copper on the prevention of refolding through aggregation of the unfolded state. *Biochem. Biophys. Res. Commun.* **422**, 442–446 (2012).

25. Enguita, F. J., Martins, L. O., Henriques, A. O. and Carrondo, M. A. Crystal structure of a bacterial endospore coat component: A laccase with enhanced thermostability properties. *J. Biol. Chem.* **278**, 19416–19425 (2003).
26. Beneyton, T., Beyl, Y., Guschin, D. A., Griffiths, A. D., Taly, V., Schuhmann, W. The thermophilic CotA Laccase from *Bacillus subtilis*: Bioelectrocatalytic evaluation of O_2 reduction in the direct and mediated electron transfer regime. *Electroanalysis* **23**, 1781–1789 (2011).
27. Liu, Z., Xie, T., Zhong, Q. and Wang, G. Crystal structure of CotA laccase complexed with 2,2-azinobis-(3-ethylbenzothiazoline-6-sulfonate) at a novel binding site. *Acta Crystallogr. Sect. Struct. Biol. Commun.* **72**, 328–335 (2016).
28. Pich, A., Bhattacharya, S., Adler, H. J. P., Wage, T., Taubenberger, A., Li, Z., van Pee, K. H., Böhmer, U., and Bley, T. Composite magnetic particles as carriers for laccase from *Trametes versicolor*. *Macromol. Biosci.* **6**, 301–310 (2006).
29. Bryjak, J., Kruczkiewicz, P., Reku, A. and Peczy, W. Laccase immobilization on copolymer of butyl acrylate and ethylene glycol dimethacrylate. **35**, 325–332 (2007).
30. Christopher, L. P., Yao, B. and Ji, Y. Lignin biodegradation with laccase-mediator systems. *Front. Energy Res.* **2**, 1–13 (2014).
31. Lindhoud, S., Norde, W. and Cohen Stuart, M. A. Effects of polyelectrolyte complex micelles and their components on the enzymatic activity of lipase. *Langmuir* **26**, 9802–9808 (2010).
32. Fulmer, G. R., Miller, A. J. M., Sherden, N. H., Gottlieb, H. E., Nudelman, A., Stoltz, B. M., Bercaw, J. E., and Goldberg, K. I. NMR chemical shifts of trace impurities: Common laboratory solvents, organics, and gases in deuterated solvents relevant to the organometallic chemist. *Organometallics* **29**, 2176–2179 (2010).
33. Durão, P., Chen, Z., Fernandes, A. T., Hildebrandt, P., Murgida, D. H., Todorovic, S., Pereira, M. M., Melo, E. P., Martins, L. O. Copper incorporation into recombinant CotA laccase from *Bacillus subtilis*: Characterization of fully copper loaded enzymes. *J. Biol. Inorg. Chem.* **13**, 183–193 (2008).
34. Rostkowski, M., Olsson, M. H., Søndergaard, C. R. and Jensen, J. H. Graphical analysis of pH-dependent properties of proteins predicted using PROPKA. *BMC Struct. Biol.* **11**, 1-6 (2011).
35. Stetefeld, J., McKenna, S. A. and Patel, T. R. Dynamic light scattering: a practical guide and applications in biomedical sciences. *Biophys. Rev.* **8**, 409–427 (2016).
36. Skakun, V. V, Engel, R., Digris, A. V, Borst, J. W. and Visser, A. J. W. G. Global analysis of autocorrelation functions and photon counting distributions. *Front. Biosci., Elite Ed.*, **2**, 489− 505 (2011).
37. Skakun, V. V., Hink, M. A., Digris, A. V., Engel, R., Novikov, E. G., Apanasovich, V. V., and Visser, A. J. W. G. Global analysis of fluorescence fluctuation data. *Eur. Biophys. J.* **34**, 323-334 (2005).
38. Singh, G., Bhalla, A., Kaur, P., Capalash, N. and Sharma, P. Laccase from prokaryotes: A new source for an old enzyme. *Rev. Environ. Sci. Biotechnol.* **10**, 309–326 (2011).
39. Solomon, E. I., Chen, P., Metz, M., Lee, S. K. and Palmer, A. E. Oxygen binding, activation, and reduction to water by copper proteins. *Angew. Chemie - Int. Ed.* **40**, 4570–4590 (2001).
40. Solomon, E. I., Augustine, A. J. and Yoon, J. O_2 Reduction to H_2O by the multicopper oxidases. *Dalt. Trans.* **9226**, 3921–3932 (2008).
41. Harada, A. and Kataoka, K. Novel polyion complex micelles entrapping enzyme molecules in the core. 2. Characterization of the micelles prepared at nonstoichiometric mixing ratios. *Langmuir* **15**, 4208–4212 (1999).
42. Toseland, C. P. Fluorescent labeling and modification of proteins. *J. Chem. Biol.* **6**, 85–95 (2013).
43. Spruijt, E., Westphal, A. H., Borst, J. W., Cohen Stuart, M. A. and Van der Gucht, J. Binodal compositions of polyelectrolyte complexes. *Macromolecules* **43**, 6476–6484 (2010).
44. Van der Kooij, H. M., Spruijt, E., Voets, I. K., Fokkink, R., Cohen Stuart, M. A., and van der Gucht, J. On the stability and morphology of complex coacervate core micelles: From spherical to wormlike micelles. *Langmuir* **28**, 14180–14191 (2012).
45. Lindhoud, S. and Claessens, M. M. A. E. Accumulation of small protein molecules in a macroscopic complex coacervate. *Soft Matter* **12**, 408–413 (2015).
46. Obermeyer, A. C., Mills, C. E., Dong, X. H., Flores, R. J. and Olsen, B. D. Complex coacervation of supercharged proteins with polyelectrolytes. *Soft Matter* **12**, 3570–3581 (2016).
47. Lindhoud, S., Voorhaar, L., de Vries, R., Schweins, R., Cohen Stuart, M. A., and Norde, W. Salt-induced disintegration of lysozyme-containing polyelectrolyte complex micelles. *Langmuir* **25**, 11425–11430 (2009).
48. Wang, J., de Keizer, A., Fokkink, R., Yan, Y., Cohen Stuart, M. A., and van der Gucht, J. Complex coacervate core micelles from iron-based coordination polymers. *J. Phys. Chem. B* **114**, 8313–8319 (2010).
49. Yan, Y., De Keizer, A., Cohen Stuart, M. A., Drechsler, M. and Besseling, N. A. M. Stability of complex coacervate core micelles containing metal coordination polymer. *J. Phys. Chem. B* **112**, 10908–10914

(2008).
50. Lindhoud, S., De Vries, R., Schweins, R., Cohen Stuart, M. A. and Norde, W. Salt-induced release of lipase from polyelectrolyte complex micelles. *Soft Matter* **5**, 242–250 (2009).
51. Nolles, A., Hooiveld, E., Westphal, A. H., van Berkel, W. J. H., Kleijn, J. M., and Borst, J. W. FRET reveals the formation and exchange dynamics of protein-containing complex coacervate core micelles. *Langmuir* **34**, 12083–12092 (2018).

Supplementary information

S2.1. ^{1}H NMR of quaternized diblock copolymer

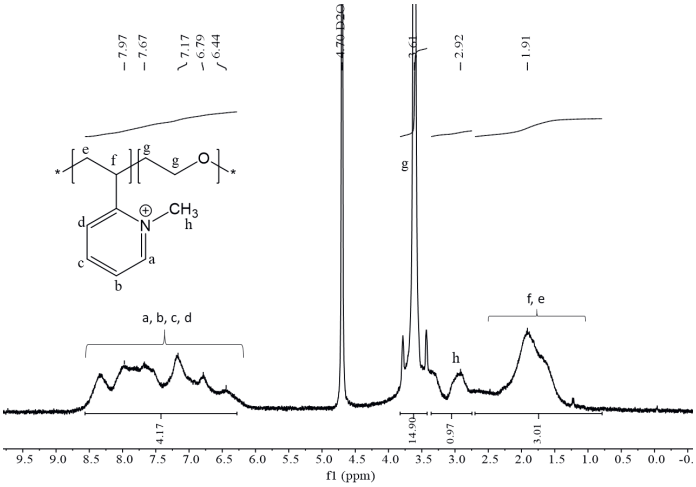

Figure S2.1. ^{1}H-NMR of PM2PV$_{128}$-*b*-PEO$_{477}$. Quaternization degree was measured by compared the integral of pyridine ring with the methyl group. The spectrum was recorded in D_2O.

S2.2. SDS-PAGE analysis

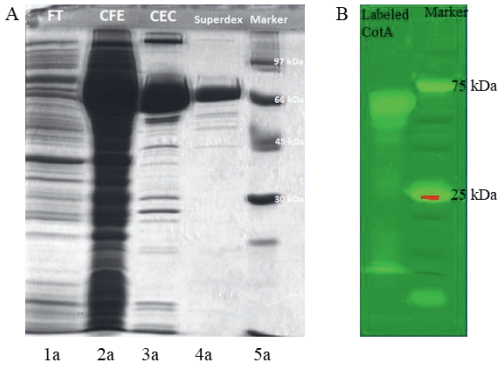

Figure S2.2. SDS-PAGE analysis for CotA laccase. (A) Holo CotA wild. 1a: flow through (FT), 2a: cell free extract (CFE), 3a: pooled from cation exchange exchanger (CEC), 4a: pooled from gel filtration column (Superdex), 5a: marker. (B) Apo CotA labeled Alexa Fluor 488 C5 maleimide.

S2.3. Charges of CotA

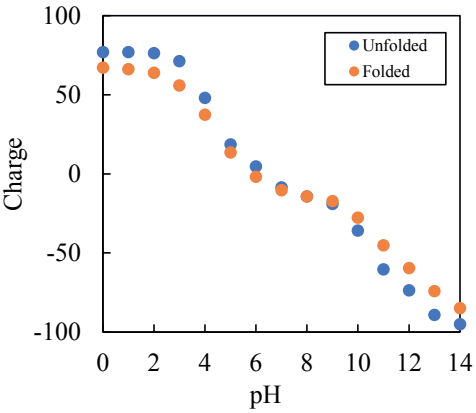

Figure S2.3. Charge of CotA as a function of pH calculated by using the PROPKA 3.1 software package.

S2.4. Effect of changing the mixing order for three-component C3Ms preparation

Effect of changing the mixing order for three-component C3Ms preparation are listed in Figure S2.4 and Figure S2.5.

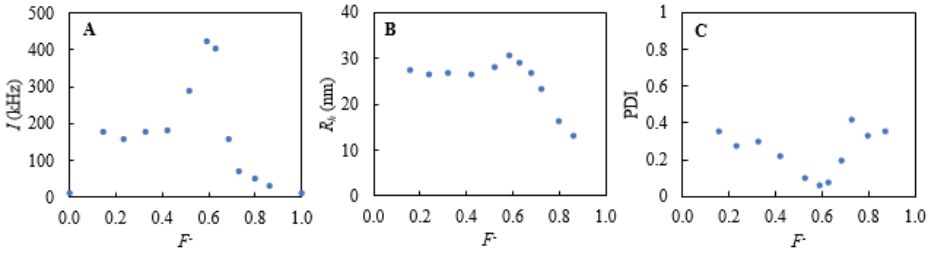

Figure S2.4. DLS results for the formation of three-component C3Ms (with a PSS/ CotA charge ratio of 2:1) as function of charge composition F^-. The three components were mixed in a different order than in the main text: first enzyme and diblock copolymer, and then PSS. (A) Scattering intensity (I), (B) hydrodynamic radius (R_h) and (C) polydispersity index (PDI). Laser power 150 mWatts.

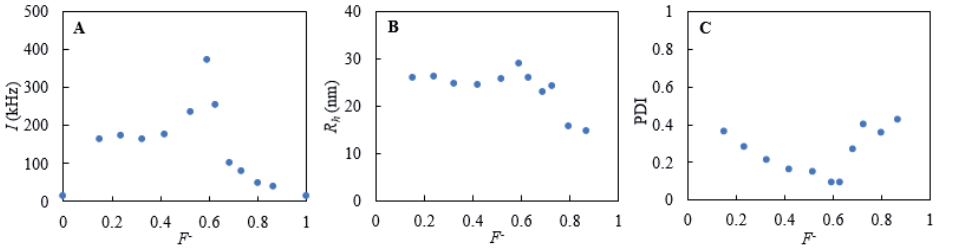

Figure S2.5. DLS results for three-component C3Ms formation (with a PSS/ CotA charge ratio of 2:1) as function of charge composition F^-. The three components were mixed as follows: PSS, diblock copolymer, and then enzyme. (A) Scattering intensity (I), (B) hydrodynamic radius (R_h) and (C) polydispersity index (PDI). Laser power 150 mWatts.

Chapter 3 :

Enzyme-polymer bioconjugation increases the salt stability of enzyme-containing complex coacervate micelles

Abstract

Enzyme-containing complex coacervate core micelles (C3Ms) are generated by mixing an aqueous charged enzyme solution with an oppositely charged-neutral hydrophilic diblock copolymer solution. The preparation of enzyme-containing C3Ms is simple and it can be used to protect enzymes against a detrimental environment and for controlled delivery. However, due to the low charge density of enzymes, enzyme-containing micelles are easily disintegrated already at moderate salt conditions. In this study, we aimed to improve the salt stability of enzyme-containing C3Ms by bioconjugation of the enzyme with a charged homopolymer. We used 1-ethyl-3-(3'-dimethylaminopropyl)carbodiimide hydrochloride (EDC) and *N*-hydroxysuccinimide (NHS) to covalently bind the enzyme CotA laccase to poly(acrylic acid) (PAA). The increase in negative charge on the enzyme after bioconjugation was determined by native agarose gel electrophoresis, SDS-PAGE, and zeta potential measurements. Circular dichroism and activity measurements showed that the structure and activity of CotA were preserved after bioconjugation; it even improved the heat resistance of the enzyme. Diblock copolymer poly(*N*-methyl-2-vinyl-pyridinium)$_{128}$-*block*-poly(ethylene oxide)$_{477}$ (PM2VP$_{128}$-*b*-PEO$_{477}$) was added to the enzyme solutions to form C3Ms. The characteristics of the enzyme-containing C3Ms and their salt stability were determined using dynamic light scattering (DLS) and fluorescence correlation spectroscopy (FCS). It was found that the micelles formed with the bioconjugated enzymes are smaller than the native CotA micelles, but their concentration is higher. Bioconjugation of the enzyme with PAA improves the stability of the enzyme-containing C3Ms against the addition of NaCl, shown by both FCS and DLS. Therefore, coupling enzymes with homopolymers of the same charge sign as the enzyme effectively improves the salt stability of enzyme-containing C3Ms.

3.1. Introduction

Protein encapsulation is important for many applications such as protein drug delivery, environmental remediation, and biocatalysis, and is used in, e.g., personal and skincare products.[1–4] Previous studies have shown that proteins can be easily encapsulated into complex coacervate core micelles (C3Ms).[5–7] These protein-containing C3Ms are soluble in an aqueous solution and have high loading efficiencies.[5,8–10] Protein-containing C3Ms are formed by mixing an aqueous solution of a charged protein and an oppositely charged-neutral hydrophilic diblock copolymer. The formation of C3Ms is driven by electrostatic attraction between the charged block of the polymer and the protein, which together form an electroneutral complex coacervate core, and by the accompanying entropy gain due to the release of counter ions. This coacervate core is surrounded by a corona formed by the neutral hydrophilic blocks of the polymers, preventing macroscopic phase separation of the coacervate and aggregation of the micelles by steric repulsion.[11–14] Protein incorporated in the core of C3Ms is protected from a harmful environment or proteases. In addition, C3Ms can be applied to control and target protein release.

One of the most significant challenges in the application of C3Ms to encapsulate proteins is to avoid disintegration of the micelles at higher salt concentrations (salt-induced disintegration). Even at moderate salt concentrations (in the order of 50-100 mM), protein-containing C3Ms appear not stable.[7,10,13] When the micelles unintentionally disintegrate, the protein will be released and is no longer protected. Improved salt-resistant enzyme-containing C3Ms can be obtained by adding a homopolymer with the same charge sign as the protein to form three-component C3Ms.[10,15] However, in a previous study,[7] we found that in assembling a three-component system, the enzymes were expelled from the micelles when salt was added, already at much lower salt concentrations than at which the micelles actually disintegrated.[7] The cause for this phenomenon is that the charged homopolymer competes with the enzyme, and when salt is added, the attraction between the protein and diblock copolymer becomes weaker. Moreover, due to the low charge density of the enzyme, with the addition of small ions, it is entropically no longer favorable to incorporate the enzyme in the core of the micelles.

Protein-containing C3Ms could be stabilized by increasing the protein net charge. This could be achieved through post-translational chemical modifications or genetic engineering.[16–22] With genetic engineering, high charged recombinant proteins can be produced in high yield and precise composition.[16,23,24] Alternatively, a homopolymer with the same charge sign as the

protein can be easily covalently coupled to protein to increase the charge. This will improve the salt stability of the C3Ms and keep the enzyme in the core of the micelles.

One method to couple biomolecules such as proteins with polyelectrolytes is bioconjugation.[16,25–32] Protein bioconjugation is usually performed by reacting to nucleophilic amino acids, such as lysine or cysteine.[16,33–36] Of these two, lysine is the most used amino acid residue for bioconjugation because proteins generally have many lysine side chains exposed on the proteins' surface, while the side chain of cysteine residues are usually buried in the protein structure. Thus, lysine typically yields higher efficiency of bioconjugation.[25] The most common linker to couple a polymer to lysine is the carbodiimide linker.[37]

This study aims to enhance the salt stability of enzyme-containing C3Ms by using bioconjugation. As in our previous studies[7,32], the spore coat protein A (CotA) laccase was used as a model enzyme to achieve this goal. Here, we made bioconjugates of this enzyme with the anionic homopolymer poly(acrylic acid) (PAA) of two different lengths and with two different ratios of PAA to CotA during bioconjugation. To link PAA to the enzyme, 1-ethyl-3-(3'-dimethylaminopropyl)carbodiimide hydrochloride (EDC) and *N*-hydroxysuccinimide (NHS) were used. C3Ms were prepared by adding the diblock copolymer poly(*N*-methyl-2-vinyl-pyridinium)$_{128}$-*block*-poly(ethylene oxide)$_{477}$ (PM2VP$_{128}$-*b*-PEO$_{477}$) to the enzyme solutions. The preferred micellar composition (PMC), structural features, and salt stability of the CotA-PAA-containing C3Ms were determined using dynamic light scattering (DLS) and fluorescence correlation spectroscopy (FCS). For the FCS experiments, we used fluorescently labeled CotA with a fluorescent dye (Alexa Fluor 488) via maleimide reaction as described previously.[7,32]

3.2. Experimental section

3.2.1. Materials

The diblock copolymer poly(2-vinyl pyridine)$_{128}$-*block*-poly(ethylene oxide)$_{477}$ (M_n = 34.5 kg/mol, M_w/ M_n = 1.1) was obtained from Polymer Source Inc. This diblock copolymer was quaternized with iodomethane following the procedure described by Lindhoud et al.,[38] resulting in a degree of quaternization (DQ) of about 70 % (measured by ^{1}H-NMR).[39] Poly(acrylic acid) (PAA) with M_n = 3.4 kg/ mol (M_w/ M_n = 1.3) (PAA$_{47}$) and M_n = 8.5 kg/ mol (M_w/ M_n = 1.07) (PAA$_{118}$) were also purchased from Polymer Source Inc. The coupling reagent 1-ethyl-3-(3'-dimethylaminopropyl)carbodiimide hydrochloride (EDC) was purchased from Thermo Fisher Scientific. *N*-Hydroxysuccinimide (NHS) was purchased from Sigma-Aldrich. Alexa Fluor 488 C5 maleimide obtained from Thermo Fisher Scientific was used to fluorescently label the native

and bioconjugated enzymes. The substrate 2,2′-azino-bis(3-ethylbenzothiazoline-6-sulfonic acid) diammonium salt (ABTS) for the activity assay was purchased from Sigma-Aldrich.

3.2.2. CotA production and purification

The CotA gene was cloned into pBAD vector and heterologously expressed in *Escherichia coli* Rosetta cells. The induction of CotA laccase overexpression was done after the optical density of the culture medium reached 0.6 - 0.8 by adding 0.15 % L-arabinose and 0.25 mM $CuSO_4$ at 25 ºC. CotA laccase was purified using two chromatography methods: cation exchange chromatography (cIEX using a SP-Sepharose FF column) and gel filtration chromatography (Superdex 200 column).

Specific fluorescence labeling of CotA with Alexa Fluor 488 C5 maleimide was done by following the procedure as described in our previous paper.[7,32] In short, a variant of CotA was obtained by changing an amino acid at position 313 from serine to cysteine (CotA S313C). During the induction of CotA S313C expression, no copper salt solution was added to the culture because copper promotes the oxidation of the sulfhydryl (thiol) group in the cysteine residue. The pooled fractions from cIEX were subsequently labeled with Alexa Fluor 488 C5 maleimide with a molar ratio of 1:10 at 4 ºC by overnight incubation in the dark. Separation of the labeled CotA from the unreacted label was performed by a Biogel-P6DG gel filtration column (BioRad) and a gel filtration column (Superdex 200 column).[7,32]

3.2.3. Bioconjugation of CotA with PAA

For protein bioconjugation in general, lysine residues are targeted by electrophilic reagents such as activated carboxylic acids through carbodiimide linker.[40] We coupled one or few carboxyl groups from PAA to the primary amines of CotA using a combination EDC/ NHS linker[41,42] (Scheme 3.1). EDC facilitates amide bond formation between the activated carboxylic acids and primary amines.[34,43] EDC is water-soluble and has been used widely for protein bioconjugation. However, the reactive intermediate, *O*-acylisourea ester, formed when EDC couple to carboxylate group, is also not stable. Using NHS improves the stability of EDC and its reactive intermediate. The combination EDC/ NHS is known to be more efficient for the coupling reaction.[36,44] EDC-mediated amide bond formation effectively occurs between pH 4.5 and 7.5. Above this pH range, the coupling reaction occurs slower with lower yields.[27]

This study used poly(acrylic acid) (PAA) of two different chain lengths: PAA_{47} and PAA_{118}. Bioconjugation to CotA was done by the following procedure. First, a 1 % w/v of PAA solution was prepared in phosphate buffer pH 7.4. A fresh solution of EDC and NHS was added

with a molar ratio of 1.2:1 and 1:1 to the carboxylic acid group of PAA, respectively. The reaction was allowed to run for 15 minutes at room temperature. Subsequently, CotA solution in sodium phosphate buffer pH 7.4 was added dropwise. This was done separately for two enzyme ratios to PAA, 1:2 and 1:5, respectively. The coupling reaction was done overnight at room temperature. Unreacted compounds and EDC–urea as a by-product were removed using Biogel-P6DG gel filtration (BioRad). Subsequently, the enzyme solutions were concentrated several times using an Amicon concentrator (cutoff of 10kDa). Successful bioconjugation of CotA with PAA was confirmed by native agarose gel electrophoresis, SDS-PAGE, zeta potential measurements, circular dichroism (CD), and activity tests. After the bioconjugation step, we had four samples of bioconjugated enzymes: CotA-PAA_{47} prepared with enzyme-PAA molar ratio 1:2, CotA-PAA_{47} with ratio 1:5, CotA-PAA_{118} with ratio 1:2, and CotA-PAA_{118} with ratio 1:5. These bioconjugates are referred to in the remainder of this paper as CotA-$2PAA_{47}$, CotA-$5PAA_{47}$, CotA-$2PAA_{118}$, and CotA-$5PAA_{118}$, respectively.

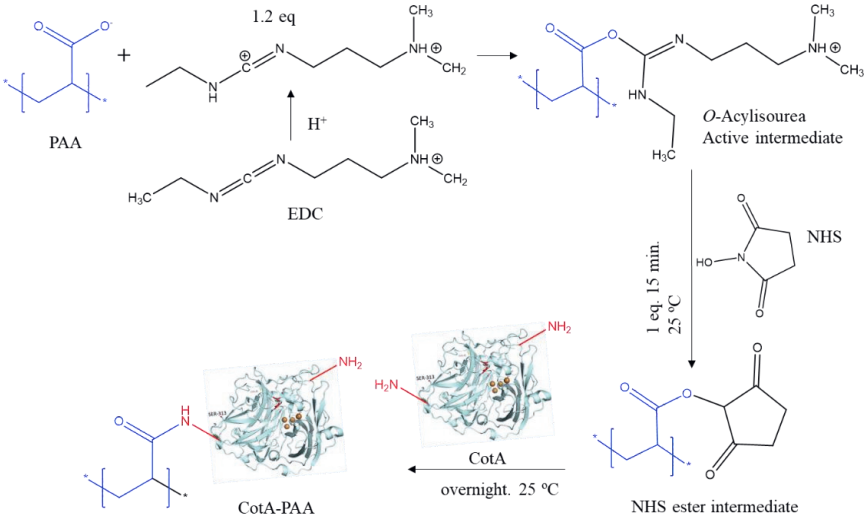

Scheme 3.1. Bioconjugation of CotA with PAA using EDC and NHS linker.

3.2.4. Native agarose gel electrophoresis and SDS-PAGE

For native agarose gel electrophoresis the procedure described by Thilakarathne et al.[45] was used. The native agarose gel was prepared by dissolving 0.5 % w/v of agarose in 40 mM Tris-acetate buffer at pH 6.5 and heating this solution in a microwave. The gel was placed in a horizontal gel electrophoresis apparatus and poured with a running buffer of 40 mM Tris-acetate of pH 6.5. The samples were mixed with loading buffer (50 % v/v glycerol and 0.1 %

w/v bromophenol blue) and then loaded into the gel wells. The electrophoresis was carried out for 45 min at 100 mV at room temperature. The gel was stained overnight with 10 % v/v acetic acid and 0.02 % m/v Coomassie brilliant blue and then destained with 10 % v/v acetic acid overnight.[45] SDS-PAGE analysis was performed by following the standard SDS-PAGE Laemmli protocol.[46–48]

3.2.5. Zeta potential measurements and circular dichroism (CD)

Zeta potential measurements were performed using a Malvern Zetasizer. The buffer of the enzyme solutions was exchanged into 10 mM sodium carbonate buffers of pH 10.8 using an ultrafiltration unit (Amicon concentrator, cutoff of 10 kDa). Samples were placed in a cuvette with Dip Cell from Malvern. We used the Smoluchowski fit from the software to calculate the zeta potential of the bioconjugated enzymes and the unconjugated enzyme.

Circular dichroism (CD) was performed to determine the protein's secondary structure. CD experiments were carried out on a JASCO J-715 spectropolarimeter with a Jasco PTC 348 WI temperature controller. The bioconjugated enzyme and the unconjugated enzyme (control) solutions were put in a quartz cuvette with an optical path length of 1 mm. The far-UV CD spectra were recorded from 200 to 260 nm with 50 nm/ min scan speed.

3.2.6. Activity and thermal stability measurements

We investigated the effect of bioconjugation on the catalytic activity of CotA by using an assay with 2,2′azino-bis-(3-ethylbenzothiazoline-6-sulfonic acid) (ABTS) as a substrate. CotA laccase oxidizes ABTS to the green-colored cationic radical $ABTS^{\bullet+}$, which was detected using a spectrophotometer at wavelength 420 nm (ε = 36 000 M^{-1} cm^{-1}). For this test, we used 1.0 mM ABTS in 100 mM sodium acetate buffer at pH 4.4. The specific activity of CotA was calculated as the activity per milligram of CotA (μmol min^{-1} mg^{-1}). The relative activity was calculated as the ratio between the specific activity of the sample of interest and the native CotA (control) activity and presented as a percentage.[49–51]

The activity of the enzymes after heating was also investigated. Solutions of native CotA and CotA-PAA bioconjugated enzymes were heated to 80 ºC and kept at that temperature for an hour. Every 10 min, small volumes were taken out and cooled to room temperature (25 ºC), and the activity of the enzymes was measured in the same way as described above.

3.2.7. Determination of the preferred micellar concentration and salt stability of the CotA-PAA containing C3Ms

For each of the CotA-PAA conjugates, we determined the preferred micellar composition (PMC), i.e., the ratio of enzyme and diblock copolymer in solution at which the concentration of C3Ms is at its maximum. To this end, solutions with different concentrations of diblock copolymer poly(*N*-methyl-2-vinyl-pyridinium)-*block*-poly(ethylene oxide) ($PM2VP_{128}$-*b*-PEO_{477}) and a constant concentration of enzyme (3 μM) were prepared (with a 1 : 1 mix volume ratio). First, the enzyme and polymer solutions were prepared separately in 10 mM sodium carbonate buffer at pH 10.8 and filtered through 0.2 μm poly(ether-sulfone) membrane syringe filters. After mixing, the solutions were left to equilibrate at room temperature overnight. The PMC for the various bioconjugated CotA variants was identified using dynamic light scattering (DLS). The salt stability of the various enzyme-containing micelles was established at their PMC. This was done by titrating a 4 M NaCl solution to the C3M solutions and observation using DLS and fluorescence correlation spectroscopy (FCS).

3.2.8. Dynamic light scattering (DLS)

DLS was performed using ALV equipment and a DPSS laser with a 660 nm wavelength and a laser power of 150 mW. Measurements of the scattering intensity (I), hydrodynamic radius (R_h), and polydispersity index (PDI) were performed at a fixed 90º angle. Cumulant analysis and the Stoke-Einstein equation for spherical particles were used to analyze the autocorrelation function and determine the hydrodynamic radius R_h.[52] The Stoke-Einstein equation for spherical particles is given by:

$$D = \frac{k_B T}{6\pi\eta R_h} \tag{3.1}$$

where D is the diffusion coefficient, k_B is the Boltzmann constant, T is the absolute temperature, and η is the solvent's viscosity. We determined the shape of the C3Ms by plotting the DLS decay rate data (Γ) obtained between detection angles from 40º to 130º as a function of the square of wave vector (q^2) for cumulant 1, 2, and 3.[32,53,54]

3.2.9. Fluorescence correlation spectroscopy (FCS)

Fluorescence correlation spectroscopy was performed on a Leica TCS SP8 X system with a 63× 1.20 NA water immersion objective and a supercontinuum laser. Fluorescently labeled enzymes (labeled with Alexa Fluor 488) were placed in a μ-Slide-8 well-chambered coverslip (Ibidi®) and excited at 488 nm with a pulse frequency of 40 MHz. Fluorescence was detected

between 495 and 550 nm using a hybrid detector coupled to a PicoHarp 300 TCSPC module (PicoQuant) with 1 Airy unit on pinhole setting. Rhodamine 110 (diffusion coefficient 4.3 × 10^{-10} m^2 s^{-1}) was used to determine the confocal structure parameter a ($a = \omega_z/\omega_{xy}$, where ω_z and ω_{xy} are axial and equatorial radii of the detection volume, respectively).

FCS data were analyzed with software FFS data processor version 2.3 (Scientific Software Technologies Software Centre, Belarus) using a two-component 3D diffusion model including a triplet state:

$$G(t) = 1 + \frac{1}{\langle N \rangle} \cdot \left(1 + \frac{F_{trip}}{1-F_{trip}}\right) e^{-t/T_{trip}} \cdot \sum_{i=1}^{n} \frac{F_i}{\left(1+\frac{t}{\tau_{dif,i}}\right) \cdot \sqrt{1 + \left(\frac{\omega_{xy}}{\omega_z}\right)^2 \cdot \frac{t}{\tau_{dif,i}}}} \quad (3.2)$$

where $\langle N \rangle$ is the average number of fluorescent particles in the confocal volume, F_{trip} is the fraction of molecules in the triplet state, T_{trip} is the average time a fluorophore resides in the triplet state, F_i is the fraction of species i, and $\tau_{dif,i}$ is the diffusion time of the species i in the confocal volume, respectively. From the diffusion time, the diffusion coefficient D can be calculated using this equation:

$$D = \frac{\omega_{xy}^2}{4 \cdot \tau_{dif}} \quad (3.3)$$

The fluorescent molecules' hydrodynamic radius can then be calculated from D using the Stokes-Einstein equation for spherical particles (Equation 3.1).

3.3. Results and discussion

3.3.1. Effect of bioconjugation on net charge and mass of CotA

In this study, we bioconjugated CotA with a weak polyanion, poly(acrylic acid) (PAA) (pK_a PAA = 4.5), thereby increasing the negative charge of this enzyme.[55] The CotA-PAA bioconjugation was confirmed using native agarose gel electrophoresis, zeta potential measurements, and SDS-PAGE. The native agarose gel electrophoresis results show the difference in electrophoretic mobility among CotA and the CotA-PAA bioconjugated enzymes that depend on the net charge of enzymes[55] (Figure 3.1A). Native CotA shows a band that has slightly moved towards the positive pole due to the net charge on this enzyme (about −12 at pH 7.4, determined using PROPKA 3.1 software).[5,7,32] As expected, the bands of the bioconjugated enzymes show significantly larger shifts towards the positive pole due to their increased negative charge. The CotA-5PAA_{118} sample, which has the longest PAA chains and the highest ratio of CotA to PAA during the bioconjugation reaction, has migrated the most to the positive

pole, indicating that has the highest negative charge. Bioconjugated enzymes have higher negative zeta potentials when measured by the Zetasizer, showing the same trend as native agarose gel electrophoresis (Figure S3.1., Supplementary information).

Figure 3.1A further shows that the bands of the samples of CotA-2PAA$_{47}$ to CotA-5PAA$_{118}$ are broader and more diffuse than the one of native CotA, which indicates that the bioconjugated enzymes have distribution in their charges due to the heterogeneity in the PAA attached to CotA (not all CotA molecules in a sample have the same amount of PAA chains attached and one chain of PAA could be attached to more than one CotA). CotA has 25 lysines in its sequence plus an N-terminus amine as the source of primary amine (NH_2). In addition, each monomer of PAA has a COOH group. The abundance of NH_2 and COOH groups increases the efficiency of bioconjugation and leads to random bioconjugation between CotA and PAA (no specific bioconjugation sites).[25]

The mixture of PAA and CotA without bioconjugation reaction in columns C1 and C2 of Figure 3.1B provides a band of similar molecular weight as native CotA. Furthermore, bioconjugation between CotA and PAA leads to heterogeneous mixtures of higher molecular weights bioconjugated enzymes due to the covalently bound PAA chains. The bands of CotA-2PAA$_{47}$, CotA-5PAA$_{47}$, CotA-2PAA$_{118}$, and CotA-5PAA$_{118}$ samples are more diffuse and smeared than the band of native CotA. However, it should be noted that all bioconjugated enzymes dissolved perfectly in buffer, and no protein aggregation was observed.

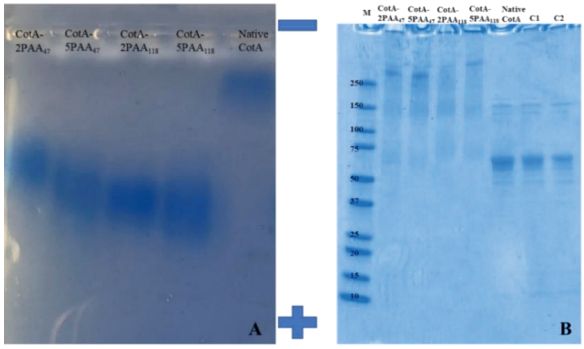

Figure 3.1. (A) Native agarose gel electrophoresis of bioconjugated enzymes (at pH 7.4): CotA-2PAA$_{47}$, CotA-5PAA$_{47}$, CotA-2PAA$_{118}$, CotA-5PAA$_{118}$ and native CotA (control). (B) SDS-PAGE for native CotA and the bioconjugated enzymes. M = marker. The size of the marker is presented in kDa. WT = native CotA. C1 = CotA mixed with PAA$_{47}$. C2 = CotA mixed with PAA$_{118}$.

3.3.2. Effect of bioconjugation on the secondary structure, activity, and temperature stability of CotA

The secondary structure of the enzymes before and after bioconjugation was determined using far-UV CD. The CD spectra show no significant differences between the secondary structures of native CotA and the bioconjugated enzymes (Figure 3.2). Thus, bioconjugation with PAA did not affect the secondary structure of the enzyme. Similarly, Thilakarathne et al. reported that hemoglobin-PAA bioconjugation did not lead to significant changes in the hemoglobin secondary structure.[45,56]

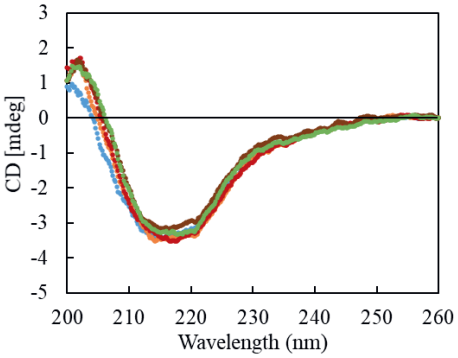

Figure 3.2. CD spectra of native CotA (blue), and bioconjugated enzymes CotA-2PAA$_{47}$ (orange), CotA-5PAA$_{47}$ (red), CotA-2PAA$_{118}$ (brown), and CotA-5PAA$_{118}$ (green).

Activity measurements were performed to evaluate the effect of bioconjugation on the catalytic activity of CotA. Figure 3.3 shows the activity of the enzymes relative to the native enzyme activity in percentage. The bioconjugated enzymes displayed relative activities of 116 ± 2 %, 85 ± 8 %, 77 ± 4 %, and 39 ± 7 % for CotA-2PAA$_{47}$, CotA-5PAA$_{47}$, CotA-2PAA$_{118}$, and CotA-5PAA$_{118}$, respectively. The activity of the CotA-2PAA$_{47}$ sample is slightly higher than that of the native CotA. This activity improvement could be due to an increase in the enzyme's solubility and improvement of the binding capacity between the enzyme and ABTS as a result of the attachment of a short PAA chain.[17] Han et al. also found an increase in the catalytic activity of several enzymes after increasing the solubility of the enzymes.[17] However, for the other samples of the CotA-PAA bioconjugated enzymes the activity decreased, especially the bioconjugated enzymes with the longer PAA chain (PAA$_{118}$) and higher concentration ratio of PAA to CotA during bioconjugation. Apparently, longer PAA chains or many PAA chains attached to CotA hinder ABTS bind to the catalytic site of CotA.

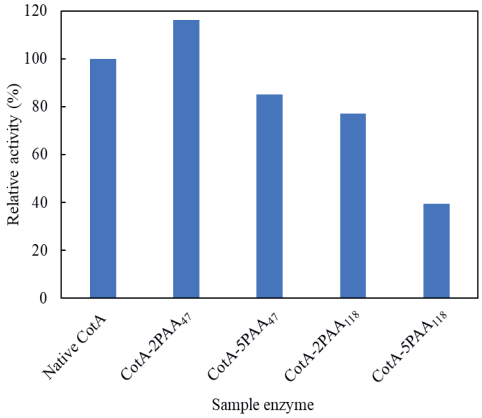

Figure 3.3. Relative activity measurements of native CotA and the various bioconjugated CotA variants.

The structural stability of the enzymes was also investigated by determining their activity after heating (80 ºC) over a certain period of time. The results are presented as relative activity to the native enzyme activity (before heating) (Figure 3.4). The activity of native CotA decreased sharply with heating time. However, all bioconjugated enzymes showed increased activity after 10 minutes of heating and a more gradual decreasing activity after longer heating times than native CotA. Possibly, a short period of heating provides better access for the substrate to the active sites of enzymes, thus resulting in faster substrate conversion.[57,58] For native CotA, heating for a shorter period (less than 10 minutes) may also increase the activity; however, it is not observed after 10 minutes of heating in this study.

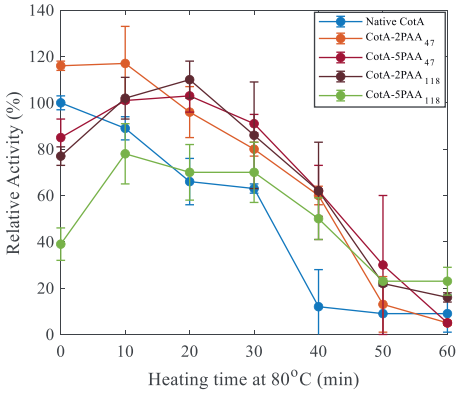

Figure 3.4. Preservation of enzyme activity after heating (80 ºC) for native CotA (blue), CotA-2PAA$_{47}$ (orange), CotA-5PAA$_{47}$ (red), CotA-2PAA$_{118}$ (brown), and CotA-5PAA$_{118}$ (green).

After 40 minutes of heating, the native CotA was completely deactivated due to denaturation, while the relative activity of bioconjugated enzymes was still above 50 %. It has been reported that bioconjugation prevents conformational transitions at high temperatures and inhibits the unfolding transition at the transition temperature.[59] Ghimire et al.[56] also reported that denaturation after thermal treatment and cooling at room temperature is reversible for hemoglobin-PAA. The relative thermal stability of bioconjugated enzymes can also because bioconjugation raises the free energy (ΔG) of denaturation and decreases the conformational entropy (ΔS) of denaturation of the enzyme.[41,55] Protein-polymer bioconjugation also benefits for improving the potential storage capacity of proteins.[60]

3.3.3. Determination of PMC and characterization of enzyme-containing C3Ms by DLS

To determine the preferred micellar composition (PMC) for the enzyme-containing C3Ms, samples were prepared with varying concentrations of PM2VP$_{128}$-*b*-PEO$_{477}$ and a constant concentration of native or bioconjugated CotA (1.5 μM). This concentration is above the critical micelles concentration of native CoA-containing C3Ms (Figure S3.4. Supplementary information). The PMC was observed using dynamic light scattering (DLS). In addition, this technique enabled us to determine the size and overall shape of the C3Ms. From the PMCs it was possible to estimate for each of the bioconjugated enzymes how much PAA chains were attached on average to each CotA molecule.

Figure 3.5 shows that with increasing PM2VP$_{128}$-*b*-PEO$_{477}$ concentration, the light scattering intensity of the samples increased due to the formation of C3Ms. The negatively charged enzymes and the positively charged PM2VP$_{128}$-*b*-PEO$_{477}$ bind and form micelles. The solutions composition that gives the maximum the light scattering intensity and lowest value of polydispersity index (PDI) is identified as PMC. If no other than electrostatic interactions drive the C3M formation, the PMC corresponds to the composition where the charge concentration ratio between enzymes and PM2VP$_{128}$-*b*-PEO$_{477}$ is about equal.

Figure 3.5 shows, as expected, that for the bioconjugated enzymes, higher concentrations of PM2VP$_{128}$-*b*-PEO$_{477}$ are needed to reach the maximum scattering intensity than for native CotA: in other words, more PM2VP$_{128}$-*b*-PEO$_{477}$ is needed to compensate for the negative charge of the bioconjugated enzymes. Among the bioconjugated enzyme samples, the PMC of the CotA-5PAA$_{118}$ sample is found at the highest concentration of diblock copolymer, indicating that this enzyme has the highest negative charge due to the longest chains of PAA, and the highest ratio of PAA to CotA during bioconjugation. At PM2VP$_{128}$-*b*-PEO$_{477}$ concentrations far above the PMC, the interaction between the enzymes and PM2VP$_{128}$-*b*-

PEO_{477} will lead to the formation of small soluble complexes resulting in low light scattering intensity and increased PDI values.

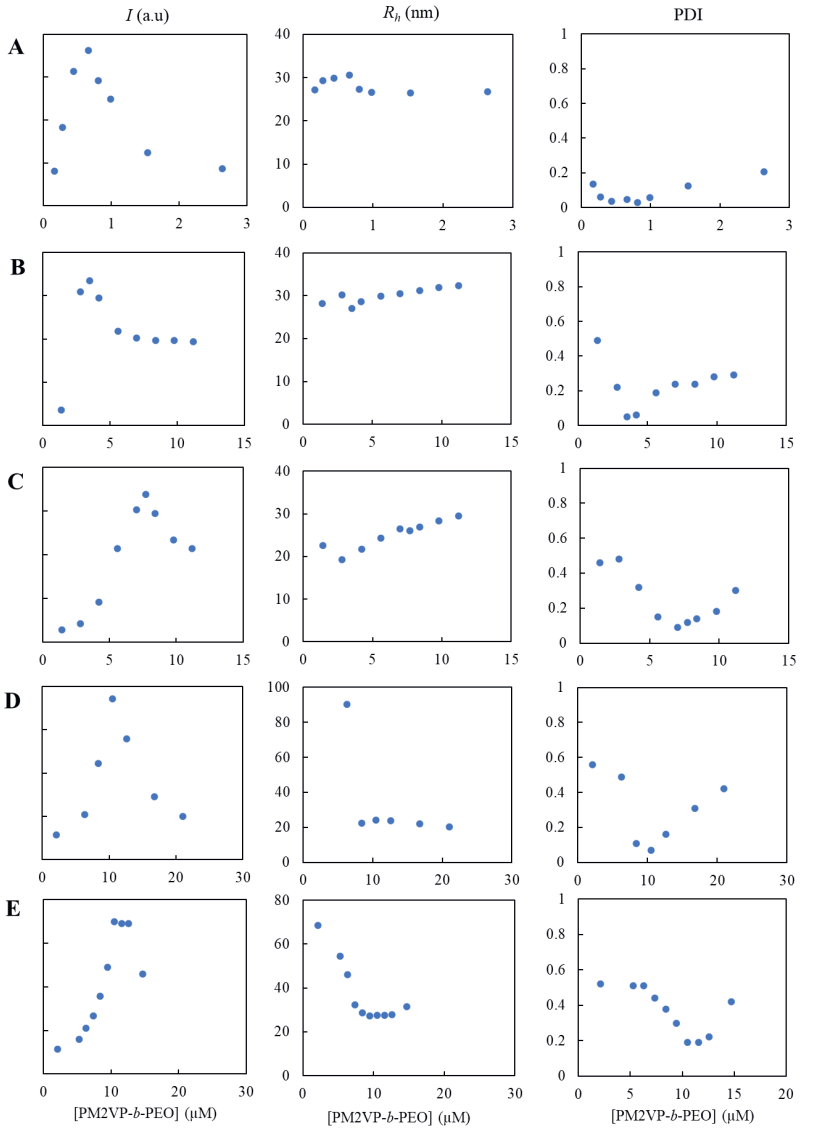

Figure 3.5. Light scattering intensity (I), hydrodynamic radius (R_h), and polydispersity index (PDI) for different mixtures of CotA-PAA bioconjugated enzymes and the diblock copolymer $PM2PV_{128}$-*b*-PEO_{477} (pH 10.8). (A) Native CotA, (B) CotA-$2PAA_{47}$, (C) CotA-$5PAA_{47}$, (D) CotA-$2PAA_{118}$, and (E) CotA-$5PAA_{118}$.

In general, the aggregation number in the core and the length of the PEO-block of the polymer influence the overall size of micelles.[61–63] DLS results show that at the PMC, the micelles have a hydrodynamic radius of 32.4 ± 0.8 nm, 27.0 ± 0.7 nm, 25.3 ± 0.6 nm, 24.9± 0.6 nm, and 26.7 ± 1.2 nm for native CotA, CotA-2PAA$_{47}$, CotA-5PAA$_{47}$, CotA-2PAA$_{118}$ and CotA-5PAA$_{118}$, respectively. The decrease in C3M size from native CotA to CotA-2PAA$_{118}$ can be explained by the presence of fewer enzyme molecules in the core, since fewer enzyme molecules are required to neutralize the charge of the diblock molecules. However, the size of the micelles containing CotA-5PAA$_{118}$ is slightly larger compared to the CotA-2PAA$_{118}$ micelles. Maybe this is because the average size of the CotA-5PAA$_{118}$ conjugates is relatively large as a result of the binding of many PAA chains to one CotA molecule during bioconjugation, and possibly more than one enzyme molecule was attached to the same PAA chain, resulting in clusters of several enzyme molecules. The DLS results also show that at the PMC the CotA-5PAA$_{118}$ C3Ms are less monodisperse than the other C3Ms: for all other C3Ms a PDI ≤ 0.1 was found, indicating a narrow size distribution of the C3Ms, while the CotA-5PAA$_{118}$ sample at the PMC has a PDI of about 0.2, which indicates a moderate size distribution.[64]

PM2VP$_{128}$-*b*-PEO$_{477}$ has a charge of about +93 (elementary units). At pH 10.8, PAA$_{47}$ and PAA$_{118}$ have charges of about −47 and −118 (elementary units), respectively. The net charge of CotA at pH 10.8 is about −41.[5,7,32] Van der Kooij et al.[65] reported that the PMC of micelles formed between PAA and PM2VP-*b*-PEO, was at a charge concentration ratio of 1:1. Furthermore, from our previous research, we know that CotA and PM2VP-*b*-PEO also have a PMC at 1:1 charge concentration ratio. Based on these findings, we assume that the PMC of CotA-PAA and PM2VP$_{128}$-*b*-PEO$_{477}$ also at equal charge concentrations of protein and diblock copolymer. With this assumption, we could estimate the average number of PAA chains attached per CotA molecule to be about 1, 4, 2, and 5 molecules for CotA-2PAA$_{47}$, CotA-5PAA$_{47}$, CotA-2PAA$_{118}$ and CotA-5PAA$_{118}$, respectively (Table S3.1., Supplementary information).

The shape of the enzyme-containing C3Ms was determined using multi-angle DLS. At each detection angle, the decay rate (Γ) of the DLS correlation function was fitted with the first, second, and third cumulant as a function of squared wave vector (q^2), resulting in three overlapping straight lines (Figure 3.6). The slope of these overlapping lines equals the diffusion coefficient. This data trend is typical for spherical particles. From this observation, we know

that the shape of the enzyme-containing C3Ms for all bioconjugated enzymes is spherical, the same as the shape of C3Ms composed of native CotA.[7,32,53,54]

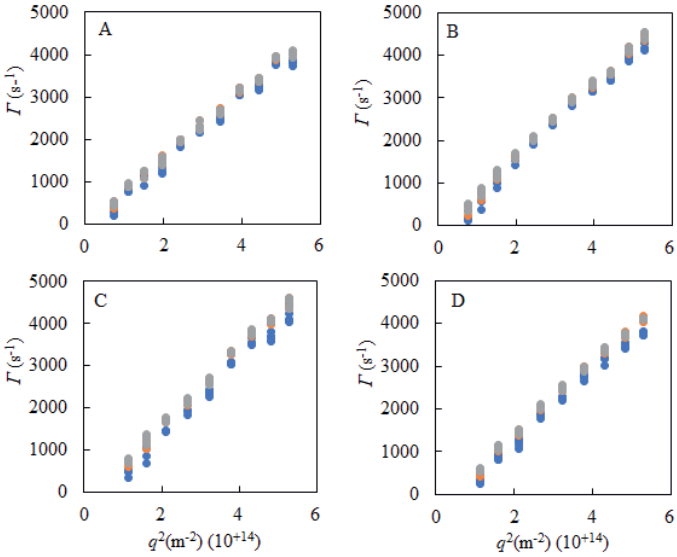

Figure 3.6. Multi-angle DLS results at the PMC of C3Ms composed of (A) CotA-2PAA$_{47}$, (B) CotA-5PAA$_{47}$, (C) CotA-2PAA$_{118}$, and (D) CotA-5PAA$_{118}$. Decay rate $\Gamma(q)$ obtained from the DLS correlation curves by a first (blue), second (orange) and third (grey) cumulant fit.

3.3.4. Encapsulation of CotA and CotA-PAA in C3Ms observed using FCS

Enzyme encapsulation was also investigated using FCS and fluorescently labeled native CotA and bioconjugated CotA (Figure S3.2, Supplementary information). FCS provides information on the size of the fluorescent free enzymes and the fluorescent C3Ms and the efficiency of protein encapsulation (the fraction of enzyme incorporated in the core of the micelles). Encapsulating enzymes into C3Ms leads to a lower diffusion coefficient and an increased fluorescence intensity per particle. The fluorescence intensity of the C3Ms is proportional to the number of fluorescent proteins inside.[5,32,66]

The FCS data in Figure 3.7B show that free CotA-PAA bioconjugated enzymes diffuse slightly slower than native CotA, due to the covalently bound PAA chains. When the diblock copolymer was added to the enzyme solutions (end composition corresponding to the PMC), the diffusion of the enzymes became significantly slower, indicating that C3Ms were formed. In addition, the number of fluorescent particles in the confocal volume (N) also decreased significantly, illustrated by the amplitude increase, due to the encapsulation of many CotA in one micelle (Figure 3.7A).

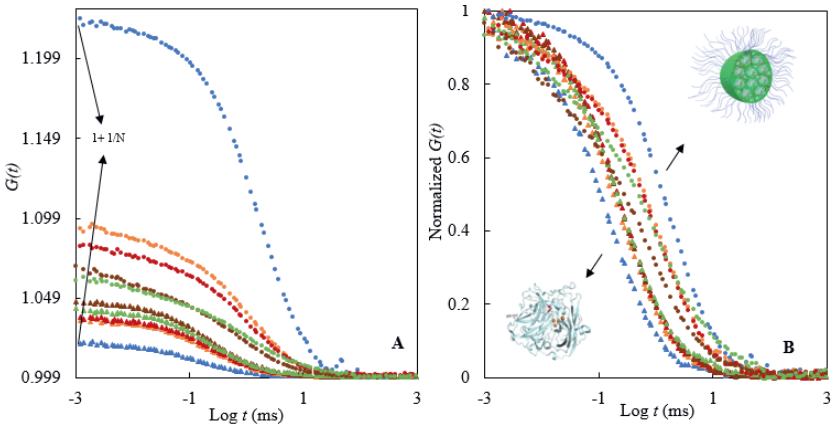

Figure 3.7. FCS measurements on free CotA and CotA-PAA enzymes and their C3Ms with the diblock copolymer PM2PV$_{128}$-*b*-PEO$_{477}$ (pH 10.8). (A) FCS autocorrelation curves ($G(t)$), (B) normalized $G(t)$. Native CotA (blue), CotA-2PAA$_{47}$ (orange), CotA-5PAA$_{47}$ (red), CotA-2PAA$_{118}$ (brown), and CotA-5PAA$_{118}$ (green). Triangles represent free enzymes and circles represent enzyme-containing C3Ms.

For the C3Ms containing CotA-PAA bioconjugated enzymes, more fluorescence particles in the confocal volume (N) were detected than for the C3Ms containing native CotA. We found N was 4 ± 1, 10 ± 2, 13 ± 1, 19 ± 3, 28 ± 13, for C3Ms composed of native CotA, CotA-2PAA$_{47}$, CotA-5PAA$_{47}$, CotA-2PAA$_{118}$, and CotA-5PAA$_{118}$, respectively. This implies that the concentration of micelles in the samples is higher for the bioconjugated enzymes than for native CotA, and the concentration increases with the length of the PAA chains and the PAA to CotA ratio during bioconjugation.

Further analysis of the FCS data showed that free native CotA has a size of 2.2 ± 0.3 nm. Encapsulation of this enzyme resulted in micelles with R_h of 31.1 ± 1.8 nm. About 77 ± 4 % of the native CotA was encapsulated in the core of micelles. The size of the free CotA-PAA enzymes was 3.6 ± 0.1 nm, 4.0 ± 0.5 nm, 2.9 ± 0.5, and 6.0 ± 2.7 nm for CotA-2PAA$_{47}$, CotA-5PAA$_{47}$, CotA-2PAA$_{118}$, and CotA-5PAA$_{118}$, respectively. The hydrodynamic radius increases with the length of the attached PAA chains and the ratio PAA to CotA applied in the bioconjugation reaction. Not only several PAA chains can be attached to CotA, but it is also likely that more than one CotA can bind to one PAA molecule, especially for the sample with the longer PAA chain and a higher ratio of PAA to CotA.

The hydrodynamic radii of the micelles formed from the CotA-PAA enzymes are 32.4 ± 3.1 nm, 26.4 ± 0.7 nm, 19.8 ± 2.4 nm, and 28.5 ± 2.7 nm for CotA-2PAA$_{47}$, CotA-5PAA$_{47}$,

CotA-2PAA$_{118}$ and CotA-5PAA$_{118}$, respectively. These sizes are similar to those obtained with DLS. Moreover, the FCS data confirm the DLS observation that the micelles containing CotA-5PAA$_{118}$ are larger than the CotA-2PAA$_{118}$ micelles.

The encapsulation efficiency of the C3Ms containing the bioconjugated enzymes is about 79 ± 1.4 %, 80 ± 0.0 %, 74 ± 4.9 %, and 67.0 ± 4.2 % for CotA-2PAA$_{47}$, CotA-5PAA$_{47}$, CotA-2PAA$_{118}$ and CotA-5PAA$_{118}$, respectively. Thus, the encapsulation efficiency for the CotA-PAA with the shorter PAA chains (PAA$_{47}$) is similar to that of native CotA. However, slightly lower encapsulation efficiencies were observed for the CotA-PAA$_{118}$ samples, possibly because from the heterogeneous conjugated enzyme mixtures, the higher charged bioconjugated enzyme molecules are preferentially incorporated into the core over the lower charged bioconjugated enzyme molecules.

3.3.5. Effect of bioconjugation on the salt stability of enzyme-containing C3Ms

We used both DLS and FCS to determine the stability of C3Ms containing native CotA and the CotA-PAA enzymes upon the addition of NaCl. With DLS, the disintegration of the micelles is reflected by a decrease in light scattering intensity. In addition, FCS provides information on the salt-induced disintegration by following the enzyme fractions encapsulated in the C3Ms and free in solution and the increase in the number of fluorescent particles detected in the confocal volume (N).

We studied the salt stability of five types of micelles by stepwise adding an NaCl solution: micelles composed of native CotA, CotA-2PAA$_{47}$, CotA-5PAA$_{47}$, CotA-2PAA$_{118}$, and CotA-5PAA$_{118}$. The DLS results in Figure 3.8 show that the light scattering intensity of the samples gradually reduces when the salt concentration increases. The increasing salt concentration decreases the entropy gain from counter ion release and screens the charged parts of the protein and polymer that weaken the electrostatic interactions. As a result, the micelles disintegrate, and the enzyme is released.[65,67] The light scattering intensity of the solution with C3Ms composed of native CotA declines significantly faster with NaCl concentration than those with C3Ms composed of the bioconjugated enzymes. After adding 140 mM NaCl, the relative scattering intensity of the native CotA-C3M solution was reduced to almost zero (< 0.05), indicating an almost complete disintegration of the C3Ms. Figure 3.8A further shows that the salt resistance of the C3Ms of the bioconjugated enzymes is higher as more negative charge is added to CotA by bioconjugation (longer PAA chains, higher PAA to enzyme ratio during bioconjugation).

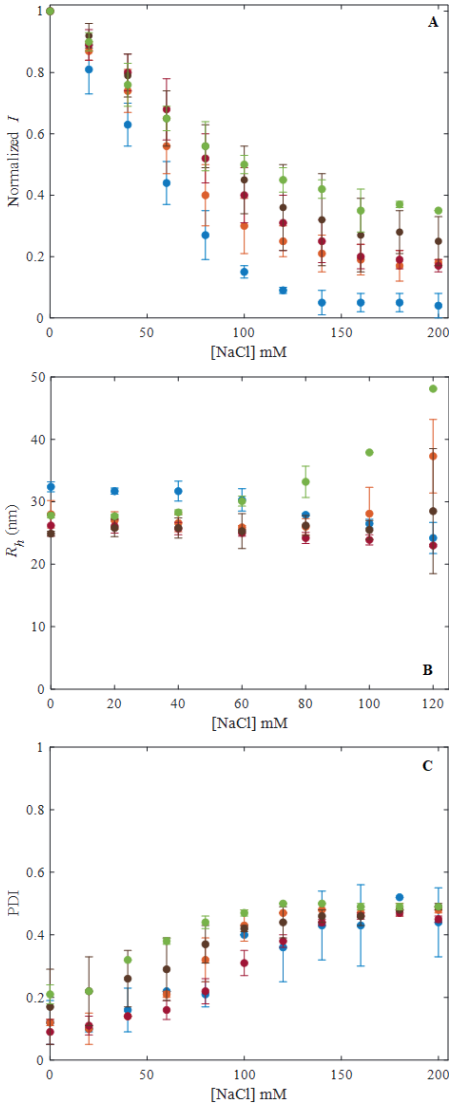

Figure 3.8. Salt stability of enzyme-containing C3Ms observed using DLS. (A) Normalized light scattering intensity (I), (B) hydrodynamic radius (R_h), and (C) polydispersity index (PDI). Native CotA (WT) (blue). CotA-2PAA$_{47}$ (orange), CotA-5PAA$_{47}$ (red), CotA-5PAA$_{118}$ (brown), and CotA-5PAA$_{118}$ (green).

Van der Kooij et al.[65] studied the stability of C3Ms composed of PM2VP-*b*-PEO and PAA and reported that the salt stability of these C3Ms is also increasing with increasing PAA chain length. They found that the micelles fully disintegrated after adding 250 mM NaCl and 400 mM

NaCl for PAA_{13} and PAA_{139}, respectively. We estimate that by conjugating enzymes with PAA, the limit to prevent total disintegration of enzyme-containing C3Ms is near 400 mM NaCl.

In Figure 3.8B, the micelles' hydrodynamic radii (R_h) as a function of NaCl concentration are given. For native CotA micelles, R_h decreased significantly compared to micelles from bioconjugated CotA. For the CotA-PAA_{47} micelles, R_h was about constant with NaCl concentration, and for CotA-$5PAA_{118}$ C3Ms, R_h increased, indicating swelling of the micelles before they disintegrated.[67] The increasing of size also can occurs due to change in the morphology of C3Ms from spherical to worm-like micelles during salt addition.[65] The PDI of all C3M samples (Figure 3.8C) increased with the addition of NaCl, indicating a broadening of size distribution upon salt addition.

FCS results regarding the salt stability of the C3Ms are presented in Figure 3.9. Figure 3.9A shows that the number of fluorescent particles detected in the confocal volume N increased with salt concentration, which indicates the release of CotA. In line with this, adding salt resulted in a decreased fraction of enzymes in C3Ms, while the fraction of free enzymes in the solution increased (Figure S3.3, Supplementary information). The results clearly show that for native CotA micelles, the enzymes were released at significantly lower salt concentrations than for micelles of the bioconjugated enzymes. After the addition of 150 mM NaCl, for native CotA C3Ms, N was almost the same as for the free enzyme sample (normalized N about equal to one), pointing to complete disintegration of the micelles. For the bioconjugated enzymes, N increased more gradually, and after the addition of 150 mM NaCl the normalized N for C3M was still less than one, indicating the micelles are more salt-resistant than the native CotA micelles. The size of the C3Ms composed of native CotA decreased significantly more upon salt addition than the size of the C3Ms composed of the various bioconjugated enzymes (Figure 3.9B). Like with DLS, we observed an increase in R_h for the CotA-$5PAA_{118}$ C3Ms during the salt titration.

The FCS and DLS results on the salt resistance of C3Ms composed of native CotA and conjugated CotA are similar. Both techniques revealed that increasing the net charge of CotA by coupling it to PAA keeps the enzyme more tightly in the micellar core because the attraction between the enzyme and the diblock copolymer is stronger, making the micelles more salt resistant. The bioconjugation strategy to improve the salt stability of enzyme-containing C3Ms works better than the so-called ‘three components strategy’, which involves adding a polymer with the same charge sign as a third component to the micelles. Our previous study[7] showed that although the homopolymer contributes to the salt stability of the micelles, there is competition between the homopolymer and CotA, and with increasing salt concentration, CotA leaves the core earlier. However, there is no competition when CotA and PAA are linked by

bioconjugation. Therefore, coupling an enzyme to a homopolymer with the same charge sign is an appropriate strategy for improving the salt stability of enzyme-containing C3Ms.

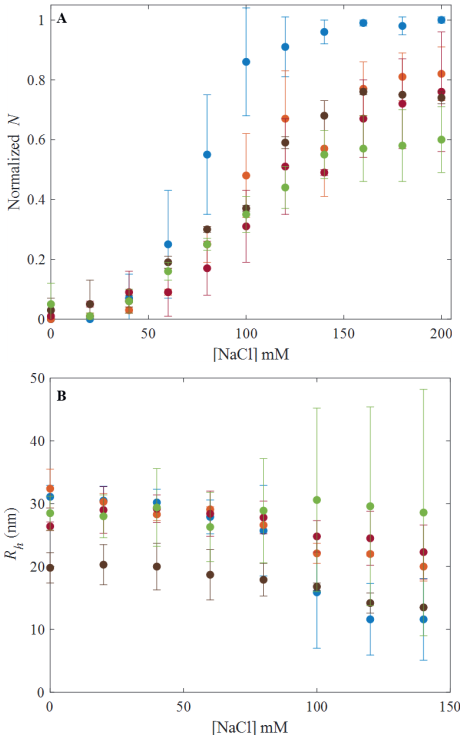

Figure 3.9. Salt stability of enzyme-containing C3Ms observed using FCS. (A) Normalized *N* and (B) hydrodynamic radius R_h for C3Ms composed of native CotA (blue), CotA-2PAA$_{47}$ (orange), CotA-5PAA$_{47}$ (red), CotA-2PAA$_{118}$ (brown), and CotA-5PAA$_{118}$ (green).

3.4. Conclusions

In this study, we enriched the net negative charge on the enzyme CotA laccase by bioconjugation with poly(acrylic acid) (PAA) of two different lengths (PAA$_{47}$ and PAA$_{118}$) and with two different PAA to CotA ratios during the bioconjugation reaction (2:1 and 5:1) using EDC/ NHS linker. Native agarose gel electrophoresis, SDS-PAGE, and zeta potential measurement showed that the bioconjugation was successful. This bioconjugation did not change the secondary structure of CotA laccase. A decrease in enzyme catalytic activity was found for the CotA- PAA$_{118}$ conjugates, probably because the longer PAA chains hinder the substrate from accessing the catalytic site of the enzyme. We also observed that the enzyme-polymer bioconjugation improved the thermal stability of CotA. FCS and DLS revealed that all CotA-PAA enzymes can be encapsulated with the diblock copolymer PM2PV-*b*-PEO into

complex coacervate core micelles at pH 10.8, as the native CotA. The CotA-PAA C3Ms are smaller than the native CotA C3Ms, but the concentration of micelles formed with the CotA-PAA enzymes is higher than with native CotA, resulting in almost the same encapsulation efficiency. DLS and FCS measurements confirmed that the CotA-PAA-containing C3Ms are more salt-resistant than CotA-containing C3Ms. This study shows that increasing the net charge of enzymes by bioconjugation is a good strategy to improve the salt stability of enzyme-containing complex coacervate core micelles (C3Ms).

References

1. Blocher McTigue, W. C. and Perry, S. L. Protein Encapsulation Using Complex Coacervates: What Nature Has to Teach Us. *Small* **16**, 1–17 (2020).
2. Fujita, D., Suzuki, K., Sato,S., Yagi-Utsumi, M., Yamaguchi, Y., Mizuno, N., Kumasaka, V., Takata, M., Noda,M., Uchiyama,S., Kato, K., and Fujita, M. Protein encapsulation within synthetic molecular hosts. *Nat. Commun.* **3**, 2–8 (2012).
3. Chakraborti, S., Lin, T. Y., Glatt, S. and Heddle, J. G. Enzyme encapsulation by protein cages. *RSC Adv.* **10**, 13293–13301 (2020).
4. Karimi, M., Zangabad, P.S., Mehdizadeh,F., Malekzad, H., Ghasemi, A., Bahrami, S., Zare, H., Moghoofei, M., Hekmatmanesh, A., and Hamblin, M.R. Nanocaged platforms: modification, drug delivery and nanotoxicity opening synthetic cages to release the tiger: nanocages for drug delivery. *Nanoscale*. **9**, 1356–1392 (2018).
5. Nolles, A., Westphal, A. H., de Hoop, J. A., Fokkink, R. G., Kleijn, J. M., van Berkel, W. J. H., Borst, J. W. Encapsulation of GFP in complex coacervate core micelles. *Biomacromolecules* **16**, 1542–1549 (2015).
6. Nolles, A., Westphal, A. H., Kleijn, J. M., van Berkel, W. J. H. and Borst, J. W. Colorful packages: Encapsulation of fluorescent proteins in complex coacervate core micelles. *Int. J. Mol. Sci.* **18**, 1557-1576 (2017).
7. Kembaren, R., Fokkink, R., Westphal, A. H., Kamperman, M., Kleijn, J. M., and Borst, J. W. Balancing Enzyme Encapsulation Efficiency and Stability in Complex Coacervate Core Micelles. *Langmuir* **36**, 8494–8502 (2020).
8. Black, K. A., Priftis, D., Perry, S. L., Yip, J., Byun, W. Y., and Tirrell, M. Protein encapsulation via polypeptide complex coacervation. *ACS Macro Lett.* **3**, 1088–1091 (2014).
9. Blocher, W. C. and Perry, S. L. Complex coacervate-based materials for biomedicine. *Wiley Interdiscip. Rev. Nanomedicine Nanobiotechnology* **9**, 76–78 (2017).
10. Lindhoud, S., de Vries, R., Norde, W. and Cohen Stuart, M. A. Structure and stability of complex coacervate core micelles with lysozyme. *Biomacromolecules* **8**, 2219–2227 (2007).
11. Cohen Stuart, M. A., Besseling, N. A. M. and Fokkink, R. G. Formation of micelles with complex coacervate cores. *Langmuir* **14**, 6846–6849 (1998).
12. Voets, I. K., de Keizer, A. and Cohen Stuart, M. A. Complex coacervate core micelles. *Adv. Colloid Interface Sci.* **147**–**148**, 300–318 (2009).
13. Nolles, A., Hooiveld, E., Westphal, A. H., van Berkel, W. J. H., Kleijn, J. M., and Borst, J. W. FRET Reveals the Formation and Exchange Dynamics of Protein-Containing Complex Coacervate Core Micelles. *Langmuir* **34**, 12083–12092 (2018).
14. Bos, I. and Sprakel, J. Langevin Dynamics Simulations of the Exchange of Complex Coacervate Core Micelles: The Role of Nonelectrostatic Attraction and Polyelectrolyte Length. *Macromolecules* **52**, 8923−8931 (2019).
15. Mills, C. E., Obermeyer, A., Dong, X., Walker, J. and Olsen, B. D. Complex Coacervate Core Micelles for the Dispersion and Stabilization of Organophosphate Hydrolase in Organic Solvents. *Langmuir* **32**, 13367–13376 (2016).
16. Ma, C., Malessa, A., Boersma, A. J., Liu, K. and Herrmann, A. Supercharged Proteins and Polypeptides. *Adv. Mater.* **32**, 1905309-1905330 (2020).
17. Han, X., Ning, W., Ma, X., Wang, X. and Zhou, K. Improving protein solubility and activity by introducing small peptide tags designed with machine learning models. *Metab. Eng. Commun.* **11**, 138-147 (2020).
18. Obermeyer, A. C., Mills, C. E., Dong, X. H., Flores, R. J. and Olsen, B. D. Complex coacervation of supercharged proteins with polyelectrolytes. *Soft Matter* **12**, 3570–3581 (2016).
19. Cummings, C. S. and Obermeyer, A. C. Phase Separation Behavior of Supercharged Proteins and Polyelectrolytes. *Biochemistry* **57**, 314–323 (2018).
20. Kapelner, R. A. and Obermeyer, A. C. Ionic polypeptide tags for protein phase separation. *Chem. Sci.* **10**, 2700–2707 (2019).
21. Van der Gucht, J., Spruijt, E., Lemmers, M. and Cohen Stuart, M. A. Polyelectrolyte complexes: Bulk phases and colloidal systems. *J. Colloid Interface Sci.* **361**, 407–422 (2011).
22. Obermeyer, A. C. and Olsen, B. D. Synthesis and application of protein-containing block copolymers. *ACS Macro Lett.* **4**, 101–110 (2015).
23. Sun, J., Xiao, L., Li, B., Zhao, K., Wang, Z., Zhou, Y., Ma, C., Li, J., Zhang, H., Hermann, A., and Liu, K. Genetically Engineered Polypeptide Adhesive Coacervates for Surgical Applications. *Angew. Chemie - Int. Ed.* **60**, 23687–23694 (2021).
24. Li, J., Li, B., Sun, J., Ma, C., Wan, S., Li, Y., Göstl, R., Herrmann,A., Liu, K.,Zhang, H. Engineered Near-Infrared Fluorescent Protein Assemblies for Robust Bioimaging and Therapeutic Applications. *Adv.*

Mater. **32**, 2000964-2000971 (2020).
25. Wilson, P. Synthesis and Applications of Protein/Peptide-Polymer Conjugates. *Macromol. Chem. Phys.* **218**, 1–15 (2017).
26. Di Marco, M., Razak, K. A., Aziz, A. A., Shamsuddin, S., Devaux, C., Borghi, E., Levy, L., and Sadun, C. Overview of the main methods used to combine proteins with nanosystems : absorption , bioconjugation , and encapsulation. *Int. J. Nanomedicine* **5**, 37–49 (2010).
27. Yadav, S. C., Kumari, A. and Yadav, R. Development of peptide and protein nanotherapeutics by nanoencapsulation and nanobioconjugation. *Peptides* **32**, 173–187 (2011).
28. Hong, J., Gong, P., Yu, J., Xu, D., Sun, H., and Yao, S. Conjugation of α-chymotrypsin on a polymeric hydrophilic nanolayer covering magnetic nanoparticles. *J. Mol. Catal. B Enzym.* **42**, 99–105 (2006).
29. Collins, J., Tanaka, J., Wilson, P., Kempe, K., Davis, T. P., McIntosh, M. P., Whittaker, M. R., and Haddleton, D. M. In situ conjugation of dithiophenol maleimide polymers and oxytocin for stable and reversible polymer-peptide conjugates. *Bioconjug. Chem.* **26**, 633–638 (2015).
30. Mudhivarthi, V. K., Cole, K. S., Novak, M. J., Kipphut, W., Deshapriya, I. K., Zhou. Y., Kasi, R. M., and Kumar C. V. Ultra-stable hemoglobin-poly(acrylic acid) conjugates. *J. Mater. Chem.* **22**, 20423–20433 (2012).
31. Wang, L., Liu, L., Wu, L., Liu, L., Wang, X., Yang, S., and Zhao, H. Environmentally responsive amino acid-bioconjugated dynamic covalent copolymer as a versatile scaffold for conjugation. *RSC Adv.* **5**, 30456–30463 (2015).
32. Kembaren, R., Westphal, A. H., Kamperman, M., Kleijn, J. M. and Borst, J. W. Charged Polypeptide Tail Boosts the Salt Resistance of Enzyme-Containing Complex Coacervate Micelles. *Biomacromolecules* **23**, 1195–1204 (2022).
33. Lee, B., Sun, S., Jiménez-Moreno, E., Neves, A. A. and Bernardes, G. J. L. Site-selective installation of an electrophilic handle on proteins for bioconjugation. *Bioorganic Med. Chem.* **26**, 3060–3064 (2018).
34. Eroglu, B. I., Kilinc, Y. B. and Mustafaeva, Z. Bioconjugation of Hepatitis B antigenic peptide with polymeric carriers through various carbodiimide chemistry. *Turkish J. Biochem.* **36**, 222–229 (2011).
35. Totaro, K. A., Liao, X., Bhattacharya, K., Finneman, J. I., Sperry, J. B., Massa, M. A., Thorn, J., Ho, S. V., and Pentelute, B. L. Systematic Investigation of EDC/sNHS-Mediated Bioconjugation Reactions for Carboxylated Peptide Substrates. *Bioconjug. Chem.* **27**, 994–1004 (2016).
36. Chouhan, R. S., Vinayaka, A. C. and Thakur, M. S. Thiol-stabilized luminescent CdTe quantum dot as biological fluorescent probe for sensitive detection of methyl parathion by a fluoroimmunochromatographic technique. *Anal. Bioanal. Chem.* **397**, 1467–1475 (2010).
37. Jain, M., Vaze, R. G., Ugrani, S. C. and Sharma, K. P. Mechanoresponsive and recyclable biocatalytic sponges from enzyme-polymer surfactant conjugates and nanoparticles. *RSC Adv.* **8**, 39029–39038 (2018).
38. Lindhoud, S., Norde, W. and Stuart, M. A. C. Effects of polyelectrolyte complex micelles and their components on the enzymatic activity of lipase. *Langmuir* **26**, 9802–9808 (2010).
39. Fulmer, G. R., Miller, A. J. M., Sherden, N. H., Gottlieb, H. E., Nudelman, A., Stoltz, B. M.; Bercaw, J. E., Goldberg, K. I. NMR chemical shifts of trace impurities: Common laboratory solvents, organics, and gases in deuterated solvents relevant to the organometallic chemist. *Organometallics* **29**, 2176–2179 (2010).
40. Gauthier, M. A. and Klok, H. A. Peptide/protein-polymer conjugates: Synthetic strategies and design concepts. *Chemical Communications* **2008**, 2591–2611 (2008).
41. Riccardi, C. M., Mistri, D., Hart, O., Anuganti, M., Lin,Y., Kasi, R.M., Kumar, C.V. Covalent interlocking of glucose oxidase and peroxidase in the voids of paper: Enzyme-polymer "spider webs. *Chem. Commun.* **52**, 2593–2596 (2016).
42. Zore, O. V., Kasi, R. M. and Kumar, C. V. Armored Enzyme–Nanohybrids and Their Catalytic Function Under Challenging Conditions. in *Methods in Enzymology* **590**, 169-192 (2017).
43. Li, Y., Gabriele, E., Samain, F., Favalli, N., Sladojevich, F., Scheuermann, J., and Neri, D. Optimized reaction conditions for amide bond formation in DNA- encoded combinatorial libraries. *ACS Comb Sci.* **18**, 438–443 (2017).
44. Keleştemur, S., Altunbek, M. and Culha, M. Influence of EDC/NHS coupling chemistry on stability and cytotoxicity of ZnO nanoparticles modified with proteins. *Appl. Surf. Sci.* **403**, 455–463 (2017).
45. Thilakarathne, V., Briand, V. A., Zhou, Y., Kasi, R. M. and Kumar, C. V. Protein Polymer Conjugates: Improving the Stability of Hemoglobin with Poly(acrylic acid). *Langmuir* **27**, 7663–7671 (2011).
46. Brunelle, J. L. and Green, R. *One-dimensional SDS-polyacrylamide gel electrophoresis (1D SDS-PAGE). Methods in Enzymology* vol. 541 (Elsevier Inc., 2014).
47. Wu, X. and Koiwa, H. One-step casting of Laemmli discontinued sodium dodecyl sulfate-polyacrylamide gel electrophoresis gel. *Anal. Biochem.* **421**, 347–349 (2012).
48. Laemmli, U. K. 227680a0. *Nature* **227**, 680–685 (1970).
49. Huang, J., Xiao, H., Li, B., Wang, J. and Jiang, D. Immobilization of Pycnoporus sanguineus laccase on

copper tetra-aminophthalocyanine–Fe3O4 nanoparticle composite. *Biotechnol. Appl. Biochem.* **44**, 93-100 (2006).
50. Kolomytseva, M. P., Myasoedova, N. M., Chernykh, A. M., Gaidina, A. S., Shebanova, A. D., Baskunov, B. P., Aschenbrenner, J., Rosengarten, J. F., Renfeld, Z. V., Gasanov, N. B., Pinchuk, I. P., Classen, T., Pietruszka, J., and Golovleva, L. A. Laccase isoform diversity in basidiomycete Lentinus strigosus 1566: Potential for phenylpropanoid polymerization. *Int. J. Biol. Macromol.* **137**, 1199–1210 (2019).
51. Xu, H. M., Sun, X. F., Wang, S. Y., Song, C. and Wang, S. G. Development of laccase/graphene oxide membrane for enhanced synthetic dyes separation and degradation. *Sep. Purif. Technol.* **204**, 255–260 (2018).
52. Stetefeld, J., McKenna, S. A. and Patel, T. R. Dynamic light scattering: a practical guide and applications in biomedical sciences. *Biophys. Rev.* **8**, 409–427 (2016).
53. Harada, A. and Kataoka, K. Chain length recognition: core-shell supramolecular assembly from oppositely charged block copolymers. *Science.* **283**, 65-67 *(*1999)..
54. Harada, A. and Kataoka, K. Novel polyion complex micelles entrapping enzyme molecules in the core. 2. Characterization of the micelles prepared at nonstoichiometric mixing ratios. *Langmuir* **15**, 4208–4212 (1999).
55. Zore, O. V., Kasi, R. M. and Kumar, C. V. *Armored Enzyme–Nanohybrids and Their Catalytic Function Under Challenging Conditions*. *Methods in Enzymology* vol. 590 (Elsevier Inc., 2017).
56. Ghimire, A., Zore, O. V., Thilakarathne, V. K. Briand, V. A., Lenehan, P. J., Lei, Y., Kasi, R. M., and Kumar, C.V. 'Stable-on-the-Table' Biosensors: Hemoglobin-Poly (Acrylic Acid) Nanogel BioElectrodes with High Thermal Stability and Enhanced Electroactivity. *Sensors* **15**, 23868–23885 (2015).
57. Riedel, C., Gabizon, R., Wilson, C.A.M., Hamadani, K., Tsekouras, K., Marqusee, S., Presse, S., and Bustamante, C. The heat released during catalytic turnover enhances the diffusion of an enzyme. *Nature* **517**, 227–230 (2015).
58. Arcus, V. L., Prentice, E.J., Hobbs, J.K., Mulholland, A.J., Van der Kamp, M.W., Pudney, C.R., Parker, E.J., and Schipper, L.A. On the Temperature Dependence of Enzyme-Catalyzed Rates. *Biochemistry* **55**, 1681–1688 (2016).
59. Suthiwangcharoen, N. and Nagarajan, R. Enhancing enzyme stability by construction of polymer-enzyme conjugate micelles for decontamination of organophosphate agents. *Biomacromolecules* **15**, 1142–1152 (2014).
60. Shakya, A. K., Sami, H., Srivastava, A. and Kumar, A. Stability of responsive polymer-protein bioconjugates. *Prog. Polym. Sci.* **35**, 459–486 (2010).
61. Yan, Y., De Keizer, A., Cohen Stuart, M. A., Drechsler, M. and Besseling, N. A. M. Stability of complex coacervate core micelles containing metal coordination polymer. *J. Phys. Chem. B* **112**, 10908–10914 (2008).
62. Rumyantsev, A. M., Zhulina, E. B. and Borisov, O. V. Scaling Theory of Complex Coacervate Core Micelles. *ACS Macro Lett.* **7**, 811–816 (2018).
63. Heo, T. Y., Kim, I., Chen, L., Lee, E., Lee, S., and Choi, S. H. Effect of ionic group on the complex coacervate core micelle structure. *Polymers* **11**, 16–19 (2019).
64. Bhattacharjee, S. Review article DLS and zeta potential – What they are and what they are not ? *J. Control. Release* **235**, 337–351 (2016).
65. Van der Kooij, H. M., Spruijt, E., Voets, I. K., Fokkink, R., Cohen Stuart, M. A., and Van der Gucht, J. On the stability and morphology of complex coacervate core micelles: From spherical to wormlike micelles. *Langmuir* **28**, 14180–14191 (2012).
66. Elson, E. L. Fluorescence correlation spectroscopy: Past, present, future. *Biophys. J.* **101**, 2855–2870 (2011).
67. Spruijt, E., Westphal, A. H., Borst, J. W., Cohen Stuart, M. A. and Van Der Gucht, J. Binodal compositions of polyelectrolyte complexes. *Macromolecules* **43**, 6476–6484 (2010).

Supplementary information

S3.1. Zeta potential measurement for native CotA, and the bioconjugated enzymes

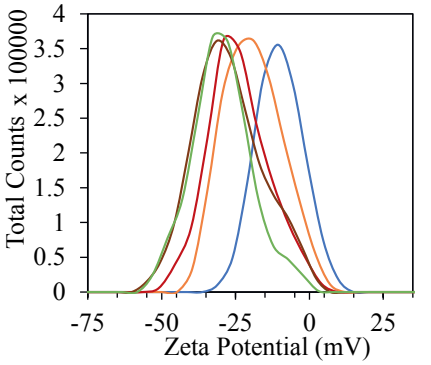

Figure S3.1. Zeta potential distribution data for native CotA (blue), and the bioconjugated enzymes (pH = 10.8): CotA-2PAA$_{47}$ (orange), CotA-5PAA$_{47}$ (red), CotA-2PAA$_{118}$ (brown), and CotA-5PAA$_{118}$ (green).

The CotA-5PAA$_{118}$ sample has the highest and native CotA has the lowest negative zeta potential. There is not much difference in zeta potential distribution of CotA-2PAA$_{118}$ and CotA-5PAA$_{118}$ as also showed from native agarose gel electrophoresis.

S3.2. Calculation of the average number of PAA chains attached to CotA based on the concentration of diblock copolymer added to enzymes that give the highest scattering intensity

In the table below the average number of PAA chains per CotA molecule is given, based on electroneutrality of the C3Ms at their PMC. Used data: the charge of $PM2VP_{128}$-*b*-PEO_{477} is about +93 (elementary units), for PAA_{47} and PAA_{118} the charge at pH 10.8 is –47 and –118 (elementary units), respectively, and the net charge of CotA at pH 10.8 is –41.[5,7,32]

Table S3.1. Estimation of PAA attached based on the preferred micellar composition (PMC)

No	Sample	[PM2VP-*b*-PEO] (μM)	(+) Charged PM2VP-*b*-PEO	(-) Charged PAA	(-) Charged CotA	[CotA-PAA] (μM)	Estimation of PAA attached
1.	CotA-PAA_{47} with ratio 1:2	1.75	90	47	41	1.5	1
2.	CotA-PAA_{47} with ratio 1:5	3.85	90	47	41	1.5	4
3.	CotA-PAA_{118} with ratio 1:2	5.25	90	118	41	1.5	2
4.	CotA-PAA_{118} with ratio 1:5	11.55	90	118	41	1.5	5

S3.3. Native agarose gel electrophoresis on fluorescent labeled enzymes

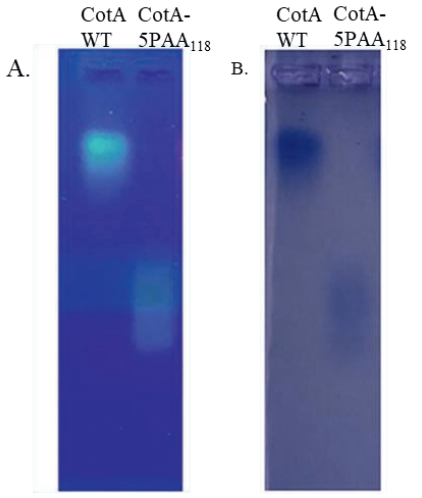

Figure S3.2. Native agarose gel electrophoresis on native CotA and CotA-5PAA$_{118}$ bioconjugated enzyme. (A) Observation under UV light, (B) after staining with Coomassie blue.

S3.4. Fractions of free enzyme and enzyme bound in C3Ms

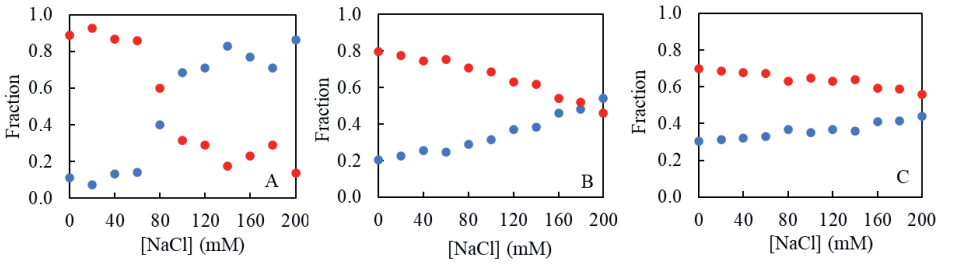

Figure S3.3. Fraction of enzyme encapsulated (red dots) and fraction of enzyme free in solution (blue dots) obtained by two-component FCS analysis. (A) Native CotA, (B) CotA-5PAA$_{47}$, and (C) CotA-5PAA$_{118}$.

S3.5. Determination of the critical micelle concentration (CMC) of CotA-containing C3Ms

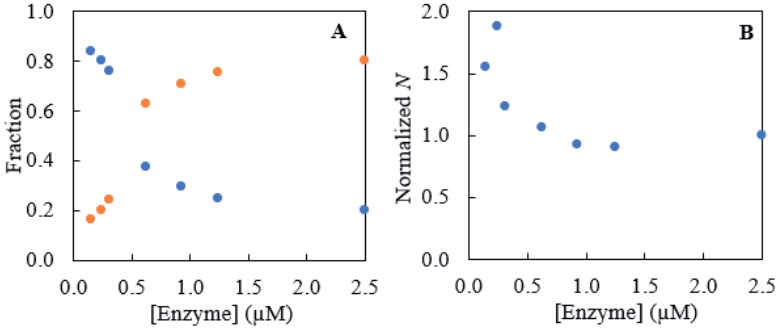

Figure S3.4. Determination of the critical micelle concentration (CMC) at the PMC as a function of enzyme concentration observed by using FCS. (A) Fraction of free enzyme (blue) and fraction encapsulated (orange). (B) Normalized number of fluorescent particles (*N*).

With FCS, the fluorescent particles can be detected at very low concentrations (nM range), allowing us to estimate the critical micelle concentration (CMC). Figure S2.6 shows that the C3Ms already appear above a concentration of 125 nM CotA-Alexa 488 with P2MVP$_{128}$-*b*-PEO$_{477}$, which we estimated as the CMC.

Chapter 4 :

Charged polypeptide tail boosts the salt resistance of enzyme-containing complex coacervate micelles

Published as:

Kembaren, R., Westphal A. H., Kamperman M., Kleijn, J. M., and Borst, J. W. Charged polypeptide tail boosts the salt resistance of enzyme-containing complex coacervate micelles. *Biomacromolecules* **23**, 1195–1204 (2022).

Abstract

Encapsulation of proteins can have advantages for their protection, stability, and delivery purposes. One of the options to encapsulate proteins is to incorporate them in complex coacervate core micelles (C3Ms). This can easily be achieved by mixing aqueous solutions of the protein and an oppositely charged-neutral hydrophilic diblock copolymer. However, protein-containing C3Ms often suffer from salt-inducible disintegration due to the low charge density of proteins. The aim of this study is to improve the salt stability of protein-containing C3Ms by increasing the net charge of the protein by tagging it with a charged polypeptide. As a model protein, we used CotA laccase and generated variants with 10, 20, 30, and 40 glutamic acids, respectively, attached at the C-terminus of CotA by using genetic engineering. Micelles were obtained by mixing the five CotA variants with poly(*N*-methyl-2-vinyl-pyridinium)-*block*-poly(ethylene oxide) ($PM2VP_{128}$-*b*-PEO_{477}) at pH 10.8. Hydrodynamic radii of the micelles of approximately 31 nm, 27 nm, and 23 nm for native CotA, CotA-E20, and CotA-E40, respectively, were determined using dynamic light scattering (DLS) and fluorescence correlation spectroscopy (FCS). The encapsulation efficiency was not affected using enzymes with a polyglutamic acid tail but resulted in more micelles with a smaller number of enzyme molecules per micelle. Furthermore, it was shown that the addition of a polyglutamic acid tail to CotA indeed resulted in improved salt stability of enzyme-containing C3Ms. Interestingly, the polyglutamic acid CotA variants showed an enhanced enzyme activity. This study demonstrates that increasing the net charge of enzymes through genetic engineering is a promising strategy to improve the practical applicability of C3Ms as enzyme delivery systems.

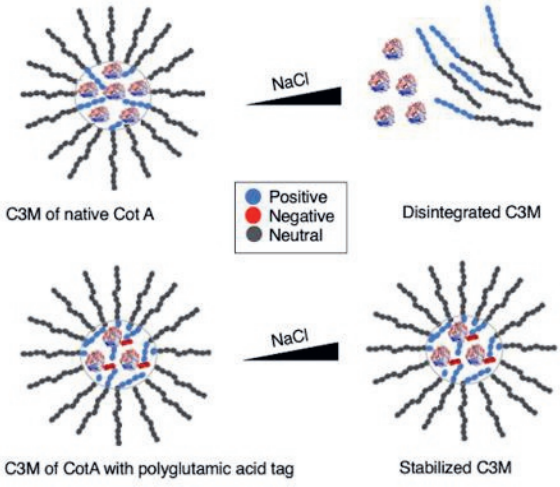

4.1. Introduction

Protein encapsulation can shield valuable proteins in denaturing or degrading environments, and also offers the possibility of targeted release, which is beneficial for many applications, especially for protein drug delivery. Many methods have been developed to encapsulate biomacromolecules and one of the most promising is the use of complex coacervate core micelles (C3Ms).[1–3] Encapsulation of proteins into C3Ms can be achieved by mixing a charged protein with a diblock copolymer, which has a counter-charged part and a neutral-hydrophilic part.[1,3–6] When these two components are mixed in a low ionic strength buffer solution, the oppositely charged parts bind electrostatically to form a complex coacervate core. The neutral-hydrophilic part of the diblock copolymer acts as shell/ corona that ensures that this core-shell structure remains soluble in an aqueous solution. The formation of C3Ms is also driven by the entropy gain upon release of counterions, which makes this packing system sensitive to high ionic strength. Therefore, a high salt environment will result in disintegration of protein-containing C3Ms. Since proteins have a pH-dependent charge, this packing system is also sensitive to pH.[1,6–10]

One way to improve the stability of protein-containing C3Ms is by increasing the net charge of the protein using post-translational chemical modification or genetic engineering.[9–15] Bioconjugation approaches allow the addition of negative charges to the protein, for example by coupling the protein with poly(acrylic acid) (PAA).[16,17] Acetylation of lysine residues using acetic anhydride has also been shown to result in protein variants with an increased negative charge.[18] However, this acetylation approach lacks bioconjugation specificity and results in heterogeneous labelling.[9] Alternatively, the net charge of proteins can be changed by the addition of a genetically engineered charged polypeptide tag at a specific site of the protein.[9,13,19,20] Genetic engineering thus allows to produce supercharged recombinant proteins with a high yield and with precise composition.[9] Kapelner and Obermeyer (2019) demonstrated that the addition of an anionic polypeptide tag at the C-terminus of green fluorescent protein (GFP) promoted coacervation at higher salt concentrations.[13]

The aim of this study is to improve the stability of protein-containing C3Ms by increasing the net charge of the protein by the addition of a charged polypeptide tag. Genetic engineering enables us to add tags or specific sequences after the start codon (N-terminus part of a protein) or before the stop codon (C-terminus part of a protein), or in exposed surface loops.[21] In comparison to N-terminus or loop tagging, introducing a tag at the C-terminus has generally less effect on protein folding and its biological function.[22,23] We used CotA laccase as a model

protein and added different polyglutamic acid tags at the C-terminus of the enzyme (Figure 4.1). C3Ms were formed in a buffer solution of pH 10.8. As described in our previous paper,[24] this pH was chosen to establish a sufficient negative charge on native CotA to form C3Ms and to eliminate the effect of the positively charged patch on its surface. The salt stability of differently charged CotA containing C3Ms was determined using dynamic light scattering (DLS) and fluorescence correlation spectroscopy (FCS). The enzyme activity of the various CotA variants was tested before and after encapsulation.

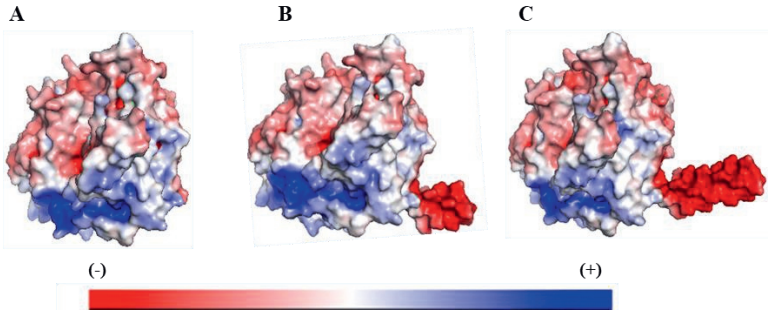

Figure 4.1. Comparison of electrostatic potentials at the molecular surface of three CotA variants. (A) Native CotA (CotA wild type), (B) CotA with additional 10 glutamic acids tags (CotA-E10), and (C) CotA with additional 20 glutamic acids tags (CotA-E20). Color surface overlay indicates the electrostatic potential in a scale from negative (red), neutral (white), and positive potential (blue). This figure was created by using the default parameters of the PyMOL APBS Tools plugin in PyMol_2.3.4 software.

4.2. Experimental section

4.2.1. Materials

The diblock copolymer poly(2-vinyl pyridine)$_{128}$-*block*-poly(ethylene oxide)$_{477}$ (P2VP$_{128}$-*b*-PEO$_{477}$) (M_n = 34.5 kg/ mol, M_w/ M_n = 1.1) was obtained from Polymer Source Inc. After quaternization with iodomethane,[25] the quaternization degree of this diblock copolymer was 73 % (measured by ^{1}H-NMR) (Figure S4.1, Supplementary information).[26] All primers for gene modification were obtained from Integrated DNA Technologies (IDT). DNA purification kits (miniprep, PCR purification, and gel purification) were purchased from Thermo Fisher Scientific. Lysogeny broth and agar medium for growth of *Escherichia coli* were purchased from Duchefa Biochemie. Columns for enzyme purification (SP-Sepharose FF, Q-Sepharose FF, Superdex 200, and Heparin Sepharose) were obtained from GE Healthcare. Alexa Fluor 488 C5 maleimide obtained from Thermo Fisher Scientific was used to fluorescently label the

CotA variants. To remove unreacted label, a Biogel-P6DG gel filtration column obtained from Bio-Rad was used. A Pierce bicinchoninic acid (BCA) protein assay kit for determination of total protein concentration was obtained from Thermo Fisher Scientific. The substrate 2,2′-azino-bis(3-ethylbenzothiazoline-6-sulfonic acid) diammonium salt (ABTS) for the activity assay was purchased from Sigma-Aldrich.

4.2.2. Modification of the CotA gene and cloning using the seamless ligation cloning extract (SLiCE) method

To clone the gene of our model protein, we used the SLiCE method. This method is based on *in vitro* recombination of short regions of homologies (about 15–52 base pairs overlap sequences between target DNA fragment and vector) in bacterial cell extracts. It is an easy and inexpensive cloning method compared to conventional cloning methods. The CotA gene was modified with primers, which contained an overlap part with the pBAD vector sequences and glutamic acid sequences of different lengths, i.e., 10 (CotA-E10), 20 (CotA-E20), 30 (CotA-E30), and 40 (CotA-E40). Native CotA was also mutated at position 313 where a serine was replaced by a cysteine (CotA-S313C). This mutation allows to specifically label the enzyme with Alexa Fluor 488 C5 maleimide. After the S313C mutation, this CotA gene was used as a template for additional glutamic acid tags with a length of 20 (CotA-S313C-E20) and 40 (CotA-S313C-E40). Agarose electrophoresis results show that the genetic engineering of CotA with several additional units of glutamic acids tags was successful (Figure S4.2, S4.3, and S4.4, Supplementary information). These modified genes were then cloned into the pBAD vector. The cloned genes were transformed in *Escherichia coli* DH5α and the bacteria were let to grow on ampicillin-containing Lysogeny broth (LB) media. After one day growing, colonies were checked by colony-PCR and the presence of correct inserts was confirmed by digestion of purified plasmids using restriction enzymes *Nde*I and *Hin*dIII. The positive plasmids were sent for sequencing to Macrogen Europe.

4.2.3. CotA Production and Purification

The CotA and modified CotA genes were transformed into *Escherichia coli* Rosetta cells. Single colonies were picked and grown overnight in LB medium containing 100 µg/mL ampicillin. The overnight culture was inoculated on 500 mL LB medium, and the cells were grown until an optical density of 0.6-0.8. CotA laccase expression was induced by adding 0.15% L-arabinose and 0.25 mM $CuSO_4$, and the cells were grown for 20 hours at 25 °C. For CotA-S313C, CotA-S313C-E20 and CotA-S313C-E40, the induction was done by only adding

0.15% L-arabinose (without copper salt solution) since copper can promote the oxidation of free sulfhydryl of the cysteine. Native CotA, CotA-S313C and CotA-E10 were purified using cation exchange chromatography (cIEX using an SP-Sepharose FF column) and gel filtration chromatography (Superdex 200 column). CotA-E20, CotA-E30, and CotA-S313C-E20 were purified using anion exchange chromatography (aIEX using a Q-Sepharose FF column) followed by gel filtration chromatography (Superdex 200 column). CotA-E40 and CotA-S313C-E40 were purified using anion exchange chromatography (aIEX using a Q-Sepharose FF column) followed by gel filtration chromatography (Superdex 200 column) and Heparin Sepharose column chromatography.

Specific fluorescence labeling of the enzyme was performed by mixing the enzyme with Alexa Fluor 488 C5 maleimide with a molar ratio of about 1:10 followed by incubation at 4 °C in the dark overnight. To remove the unreacted label, the mixture was loaded to a Biogel-P6DG gel filtration column using buffer 20 mM Tris HCl containing 10 mM NaCl. The fractions that showed fluorescence and contained protein were pooled and concentrated using a spin filter concentrator. Next, the labeled CotA was further purified on a gel filtration column (Superdex 200 column). The fractions that showed absorption at both 280 and 490 nm were collected and concentrated using a spin filter concentrator. The purity of CotA was analyzed by SDS-PAGE.

4.2.4. CotA activity measurement

We investigated the effect of polyglutamic acid tags on the CotA C-terminus by measuring the enzyme activity using 2,2′azino-bis-(3-ethylbenzothiazoline-6-sulphonic acid) (ABTS) as a substrate for the assay. The activity of the CotA variants before and after C3M formation has been measured. We used 1.0 mM ABTS in 100 mM sodium acetate buffer at pH 4.4. CotA will oxidize ABTS resulting in a green-colored cationic radical ($ABTS^{\bullet+}$), which can be detected by measuring the absorption at wavelength 420 nm ($\varepsilon = 36\,000\ M^{-1}\ cm^{-1}$). The relative activity was defined as the ratio between the specific activity of modified CotA and the specific activity of native CotA and expressed as a percentage.[27–29] The total protein concentration was determined using the BCA protein assay.

4.2.5. Formation of C3Ms containing CotA and CotA variants and determination of their salt stability

Enzyme solutions and solutions of the polymer $PM2VP_{128}$-*b*-PEO_{477} were prepared separately in a 10 mM sodium carbonate buffer at pH 10.8. All solutions were filtered through 0.2 µm poly(ether-sulfone) membrane syringe filters (Advanced Microdevices Pvt. Ltd). Mixtures of

these solutions were prepared with the same final enzyme concentration but increasing concentrations of the diblock copolymer and stored at room temperature overnight before measurement. The mixed ratio composition F^- is calculated by using the equation $F^- = \frac{[n^-]}{[n^+] + [n^-]}$, where n^- refers to the concentration of net negative charge on the enzyme molecules and n^+ refers to the positive charge concentration on the diblock copolymer. $PM2VP_{128}$-*b*-PEO_{477} has a charge of about +93 (elementary units). We used software PROPKA 3.1 to calculate the net charge of the various CotA variants from their three-dimensional structure (Figure S4.5, Supplementary information).[4,5] This resulted for native CotA laccase in buffer pH 10.8 in a net charge of about −41, while the genetically engineered CotA-E10, CotA-E20, CotA-E30, and CotA-E40 have net charges of about −51, −61, −71, and −81, respectively.

For salt stability determination, 4 M NaCl solution was titrated to solutions of enzyme-containing micelles, and the effect on the micelles was followed using dynamic light scattering (DLS) and fluorescence correlation spectroscopy (FCS). For the DLS and FCS measurements, (each n = 3) were performed and these measurements consisted of 10 repetitions of 10 s duration for DLS and 8 repetitions of 20 s duration for FCS. Each of these repetitions were composed of 10 measurements of 10 s for DLS and 8 measurements of 20 s for FCS were done. For FCS measurements, Alexa Fluor 488 labeled enzymes of native CotA, CotA-E20, and CotA-E40 were used. FCS data were analyzed with the software FFS data processor, version 2.3 (Scientific Software Technologies Software Centre, Belarus), using a 3D-diffusion including triplet state model.[4,5,24]

4.2.6. Dynamic light scattering

DLS was performed with an ALV-LSE 41/ CGS-8F goniometer instrument equipped with a DPSS laser operating at 660 nm, and the laser power used was 200 mW. Measurements of scattering intensity, hydrodynamic radius (R_h), and polydispersity index (PDI) were performed at a fixed scattering angle of 90°. The shape of the C3Ms was determined by using multi-angle DLS.

The principle of DLS is to measure the fluctuation of scattered light intensity which occurs when laser light hits the diffusing particles. This fluctuation of scattered light intensity depends on particle movement caused by Brownian motion.[30] Tracing this fluctuating intensity over time (t) enables us to plot a second-order autocorrelation function as shown in equation:

$$G_2(\tau) = \frac{\langle I(t)\rangle \, . \, I\,(t+\tau)\rangle}{\langle I(t)\rangle^2} \qquad (4.1)$$

where $I(t)$ is the time-dependent scattered light intensity. The field-correlation function of monodisperse particles can be described with an equation featuring the decay rate (Γ) and the passed time (τ):

$$G_1(q,\tau) = e^{-\Gamma\tau} \tag{4.2}$$

The relation of the decay rate (Γ) and the diffusion coefficient (D) is given by

$$\Gamma = q^2.D \tag{4.3}$$

where q is the wave vector, which is defined by the used wavelength (λ_0), the refractive index of the medium (n), and the detection angle (θ) according to the equation:

$$q = \frac{4\pi n}{\lambda_0}\sin\left(\frac{\theta}{2}\right) \tag{4.4}$$

The hydrodynamic radius (R_h) was calculated from the diffusion coefficient (D) obtained from the autocorrelation function by a cumulant fit method, and the Stokes−Einstein equation for spherical particles:

$$D = \frac{k_B T}{6\pi\eta R_h} \tag{4.5}$$

where k_B is the Boltzmann constant, T is the absolute temperature, and η is the viscosity of the solution. The polydispersity index (PDI) is a representation of the particle size heterogeneity in a sample and is in DLS usually calculated from the width at half height of the relevant peak in the particle size distribution using the equation:

$$\text{PDI} = \left(\frac{\text{width}}{\text{radius}}\right)^2 \tag{4.6}$$

where the radius is the mean hydrodynamic radii of the peak. Samples with a PDI of 0.0 - 0.1 are considered to be very monodisperse, while PDI values ranging from 0.1 - 0.4 indicate a moderate polydisperse sample and PDI values > 0.4 are indicative for highly polydisperse samples.[31]

4.2.7. Fluorescence correlation spectroscopy

FCS was performed using a Leica TCS SP8 X system equipped with a 63× 1.20 NA water immersion objective and a supercontinuum laser. CotA labeled with Alexa Fluor 488 was excited at 488 nm with a pulse frequency of 40 MHz. Fluorescence was detected between 495-550 nm using a hybrid detector coupled to a PicoHarp 300 TCSPC module (PicoQuant) with a pinhole setting of 1 Airy unit. FCS data were analyzed with software FFS-data processor

version 2.3 (Scientific Software Technologies Software Centre, Belarus), using a two-component 3D-diffusion model including triplet state.[32] Rhodamine 110 (diffusion coefficient 4.3 x 10^{-10} m^2s^{-1}) was used to determine the confocal structure *a* parameter ($a = \omega_z/\omega_{xy}$ with ω_{xy} and ω_z the equatorial and axial radii of the detection volume).

In FCS, the fluctuations in fluorescence intensity, resulting from fluorescent particles traversing the confocal detection volume, are recorded over time and used to calculate the autocorrelation function $G(t)$ as follows:

$$G(t) = \frac{\langle I(t)\rangle \cdot I(t+\tau)\rangle}{\langle I(t)\rangle^2} \tag{4.7}$$

where $I(t)$ is the time-dependent fluorescence intensity. After excitation of a fluorophore, transition from the singlet state to the triplet state (intersystem crossing) may occur. Relaxation from the triplet state to the ground state (microsecond time scale) can occur without emission of photons. This intersystem crossing may lead to an additional component in the autocorrelation function. In the following autocorrelation equation, the triplet state component is included:

$$G(t) = 1 + \frac{1}{\langle N\rangle} \cdot \left(1 + \frac{F_{trip}}{1-F_{trip}}\right) e^{-t/T_{trip}} \cdot \sum_{i=1}^{n} \frac{F_i}{\left(1+\frac{t}{\tau_{dif,i}}\right) \cdot \sqrt{1 + \left(\frac{\omega_{xy}}{\omega_z}\right)^2 \cdot \frac{t}{\tau_{dif,i}}}} \tag{4.8}$$

where $\langle N\rangle$ is the average number of fluorescent particles in the confocal volume, F_{trip} is the fraction of molecules in the triplet state, T_{trip} is the average time a fluorophore resides in the triplet state, F_i is the fraction of species *i*, $\tau_{dif,i}$ is the diffusion time of the species *i* in the confocal volume, and ω_{xy} and ω_z are the equatorial and axial radii of the detection volume, respectively. From the diffusion time, the diffusion coefficient *D* can be calculated using this equation:

$$D = \frac{\omega_{xy}^2}{4 \cdot \tau_{dif}} \tag{4.9}$$

Subsequently, from *D* the hydrodynamic radius of the fluorescent particle can be calculated using the Stokes-Einstein relation (Equation 4.5).

4.3. Results and discussion

4.3.1. CotA production and purification

The engineered CotA proteins were overexpressed in the *Escherichia coli* Rosetta strain and purified by a combination of ion exchange chromatography and size exclusion chromatography.

Figure 4.2 shows the results of an SDS-PAGE of the purified native CotA and the glutamic acid CotA variants. The purified CotA samples are 85-95 % pure (analyzed by using ImageJ software). The addition of polyglutamic acid tags resulted in a stepwise increase in molecular weight, more precisely from 65 kDa (native CotA) to 66.5 kDa (CotA-E10), 67.9 kDa (CotA-E20), 69.4 kDa (CotA-E30), and 70.9 kDa (CotA-E40). Moreover, the purified native CotA and glutamic acid CotA variants also show an intense blue color as a sign of incorporation of the copper ion (T1 Cu ion)[22,33] in the enzyme (Figure S4.6, Supplementary information). From these results, we conclude that the CotA variants are well expressed and purified.

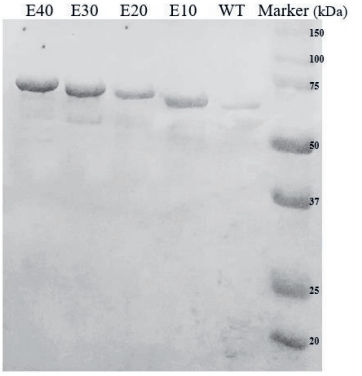

Figure 4.2. SDS-PAGE of purified CotA WT, CotA-E10, CotA-E20, CotA-E30 and CotA-E40.

4.3.2. Encapsulation of CotA and CotA variants in C3Ms

In this study, we encapsulated CotA and the higher charged CotA variants using a cationic-neutral hydrophilic diblock copolymer, $PM2VP_{128}$-*b*-PEO_{477}. For each CotA variant several mixed ratio compositions (F^-) were prepared with a constant concentration of enzyme and an increasing concentration of diblock copolymer. The different mixtures were analyzed with DLS (Figure 4.3). The negatively charged enzymes and the positively charged block of $PM2VP_{128}$-*b*-PEO_{477} bind electrostatically, which is the foundation to generate C3Ms.[1,4,6,34–36] When the charge ratio between enzyme and $PM2VP_{128}$-*b*-PEO_{477} is about equal, the number of C3Ms in solution is expected to be highest. This composition is known as the preferred micellar composition (PMC) and is manifested by a maximum in light scattering intensity. Figure 4.3 shows that the PMC for native CotA and all CotA variants is indeed observed at a mixing composition (F^-) of about 0.5.

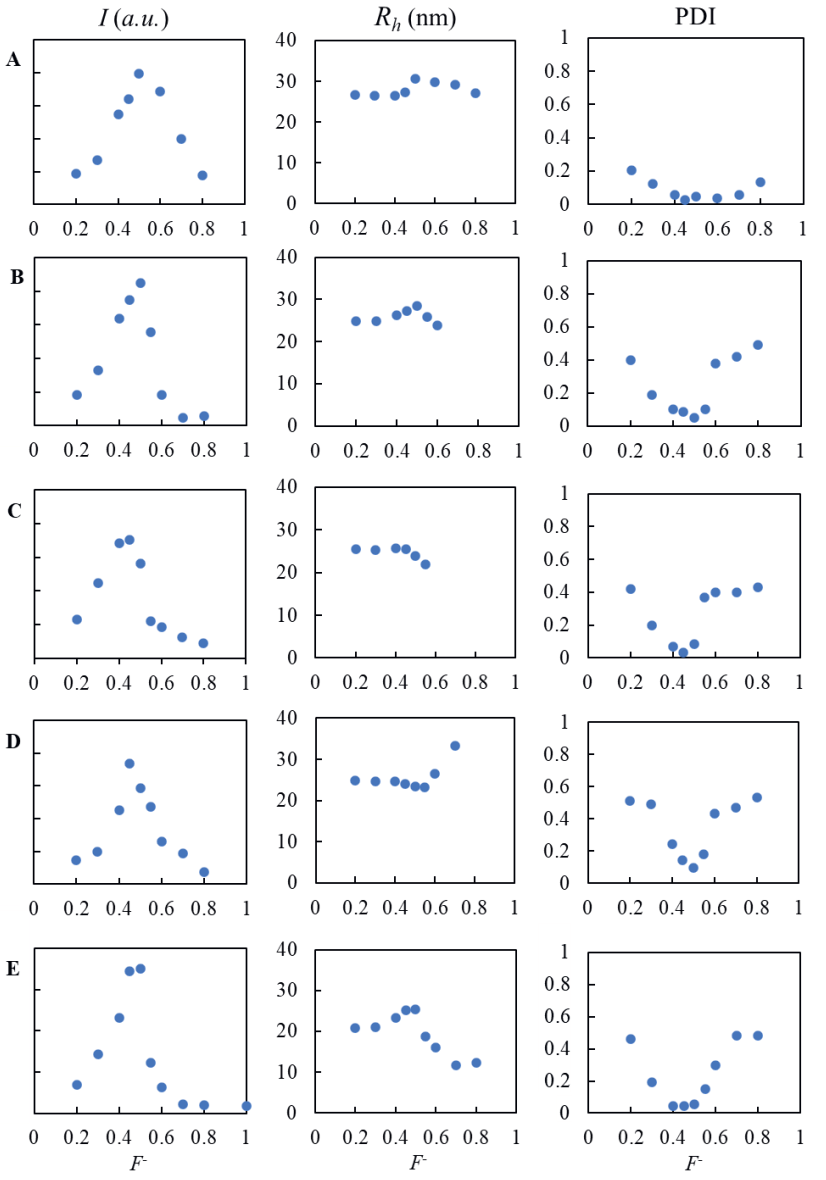

Figure 4.3. Light scattering intensity (*I*), hydrodynamic radius (R_h), and polydispersity index (PDI) for mixtures of different CotA variants with the diblock copolymer PM2PV$_{128}$-*b*-PEO$_{477}$ observed with DLS. (A) Native CotA, (B) CotA-E10, (C) CotA-E20, (D) CotA-E30, (E) CotA-E40. The maximum in light scattering intensity as a function of F^- corresponds to the preferred micellar composition (PMC).

At the PMC, the C3Ms containing native CotA have a hydrodynamic radius (R_h) of 32.0 ± 3.1 nm. For the C3Ms containing CotA with additional charges this is 31.2 ± 1.3 nm, 28.4 ± 1.3 nm, 25.9 ± 2.3 nm, and 25.4 ± 2.1 nm for CotA-E10, CotA-E20, CotA-E30, and CotA-E40, respectively. The decrease in micellar size with increasing charge on the enzyme probably results from the fact that less enzyme molecules are needed to neutralize the charge of the diblock molecules and therefore the number of CotA molecules within one micelle is lower. At the PMC, all C3Ms show a minimum in the polydispersity index (PDI) compared to other mixing compositions. This indicates a narrow size distribution of the C3Ms around the PMC. At other mixing compositions, charged soluble complexes have been formed, resulting in lower light scattering intensities and higher PDI values.[1,4–6,8,37,38]

We conducted multi-angle DLS to determine the shape of CotA containing C3Ms. If C3Ms have a spherical shape, multi-angle DLS will result in a linear relationship between the squared wave vector (q^2) and the decay rate (Γ).[39,40] Figure 4.4 shows the decay rate (Γ) of the first, second, and third cumulants as a function of the squared wave vector (q^2) on C3Ms composed of native CotA (Figure 4.4A) and CotA-E40 (Figure 4.4B). Three overlapping straight lines were obtained, indicating that from native CotA and CotA-E40 variants C3Ms with a spherical shape are formed.[39,40] Similar results were found for C3Ms composed of CotA-E10, CotA-E20 and CotA-E30 variants (Figure S4.7, Supplementary information).

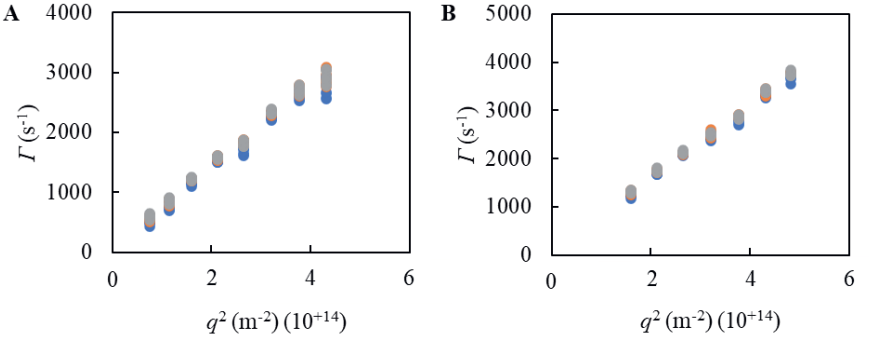

Figure 4.4. Multi-angle DLS results of C3M solutions containing (A) native CotA and (B) CotA-E40. The decay rate Γ obtained from the DLS correlation curves by a first (blue), second (orange), and third (gray) cumulant fit with squared wave vector q^2.

4.3.4. Higher charged CotA variants show improved C3M stability against salt

The addition of salt to a solution of enzyme-containing C3Ms will decrease the entropy gain of counterion release and at the same time will weaken the electrostatic interaction between the enzyme and polymer resulting in disintegration of micelles.[1,4–6,14,38,41,42] To reveal if the additional charges fused at the C-terminus of CotA affect C3M stability, we performed DLS measurements monitoring the scattering intensity versus salt concentration.

Figure 4.5A shows the scattering intensity, normalized to its value at zero added salt, against NaCl concentration for C3Ms composed of native CotA, CotA-E20 and CotA-E40 (see Figure S4.8 in Supplementary information for the results for all CotA variants). For C3Ms composed of native CotA, the addition of salt results in a faster decline of light scattering intensity compared to C3Ms composed of additionally charged CotA variants. At a concentration of 140 mM NaCl, the normalized scattering intensity is zero, meaning there are no native CotA-C3Ms present anymore. Increasing the negative charge of CotA results in an improved salt stability of the C3Ms. Notably, the more negative charge is added to CotA, the better the resistance of the C3Ms against salt.

Differences in salt stability of C3Ms containing CotA variants are also reflected by their difference in hydrodynamic radii (R_h) as a function of NaCl concentration. Figure 4.5B shows that the R_h of C3Ms composed of native CotA decreases significantly with increasing NaCl concentration. After the addition of 100 mM NaCl, the size of the micelles was reduced by about 25 %. However, for the higher charged CotA variants CotA-E20 and CotA-E40 the size of the C3Ms remained fairly constant (reduction about 3 %).

During the addition of NaCl to the C3Ms samples also an increase in PDI was observed, ranging from 0.1 at zero salt (monodisperse) to values above 0.4 (highly polydisperse) at 140 mM NaCl (Figure 4.5C). We observed that at the higher salt concentrations not only the particle size distributions were broadened, but that they also showed multiple peaks. These findings indicate disintegration of the micelles and release of the enzyme from the micellar cores. Cumulant fitting on such heterogeneous/ polydisperse samples may result in inaccurate R_h values.

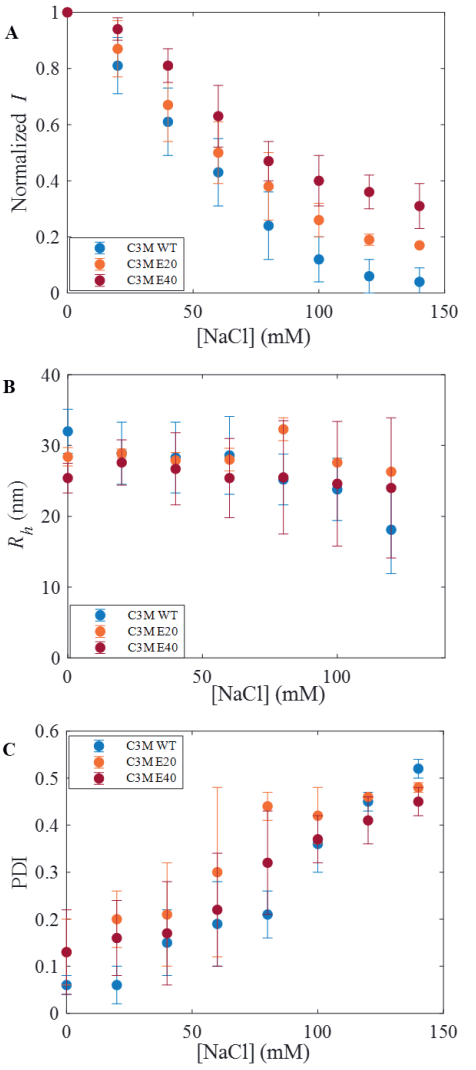

Figure 4.5. Salt stability of enzyme-containing C3Ms was observed by using DLS. (A) Normalized light scattering intensity (I), (B) hydrodynamic radius (R_h), (C) polydispersity index (PDI). C3Ms composed of native CotA (blue), CotA E-20 (orange), and CotA-E40 (dark red). Error bars represent the standard deviation from three repetitions (n = 3).

4.3.5. C3Ms formation and salt stability observed with FCS

Micelle formation and the effect of increasing the net charge of CotA on the salt stability of enzyme-containing C3Ms were also monitored by FCS. FCS and DLS are based on similar principles, but the main difference is the ability of FCS to discriminate between free enzymes

in solution and encapsulated enzymes. However, for FCS CotA needs to be labeled with a fluorescent probe, for which we used Alexa Fluor 488.

Figure 4.6 shows FCS measurements on solutions of free CotA and CotA encapsulated in C3Ms. It becomes clear that the addition of diblock copolymer to the CotA solution shifts the auto-correlation function to a higher diffusion time, indicating that the diffusion of enzymes becomes slower due to the formation of C3Ms (Figure 4.6D). Moreover, FCS allows to quantify the number of fluorescent species in the confocal volume indicated at the intercept of the Y-axis (Figure 4.6A-C). Encapsulation of CotA results in a decrease of the number of fluorescent particles detected in the confocal volume (*N*). Furthermore, the brightness of the micelles increases with the number of fluorescent CotA molecules encapsulated.[4,5,24,43]

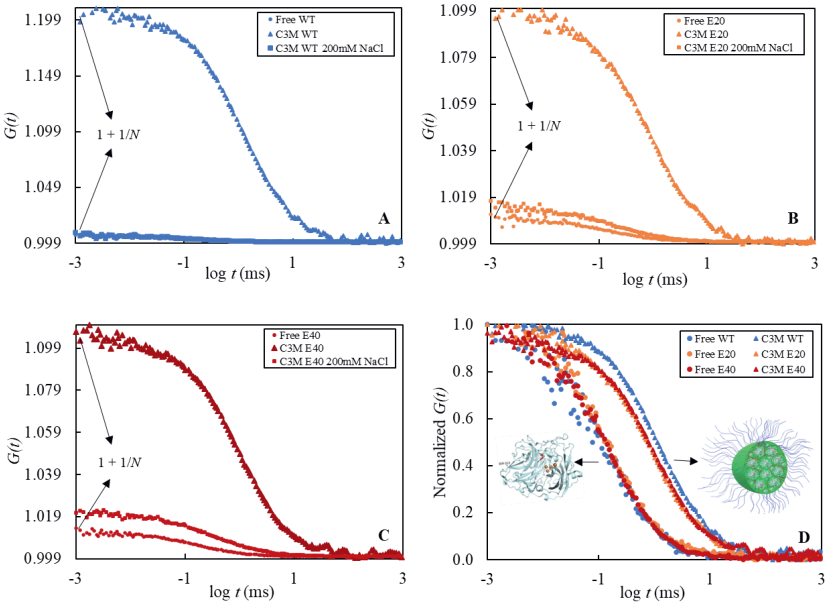

Figure 4.6. FCS measurements on C3Ms composed of labeled enzymes. FCS autocorrelation curves ($G(t)$) for: (A) Native CotA (blue), (B) CotA-E20 (orange), and (C) CotA-E40 (dark red). The spheres represent the free enzyme, the triangles represent enzyme-containing C3Ms, and the squares represent enzyme-containing C3Ms with an additional 200 mM NaCl. (D) Normalized $G(t)$ for free enzymes and C3Ms samples of native CotA and higher charged CotA variants.

The autocorrelation functions were analyzed using a two-component 3D diffusion model including triplet state (Equation 4.8). The fraction of encapsulated enzyme was found to be

about 77 ± 4 %, 77 ± 1 %, and 75 ± 7 % for native CotA, CotA-E20, and CotA-E40, respectively. These results show that the encapsulation efficiency for all enzymes is approximately the same. However, the concentration of C3Ms composed of the higher charged CotA variants is higher than that of the native CotA containing C3Ms, illustrated by the higher number of fluorescent particles detected in the confocal volume (*N*) (Table 4.1).

Furthermore, for native CotA free in solution, FCS analysis revealed a R_h of about 2.2 ± 0.3 nm, and for C3Ms containing native CotA a R_h of 30.5 ± 2.1 nm was obtained. Free CotA-E20 and CotA-E40 have a size of 3.5 ± 0.4 nm, and 3.1 ± 1.6 nm, respectively, whereas the R_h of micelles formed from CotA-E20 and CotA-E40 is 26.0 ± 1.3 nm and 22.3 ± 1.6 nm, respectively. Micellar sizes determined with FCS and DLS are in good agreement (Table 4.1). In conclusion, more charge added to CotA results in a higher concentration of micelles of smaller size, while the encapsulation efficiency is not significantly affected.

Table 4.1. Characterization of C3Ms by FCS and DLS

Sample	*N* (FCS)	Fraction encapsulated (FCS)	R_h (nm) (FCS)	R_h (nm) (DLS)
C3M Native CotA	4.9 ± 0.1	77 ± 4 %	30.5 ± 2.1	32.0 ± 3.1
C3M CotA-E20	6.5 ± 3.6	77 ± 1 %	26.0 ± 1.3	28.4 ± 1.3
C3M CotA-E40	10.7 ± 1.5	75 ± 7 %	22.3 ± 1.6	25.4 ± 2.1

Error margins represent the standard deviation from three repetitions (n = 3)

FCS was also used to monitor the salt stability of CotA containing C3Ms. This was done by quantifying the total number of fluorescent particles in the confocal volume (*N*) as a function of NaCl concentration. Figure 4.7A shows that *N,* normalized to the number of particles detected in a solution of free CotA with the same protein concentration as the C3M systems, increases with salt concentration, which indicates the release of CotA from the core of the micelles. These results clearly show that native CotA is released at a lower salt concentration from the micelles than the higher charged CotA variants. Native CotA-containing micelles reached a normalized *N* of 1.0 above 80 mM salt, pointing to a total disintegration of the micelles. For micelles containing CotA-E20 and CotA-E40, *N* increased much more gradually compared to micelles containing native CotA, and these C3Ms do not completely fall apart even at the highest salt concentration applied. In addition, the more negative charge is added to CotA, the better the resistance of the C3Ms against salt.

Figure 4.7B shows the hydrodynamic radius (R_h) of the various C3Ms as a function of NaCl concentration. The R_h of C3Ms composed of native CotA decreases significantly more

with increasing NaCl concentration than the R_h of C3Ms composed of the higher charged CotA variants: after addition of 100 mM NaCl, the size of the native CotA micelles was decreased by about 64 %, while the reduction in R_h for CotA-E20 and CotA-E40 was about 29 % and 33 %, respectively. These FCS measurements confirm the conclusions from the DLS measurements that the addition of polyglutamic acid tags to CotA results in improved salt stability of CotA-containing C3Ms, and that the salt stability of the C3Ms increases with increasing charge on the CotA variants.

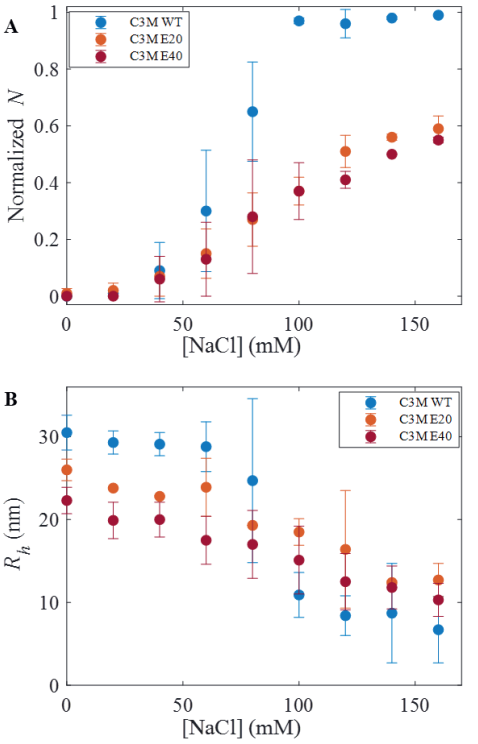

Figure 4.7. Salt stability of enzyme-containing C3Ms was observed by using FCS. (A) Normalized number of fluorescent particles in the confocal volume (N), (B) hydrodynamic radius (R_h). C3Ms composed of native CotA (blue), CotA E-20 (orange), and CotA-E40 (dark red). Error bars represent the standard deviation from three repetitions (n = 3).

Quenching of fluorescence upon enzyme encapsulation was observed by a reduced fluorescence intensity (Figure S4.9, Supplementary information).[4,5,7] However, this quenching has no implication for the present study, since we use only the number of fluorescent objects (C3Ms and free protein) in the confocal volume and their diffusion times to calculate their hydrodynamic size.

4.3.6. Comparison of FCS and DLS results

Although the DLS and FCS results show the same trends and lead to the same conclusions, there are quantitative differences in the values obtained for the mean hydrodynamic radius R_h. As long as the particle size distribution in the samples is relatively narrow (before the addition of salt), FCS and DLS measurements on R_h are in good agreement (Table 4.1). However, after the addition of salt the results start to deviate. Especially above a concentration of 50 mM NaCl the R_h values obtained from FCS clearly decrease faster with the addition of salt than those obtained with DLS. Under these conditions, we are dealing with a mixture of free enzyme molecules, C3Ms and/ or soluble complexes. Thus, with the addition of salt a broadening of the particle size distribution and the development of multiple peaks takes place, reflected in increasing PDI values. These changes in the particle size distribution can explain the observed deviations in R_h values from DLS and FCS as follows. In DLS the scattered intensity of small particles (i.e., the free enzymes) is negligible with respect to that of the larger particles (C3Ms and soluble complexes), so the calculated R_h value is dominated by the contribution of the C3Ms and soluble complexes.[28,41] On the other hand, in FCS every fluorescent particle in the confocal volume contributes equally to the determination of the average diffusion time and thus to the mean hydrodynamic radius (see Equations 4.5, 4.8, and 4.9). This leads to lower R_h values than those following from the DLS analysis.[30,41] Hirschle et al. also observed larger average particle sizes by using DLS compared to FCS on broader size distribution samples.[28] Moreover, at very low scattered light intensities, R_h determination using DLS becomes inaccurate. Overall, the R_h results of FCS are considered more reliable.

Finally, we note that the deviations in the R_h values may be also partly due to the different fitting models used in DLS and FCS. In DLS, the autocorrelation function was fitted using the cumulant method, while in FCS the autocorrelation function was fitted using a two-components model.

4.3.7. The effect of genetic modification and encapsulation on the activity of CotA

Enzyme activity measurements were conducted to evaluate whether the addition of charged amino acids influences the enzyme function. Here, CotA activity measurements were done with the substrate ABTS (for details see experimental section). Figure 4.8 shows a relative activity histogram for native CotA and CotA variants free in solution as well as after being encapsulated in C3Ms. The activity of native CotA free in solution is set to 100 %. Remarkably, the higher charged CotA variants showed significantly higher activities than native CotA: their relative activities amount to about 170 ± 1.1 %, 140 ± 0.5 %, 140 ± 0.5 % and 160 ± 1 % for CotA-E10,

CotA-E20, CotA-30, and CotA-40, respectively. A possible explanation for the enhanced activity of the charged variants is the improvement of their solubility.[10,45,46] Han et al. also found an increased solubility and catalytic activity of several enzymes (tyrosine ammonia lyase, aldehyde dehydrogenase, and 1-deoxy-D-xylulose-5-phosphate synthase) after the addition of short polyglutamic acid tags.[10]

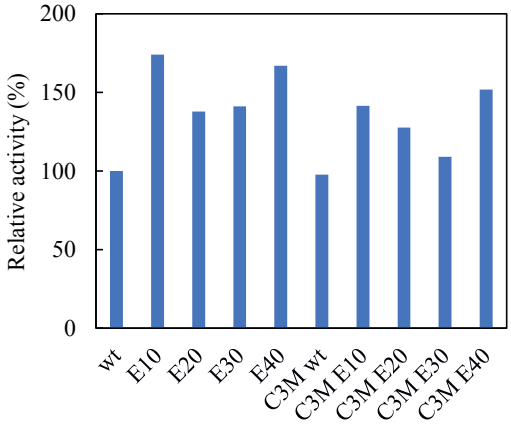

Figure 4.8. Activity measurement of native CotA (CotA-WT), CotA-E10, CotA-E20, CotA-E30, and CotA-E40 and its C3Ms.

Next, we aimed at measuring the activity of CotA when encapsulated in C3Ms also with the substrate ABTS. However, this was not possible since the ABTS assay procedure involves a low pH buffer (pH 4.4), resulting in a positive net charge on the enzyme (pI at pH 5.84 for native CotA) and therefore disintegration of the C3Ms. C3Ms composed of higher charged CotA variants also disintegrate at this pH (Figure S4.10, Supplementary information). Figure 4.8 shows that encapsulation and subsequent release in the ABTS assay buffer does not affect the activity of native CotA. For the higher charged CotA variants the activity decreases somewhat as a result of encapsulation and pH induced release, but it is still higher than that of native CotA free in solution.

4.4. Conclusions

In this study we produced variants of CotA that have polyglutamic acid tags of different lengths at the C-terminus. These polyglutamic acid tags contribute to a higher negative charge of the enzyme and are therefore expected to increase the salt stability of C3Ms containing the enzyme. DLS measurements revealed that for all CotA variants the PMC for C3M formation with the

cationic-neutral hydrophilic diblock copolymer PM2PV$_{128}$-*b*-PEO$_{477}$ is at a mixing composition (F^-) of about 0.5. FCS measurements showed that increasing the net charge of CotA results in the formation of more C3Ms, but with a lower number of CotA molecules within one micelle. The overall encapsulation of the native and modified enzymes was approximately the same, i.e., 75 – 77 % of the enzyme molecules were incorporated in the micelles. DLS and FCS measurements confirmed that C3Ms composed of CotA with additional charges are significantly more salt-resistant than native CotA-containing micelles. The more extra charge is added to the CotA, the better the salt stability of C3Ms. Furthermore, it was found that adding a polyglutamic tag to the enzyme enhances its activity, which is largely maintained upon encapsulation and pH induced release from the C3Ms. This study therefore shows that increasing the net charge of enzymes by genetic engineering is a promising strategy to improve the practical applicability of C3Ms as enzyme delivery systems.

References

1. Voets, I. K., de Keizer, A. and Cohen Stuart, M. A. Complex coacervate core micelles. *Adv. Colloid Interface Sci.* **147–148**, 300–318 (2009).
2. Blocher, W. C. and Perry, S. L. Complex coacervate-based materials for biomedicine. *Wiley Interdiscip. Rev. Nanomedicine Nanobiotechnology* **9**, 76–78 (2017).
3. Blocher McTigue, W. C. and Perry, S. L. Protein encapsulation using complex coacervates: what nature has to teach us. *Small* **16**, 1–17 (2020).
4. Nolles, A., Westphal, A. H., de Hoop, J. A., Fokkink, R. G., Kleijn, J. M., van Berkel, W. J. H., and Borst, J. W. Encapsulation of GFP in complex coacervate core micelles. *Biomacromolecules* **16**, 1542–1549 (2015).
5. Nolles, A., Westphal, A. H., Kleijn, J. M., van Berkel, W. J. H. and Borst, J. W. Colorful packages: Encapsulation of fluorescent proteins in complex coacervate core micelles. *Int. J. Mol. Sci.* **18**, 1557-1576 (2017).
6. Lindhoud, S., de Vries, R., Norde, W. and Stuart, M. A. C. Structure and stability of complex coacervate core micelles with lysozyme. *Biomacromolecules* **8**, 2219–2227 (2007).
7. Nolles, A., Hooiveld, E., Westphal, A. H., van Berkel, W. J. H., Kleijn, J. M., and Borst, J. W. FRET Reveals the formation and exchange dynamics of protein-containing complex coacervate core micelles. *Langmuir* **34**, 12083–12092 (2018).
8. Lindhoud, S., De Vries, R., Schweins, R., Cohen Stuart, M. A. and Norde, W. Salt-induced release of lipase from polyelectrolyte complex micelles. *Soft Matter* **5**, 242–250 (2009).
9. Ma, C., Malessa, A., Boersma, A. J., Liu, K. and Herrmann, A. Supercharged Proteins and Polypeptides. *Adv. Mater.* **32**, 1905309-1905330 (2020).
10. Han, X., Ning, W., Ma, X., Wang, X. and Zhou, K. Improving protein solubility and activity by introducing small peptide tags designed with machine learning models. *Metab. Eng. Commun.* **11**, 138-147 (2020).
11. Obermeyer, A. C., Mills, C. E., Dong, X. H., Flores, R. J. and Olsen, B. D. Complex coacervation of supercharged proteins with polyelectrolytes. *Soft Matter* **12**, 3570–3581 (2016).
12. Cummings, C. S. and Obermeyer, A. C. Phase Separation Behavior of Supercharged Proteins and Polyelectrolytes. *Biochemistry* **57**, 314–323 (2018).
13. Kapelner, R. A. and Obermeyer, A. C. Ionic polypeptide tags for protein phase separation. *Chem. Sci.* **10**, 2700–2707 (2019).
14. van der Gucht, J., Spruijt, E., Lemmers, M. and Cohen Stuart, M. A. Polyelectrolyte complexes: Bulk phases and colloidal systems. *J. Colloid Interface Sci.* **361**, 407–422 (2011).
15. Obermeyer, A. C. and Olsen, B. D. Synthesis and application of protein-containing block copolymers. *ACS Macro Lett.* **4**, 101–110 (2015).
16. Collins, J., Tanaka, J., Wilson, P., Kempe, K., Davis, T. P., McIntosh, M. P., Whittaker, M. R., and Haddleton, D. M. In situ conjugation of dithiophenol maleimide polymers and oxytocin for stable and reversible polymer-peptide conjugates. *Bioconjug. Chem.* **26**, 633–638 (2015).
17. Di Marco, M., Razak, K. A., Aziz, A. A., Shamsuddin, S., Devaux, C., Borghi, E., Levy, L., and Sadun, C. Overview of the main methods used to combine proteins with nanosystems : absorption , bioconjugation , and encapsulation. *Int. J. Nanomedicine* **5**, 37–49 (2010).
18. Shaw, B. F., Arthanari, H., Narovlyansky, M., Durazo, A., Frueh, D. P., Pollastri, M. P., Lee, A., Bilgicer, B., Gygi, S. P., Wagner, G., and Whitesides, G. M. Neutralizing positive charges at the surface of a protein lowers its rate of amide hydrogen exchange without altering its structure or increasing its thermostability. *J. Am. Chem. Soc.* **132**, 17411–17425 (2010).
19. Sun, J., Xiao, L., Li, B., Zhao, K., Wang, Z., Zhou, Y., Ma, C., Li, J., Zhang, H., Hermann, A., and Liu, K. Genetically Engineered Polypeptide Adhesive Coacervates for Surgical Applications. *Angew. Chemie - Int. Ed.* **60**, 23687–23694 (2021).
20. Li, J., Li, B., Sun, J., Ma, C., Wan, S., Li, Y., Göstl, R., Herrmann,A., Liu, K.,Zhang, H. Engineered Near-Infrared fluorescent protein assemblies for robust bioimaging and therapeutic applications. *Adv. Mater.* **32**, 2000964-2000971 (2020).
21. Kanca, O., Bellen, H. J. and Schnorrer, F. Gene tagging strategies to assess protein expression, localization, and function in Drosophila. *Genetics* **207**, 389–412 (2017).
22. Booher, K. R. and Kaiser, P. A PCR-based strategy to generate yeast strains expressing endogenous levels of amino-terminal epitope-tagged proteins. *Biotechnol. J.* **3**, 524–529 (2008).
23. Wang, Q., Xue, H., Li, S., Chen, Y., Tian, X., Xu, X., Xiao, W., Fu, Y. V. A method for labeling proteins with tags at the native genomic loci in budding yeast. *PLoS One* **12**, 1–15 (2017).
24. Kembaren, R., Fokkink, R., Westphal, A. H., Kamperman, M., Kleijn, J. M., and Borst, J. W. Balancing enzyme encapsulation efficiency and stability in complex coacervate core micelles. *Langmuir* **36**, 8494–8502 (2020).

25. Lindhoud, S., Norde, W. and Cohen Stuart, M. A. Effects of polyelectrolyte complex micelles and their components on the enzymatic activity of lipase. *Langmuir* **26**, 9802–9808 (2010).
26. Fulmer, G. R., Miller, A. J. M., Sherden, N. H., Gottlieb, H. E., Nudelman, A., Stoltz, B. M., Bercaw, J. E., and Goldberg, K. I. NMR chemical shifts of trace impurities: Common laboratory solvents, organics, and gases in deuterated solvents relevant to the organometallic chemist. *Organometallics* **29**, 2176–2179 (2010).
27. Huang, J., Xiao, H., Li, B., Wang, J. and Jiang, D. Immobilization of *Pycnoporus sanguineus* laccase on copper tetra-aminophthalocyanine–Fe3O4 nanoparticle composite. *Biotechnol. Appl. Biochem.* **44**, 93-100 (2006).
28. Kolomytseva, M. P., Myasoedova, N. M., Chernykh, A. M., Gaidina, A. S., Shebanova, A. D., Baskunov, B. P., Aschenbrenner, J., Rosengarten, J. F., Renfeld, Z. V., Gasanov, N. B., Pinchuk, I. P., Classen, T., Pietruszka, J., and Golovleva, L. A. Laccase isoform diversity in *basidiomycete Lentinus strigosus* 1566: Potential for phenylpropanoid polymerization. *Int. J. Biol. Macromol.* **137**, 1199–1210 (2019).
29. Xu, H. M., Sun, X. F., Wang, S. Y., Song, C. and Wang, S. G. Development of laccase/graphene oxide membrane for enhanced synthetic dyes separation and degradation. *Sep. Purif. Technol.* **204**, 255–260 (2018).
30. Hirschle, P., Preiß, T., Auras, F., Pick, A., Volkner, J., Valdeperez, D., Witte, G., Parak, W. J., Radler, J. O., Wuttke, S. Exploration of MOF nanoparticle sizes using various physical characterization methods-is what you measure what you get? *CrystEngComm* **18**, 4359–4368 (2016).
31. Bhattacharjee, S. Review article DLS and zeta potential – What they are and what they are not ? *J. Control. Release* **235**, 337–351 (2016).
32. Skakun, V. V., Hink, M. A., Digris, A. V., Engel, R., Novikov, E. G., Apanasovich, V. V., and Visser, A. J. W. G. Erratum: Global analysis of fluorescence fluctuation data. *Eur. Biophys. J.* **34**, 972 (2005).
33. Durão, P., Chen, Z., Fernandes, A. T., Hildebrandt, P., Murgida, D. H., Todorovic, S., Pereira, M. M., Melo, E. P., and Martins, L. O. Copper incorporation into recombinant CotA laccase from *Bacillus subtilis*: Characterization of fully copper loaded enzymes. *J. Biol. Inorg. Chem.* **13**, 183–193 (2008).
34. Cohen Stuart, M. A., Besseling, N. A. M. and Fokkink, R. G. Formation of micelles with complex coacervate cores. *Langmuir* **14**, 6846–6849 (1998).
35. Olijve, L. L. C. and Voets, I. K. Morphological evolution of complex coacervate core micelles revealed by iPAINT microscopy. **107**, 450–455 (2016).
36. Magana, J. R., Sproncken, C. C. M. and Voets, I. K. On complex coacervate core micelles: Structure-function perspectives. *Polymers* **12**, 1953-1990 (2020).
37. Lindhoud, S., Norde, W. and Stuart, M. A. C. Reversibility and relaxation behavior of polyelectrolyte complex micelle formation. *J. Phys. Chem. B* **113**, 5431–5439 (2009).
38. Van der Kooij, H. M., Spruijt, E., Voets, I. K., Fokkink, R., Cohen Stuart, M. A., and van der Gucht, J. On the stability and morphology of complex coacervate core micelles: From spherical to wormlike micelles. *Langmuir* **28**, 14180–14191 (2012).
39. Harada, A. and Kataoka, K. Chain length recognition: core-shell supramolecular assembly from oppositely charged block copolymers. *Science* **283**,65−67 (1999).
40. Harada, A. and Kataoka, K. Novel polyion complex micelles entrapping enzyme molecules in the core. 2. Characterization of the micelles prepared at nonstoichiometric mixing ratios. *Langmuir* **15**, 4208–4212 (1999).
41. Shah, S. and Leon, L. Structural dynamics, phase behavior, and applications of polyelectrolyte complex micelles. *Curr. Opin. Colloid Interface Sci.* **53**, 101424 (2021).
42. Heo, T. Y., Kim, I., Chen, L., Lee, E., Lee, S., and Choi, S. H. Effect of ionic group on the complex coacervate core micelle structure. *Polymers* **11**, 16–19 (2019).
43. Elson, E. L. Fluorescence correlation spectroscopy: Past, present, future. *Biophys. J.* **101**, 2855–2870 (2011).

Supplementary information

S4.1. ^{1}H NMR spectrum of the quaternized diblock copolymer

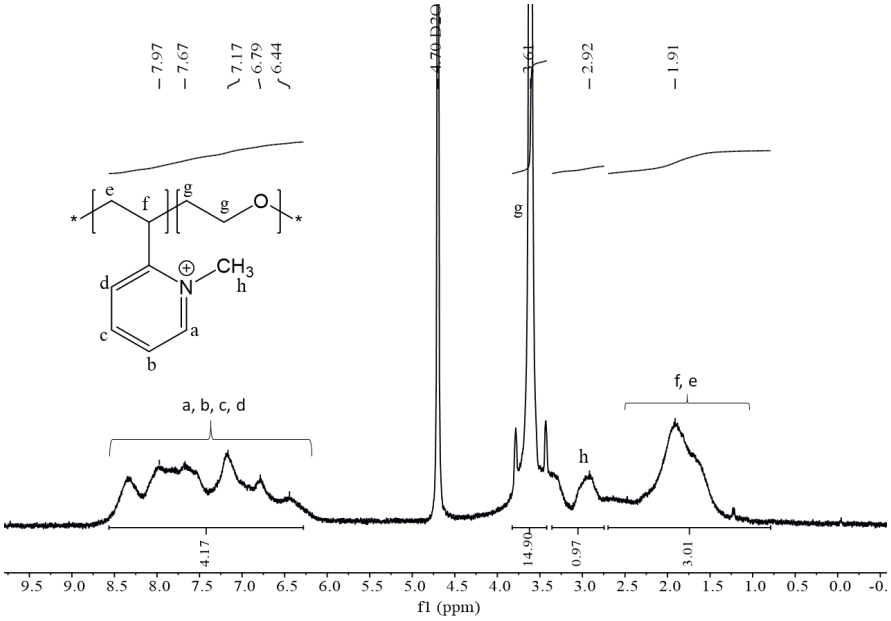

Figure S4.1. ^{1}H-NMR spectrum of PM2PV$_{128}$-*b*-PEO$_{477}$ was recorded in D_2O. The degree of quaternization (DQ) was calculated by comparing the sum integral of the pyridine ring peak with that of the methyl group.

DQ = ((4.17 + 0.97) / (4+3)) *100 % = 73 %.

S4.2. Primer sequences for cloning

Primers that were used to add polyglutamic acid tags were purchased from IDT. For PCR, the template that has been used is the native CotA gene. The primer sequences used are listed below:

a. **Forward primer (for all engineered CotA): CotA-N-forward 5'-**
GGCTAACAGGAGGAATTACATATGACACTTGAAAAATTTGTGGATGCTC

b. **Reverse primer for native CotA: CotA-wt-rev 5'-**
GAGTTTTTGTTCGGGCCCAAGCTTTTATTTATGGGGATCAGTTATATCCATCGG

c. **Reverse primer for CotA-E10: CotA-E10-rev 5'-**
GAGTTTTTGTTCGGGCCCAAGCTTTTATTCCTCTTCTTCCTCTTCTTCCTCTTCTTCT
TTATGGGGATCAGTTATATCCATCGG

d. **Reverse primer for CotA-E20: CotA-E20-rev 5'-**
GAGTTTTTGTTCGGGCCCAAGCTTTTATTCTTCCTCTTCTTCCTCTTCTTCCTCTTCT
TCCTCTTCTTCCTCTTCTTCCTCTTCTTCTTTATGGGGATCAGTTATATCCATCGG

e. **Reverse primer for CotA-E30: CotA-E30-rev 5'-**
GAGTTTTTGTTCGGGCCCAAGCTTTTACTCTTCTTCCTCTTCTTCCTCTTCTTCCTCT
TCTTCCTCTTCTTCCTCTTCTTCCTCTTCTTCCTCTTCTTCCTCTTCTTCCTCTTCTTC
TTTATGGGGATCAGTTATATCCATCGG

f. **Reverse primer for CotA-E40: CotA-E40-rev 5' –**
GAGTTTTTGTTCGGGCCCAAGCTTTTATTCCTCTTCTTCCTCTTCTTCCTCTTCTTCC
TCTTCTTCCTCTTCTTCCTCTTCTTCCTCTTCTTCCTCTTCTTCCTCTTCTTCCTCTTC
TTCCTCTTCTTCCTCTTCTTCCTCTTCTTCTTTATGGGGATCAGTTATATCCATCGG

S4.3. Agarose gel electrophoresis

CotA-E10

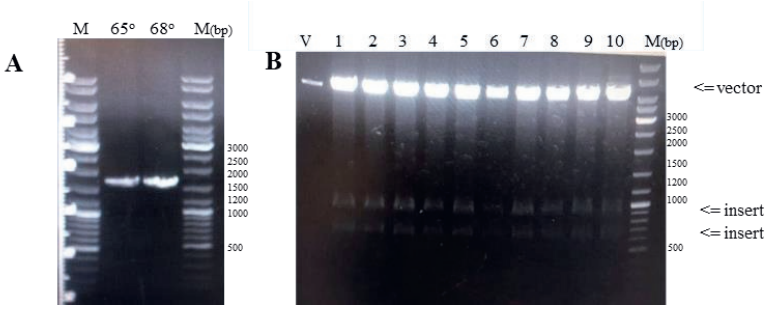

Figure S4.2. Agarose gel electrophoresis results for CotA-E10. (A) After running PCR, (B) after digestion using restriction enzymes *Nde*I and *Hin*dIII on the isolated plasmid after cloning and transformation. V is vector, M are markers.

Figure S4.2A shows the successful modification of the CotA with 10 additional glutamic acid residues by PCR using annealing temperatures of 65 ºC or 68 ºC. Figure S4.2B shows that 10 randomly selected *E. coli* colonies contain the inserted gene of CotA-E10.

CotA-E20

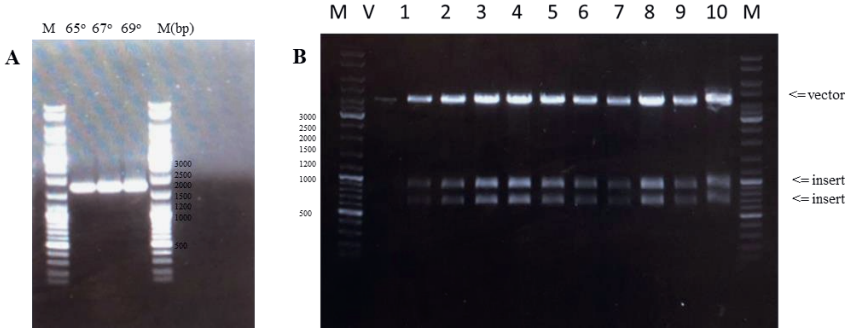

Figure S4.3. Agarose gel electrophoresis results for CotA-E20. (A) After running PCR, (B) after digestion using restriction enzymes *Nde*I and *Hin*dIII on the isolated plasmid after cloning and transformation. V is vector, M are markers.

Figure S4.3A shows the successful modification of the CotA with 20 additional glutamic acid residues by PCR using annealing temperatures of 65 ºC or 67 ºC or 69 ºC. Figure S4.3B shows that 10 randomly selected *E. coli* colonies contain the inserted gene of CotA-E20.

CotA-E40

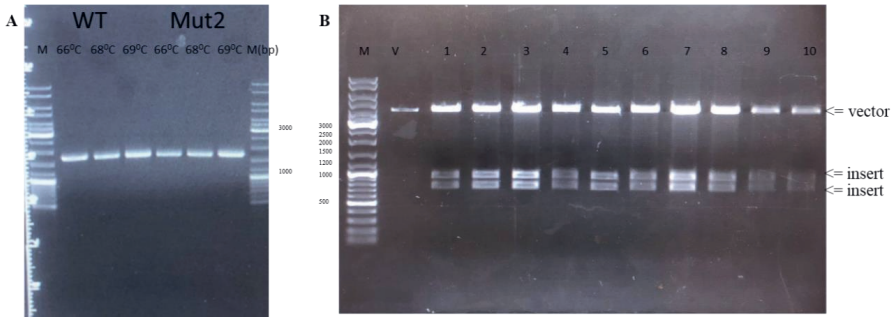

Figure S4.4. Agarose gel electrophoresis results for CotA-E40. (A) After running PCR, (B) after digestion using restriction enzymes *Nde*I and *Hin*dIII on the isolated plasmid after cloning and transformation. V is vector, M are markers.

Figure S4.5A shows the successful modification of the CotA with 40 additional glutamic acid residues by PCR using annealing temperatures of 66 ºC or 68 ºC or 69 ºC. Figure S4.4B shows that 10 randomly selected *E. coli* colonies contain the inserted gene of CotA-E40.

S4.4. Calculated charge of CotA as a function of pH

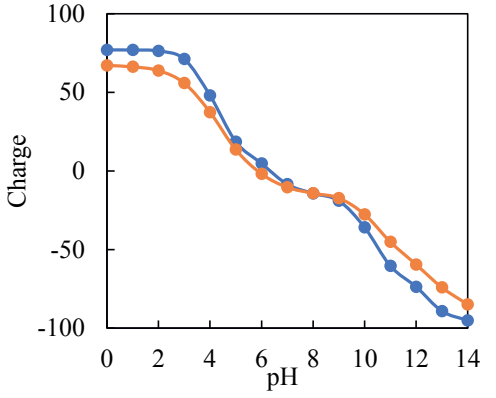

Figure S4.5. Charge of CotA as a function of pH calculated by using the PROPKA 3.1 software package. Blue dots and line represent the unfolded state of CotA, and orange dots and line represent the folded state of CotA.

S4.5. Color of the solutions of purified native CotA and the glutamic acid CotA variants

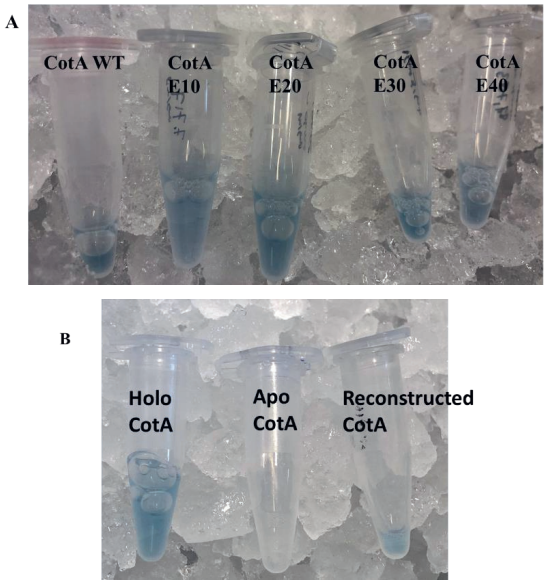

Figure S4.6. The color of the enzyme solutions: (A) the purified native CotA and the glutamic acid CotA variants (CotA-E10, CotA-E20, CotA-30, and CotA-E40). (B) holoprotein, apoprotein and reconstructed protein. The blue color (absent in apo CotA) is a sign of the copper ion (T1 Cu ion) incorporated in the protein resulting in active enzyme.

S4.6. DLS multi-angle results on C3Ms containing higher charged enzyme variants

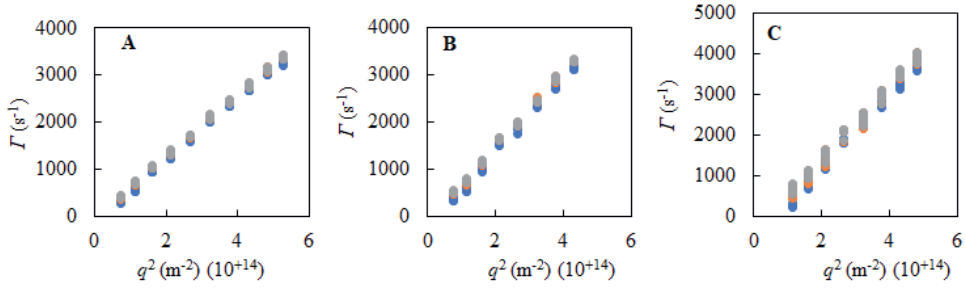

Figure S4.7. Multi-angle DLS results of C3M solutions containing (A) CotA-E10, (B) CotA-E20, (C) CotA-E30. The decay rate Γ obtained from the DLS correlation curves by a first (blue), second (orange), and third (gray) cumulant fit with squared wave vector q^2.

S4.7. DLS results on salt stability of enzyme-containing C3Ms for all C3Ms samples

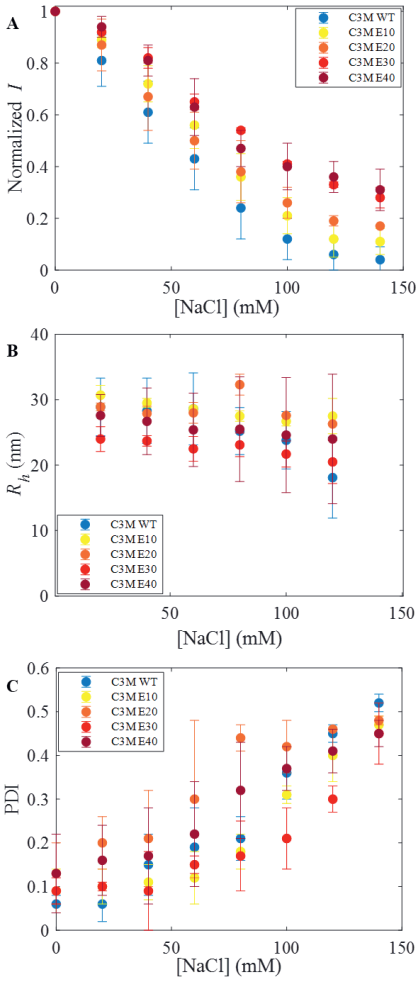

Figure S4.8. Salt stability of enzyme-containing C3Ms observed by using DLS. (A) Normalized light scattering intensity (I), (B) hydrodynamic radius (R_h), (C) polydispersity index (PDI). C3Ms composed of native CotA (blue), CotA E-10 (yellow), CotA E-20 (orange), CotA E-30 (red), and CotA-E40 (dark red). Error bars represent the standard deviation from three repetitions (n = 3), and for each of these repetitions the result was the average of 10 measurements of 10 seconds.

S4.8. Fluorescence spectra of labeled enzymes free in solution and encapsulated in C3Ms

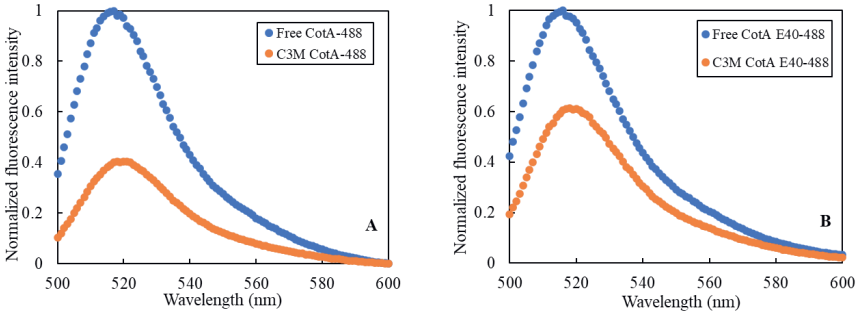

Figure S4.9. Normalized fluorescence emission spectra showing the effect of quenching upon encapsulation of CotA (A) Native CotA (CotA WT), (B) CotA-E40. Free enzyme (blue), C3Ms (orange). The fluorescence emission spectra were recorded using Cary Eclipse Spectrofluorimeter (Varian Inc.) by exciting Alexa-488 CotA at a wavelength of 490 nm and scanning the fluorescence emission from 500 to 600 nm.

S4.9. DLS results on pH stability of enzyme-containing C3Ms

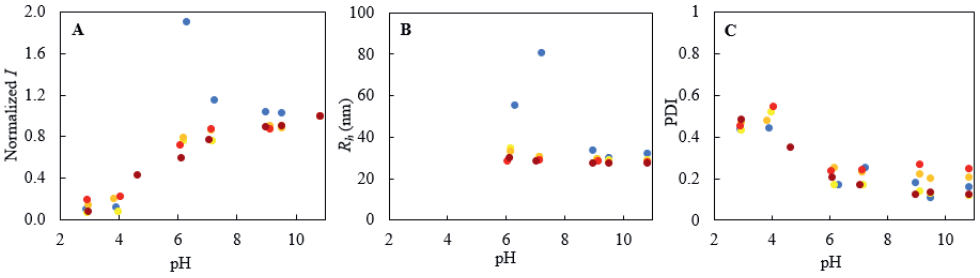

Figure S4.10. pH stability of enzyme-containing C3Ms observed by using DLS. (A) Normalized light scattering intensity (I)), (B) hydrodynamic radius (R_h), (C) polydispersity index (PDI). C3Ms composed of native CotA (blue), CotA E-10 (yellow), CotA E-20 (orange), CotA E-30 (red), and CotA-E40 (dark red).

Chapter 5 :

Enhanced stability of complex coacervate core micelles following different core-crosslinking strategies

Published as:

Kembaren, R., Kleijn, J. M., Borst, J. W, Kamperman, M., and Hofman, A. A. Enhanced stability of complex coacervate core micelles following different core-crosslinking strategies. *Soft matter* **18**, 3052 – 3062 (2022).

Abstract

Complex coacervate core micelles (C3Ms) are formed by mixing aqueous solutions of a charged (bio)macromolecule with an oppositely charged-neutral hydrophilic diblock copolymer. The stability of these structures is dependent on the ionic strength of the solution; above a critical ionic strength the micelles will completely disintegrate. This instability at high ionic strengths is the main drawback for their application in, e.g., drug delivery systems or protein protection. In addition, the stability of C3Ms composed of weak polyelectrolytes is pH-dependent as well. The aim of this study is to assess the effectiveness of covalent crosslinking of the complex coacervate core to improve the stability of C3Ms. We studied the formation of C3Ms using a quaternized and amine-functionalized cationic-neutral diblock copolymer, poly(2-vinylpyridine)-*block*-poly(ethylene oxide) (QP2VP-*b*-PEO), and an anionic homopolymer, poly(acrylic acid) (PAA). Two different core-crosslinking strategies were employed that resulted in crosslinks between both types of polyelectrolyte chains in the core (i.e., between QP2VP and PAA) or in crosslinks between polyelectrolyte chains of the same type only (i.e., QP2VP). For these two strategies we used the crosslinkers 1-ethyl-3-(3'-dimethylaminopropyl)carbodiimide hydrochloride (EDC) and dimethyl 3,3′-dithiopropionimidate dihydrochloride (DTBP), respectively. EDC provides permanent crosslinks, while DTBP crosslinks can be broken by a reducing agent. Dynamic light scattering showed that both approaches significantly improved the stability of C3Ms against salt and pH changes. Furthermore, reduction of the disulfide bridges in the DTBP core-crosslinked micelles largely restored the original salt-stability profile. Therefore, this feature provides an excellent starting point for the application of C3Ms in controlled release formulations.

5.1. Introduction

Complex coacervate core micelles (C3Ms), also known as block ionomer complexes[1] or polyion complex micelles[2] are polymeric nanostructures with a complex coacervate core and a neutral hydrophilic shell.[3–5] C3M formation is based on self-assembly of ionic-neutral hydrophilic diblock copolymers and oppositely charged macromolecules at concentrations exceeding the critical micelle concentration (CMC).[3,6–8] The driving forces for C3M formation are Coulombic attraction between the oppositely charged parts of the polyelectrolyte chains and the entropy gain from the release of the counterions upon complex formation.[3,9–11] C3Ms are easy to prepare as it only involves a simple mixing step of aqueous solutions. C3Ms can be used as carrier for charged macromolecules such as proteins, DNA, and RNA.[3,12,13] Furthermore, C3Ms are interesting for many other applications, including their use as bionanoreactors or nanoprobes, for the encapsulation of biomolecules, and as drug delivery systems.[2,3,14–18]

Despite their ease of preparation, C3Ms can easily disintegrate, in particular at high ionic strength, which is the main limitation for their practical application.[3,14,18–21] Increasing the salt concentration decreases the driving forces for C3M formation, resulting in a reduced stability of the C3Ms. Above a certain salt concentration, also known as the critical salt concentration (CSC), C3Ms will completely disintegrate. In addition, in case of weak polyelectrolytes, the pH is an essential parameter for the stability of C3Ms as well.[3,14]

A strategy to overcome undesired disintegration of C3Ms is by crosslinking the polymers. This can be done reversibly or irreversibly, either in the core or in the corona of the micelles.[14,22–25] However, crosslinking the corona/ shell may affect the surface characteristics and reduces the hydrophilicity and thus the solubility of the micelles.[24] With the core-crosslinking strategy, on the other hand, we expect that the micelles' surface characteristics will remain the same. Core-crosslinking of C3Ms can be achieved by binding together one or both types of polymers present in the core of C3Ms, either physically or covalently.[26–28] Chemical crosslinking of the components in the core will provide a more stable network. Chemical crosslinks can be introduced, for example, by irradiation (photo-polymerization), an enzymatic reaction, or by using "click" chemistry.[27] To crosslink C3Ms, the polymers must contain reactive functional groups, such as amines, thiols, carboxylates, hydroxyls, acetoacetyl groups, acetal groups, acrylamide derivates, or carbonyl groups.[29,30]

The aim of this study is to determine the effectiveness of covalently crosslinking the core of C3Ms to improve their stability against salt addition and pH changes. C3Ms were prepared using a cationic-neutral diblock copolymer, poly(2-vinylpyridine)$_{128}$-*b*-poly(ethylene oxide)$_{477}$

($P2VP_{128}$-*b*-PEO_{477}), and an anionic homopolymer, poly(acrylic acid)$_{118}$ (PAA_{118}). Beforehand, the P2VP-containing diblock copolymer was functionalized with primary amine groups via quaternization. Since primary amines are known to participate in quaternization reactions themselves, protection chemistry was required during the quaternization procedure. Several amine protecting groups are convenient to use like 9-fluorenylmethyl carbamate (FMOC), *t*-butyl carbamate (BOC), and phthalimides.[31–33] We have chosen *N*-(2-bromoethyl)phthalimide because of its stability under the conditions required for the quaternization reaction (including heating to 150 °C). After deprotection, the amine can be used for core-crosslinking by adding a bifunctional crosslinker to the C3M solution.[14,24] In this study, we used two types of crosslinkers, 1-ethyl-3-(3'-dimethylaminopropyl)carbodiimide hydrochloride (EDC) and dimethyl 3,3′-dithiopropionimidate dihydrochloride (DTBP). EDC forms irreversible crosslinks between amine and carboxylic groups, while DTBP connects two amine groups. Furthermore, since DTBP crosslinks contain disulfide bridges, these crosslinks can be broken again by addition of a reducing agent. We have investigated these two types of crosslinkers to crosslink the core of C3Ms (Scheme 5.1).

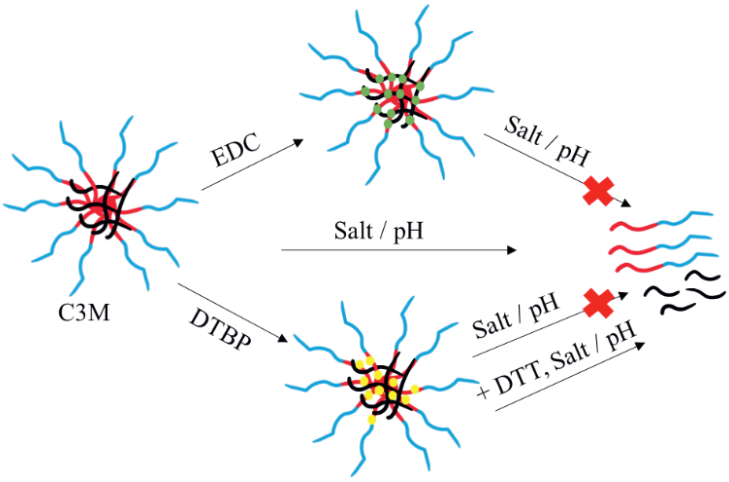

Scheme 5.1. Schematic overview of core-crosslinking strategies of C3Ms using the crosslinkers EDC and DTBP. The use of EDC results in permanent crosslinks, whereas DTBP provides crosslinks that can be broken by reducing agents like 1,4-dithiothreitol (DTT). Red-blue: charged-neutral diblock copolymer. Black: oppositely charged homopolymer. Green and yellow: crosslinks formed by EDC and DTBP, respectively.

We have compared these different core-crosslinking strategies, i.e., network formation between only one or between both types of polymers in the core, and permanent versus reversible crosslinking. Using dynamic light scattering (DLS), we investigated the formation of C3Ms, their size and stability as a function of ionic strength and pH before and after crosslinking, and in case of DTBP also after breaking the crosslinks.

5.2. Experimental section

5.2.1. Materials

The diblock copolymer poly(2-vinylpyridine)$_{128}$-*block*-poly(ethylene oxide)$_{477}$ (P2VP$_{128}$-*b*-PEO$_{477}$) (M_n = 34.5 kg/ mol, M_w/ M_n = 1.1) and homopolymer poly(acrylic acid)$_{118}$ (PAA$_{118}$) (M_n = 8.5 kg/mol, M_w/ M_n = 1.07) were obtained from Polymer Source Inc. The crosslinkers 1-ethyl-3-(3'-dimethylaminopropyl)carbodiimide hydrochloride (EDC) and dimethyl 3,3′-dithiopropionimidate dihydrochloride (DTBP) were purchased from Thermo Fisher Scientific. The quaternization reagent *N*-(2-bromoethyl)phthalimide and the hydrazine hydrate solution (78-82 % in H_2O) were obtained from Sigma-Aldrich. 1,4-dithiothreitol (DTT) was purchased from Carl Roth.

5.2.2. Polymer quaternization

N-(2-bromoethyl) phthalimide (5 eq. with respect to 2VP, 1.18 g, 4.64 mmol) and diblock copolymer poly(2-vinylpyridine)$_{128}$-*block*-poly(ethylene oxide)$_{477}$ (0.25 g, 0.93 mmol of 2VP units) were mixed and subsequently heated at 150 °C for 2 hours in a small vial with stirring bar. No additional solvents were added; the molten quaternization agent simultaneously acts as a solvent (T_m = 82 °C). After cooling to room temperature, about 5 mL of dichloromethane was added to dissolve the solidified product and then the solution was precipitated in diethyl ether. The precipitated polymer was filtered and washed five times with diethyl ether. Finally, the polymer was dried in a vacuum oven, resulting in an off-white powder.

5.2.3. Deprotection of the quaternized diblock copolymer

The polymer powder (0.3 g) that was obtained after the quaternization reaction was dissolved in 8 mL of ethanol and heated at 80 °C with reflux under an N_2 atmosphere. Subsequently, hydrazine hydrate solution (78-82 % in H_2O) (10 eq. with respect to 2VP) was added for deprotection of the quaternized diblock copolymer. The mixture was kept at 80 °C for 18 hours. After that, the mixture was cooled to 4 °C and filtered to remove phthalhydrazide. The filtrate

was collected, and the volume of filtrate was reduced to about 3 mL by using a rotary evaporator. The solution was then dialyzed (MWCO 3.5 kg/mol) for three days against water to remove excess hydrazine hydrate and the side product phthalhydrazide.[34] After lyophilization the polymer product was obtained as a white powder and analyzed by using ^{1}H-NMR (using a Bruker Avance III 400 MHz NMR spectrometer), FTIR (using a Bruker Tensor 27 IR spectrometer), and a ninhydrin assay. For the ninhydrin assay, the polymer (0.5 mg) was dissolved in 50 µL of water, then 200 µL of ninhydrin solution (2 % in ethanol) was added. The solution was heated at 90 °C for 3 min, then cooled to room temperature. An overview of the quaternization and deprotection reactions is presented in Scheme 5.2.

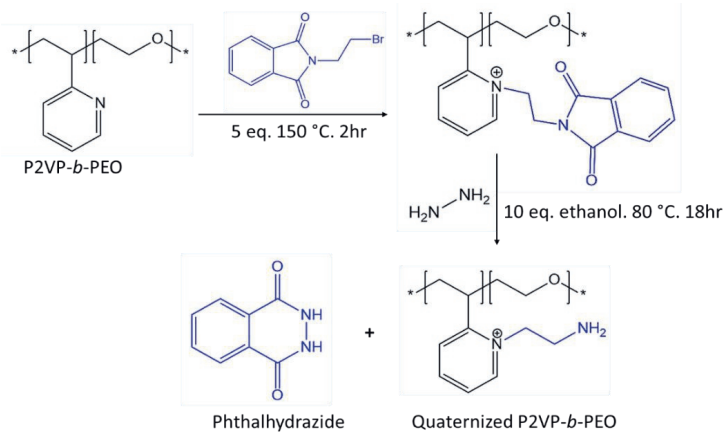

Scheme 5.2. Synthetic pathway for the preparation of amine-functionalized diblock copolymer, $P2VP_{128}$-*b*-PEO_{477}, via quaternization and deprotection.

5.2.4. Formation of C3Ms

PAA and quaternized diblock copolymer solutions were prepared separately in a 10 mM sodium phosphate buffer at pH 7.4. All solutions were filtered through 0.2 µm polyethersulfone membrane syringe filters. To determine the preferred micellar composition (PMC), i.e., the optimal polymer composition for C3M formation, different concentrations of poly(acrylic acid) from the stock solution of 60 µM were added to a constant concentration of quaternized diblock copolymer solution (5 µM) with a 1:1 volume ratio (volume total of 1 mL). The mixed solutions were left to equilibrate at room temperature overnight before measurement. The extent of C3M formation was determined by using DLS. After establishment of the PMC, all C3M preparations were made at the PMC and several dilution series with 10 mM sodium phosphate buffer at pH 7.4 were prepared to determine the critical micelle concentration (CMC).

5.2.5. Core-crosslinking of C3Ms

Core-crosslinking of the C3Ms (at the PMC) was achieved by using two different kinds of crosslinking agents. After mixing of the quaternized diblock copolymer with PAA to form C3Ms (total volume of 5 mL), either EDC (2.0 eq. to amine) or DTBP (3.9 eq. to amine) crosslinker was added to the micellar solutions. The crosslinking reaction was performed in 10 mM buffer sodium phosphate pH 7.4 at room temperature. The solution was stirred for at least 3 hours. Unreacted crosslinking agent is expected to degrade eventually due to the hydrolysis of linker.

5.2.6. C3M stability

The stability of C3Ms was investigated by salt and acid-base titrations while monitoring the scattering intensity of the micelles by using DLS. For salt stability observation, a 4.0 M NaCl solution was titrated into the C3M solution. For assessment of the pH stability, 0.1 M NaOH and 0.1 M HCl solutions were titrated into the C3M solutions. To cleave the crosslinks originating from DTBP, a final DTT concentration of 50 mM was added to DTBP core-crosslinked C3Ms and incubated for 30 minutes. Subsequently, the solution was titrated with a 4 M NaCl and the extent of micelle disintegration was monitored by using DLS.

5.2.7. Dynamic light scattering (DLS)

Light scattering measurements were performed on an ALV-LSE 41/ CGS-8F goniometer system equipped with a DPSS laser (λ = 660 nm, 200 mW).[6,35] The PMC, mean hydrodynamic radius of the micelles (R_h), and polydispersity index (PDI) were measured at a fixed 90° angle. The shape of the C3Ms was resolved by using multi-angle DLS at angles ranging from 50° to 120° in steps of 10°. Intensity correlation functions were recorded for 10 seconds and averaged over 8 runs per angle. Hydrodynamic radii and polydispersity indices were acquired through a second order cumulant analysis.

5.3. Results and discussion

5.3.1. Functionalization of the diblock copolymer for crosslinking purposes

Quaternization of P2VP using *N*-(2-bromoethyl)phthalimide aims to simultaneously introduce positive charges and primary amine functional groups onto the P2VP-*b*-PEO diblock copolymer.[36–39] Primary amines are interesting, as they allow a large variety of click reactions for crosslinking. We used a phthalimide-protected primary amine group in order to prevent self-

cyclization or polymerization during the quaternization reaction, which can be easily deprotected afterwards by hydrazinolysis using hydrazine hydrate.[33,40] In this study, we tested the homopolymer P2VP first before using the diblock copolymer $P2VP_{128}$-*b*-PEO_{477}. The homopolymer functionalization was successful with a degree of quaternization (DQ) of 92 % (Figure S5.1 and S5.2, Supplementary information).

Figure 5.1A shows the ^{1}H-NMR spectrum of the $P2VP_{128}$-*b*-PEO_{477} copolymer before quaternization. After quaternization with *N*-(2-bromoethyl)phthalimide, the signals from P2VP's aromatic ring are clearly shifted (6-8.5 ppm) and an intense peak appeared at 7.78 ppm from the phthalimide aromatic rings (Figure 5.1B; protons [j] and [k]). Moreover, a new broad signal showed up around 3.5-5.5 ppm originating from the two CH_2 groups of ethyl phthalimide (protons [h] and [i]). This result indicates that the polymer was successfully quaternized and a degree of quaternization of about 85 % was calculated from the ratio of the integral area of the aromatic rings and the integral area of P2VP's backbone (Figure S5.3 and S5.4, Supplementary information). After treatment of the quaternized diblock copolymer with hydrazine hydrate, the disappearance of the peak at 7.78 ppm originating from protons [j] and [k] indicates full deprotection of the primary amine groups (Figure 5.1C).[36,40,41]

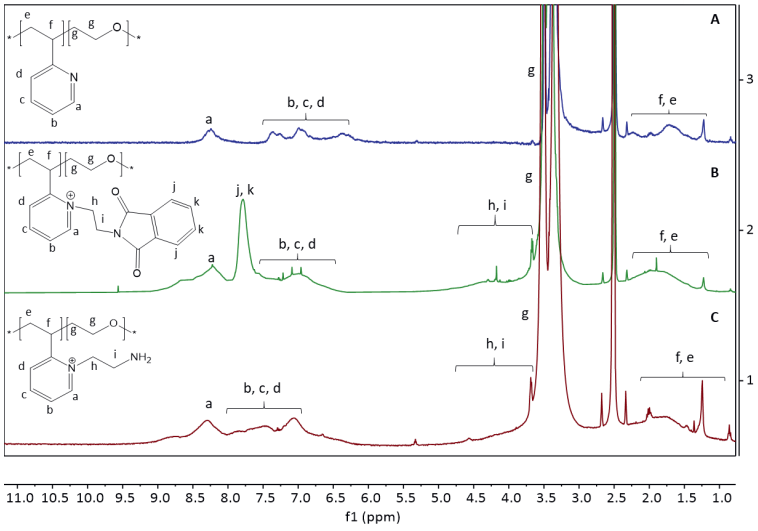

Figure 5.1. ^{1}H-NMR spectra of the functionalized diblock copolymer $P2VP_{128}$-*b*-PEO_{477}. (A) Diblock copolymer before quaternization, (B) diblock copolymer after quaternization using N-(2-bromoethyl)phthalimide, (C) quaternized diblock copolymer after deprotection using hydrazine hydrate. Spectra A, B, and C were recorded in DMSO-d_6.

Next, we conducted Fourier-transform infrared spectroscopy (FTIR) to further characterize the functionalized diblock copolymer. Figure 5.2 demonstrates FTIR spectra of quaternized P2VP$_{128}$-*b*-PEO$_{477}$. After quaternization of P2VP$_{128}$-*b*-PEO$_{477}$, the spectrum of the diblock copolymer shows new bands at 1774 cm^{-1} and 1710 cm^{-1} originating from the carbonyls (C=O stretching) of the phthalimide groups (Figure 5.2B). These changes confirm that the copolymer was successfully quaternized with *N*-(2-bromoethyl)phthalimide. After hydrazinolysis and dialysis (Figure 5.2C), the removal of the phthalimide groups led to the disappearance of the stretching modes of the carbonyl group (C=O) in the 1774 - 1710 cm^{-1} region. This result proves that the deprotection reaction was successful and that the phthalhydrazide by-product was completely removed.[42–44] Furthermore, a new band appeared at 1641 cm^{-1} which can be assigned to the bending vibration of the NH group, as well as an increase in the intensity of the bands in the 3250–3400 cm^{-1} region that can be assigned to the stretching vibration of –NH$_2$. This confirms the successful formation of primary amine groups.

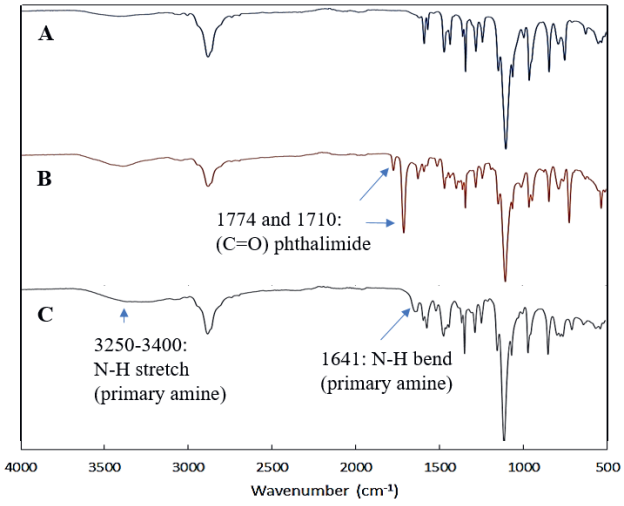

Figure 5.2. FTIR spectra of the functionalized diblock copolymer P2VP$_{128}$-*b*-PEO$_{477}$. (A) Diblock copolymer before quaternization, (B) diblock copolymer after quaternization using N-(2-bromoethyl)phthalimide, (C) quaternized diblock copolymer after deprotection using hydrazine hydrate.

To further support the presence of accessible primary amines in the deprotected diblock copolymer, we have conducted a ninhydrin assay. This assay is a colorimetric method that enables qualitative and quantitative determination of amino groups.[45–47] The

presence of primary amines will give a dark purple product known as “Ruhemann’s purple”. Figure 5.3 shows that the diblock copolymer solutions before quaternization and deprotection only give a pale-yellow color, identical to the control sample, indicating that there are no primary amines in these polymer samples present. This is in large contrast to the deprotected diblock copolymer, for which the solution turned deep purple upon addition of ninhydrin as a direct result of ninhydrin-amine complex formation. Taken together, we have generated diblock copolymers that have accessible primary amines suitable for crosslinking validated by different approaches like ^{1}H-NMR and FTIR.

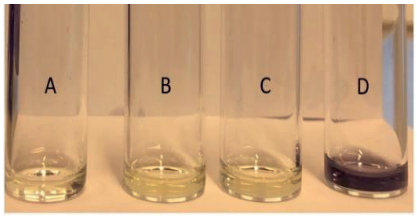

Figure 5.3. Ninhydrin test (using ninhydrin 2 %) of the functionalized diblock copolymer (2 mg/mL). (A) Blank/ negative control, (B) diblock copolymer before quaternization, (C) diblock copolymer after quaternization, (D) diblock copolymer after being deprotected.

5.3.2. C3M formation between the functionalized diblock copolymer and homopolymer

After successful quaternization of the diblock copolymer, this copolymer was mixed with homopolymer to form C3Ms. DLS measurements were performed to observe the formation of these C3Ms. Different aliquots of a solution of the anionic homopolymer (PAA_{118}) were added to solutions with a constant concentration of cationic-neutral hydrophilic diblock copolymer, quaternized $P2VP_{128}$-*b*-PEO_{477}, to determine the preferred micellar composition (PMC). The PMC is identified as the mixing composition where the scattering intensity reaches its maximum. After equilibrating the mixtures overnight, the light scattering intensity (I), the hydrodynamic radius of the micelles (R_h), and the polydispersity index (PDI) were determined as a function of the PAA concentration.

Figure 5.4 shows the DLS results for mixtures with different concentrations of PAA and a constant concentration of quaternized $P2VP_{128}$-*b*-PEO_{477} (final polymer concentration of 2.50 µM). The light scattering intensity (Figure 5.4A) increases rapidly with increasing PAA concentration, indicating formation of C3Ms. At a concentration of 1.81 µM PAA_{118}, the light scattering intensity reached a maximum, implying that this

mixing composition contains the highest number and most well-defined micelles. Thus, this point is considered to be the PMC.

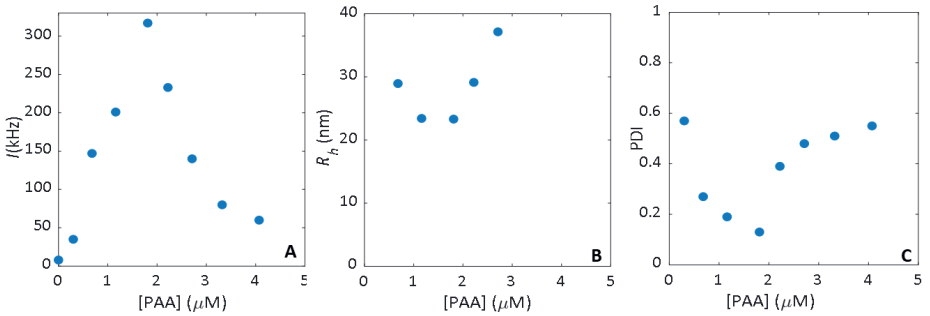

Figure 5.4. DLS results for mixtures of different concentrations of PAA and a constant concentration of quaternized P2VP$_{128}$-*b*-PEO$_{477}$ (final polymer concentration of 2.5 μM). (A) Scattering intensity (*I*), (B) hydrodynamic radius (R_h), and (C) polydispersity index (PDI).

At the pH used (pH 7.4), the primary amines of the quaternized diblock copolymer are protonated (pK_a of ethyleneamine = 10.4)[48,49] and bear a positive charge, thereby contribute to the total number of positive charges on this polymer; it amounts to 218 elementary charges per molecule (DQ * n(2VP) * 2 = 0.85 * 128 * 2 = 218). At this pH the carboxylic groups of PAA are all deprotonated, so the number of negative charges on PAA is 118. Thus, at the PMC, the ratio between the total concentration of negative charges on the PAA and the total concentration of positive charges on the diblock ([–]/[+]) is 0.39 ((1.81*118) / (2.5*218) = 0.39). Clearly, the PMC of these C3Ms is far from charge stoichiometry ([–]/[+] = 1), indicating that interactions other than electrostatic play a role in micelle formation for this polymer couple. These are probably hydrophobic interactions, since the diblock copolymer still contains hydrophobic pyridine units due to incomplete quaternization.[3,12,14]

At the PMC, the C3Ms have a hydrodynamic radius of 25.1 ± 1.0 nm (Figure 5. 4B), and a minimum value for the PDI of 0.1 ± 0.03 is found (Figure 5.4C), indicating a narrow size distribution of the C3Ms.[50] Addition of PAA beyond the PMC leads to excess charge and results in reduction of light scattering intensity because of disintegration of micelles into negatively charged soluble complexes.[20,51]

Besides the ratio between the charged homopolymers and diblock copolymers, micelle formation also depends on their absolute concentration: micelles are only formed above a certain concentration, the CMC.[1] Diluting a 2.50 μM C3M stock solution

prepared at the PMC with 10 mM sodium phosphate buffer (pH 7.4) initially leads to a linear decrease of the scattering intensity as observed by DLS (Figure S5, Supplementary information), reflecting the decrease in number of micelles.[52,53] Although the intensity becomes small compared to the background at low polymer concentrations, from this dilution series it is safe to assume the CMC being equal or possibly even lower than 0.59 μM, the concentration at which C3Ms can still be identified. For comparison, the typical range of CMC values reported for polymeric micelles is in the order of 10^{-6} to 10^{-7} M.[3,52–54] The CMC of low molecular weight surfactant micelles is in the order of 10^{-3} to 10^{-4} M. This makes polymeric micelles less prone to dissociation at low concentrations compared to surfactant-based micelles.[55]

5.3.3. Core-crosslinking of C3Ms using two different strategies

The aim of our present study is to enhance the stability of the micelles for which we have explored different crosslinking strategies. Here, we used two types of crosslinking agents that allow crosslinking of the core of C3Ms: EDC and DTBP. After 3 hours, the crosslinking reaction was expected to stop due to the short half-life of these linkers in aqueous solution.[56–58] EDC facilitates formation of a permanent amide bond between the primary amine groups of the quaternized P2VP-*b*-PEO diblock copolymer and the carboxylic acid groups of PAA in the core of C3Ms. This amide bond formation is irreversible (Scheme 5.3). Efficient amide formation by the EDC linker can be achieved at a pH in the range of 4.5-7.5.[59–61]

On the other hand, DTBP has imido ester groups that can only react with amine-containing polymers to form an amidine bond, and works best in a pH range of 7 to 10. DTBP has an internal disulfide group that can be cleaved using a reducing agent.[62–65] The addition of DTBP to a solution of C3Ms results in crosslinking of the core of the micelles by amidine bond formation between amine groups of two P2VP units of the quaternized diblock copolymer (Scheme 5.4). Thus, if DTBP is used as crosslinker, PAA is not incorporated in the crosslinked network. Furthermore, the imido ester groups of DTBP maintain the overall positive charge on the diblock copolymer after reacting with primary amines[66] ensuring that the negatively charged PAA remains in the core. The addition of reducing agents such as 1,4-dithiothreitol (DTT) and tris(2-carboxyethyl)phosphine (TCEP) results in dissociation of the crosslinks. DLS demonstrated that the hydrodynamic radius of EDC and DTBP core-crosslinked micelles was 23.9 ± 0.9 nm and 24.3 ± 1.4 nm, respectively. These sizes are similar to the size of the non-crosslinked micelles. Multi-angle DLS revealed that their shape remained spherical (Figure 5.5), which can be deduced from the three overlapping linear relationships between the decay

rate Γ and wave vector q for each type of micelle[67,68] which are unaffected by the crosslinking agents.

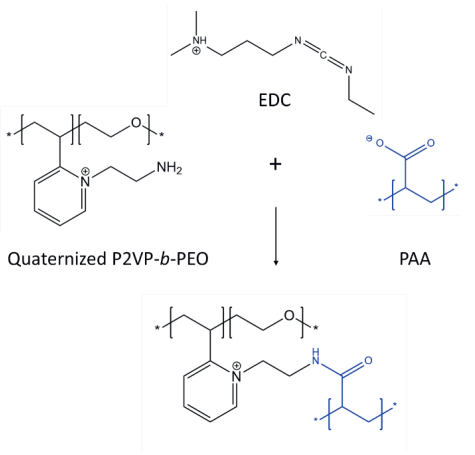

Scheme 5.3. Crosslink formation between a primary amine group of the quaternized diblock copolymer P2VP-*b*-PEO and a carboxylate group of the homopolymer PAA using EDC.

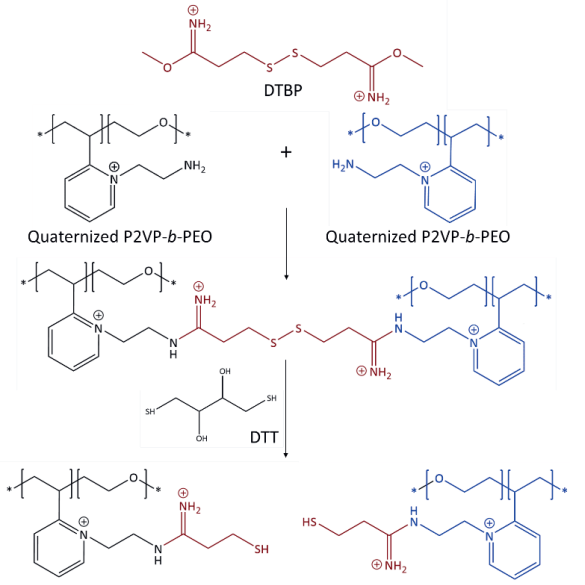

Scheme 5.4. Crosslink formation between primary amine groups of the quaternized diblock copolymer P2VP-*b*-PEO using DTBP. The crosslinks can be cleaved using reducing agents such as DTT.

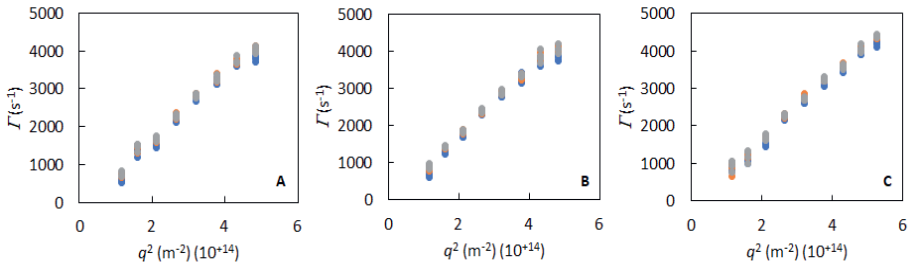

Figure 5.5. Multi-angle DLS results for all C3M formulations. The decay rate Γ as a function of the wave vector q was obtained from the DLS correlation curves by a first (blue), second (orange), and third (grey) order cumulant fit. (A) C3Ms without crosslinks, (B) C3Ms core-crosslinked with EDC, (C) C3Ms core-crosslinked with DTBP.

5.3.4. Stability of C3Ms

The stability of the micelles, prepared at the PMC, was studied using a salt titration. In Figure 5.6., the normalized scattering intensity, R_h and PDI for four different C3Ms samples (C3M control, C3M crosslinked by EDC, C3M crosslinked by DTBP, and C3M crosslinked by DTBP and treated with DTT) are plotted against the salt concentration, up to 1.0 M of NaCl. All samples showed a decrease in scattering intensity with increasing salt concentration. However, for non-crosslinked C3Ms, the scattering intensity decreases significantly faster than for core-crosslinked C3Ms. At 1.0 M NaCl, the scattering intensity of non-crosslinked C3Ms is practically zero, indicating total disintegration of the micelles. However, core-crosslinked micelles turned out to be much more resistant to salt addition. Both EDC and DTBP core-crosslinked C3Ms demonstrate a more gradual decrease in scattering intensity, which seems to reach a plateau at the highest NaCl concentrations applied. At 1.0 M NaCl a large fraction of the micelles was still present. The salt stability of EDC core-crosslinked micelles seems to be higher than that of the DTBP core-crosslinked ones, which can be explained from the fact that in EDC core-crosslinked micelles the two types of polymer chains are bonded together in the core. For EDC crosslinked micelles the scattering intensity at 1.0 M NaCl was about 77 % of its initial value. This may be caused by the loss of some polymer chains that where not properly connected via crosslinks. For DTBP core-crosslinked micelles the scattering intensity at 1.0 M salt is about 55 % of its value before NaCl addition. Since the PAA chains are not covalently attached to the crosslinked P2VP chains, they can diffuse out from the micelles via reptation[69,70] at high salt conditions when all charges are screened. However, possibly a part of the PAA

chains remains entangled in the cross-linked network formed by the P2VP chains and cannot dissociate from the complexes, even at very high salt concentrations.[14,66]

An additional feature of DTBP crosslinking is the presence of a disulfide bridge, offering the possibility to cleave the network by simply adding a reducing agent. We treated DTBP core-crosslinked C3Ms with the reducing agent DTT and observed a gradual disintegration of C3Ms upon addition of salt (see Figure 5.6A). After core-crosslinking using DTBP and subsequently reducing the disulfide bridges, the original salt-stability profile of the non-crosslinked C3Ms was largely restored.

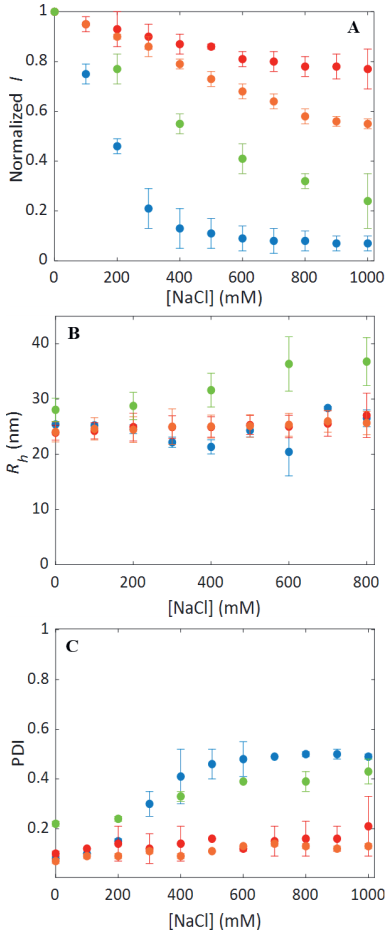

Figure 5.6. Stability measurements of C3Ms as a function of salt concentration using DLS. C3Ms without crosslinks (control) (blue), C3Ms core-crosslinked with EDC (red), C3Ms core-crosslinked with DTBP (orange), C3Ms core-crosslinked with DTBP after addition of 50 mM DTT (green). (A) Normalized scattering intensity (I), (B) hydrodynamic radius (R_h), (C) polydispersity index (PDI).

Figure 5.6B presents the hydrodynamic radii of different C3Ms as a function of NaCl concentration, showing that these are rather constant in all cases. It should be noted that for low scattering intensities the error in R_h is relatively large. DTT-treated crosslinked micelles are larger than non-crosslinked micelles, presumably due to the (cleaved) DTBP moieties present in the cores. These micelles seem to have a much stronger tendency to swell than other C3Ms.[14,54] The PDI of non-crosslinked C3Ms and DTT-treated crosslinked micelles increased with increasing salt concentration and reached above 0.4 at 1.0 M NaCl, pointing to highly polydisperse samples due to disintegration of the micelles (Figure 5.6C). However, the PDI of crosslinked C3Ms only slightly increased with increasing salt concentration, and reached PDI values of 0.2 at most at 1.0 M salt, which indicates moderately polydisperse samples with the micelles still being intact.[50]

We also investigated the effect of pH on micelle stability since the pH determines the degree of dissociation of carboxylic groups of poly(acrylic acid) and amine functional groups of the quaternized diblock copolymer. In Figure 5.7 and Figure 5.8, the pH-dependence of the scattering intensity, R_h, and PDI are plotted for the different micellar systems: non-crosslinked C3Ms, EDC core-crosslinked C3Ms, and DTBP core-crosslinked C3Ms. When the pH decreases by the addition of 0.1 M HCl, the negative charge on PAA becomes lower (pK_a of PAA = 4.5). At pH 3 the charge of the PAA functional groups is practically zero (dissociation degree α = 0.03). For the non-crosslinked micelles, we observed a decrease in scattering intensity with decreasing pH and especially below pH 4 the intensity decreased sharply (Figure 5.7A). Obviously, in this case the reduction of negative charge on PAA results in disruption of the C3Ms. On the other hand, core-crosslinked C3Ms are stable over the full pH range covered by the HCl titration, as evidenced by a constant high scattering intensity. For crosslinking using EDC, the core-crosslinked C3Ms cannot fall apart because a network between PAA and diblock copolymer is established. Surprisingly, for the crosslinking using DTBP, which only connects the QP2VP chains, the PAA apparently also remains trapped inside the core. At low pH, PAA adopts a globular conformation (but not collapsed for PAA with molar mass less than 16.5 kg/ mol).[71] This globular structure is most likely the cause that PAA cannot diffuse out of the QP2VP network in the core of micelles.[71]

The size of the non-crosslinked micelles decreased at a pH close to the pK_a of PAA, suggesting that some PAA and also diblock copolymer leave the micelles before they fully disintegrate (Figure 5.7B). The PDIs of these non-crosslinked micelles increased upon addition of acid (Figure 5.7C) and measured values above 0.4 at a pH below the pK_a

of PAA, an indication for highly polydisperse samples.[50] However, for the core-crosslinked C3Ms, both EDC and DTBP, the size of the micelles and the PDI are rather constant upon the addition of acid.

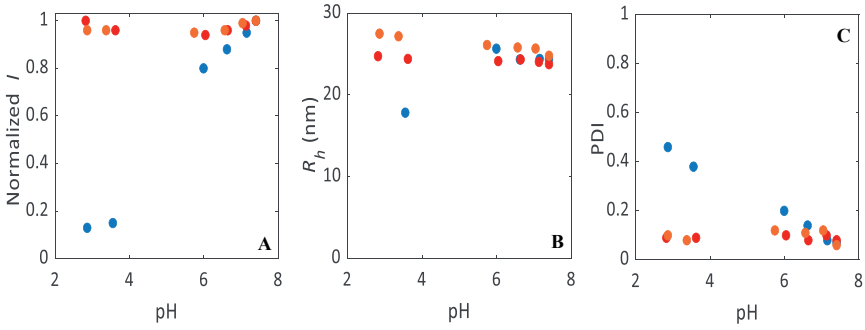

Figure 5.7. Stability measurements as a function of the pH (with addition of 0.1 M HCl) as observed by using DLS. Blue (C3Ms without crosslinks/ control), red (C3Ms core-crosslinked with EDC), orange (C3Ms core-crosslinked with DTBP). (A) Normalized scattering intensity (I), (B) hydrodynamic radius (R_h), (C) polydispersity index (PDI).

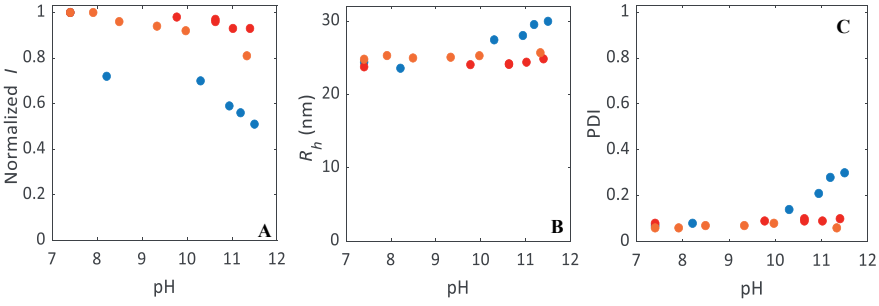

Figure 5.8. Stability measurements as a function of the pH (with addition of 0.1 M NaOH) as observed by using DLS. Blue (C3Ms without crosslinks/ control), red (C3Ms core-crosslinked with EDC), orange (C3Ms core-crosslinked with DTBP). (A) Normalized scattering intensity (I), (B) hydrodynamic radius (R_h), (C) polydispersity index.

When the pH is increased by addition of 0.1 M NaOH, the total number of positive charges on the diblock copolymer decreases because the deprotected amino groups become deprotonated (pK_a of ethyleneamine = 10.4).[48,49] Above pH 11, these groups are barely charged anymore. However, as the quaternization reaction leads to permanent (pH-independent) charges on the pyridine rings, a high pH does not lead to such a

dramatic decrease in scattering intensity of the non-crosslinked C3Ms compared to the addition of acid. In other words, non-crosslinked C3Ms do not entirely fall apart since the positive charges of the quaternized pyridine ring are still present at a high pH (Figure 5.8A). However, we still observe a lower C3M stability than for the core-crosslinked C3Ms.

The size of the non-crosslinked micelles slightly increased at a pH above the pK_a of ethyleneamine, and is accompanied by an increase of the PDI (Figure 5.8B and Figure 5.8C). This suggests a slight swelling of the micelles and possibly a structural rearrangement and some loss of PAA due to the deprotonation of amino groups. However, with the addition of base, the R_h and PDI of the core-crosslinked C3Ms, both EDC and DTBP, are rather constant showing that the micelles stay intact and unchanged. In summary, crosslinks between the two components in the core (EDC) result in a slightly higher stability against pH changes compared to crosslinks between only one component (DTBP). Again, this is likely a result of EDC being able to keep both components of the C3Ms together in the core, while with DTBP, PAA may diffuse out as it is not included in the network. We note that the difference between the two crosslinking strategies is less pronounced for stability against pH changes than for the stability against salt addition. In the latter case all charges on both polymers gradually become effectively screened, while changing the pH has no effect on the permanent positive charges of the diblock copolymer and only limited effect (at low pH) on the charges of the PAA homopolymer.

5.4. Conclusions

In this study, we modified a P2VP-*b*-PEO diblock copolymer via quaternization that simultaneously resulted in permanent positive charges on the pyridine rings and, after deprotection, in primary amine functional groups. C3Ms were prepared by mixing aqueous solutions of the anionic homopolymer PAA and the quaternized diblock copolymer. DLS measurements confirmed the formation of C3Ms. The PMC of the C3Ms was not found at the charge balance between negative charges on PAA and positive charges on the quaternized P2VP-*b*-PEO but at a lower ratio ([-]/ [+] = 0.39). This points to the role of other types of interactions besides electrostatic attraction in the complex formation, such as hydrophobic interactions. Covalent core-crosslinking of the micelles resulted in a significant improvement of the stability of C3Ms against salt addition and pH changes. Using the crosslinker EDC,

permanent crosslinks between PAA and quaternized P2VP in the micellar core are formed; the crosslinker DTBP provides cleavable (reversible) bonds between P2VP chains only. Core-crosslinking using EDC provides a slightly higher stability compared to core-crosslinking using DTBP because it keeps these two components of the C3Ms together in the micelle core. In case of DTBP-crosslinked micelles, PAA can diffuse out of the core due to charge screening when the salt concentration is increased, although some of the polymer chains may remain trapped in the crosslinked network. An advantage of the second approach is the ability to cleave the internal disulfide bridges via addition of a reducing agent (DTT), thereby largely restoring the original disintegration profile of C3Ms as a function of salt concentration. This type of reversible crosslinkers offers great opportunities for controlled release of functional ingredients using C3Ms.

References

1. Bronich, T. K., Kabanov, A. V and Kabanov, V. A. Soluble complexes from poly (ethylene oxide) - block -polymethacrylate anions and n -alkylpyridinium cations. *Macromolecules* **9297**, 3519–3525 (1997).
2. Harada, A. and Kataoka, K. Formation of polyion complex micelles in an aqueous milieu from a pair of oppositely-charged block copolymers with poly(ethylene glycol) Segments. *Macromolecules* **28**, 5294–5299 (1995)
3. Voets, I. K., de Keizer, A. and Cohen Stuart, M. A. Complex coacervate core micelles. *Adv. Colloid Interface Sci.* **147**–**148**, 300–318 (2009).
4. Cohen Stuart, M. A., Besseling, N. A. M. and Fokkink, R. G. Formation of micelles with complex coacervate cores. *Langmuir* **14**, 6846–6849 (1998).
5. Harada, A. and Kataoka, K. Polyion complex micelle formation from double-hydrophilic block copolymers composed of charged and non-charged segments in aqueous media. *Polym. J.* **50**, 95–100 (2018).
6. Dähling, C., Houston, J. E., Radulescu, A., Drechsler, M., Brugnoni, M., Mori, H. Pergushov, D. V. and Plamper, F. A. Self-templated generation of triggerable and restorable nonequilibrium micelles. *ACS Macro Lett.* **7**, 341–346 (2018).
7. Sproncken, C. C. M., Magana, J. R. and Voets, I. K. 100th anniversary of macromolecular science viewpoint: attractive soft matter: association kinetics, dynamics, and pathway complexity in electrostatically coassembled micelles. *ACS Macro Lett.* **10**, 167–179 (2021).
8. Magana, J. R., Sproncken, C. C. M. and Voets, I. K. On complex coacervate core micelles: Structure-function perspectives. *Polymers* **12**, 1953-1990 (2020).
9. Marras, A. E., Ting, M., Stevens, K. C. and Tirrell, M. V. Advances in the structural design of polyelectrolyte complex micelles. *J. Phys. Chem. B* **125**, 7076–7089 (2021).
10. Marras, A. E., Campagna, T. R., Vieregg, J. R. and Tirrell, M. V. Physical property scaling relationships for polyelectrolyte complex micelles. *Macromolecules* **54**, 6585–6594 (2021).
11. Amann, M., Diget, J. S., Lyngsø, J., Pedersen, J. S., T. Narayanan and Lund, R. Kinetic pathways for polyelectrolyte coacervate micelle formation revealed by time-resolved synchrotron SAXS. *Macromolecules* **52**, 8227–8237 (2019).
12. Nolles, A., Westphal, A. H., de Hoop, J. A., Fokkink, R. G., Kleijn, J. M., van Berkel, W. J. H., and Borst, J. W. Encapsulation of GFP in complex coacervate core micelles. *Biomacromolecules* **16**, 1542–1549 (2015).
13. Agarwal, N. P., Matthies, M., Gür, F. N., Osada, K. and Schmidt, T. L. Block copolymer micellization as a protection strategy for DNA origami. *Angew. Chemie - Int. Ed.* **56**, 5460–5464 (2017).
14. Bourouina, N., Cohen Stuart, M. A. and Kleijn, J. M. Complex coacervate core micelles as diffusional nanoprobes. *Soft Matter* **10**, 320–331 (2014).
15. Lindhoud, S., de Vries, R., Norde, W., and Cohen Stuart, M. A. Structure and stability of complex coacervate core micelles with lysozyme. *Biomacromolecules* **8**, 2219–2227 (2007).
16. Mills, C. E., Obermeyer, A., Dong, X., Walker, J. and Olsen, B. D. Complex coacervate core micelles for the dispersion and stabilization of organophosphate hydrolase in organic solvents. *Langmuir* **32**, 13367–13376 (2016).
17. Jaturanpinyo, M., Harada, A., Yuan, X. and Kataoka, K. Preparation of bionanoreactor based on core-shell structured polyion complex micelles entrapping trypsin in the core cross-linked with glutaraldehyde. *Bioconjug. Chem.* **15**, 344–348 (2004).
18. Blocher McTigue, W. C. and Perry, S. L. Protein encapsulation using complex coacervates: What nature has to teach us. *Small* **16**, 1–17 (2020).
19. Lindhoud, S., de Vries, R., Schweins, R., Cohen Stuart, M. A. and Norde, W. Salt-induced release of lipase from polyelectrolyte complex micelles. *Soft Matter* **5**, 242–250 (2009).
20. Nolles, A., Hooiveld, E., Westphal, A. H., van Berkel, W. J. H., Kleijn, J. M., and Borst, J. W. FRET reveals the formation and exchange dynamics of protein-containing complex coacervate core micelles. *Langmuir* **34**, 12083–12092 (2018).
21. Gao, S., Holkar, A. and Srivastava, S. polymers Protein-Polyelectrolyte Complexes and Micellar Assemblies. *Int. J. Polym. Sci.*, **2011**, 1–8 (2015).
22. Shao, Y., Huang, W., Shi, C., Atkinson, S. T. and Luo, J. Reversibly crosslinked nanocarriers for on-demand drug delivery in cancer treatment. *Ther. Deliv.* **3**, 1409–1427 (2012).
23. Ma, X., Liu, J., Lei, L., Yang, H. and Lei, Z. Synthesis of light and dual-redox triple-stimuli-responsive core-crosslinked micelles as nanocarriers for controlled release. *J. Appl. Polym. Sci.* **136**, 1–8 (2019).
24. Talelli, M., Barz, M., Rijcken, C. J. F., Kiessling, F., Hennink, W.E., Lammers, T. Core-crosslinked polymeric micelles: Principles, preparation, biomedical applications and clinical translation. *Nano Today* **10,** 93-117 (2015).

25. Shim, M. S. and Kwon, Y. J. Acid-transforming polypeptide micelles for targeted nonviral gene delivery. *Biomaterials* **31**, 3404–3413 (2010).
26. Krishnakumar, G. S., Sampath, S., Muthusamy, S. and John, M. A. Importance of crosslinking strategies in designing smart biomaterials for bone tissue engineering: A systematic review. *Materials Science and Engineering C* **96**, 941–954 (2019).
27. Hennink, W. E. and van Nostrum, C. F. Novel crosslinking methods to design hydrogels. *Advanced Drug Delivery Reviews* **64**, 223–236 (2012).
28. van Nostrum, C. F. Covalently cross-linked amphiphilic block copolymer micelles. *Soft Matter* **7**, 3246–3259 (2011).
29. Tillet, G., Boutevin, B. and Ameduri, B. Chemical reactions of polymer crosslinking and post-crosslinking at room and medium temperature. *Progress in Polymer Science* **36**, 191–217 (2011).
30. Ayyub, O. B., Ibrahim, M. B. and Kofinas, P. Synthesis and characterization of microphase separated primary amine functionalized polystyrene-*b*-poly(2-vinylpyridine). *Polymer* **55**, 6227–6231 (2014).
31. Mantovani, G., Lecolley, F., Tao, L., Haddleton, D. M., Clerx, J., Cornelissen, J. J. L. M. and Velonia, K. Design and synthesis of *N*-maleimido-functionalized hydrophilic polymers via copper-mediated living radical polymerization: A suitable alternative to pegylation chemistry. *J. Am. Chem. Soc.* **127**, 2966–2973 (2005).
32. Ju, M., Gong, F., Cheng, S. and Gao, Y. Fast and convenient synthesis of amine-terminated polylactide as a macroinitiator for ω-benzyloxycarbonyl-L-lysine-N-carboxyanhydrides. *Int. J. Polym. Sci.* **2011**, 1–8 (2011).
33. McMaster, P. D., Byrnes, E. W., Block, A. J. and Tenthorey, P. A. New antiarrhythmic agents. 5. α-Aminoaceto-2,6-xylidides with functionalized amide alkyl substituents. *J. Med. Chem.* **24**, 53–58 (1981).
34. Nielsen, J. and Rasmussen, P. H. Implementation of a combinatorial cleavage and deprotection scheme. 1. Synthesis of phthalhydrazide libraries. *Tetrahedron Lett.* **37**, 3351–3354 (1996).
35. Kembaren, R., Fokkink, R., Westphal, A. H., Kamperman, M., Kleijn, J. M., and Borst, J. W. Balancing enzyme encapsulation efficiency and stability in complex coacervate core micelles. *Langmuir* **36**, 8494–8502 (2020).
36. Dehghani-Firouzabadi, A. A. and Firouzmandi, S. Synthesis and characterization of a new unsymmetrical potentially pentadentate Schiff base ligand and related complexes with manganese(II), nickel(II), copper(II), zinc(II) and cadmium(II). *J. Braz. Chem. Soc.* **28**, 768–774 (2017).
37. Malkov, A. V., Stewart-Liddon, A. J. P., Teplý, F., Kobr, L., Muir, K. W., Haigh, D., and Kočovský, P. New pinene-derived pyridines as bidentate chiral ligands. *Tetrahedron* **64**, 4011–4025 (2008).
38. Chamoulaud, G. and Bélanger, D. Chemical modification of the surface of a sulfonated membrane by formation of a sulfonamide bond. *Langmuir* **20**, 4989–4995 (2004).
39. Sadman, K., Wang, Q., Chen, Y., Keshavarz, B., Jiang, Z. and Shull, K. R. Influence of hydrophobicity on polyelectrolyte complexation. *Macromolecules* **50**, 9417–9426 (2017).
40. Nosov, R., Padnya, P., Shurpik, D. and Stoikov, I. Synthesis of water-soluble amino functionalized multithiacalix[4]arene via quaternization of tertiary amino groups. *Molecules* **23**, 1–11 (2018).
41. Attia, M. I., El-Emam, A. A., Al-Turkistani, A. A., Kansoh, A. L. and El-Brollosy, N. R. Synthesis of novel 2-(Substituted amino)alkylthiopyrimidin-4(3H)-ones as potential antimicrobial agents. *Molecules* **19**, 279–290 (2014).
42. Akrami, S., Karami, B. and Farahi, M. Preparation and characterization of novel phthalhydrazide-functionalized MCM-41 and its application in the one-pot synthesis of coumarin-fused triazolopyrimidines. *RSC Adv.* **7**, 34315–34320 (2017).
43. Luan, F., Wei, L., Zhang, J., Tan, W., Chen, Y., Dong, F., Li, Q. and Guo, Z. Preparation and characterization of quaternized chitosan derivatives and assessment of their antioxidant activity. *Molecules* **23**, 516-529 (2018).
44. Hill, M. R., Mukherjee, S., Costanzo, P. J. and Sumerlin, B. S. Modular oxime functionalization of well-defined alkoxyamine-containing polymers. *Polym. Chem.* **3**, 1758–1762 (2012).
45. Yemm, E. W., Cocking, E. C. and Ricketts, R. E. The determination of amino-acids with ninhydrin. *Analyst* **80**, 209–214 (1955).
46. Sun, S. W., Lin, Y. C., Weng, Y. M. and Chen, M. J. Efficiency improvements on ninhydrin method for amino acid quantification. *J. Food Compos. Anal.* **19**, 112–117 (2006).
47. Friedman, M. Applications of the ninhydrin reaction for analysis of amino acids, peptides, and proteins to agricultural and biomedical sciences. *J. Agric. Food Chem.* **52**, 385–406 (2004).
48. Vijisha K., R. and Muraleedharan, K. The pKa values of amine based solvents for CO_2 capture and its temperature dependence—An analysis by density functional theory. *Int. J. Greenh. Gas Control* **58**, 62–70 (2017).
49. Juranić, I. Simple method for the estimation of pKa of amines. *Croat. Chem. Acta* **87**, 343–347 (2014).
50. Bhattacharjee, S. DLS and zeta potential - What they are and what they are not? *J. Control. Release* **235**,

337–351 (2016).
51. Lindhoud, S., Norde, W. and Cohen Stuart, M. A. Effects of polyelectrolyte complex micelles and their components on the enzymatic activity of lipase. *Langmuir* **26**, 9802–9808 (2010).
52. Topel, Ö., Çakir, B. A., Budama, L. and Hoda, N. Determination of critical micelle concentration of polybutadiene-block- poly(ethyleneoxide) diblock copolymer by fluorescence spectroscopy and dynamic light scattering. *J. Mol. Liq.* **177**, 40–43 (2013).
53. Santos, M. S., Tavares, F. W. and Biscaia, E. C. Molecular thermodynamics of micellization: Micelle size distributions and geometry transitions. *Brazilian J. Chem. Eng.* **33**, 515–523 (2016).
54. van der Kooij, H. M., Spruijt, E., Voets, I. K., Fokkink, R., Cohen Stuart, M. A., and van der Gucht, J. On the stability and morphology of complex coacervate core micelles: From spherical to wormlike micelles. *Langmuir* **28**, 14180–14191 (2012).
55. Rijcken, C. J. F., Soga, O., Hennink, W. E. and van Nostrum, C. F. Triggered destabilisation of polymeric micelles and vesicles by changing polymers polarity: An attractive tool for drug delivery. *J. Control. Release* **120**, 131–148 (2007).
56. Gilles, M. A., Hudson, A. Q. and Borders, C. L. Stability of water-soluble carbodiimides in aqueous solution. *Anal. Biochem.* **184**, 244–248 (1990).
57. Douglas T. Browne, S. B. and Kent, H. Formation of non-amidine products in the reaction of primary amines with imido esters. **67**, 126–132 (1975).
58. Hunter, M. J. and Ludwig, M. L. The Reaction of Imidoesters with Proteins and Related Small Molecules. *J. Am. Chem. Soc.* **84**, 3491–3504 (1962).
59. Keleştemur, S., Altunbek, M. and Culha, M. Influence of EDC/NHS coupling chemistry on stability and cytotoxicity of ZnO nanoparticles modified with proteins. *Appl. Surf. Sci.* **403**, 455–463 (2017).
60. Totaro, K. A. Liao, X., Bhattacharya, K., Finneman, J. I., Sperry, J. B., Massa, M. A., Thorn, J., Ho, S. V. and Pentelute, B. L. Systematic investigation of EDC/sNHS-mediated bioconjugation reactions for carboxylated peptide substrates. *Bioconjug. Chem.* **27**, 994–1004 (2016).
61. Eroglu, B. I., Kilinc, Y. B. and Mustafaeva, Z. Bioconjugation of Hepatitis B antigenic peptide with polymeric carriers through various carbodiimide chemistry. *Turkish J. Biochem.* **36**, 222–229 (2011).
62. Liu, H., Zhao, F., Koo, B., Luan, Y., Zhong, L., Yun, K., and Shin, Y. Dimethyl 3,3″-dithiobispropionimidate (DTBP) as a cleavable disulfide-based polymer to encapsulate nucleic acids in biological sample preparation. *Sensors Actuators, B Chem.* **288**, 225–231 (2019).
63. Xu, X., Smith, A. E. and McCormick, C. L. Facile 'One-Pot' preparation of reversible, disulfide-containing shell cross-linked micelles from a RAFT-synthesized, pH-responsive triblock copolymer in water at room temperature. *Aust. J. Chem.* **62**, 1520–1527 (2009).
64. Durney, A. R., Kawaguchi, S., Pennamon, G. and Mukaibo, H. Polymeric hydrogel thin film synthesis via diffusion through a porous membrane. *Mater. Lett.* **133**, 171–174 (2014).
65. Koniev, O. and Wagner, A. Developments and recent advancements in the field of endogenous amino acid selective bond forming reactions for bioconjugation. *Chem. Soc. Rev.* **44**, 5495–5551 (2015).
66. Oupický, D., Carlisle, R. C. and Seymour, L. W. Triggered intracellular activation of disulfide crosslinked polyelectrolyte gene delivery complexes with extended systemic circulation in vivo. *Gene Ther.* **8**, 713–724 (2001).
67. Harada, A. and Kataoka, K. Chain length recognition: Core-shell supramolecular assembly from oppositely charged block copolymers. *Science* **283**, 65-67 (1999).
68. Harada, A. and Kataoka, K. Novel polyion complex micelles entrapping enzyme molecules in the core. 2. Characterization of the micelles prepared at nonstoichiometric mixing ratios. *Langmuir* **15**, 4208–4212 (1999).
69. Cates, M. E. Reptation of living polymers: Dynamics of entangled polymers in the presence of reversible chain-scission reactions. *Macromolecules* **20**, 2289–2296 (1987).
70. Klein, J. Evidence for reptation in an entangled polymer melt. *Nature* **271**, 143–145 (1978).
71. Swift, T., Swanson, L., Geoghegan, M. and Rimmer, S. The pH-responsive behaviour of poly(acrylic acid) in aqueous solution is dependent on molar mass. *Soft Matter* **12**, 2542-2549 (2016).

Supplementary information

S5.1. ^{1}H NMR spectra of the homopolymer poly(2-vinylpyridine)$_{44}$ (P2VP$_{44}$) before and after quaternization

These data show that the quaternization and deprotection of the homopolymer were successful, so that the quaternization procedure could also be applied to the diblock copolymer poly(2-vinylpyridine)$_{128}$-*block*-poly(ethylene oxide)$_{477}$ (P2VP$_{128}$-*b*-PEO$_{477}$).

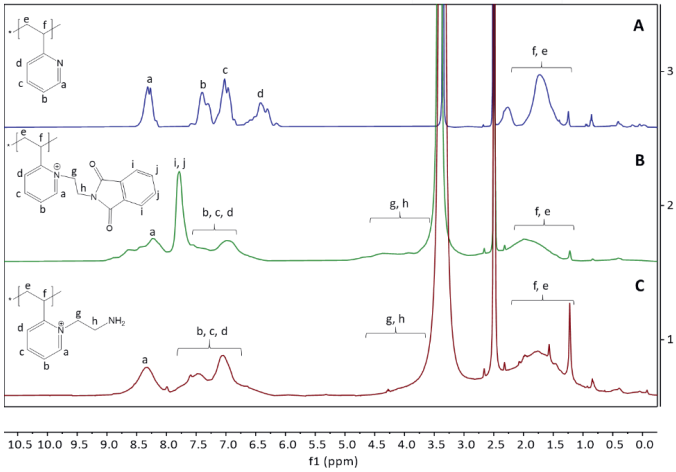

Figure S5.1. ^{1}H NMR spectra of the homopolymer P2VP$_{44}$. (A) Homopolymer before quaternization, (B) homopolymer after quaternization using *N*-(2-bromoethyl)phthalimide, (C) quaternized homopolymer after deprotection using hydrazine hydrate. Spectra A, B, and C were recorded in DMSO-d_6

S5.2. The quaternization degree of the homopolymer P2VP$_{44}$ was calculated from the ratio of the integral area of the aromatic rings and the integral area of P2VP's backbone

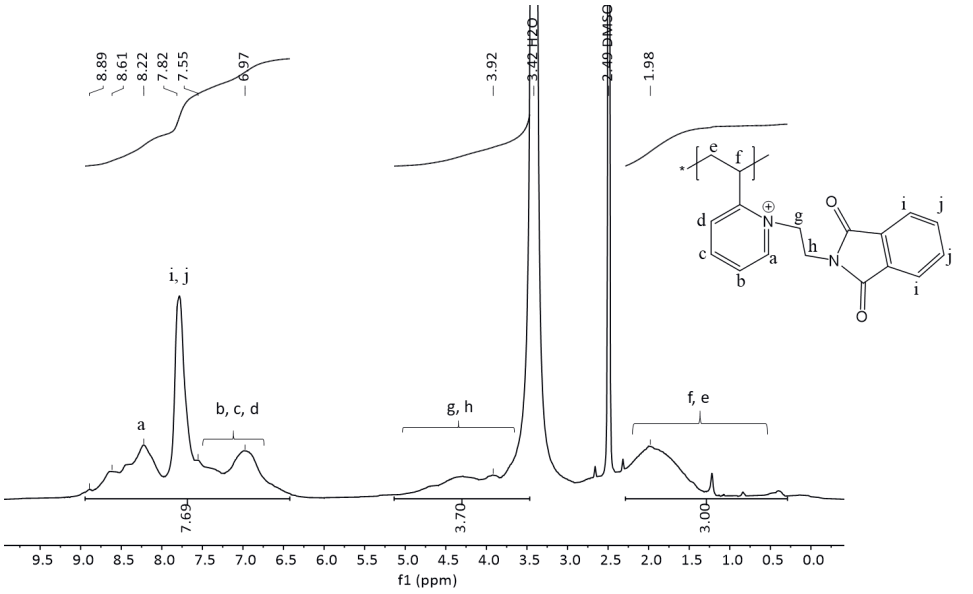

Figure S5.2. ^{1}H NMR spectrum of the homopolymer P2VP$_{44}$ after quaternization using *N*-(2-bromoethyl)phthalimide. The spectrum was recorded in DMSO-d_6. Degree of quaternization (DQ) was calculated from the ratio of the integral area of the aromatic rings and the integral area of P2VP's backbone. DQ = (((7.69 – 4)/4) : (3/3)) * 100 % = 92%.

S5.3. ^{1}H NMR spectrum of the diblock copolymer poly(2-vinylpyridine)$_{128}$-*block*-poly(ethylene oxide)$_{477}$ (P2VP$_{128}$-*b*-PEO$_{477}$) before quaternization in $CDCl_3$, to confirm the composition of P2VP-*b*-PEO before quaternization

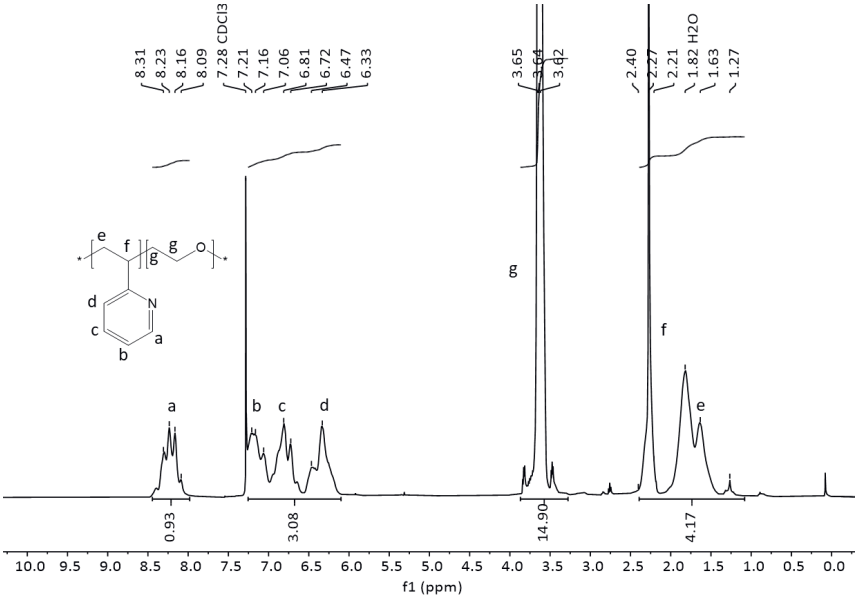

Figure S5.3. ^{1}H-NMR spectrum of the neat diblock copolymer P2VP$_{128}$-*b*-PEO$_{477}$ in $CDCl_3$. The block ratio of P2VP and PEO was calculated from the ratio of the integral area of the aromatic rings and the integral area of PEO. Block ratio = (0.93 + 3.08) : 14.9 = 4.0 : 14.9 = 128 : 477.

S5.4. The quaternization degree of the diblock copolymer P2VP$_{128}$-*b*-PEO$_{477}$ was calculated from the ratio of the integral area of the aromatic region and the integral area of P2VP's backbone

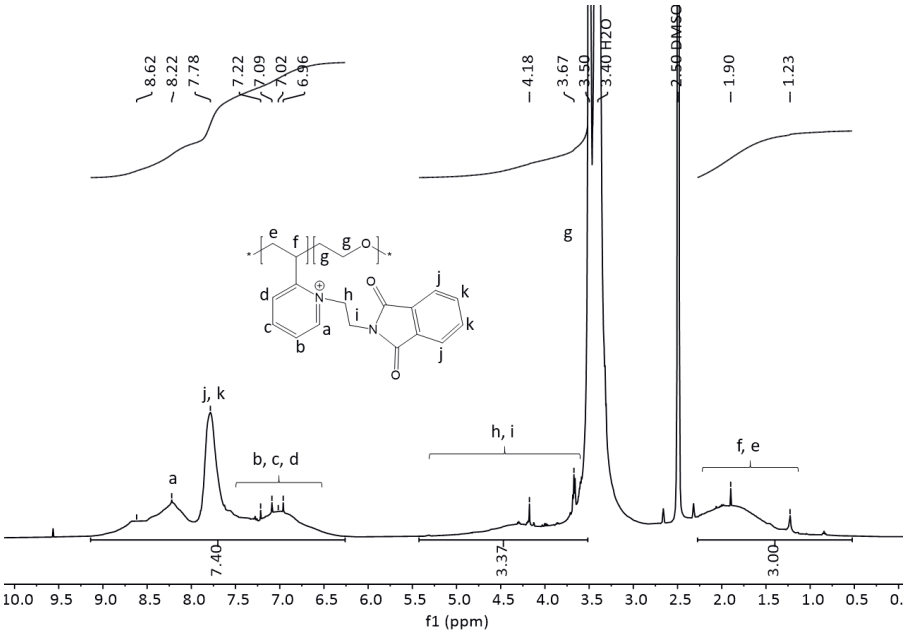

Figure S5.4. ^{1}H-NMR spectrum of the diblock copolymer P2VP$_{128}$-*b*-PEO$_{477}$ after quaternization using *N*-(2-bromoethyl)phthalimide. The spectrum was recorded in DMSO-d_6. The degree of quaternization (DQ) was calculated from the ratio of the integral area of the aromatic rings and the integral area of P2VP's backbone. DQ = (((7.4 – 4)/4) : (3/3)) * 100 % = 85 %.

S5.5. For determination of the CMC, a 2.50 µM C3M stock solution was diluted with buffer and analyzed by dynamic light scattering (DLS)

From this dilution series, the CMC was estimated to be equal to or lower than 0.59 µM. at even lower polymer concentrations the measurement becomes inaccurate due to relatively strong scattering of the buffer (17 – 20 kHz).

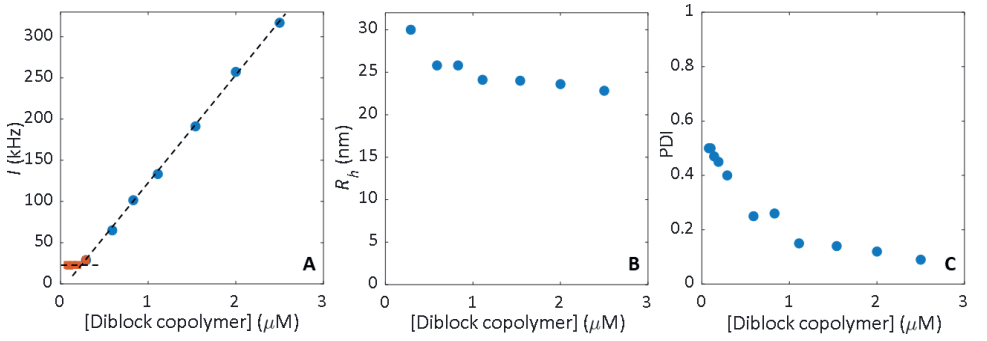

Figure S5.5. Determination of the critical micelle concentration (CMC) at the PMC. DLS results are plotted as a function of the quaternized $P2VP_{128}$-*b*-PEO_{477} concentration. (A) Absolute scattering intensity (I), (B) hydrodynamic radius (R_h), and (C) polydispersity index (PDI). Dashed lines indicate the slope of the scattering intensity values during dilution. Orange data points indicate weak scattering below the estimated CMC.

Chapter 6 :

Core-crosslinking enhances the salt resistance of enzyme-containing complex coacervate core micelles

Manuscript in preparation as:

Kembaren, R., Kleijn, J. M., Borst, J. W, Kamperman, M., and Hofman, A. H. Core-crosslinking enhances the salt resistance of enzyme-containing complex coacervate cores micelles.

Abstract

Enzymes are biomolecules that are often used in pharmaceutical and food applications. Enzymes can lose their enzymatic activity upon denaturation or degradation by proteases. Protection of enzymes can be achieved by encapsulating them in complex coacervate core micelles (C3Ms). The encapsulation of enzymes into C3Ms is easily achieved by mixing solutions of enzyme and oppositely charged-neutral hydrophilic diblock copolymer. Despite the simple preparation, the application of C3Ms is limited because they quickly disintegrate when salt is added, even when salt concentrations are moderate. In the previous chapter, we studied C3Ms composed of purely synthetic polyelectrolytes and found that core-crosslinking significantly improved the stability of C3Ms against high salt concentrations and pH changes. This chapter aims to increase the salt stability of enzyme-containing C3Ms by applying the same crosslinking strategy. The C3Ms were composed of a quaternized amine-functionalized cationic-neutral diblock copolymer and a negatively charged enzyme, CotA laccase. Dimethyl-3,3'-dithiobispropionimidate (DTBP) was used as a crosslinker. Based on DLS and FCS results, it was concluded that crosslinked enzyme-containing C3Ms are more stable against salt than non-crosslinked C3Ms. Only a slight reduction in enzyme activity was observed, which was attributed to the polymer network in the core that hinders the substrate from binding to CotA. Core-crosslinking is a very effective strategy for encapsulating proteins in C3Ms.

6.1. Introduction

Complex coacervate core micelles (C3Ms) are formed by mixing aqueous solutions of ionic-neutral hydrophilic diblock copolymers with oppositely charged macromolecules at concentrations above their critical micelle concentration (CMC).[1–4] The structure of C3Ms consists of a complex coacervate core and a neutral hydrophilic shell/ corona.[5–7] The core of a C3M contains a significant amount of water, making this nanostructure suitable for the encapsulation of charged and hydrophilic biomolecules, such as proteins, DNA, and RNA.[2,5,8–13] Moreover, the corona of C3Ms can protect the encapsulated material against the external environment. Therefore, C3Ms can be useful for many applications such as gene and drug delivery,[14] nanobioreactors,[13] biosensors,[15] and nanoprobes.[8]

The driving force for the formation of C3Ms is the electrostatic attraction between the oppositely charged polyelectrolyte chains and the entropy gain from the release of counterions upon complex formation. The application of C3Ms is limited since they quickly disintegrate when salt is added. Moreover, due to the lower charge density of proteins, C3Ms composed of proteins are even more vulnerable to disintegration than C3Ms composed of synthetic polyelectrolytes.[16–19] C3Ms typically disintegrate completely above a certain salt concentration, the so-called critical salt concentration (CSC).[5,8]

In the previous chapter, we demonstrated that by crosslinking the core of C3Ms, which is composed of a primary amine-functionalized cationic-neutral hydrophilic diblock copolymer and an anionic homopolymer, the C3Ms' stability is significantly improved against salt and pH changes.[20–22] In this chapter, we implemented this core-crosslink strategy to improve the salt stability of enzyme-containing C3Ms. Moreover, by using an active enzyme, we were able to measure the effect of crosslinking on the enzyme's catalytic activity. To achieve this goal, we used the amine-functionalized diblock copolymer poly(*N*-methyl-2-vinyl-pyridinium)$_{128}$-*block*-poly(ethylene oxide)$_{477}$ (Q_{NH_2}PM2VP$_{128}$-*b*-PEO$_{477}$). This diblock copolymer was generated via a two-step quaternization reaction, by first using *N*-(2-bromoethyl)phthalimide and then iodomethane as reagents. We used this two-step quaternization procedure to increase the degree of quaternization and enzyme encapsulation efficiency into C3Ms.

In this study, we used CotA laccase as a model enzyme. The crosslinker dimethyl-3,3′-dithiopropionimidate dihydrochloride (DTBP) was used because it can form a covalent link between primary amines at high pH and contains a cleavable disulfide bond in its structure. The ability to disrupt a disulfide-bond is beneficial for drug delivery as the reduction (cleavage)

occurs inside a cell in response to glutathione concentrations higher than those at the cell's exterior.[23]

The formation, structural features, and the salt stability of the enzyme-containing C3Ms were investigated using dynamic light scattering (DLS) and fluorescence correlation spectroscopy (FCS). With DLS and FCS, we can observe the C3M formation and stability. In addition, with FCS, we can observe the encapsulation efficiency since FCS can discriminate between fluorescently labeled enzymes in micelles and free in solution. We also examined the effect of crosslinking on enzyme activity in this study.

6.2. Experimental section

6.2.1. Materials

The diblock copolymer poly(2-vinylpyridine)$_{128}$-*block*-poly(ethylene oxide)$_{477}$ (P2VP$_{128}$-*b*-PEO$_{477}$) (M_n = 34.5 kg/ mol, M_w/ M_n = 1.1) was obtained from Polymer Source Inc. Dimethyl-3,3′-dithiopropionimidate dihydrochloride (DTBP) and the fluorescent probe for the enzyme, Alexa Fluor 488 C5 maleimide, were obtained from Thermo Fisher Scientific. The quaternization agents *N*-(2-bromoethyl)phthalimide and iodomethane (99 %, stabilized with copper), and the substrate for the activity assay, 2,2′-azino-bis(3-ethylbenzothiazoline-6-sulfonic acid) diammonium salt (ABTS) were purchased from Sigma-Aldrich. The reducing agent 1,4-dithiothreitol (DTT) was purchased from Carl Roth.

6.2.2. Amine-functionalization of diblock copolymer

Quaternization of the diblock copolymer poly(2-vinylpyridine)$_{128}$-*block*-poly(ethylene oxide)$_{477}$ was performed following a modified procedure that was described previously.[24] The diblock copolymer (0.21 g, 0.78 mmol of 2VP units) was added to *N*-(2-bromoethyl)phthalimide (5 eq. with respect to 2VP, 0.99 g, 3.88 mmol) in a small vial under continuous stirring and subsequently heated at 120 ºC for 2 hours (Scheme 6.1). After allowing the mixture to cool down to room temperature, 5 mL dichloromethane was added to dissolve the solidified product, and the solution was then precipitated into diethyl ether. The precipitated polymer was filtered and washed with diethyl ether five times and subsequently dried in a vacuum oven, yielding 0.20 g of off-white powder (yield 95 %).

The remaining 2VP groups were quaternized by adding 0.8 mL iodomethane (13.5 mmol) to the polymer (0.20 g, 0.68 mmol of 2VP units) in 10 mL acetonitrile. The reaction was allowed to proceed overnight at reflux under an N_2 atmosphere. The

solution was then precipitated into diethyl ether. The precipitated polymer was filtered, washed five times with diethyl ether, and dried in a vacuum oven. Further purification was achieved by dialysis against water. After that, the polymer was dried using freeze-drying (0.15 g, yield 75 %).

The deprotection of the phthalimide was done using a slightly modified procedure described in our previous study.[24] After the quaternization procedure, the polymer powder (0.15 g) was dissolved in 8 mL of ethanol and heated at 80 ºC with reflux in an N_2 environment. The deprotection was done by mixing the quaternized diblock copolymer with hydrazine hydrate solution (78-82 % in H_2O) (10 eq. with respect to 2VP, 8.3 mmol) for 18 hours at 80 ºC. The mixture was then cooled to 4 ºC before being filtered to remove phthalhydrazide. The filtrate was collected, and the volume of the filtrate was decreased to roughly 3 mL using a rotary evaporator. The solution was subsequently dialyzed against water for three days to eliminate excess hydrazine hydrate and the side product phthalhydrazide (MWCO 3.5 kg/mol).[25] The polymer solution was then freeze-dried. The quaternization degree was determined by using ^{1}H-NMR (using a Bruker Avance III 400 MHz NMR spectrometer) to be about 97 %.

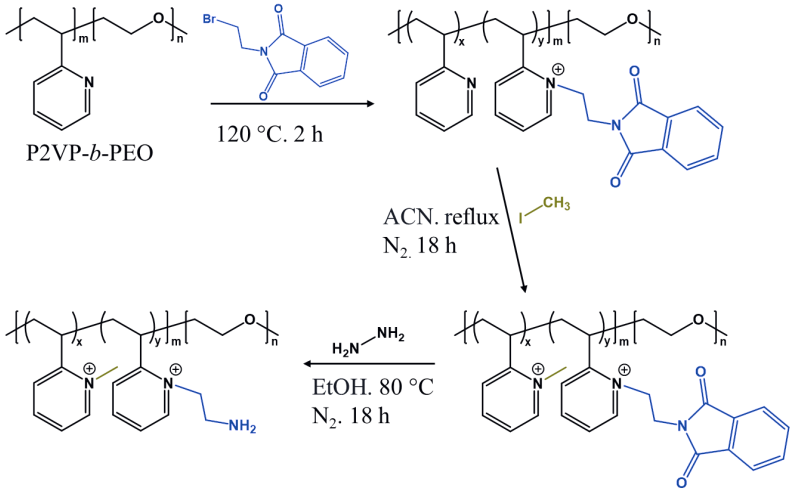

Scheme 6.1. Synthesis of an amine-functionalized diblock copolymer, $Q_{NH_2}PM2VP_{128}$-*b*-PEO_{477}, via a two-step quaternization process, then followed by deprotection.

6.2.3. CotA production and purification

The production and purification of CotA laccase (65 kDa, pI = 5.8) were carried out as described in our earlier studies.[17,26] *Escherichia coli* Rosetta cells with the CotA gene in the pBAD vector were cultured at 37 ºC in ampicillin and chloramphenicol-containing lysogeny broth (LB)

medium. The induction of CotA overexpression was done by adding 0.15 % L-arabinose and 0.25 mM $CuSO_4$ to the cell culture when the optical density of the cultured medium reached a value of 0.6–0.8. The cell culture was then incubated at 25 ºC for 20 hours. Because copper could accelerate the oxidation of the free thiol group of the cysteine, the induction of CotA-S313C was carried out with just 0.15 % L-arabinose (without copper salt solution). Cation exchange chromatography (SP-Sepharose FF column) and gel filtration chromatography (Superdex 200 column) were applied to purify CotA.

The enzyme was fluorescently labeled by combining CotA-S313C with Alexa Fluor 488 C5 maleimide at a molar ratio of approximately 1:10, then incubating it at 4 ºC in the dark overnight. The mixture was passed through a Biogel-P6DG gel filtration column with a 20 mM Tris HCl buffer containing 10 mM NaCl to remove unreacted labels. A spin filter concentrator was used to capture and concentrate the fluorescent protein-containing fractions. The labeled CotA was then further purified on a gel filtration column (Superdex 200 column). Fractions showing absorption at 280 and 490 nm were collected and concentrated using a spin filter concentrator. SDS-PAGE was used to determine the purity of CotA: the purity of the enzyme is about 90 %, analyzed using ImageJ software.

6.2.4. Formation of enzyme-containing complex coacervate core micelles

To form C3Ms, mixtures with a varying concentration of the amine-functionalized diblock copolymer, $Q_{NH_2}PM2VP_{128}$-*b*-PEO_{477}, and a constant concentration of enzyme (1 μM) were prepared. CotA and quaternized diblock copolymer solutions were prepared separately in a 10 mM sodium carbonate buffer at pH 10.8, and filtered through a 0.2 μm polyethersulfone membrane syringe filter. After being mixed, the solutions were stored at room temperature overnight before measurement. $Q_{NH_2}PM2VP_{128}$-*b*-PEO_{477} has a charge of about +124 (elementary units) at pH 10.8 (based on the quaternization degree of the pyridine rings under the assumption that primary amines are uncharged at pH 10.8). The net charge of the CotA laccase was calculated using PROPKA 3.1 software based on its three-dimensional structure.[17,27,28] This resulted in a predicted net charge value of about −41 for CotA laccase in buffer at pH 10.8. C3M formation was observed using dynamic light scattering (DLS) and fluorescence correlation spectroscopy (FCS).

6.2.5. Core-crosslinking of micelles

Core-crosslinked C3Ms were prepared by using DTBP as a crosslinker. After mixing quaternized diblock copolymer with CotA laccase, different concentrations of DTBP (0.25 and 0.5 eq. relative to the amine groups of the diblock copolymer) were added to the micellar solution. The crosslinking reaction was performed in 10 mM sodium carbonate buffer at pH 10.8, at room temperature for 3 hours.

6.2.6. Salt stability of C3Ms

The stability of C3Ms was determined by using salt titration: a concentrated salt solution (4 M NaCl) was titrated into the enzyme-containing C3M dispersion and was followed by DLS and FCS measurements. To cleave the disulfide bridges in the DTBP linker, a final concentration of 10 mM DTT was added to the DTBP-core crosslinked C3Ms and allowed to react for 30 minutes. After this, salt was again titrated into the C3M solutions while being monitored by DLS and FCS. Fluorescently labeled CotA with Alexa Fluor 488 was used for the FCS measurements.

6.2.7. Activity measurement

We investigated the effect of the core-crosslinking on the activity of CotA by using 2,2′-azino-bis-(3-ethylbenzothiazoline-6-sulfonic acid) diammonium salt (ABTS) as a substrate for the activity assay. CotA oxidizes ABTS to produce a green-colored cationic radical ($ABTS^{\bullet+}$), which can be identified by measuring the absorbance at 420 nm (ε = 36 000 M^{-1} cm^{-1}). The activity of free CotA, of CotA-C3Ms (control), and of core-crosslinked C3Ms samples was assessed using 1.0 mM ABTS in a 100 mM sodium acetate buffer at pH 4.4. The relative activity was calculated as the ratio between the specific activity of the sample of interest and the specific activity of free CotA. The total protein concentration was determined using the BCA protein assay.

The effect of DTT on the CotA activity was also measured. This was done by adding a final concentration of 10 mM DTT to the sample, after which DTT was removed by an Amicon concentrator (cutoff of 10 kDa). The activity was then determined using the same procedure as described above.

6.2.8. Dynamic light scattering (DLS)

DLS was performed on an ALV-LSE 41/ CGS-8F goniometer system equipped with a DPSS laser (λ = 660 nm, 200 mW). Measurements of the preferred micellar composition (PMC),

hydrodynamic radius (R_h), and polydispersity index (PDI) were done at a fixed 90º angle. Cumulants fit analysis and the Stoke-Einstein equation for spherical particles were applied to analyze the autocorrelation functions and determination of R_h. The shape of the C3M samples was determined using multi-angle DLS at angles ranging from 50º to 130º in steps of 10º. Intensity correlation functions were recorded for 10 seconds and averaged over 8 runs per angle.

6.2.9. Fluorescence correlation spectroscopy (FCS)

FCS was performed on a Leica TCS SP8 X SMD system equipped with a 63× 1.20 NA (numerical aperture) water immersion objective. Measurements were performed in a µ-Slide 8-wells chambered coverslip (Ibidi®). A supercontinuum laser was used to excite the samples by selecting a 488 nm laser line with a pulse frequency of 40 MHz. The size-adjustable pinhole was set at 1 Airy unit for all measurements. Fluorescence emission was detected between 495 and 550 nm using a hybrid detector coupled to a PicoHarp 300 TCSPC module (PicoQuant). Rhodamine 110 (diffusion coefficient D = 4.3 × 10^{-10} m^2 s^{-1}) was used to determine the confocal structure parameter a (expressed as ω_z/ω_{xy}, where ω_{xy} and ω_z are the equatorial and axial radii of the detection volume, respectively).

In FCS, the autocorrelation function $G(t)$ curves enable the estimation of the diffusion time and the number of fluorescent particles detected in the confocal volume.[29,30] The FFS-data processor version 2.3 (Scientific Software Technologies Software Centre, Belarus) was used for the FCS data analysis.[27,28,17] The equation used to fit translational data, which includes the triplet state, is as follows:

$$G(t) = 1 + \frac{1}{\langle N \rangle} \cdot \left(1 + \frac{F_{trip}}{1-F_{trip}}\right) e^{-t/T_{trip}} \cdot \sum_{i=1}^{n} \frac{F_i}{\left(1+\frac{t}{\tau_{dif,i}}\right) \cdot \sqrt{1+\left(\frac{\omega_{xy}}{\omega_z}\right)^2 \cdot \frac{t}{\tau_{dif,i}}}} \quad (6.1)$$

This equation was used to obtain N for the different samples, where N represents the average number of fluorescent particles in the confocal volume, F_{trip} represents the fraction of molecules in the triplet state, and T_{trip} represents the average time a molecule resides in the triplet state. The last part of the equation describes the diffusion behavior of the molecules, where F_i represents the fraction of species i, and $\tau_{dif,i}$ represents the diffusion time of species i. From the diffusion time, the diffusion coefficient D can be calculated using the following equation:

$$D = \frac{{\omega_{xy}}^2}{4\tau_{dif}} \quad (6.2)$$

The hydrodynamic radius of the fluorescent particle, derived from D, was calculated using the Stokes-Einstein relation for spherical particles:

$$D = \frac{k_B T}{6\pi\eta R_h} \quad (6.3)$$

Where k_B is the Boltzmann constant, T is the absolute temperature, and η is the viscosity of the solution.

6.3. Results and discussion

6.3.1. Functionalization of the diblock copolymer

Sequential quaternization of the diblock copolymer using *N*-(2-bromoethyl)phthalimide and iodomethane aims to introduce both positive charges and primary amines onto the diblock copolymer.[31–34] In our previous study, we found that quaternization using a phthalimide-protected primary amine group prevents self-cyclization and polymerization. Lowering the reaction temperature from 150 to 120 °C in step 1, and additional quaternization using iodomethane (step 2) reduced the number of primary amines and increased the total degree of quaternization of the diblock copolymer. The quaternization and deprotection of the diblock copolymer were confirmed by using ^{1}H-NMR. After quaternization with *N*-(2-bromoethyl)phthalimide, the signals from P2VP's aromatic ring are shifted (6-8.5 ppm), and an intense peak appeared at 7.75 ppm from the phthalimide aromatic rings (Figure 6.1A vs 6.1B; protons [j] and [k]). Moreover, a new broad signal appeared around 3.5-5.5 ppm originating from the two CH_2 groups of ethyl phthalimide (protons [h] and [i]). These results show that quaternization of the diblock copolymer was successful, with a degree of quaternization (DQ) of about 48 % (calculated from the ratio of the integral area of the aromatic rings and the integral area of P2VP's backbone) (Figure S6.1, Supplementary information). The DQ in this study is significantly lower than what we achieved in the previous study (DQ of about 85 %)[24] due to the lower reaction temperature (120 ºC) that we used during the quaternization. The reason for using a lower temperature is that we intended to leave some unquaternized pyridine units for the second quaternization step using iodomethane. After quaternization using iodomethane, an increased intensity of the peak at 3.9 ppm is observed, originating from the methyl group (Figure 6.1C; protons [l]). This result indicates that this second quaternization step was successful as well. The degree of quaternization increased to about 97 % (calculated from the ratio of the aromatic rings' integral, the integral value of the methyl group, and the integral value of P2VP's backbone) (Figure S6.2, Supplementary information). Treatment of the quaternized diblock copolymer with hydrazine hydrate resulted in the disappearance of the peak at 7.78 ppm due to the removal of the phthalimide group.[31,35,36] The deprotection using hydrazine hydrate resulted in primary amines that are accessible for the crosslinking reaction.[35,37]

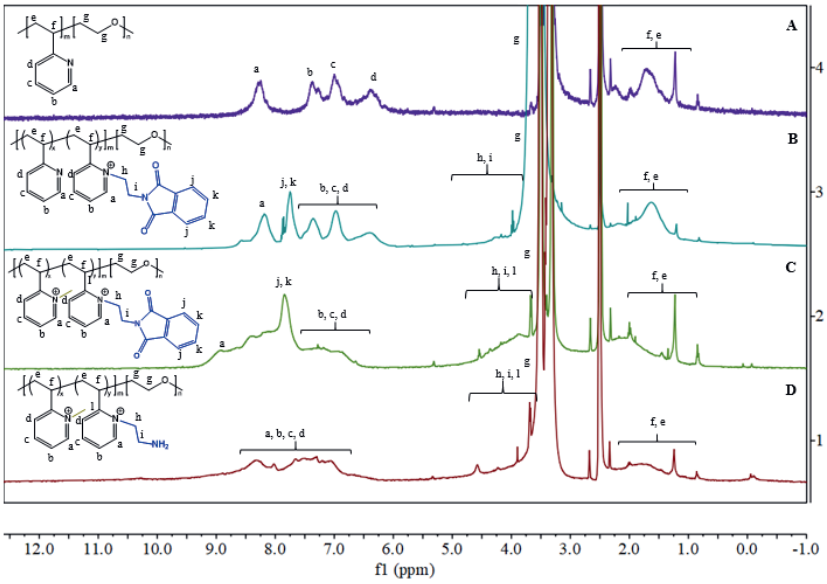

Figure 6.1. ^{1}H-NMR spectra of the quaternized diblock copolymer Q_{NH_2}PM2VP$_{128}$-*b*-PEO$_{477}$. (A) Diblock copolymer before quaternization, (B) diblock copolymer after quaternization using *N*-(2-bromoethyl)phthalimide, (C) diblock copolymer after second quaternization step using iodomethane, (D) quaternized diblock copolymer after deprotection using hydrazine hydrate. Spectra A, B, C, and D were recorded in DMSO-d_6.

6.3.2. Encapsulation of CotA into C3Ms

C3Ms were generated by mixing aqueous solutions of CotA and the quaternized amine-functionalized diblock copolymer Q_{NH_2}PM2VP$_{128}$-*b*-PEO$_{477}$ at pH 10.8. CotA-containing C3Ms cannot be formed at physiological pH due to insufficient net charges of CotA (only −10) and a positively charged patch (+15) on the CotA surface.[17] Mixing of CotA and diblock copolymer at a pH of around 7 led to the formation of large heterogeneous aggregates, and C3Ms are not forming (Figure S6.3, Supplementary information). Our previous study showed that a pH of 10.8 provides a sufficient net negative charge on CotA and eliminates the influence of the positively charged patch on the CotA surface. At pH 10.8, CotA is still active and maintains its secondary structure.[17] At this pH, the quaternized pyridine block of the polymer carries a pH-independent positive charge, while the primary amine part of the diblock has no charge. The positively charged pyridine block of Q_{NH_2}PM2VP$_{128}$-*b*-PEO$_{477}$ binds electrostatically to the negatively charged CotA, generating C3Ms.

Dynamic light scattering (DLS) was used to determine that C3Ms had been formed. Different mixtures with a varying concentration of diblock copolymer and a constant concentration of CotA were prepared. After equilibration, the scattering intensity (I), the hydrodynamic radius (R_h), and the polydispersity index (PDI) were measured as a function of diblock copolymer concentration. This experiment was performed to find the preferred micellar composition (PMC), which is identified as the mixing composition for which the scattering intensity reaches a maximum. The results are given in Figure 6.2.

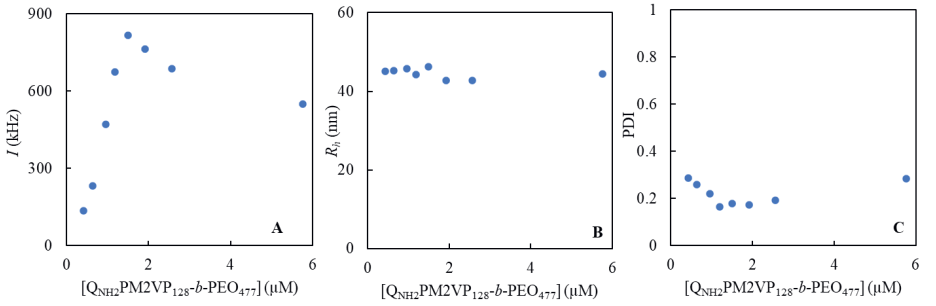

Figure 6.2. DLS results for mixtures with a constant concentration of CotA (1.0 μM) and different concentrations of diblock copolymer Q_{NH_2}PM2VP$_{128}$-*b*-PEO$_{477}$. (A) Scattering intensity (I), (B) hydrodynamic radius (R_h), and (C) PDI.

The light scattering intensity (Figure 6.2A) increases with the concentration of diblock copolymer, indicating the formation of C3Ms. The addition of 1.49 μM of quaternized diblock copolymer to 1.0 μM of CotA laccase resulted in a maximum scattering intensity, meaning that this composition contains the highest number and most well-defined micelles. The mixed ratio composition (F^-) is calculated by using the equation $F^- = \frac{[n^-]}{[n^+] + [n^-]}$, where $[n^-]$ refers to the concentration of net negative charge on the enzyme molecules, and $[n^+]$ refers to the concentration of positive charge on the diblock copolymer. The DLS results show that the PMC was at $F^- = 0.18$ ((1*41) / ((1.49*124) + (1*41)) = 0.18), where 41 is the net number of negative charges per enzyme molecule and 124 is the average number of positive charges per diblock copolymer. The PMC of these C3Ms is not at charge stoichiometry ($F^- = 0.5$) because additional interactions play a role in the micelle formation, such as hydrophobic, cation-π, π-π interactions, and potentially also hydrogen-bonding between the neutral amines.[5,8,27,38–42] Another reason for the PMC being shifted is steric hindrance: the location of the positively charged pyridine group is close to the vinyl backbone and uncharged ethyleneamine group, which makes it more

difficult to access by the negatively charged part of CotA, resulting in more diblock copolymer needed to compensate for the charge of CotA.[43,44]

At the PMC, the C3Ms have a hydrodynamic radius of 47.8 ± 5.7 nm (Figure 6.2B), and a minimum in the PDI is found (PDI = 0.12 ± 0.02) (Figure 6.2C), indicating a narrow size distribution.[45] In addition, multi-angle DLS showed that the C3Ms have a spherical shape (Figure S6.4, Supplementary information).[14,46,47] The addition of quaternized diblock above 1.49 μM leads to an excess of positive charge (more block copolymer as compared to enzyme), and a subsequent decrease in the concentration of well-defined micelles, which is observed as decreased light scattering intensity and increased PDI.[5,6,8]

6.3.3. Core-crosslinked C3Ms observed by DLS

Core-crosslinked C3Ms were prepared at the PMC. The core-crosslinking reaction was done by adding an imidoester crosslinker, DTBP, to the C3Ms at pH 10.8. At pH 10.8, the primary amines are deprotonated and become more nucleophilic. Consequently, primary amines are more reactive toward electrophiles at this pH.[48] Moreover, at a high pH, imidoesters also have the highest specificity for amine reactions.[48–50] Crosslinking of amines in the core of the micelles, resulting in formation of amidine bonds, was achieved by a 3 hours reaction with DTBP.[21,51] Proteins also contain multiple primary amines in their structure (at the N-terminus and in the side-chain of lysine residues, of which CotA has 25 units). However, it should be noted that the number of primary amine groups on CotA is lower than that on the diblock copolymer (the diblock copolymer has about 61 primary amines). In the PMC, the concentration of diblock copolymer is higher than the concentration of enzyme. Therefore, crosslinking between the diblock copolymer chains is dominantly/ more likely to happen, especially at a low concentration of crosslinker. However, there may also be small amounts of crosslinking between enzyme and diblock or between enzyme molecules. After performing the reaction with 0.25 and 0.5 eq. DTBP with respect to the number of amine groups of the diblock copolymer, the micelles had an R_h of 46.7 ± 4.1, and 45.8 ± 7.2, respectively. These sizes are comparable to that of untreated micelles (R_h = 47.8 ± 5.7 nm). Furthermore, multi-angle DLS revealed that the spherical shape remained unaffected after crosslinking (Figure S6.4, Supplementary information).

6.3.4. C3Ms characteristics measured by FCS

The properties of the C3Ms and the effect of core-crosslinking were also investigated using FCS because it is possible to distinguish between free enzymes in solution and encapsulated

enzymes with FCS. To make our system suitable for FCS measurements, CotA was labeled with a fluorescent probe, Alexa Fluor 488. Figure 6.3 shows FCS measurements on solutions of free CotA and CotA-containing C3Ms with and without the addition of the DTBP crosslinker. From Figure 6.3A, it can be seen that the addition of diblock copolymer into a solution of CotA increases the diffusion time, which implies a decrease in the diffusion coefficient of the CotA, and is a result of the formation of C3Ms.[17,26–28,52]

In addition, that C3Ms are formed can also be observed by FCS based on the number of fluorescent particles detected in the confocal volume (N). When the fluorescently labeled CotA molecules are encapsulated, the number of fluorescent particles detected in the confocal volume is low, whereas the micelles have a high brightness because many fluorescent CotA molecules are encapsulated in one micelle.[17,27,28,53] The number of species detected in the confocal volume (N) can be quantified by looking at the intercept of the correlation function $G(t)$ with the Y-axis, which equals $1+1/N$ (Figure 6.3B). FCS analysis on the C3M samples show that N is about 5 ± 1, 5 ± 2, and 6 ± 1 for non-crosslinked C3Ms (control), core-crosslinked C3Ms with 0.25 eq DTBP, and core-crosslinked C3Ms with 0.5 eq. DTBP, respectively. The core-crosslinked C3Ms having a similar N to the C3M control sample suggests that they have the same concentration of micelles.

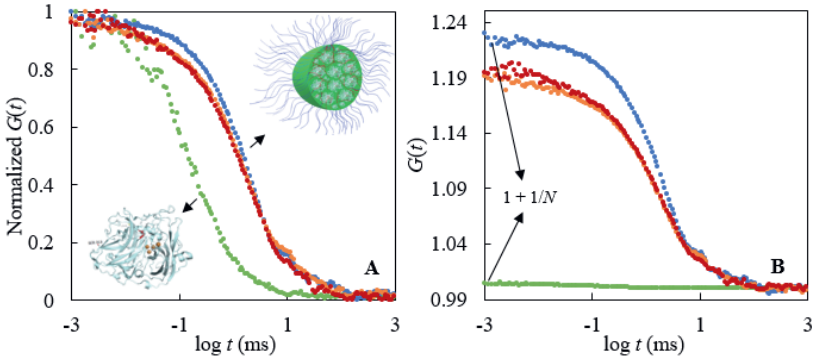

Figure 6.3. FCS measurements on C3Ms composed of fluorescently labeled CotA. (A) Normalized FCS autocorrelation curves ($G(t)$) for free CotA (green), C3M control (blue), core-crosslinked C3M with 0.25 eq. DTBP (orange) and core-crosslinked C3M with 0.5 eq. DTBP (red). (B) $G(t)$ for free enzyme, C3Ms control and core-crosslinked C3Ms.

The size of the fluorescent particles was calculated using the diffusion time generated from Equations 6.1 and 6.2. For CotA labeled with Alexa 488 free in solution, FCS analysis revealed an R_h of about 2.2 ± 0.5 nm, and for C3Ms containing CotA labeled with Alexa 488, an R_h of

44.3 ± 4.11 nm was obtained. The R_h of the core-crosslinked C3Ms was 39.6 ± 6.2 nm (0.25 eq. DTBP) and 37.8 ± 14.0 nm (0.5 eq. DTBP). The size information provided by FCS and DLS measurements is in good agreement. The autocorrelation functions $G(t)$ were analyzed using a two-component 3D diffusion model including a triplet state to estimate the fraction of enzyme free in solution and encapsulated in C3Ms (Equation 6.1). From this analysis, the fraction of encapsulated CotA was found to be 91.5 ± 5.9 %. After core-crosslinking of the C3Ms, the fraction of encapsulated enzyme was 85.9 ± 9.7 % and 86.7 ± 2.1 % when treated with 0.25 and 0.5 eq. DTBP, respectively. These results demonstrate that the encapsulation efficiency for core-crosslinked C3Ms is similar to that of non-crosslinked C3Ms, meaning that enzymes are maintained in the core and are thus not expelled. Quaternization of $P2VP_{128}$-*b*-PEO_{477} using *N*-(2-bromoethyl) phthalimide and iodomethane results in a higher encapsulation efficiency of the C3Ms: previously, we found encapsulation efficiency of around 77 ± 4 % for CotA encapsulation with quaternized $P2VP_{128}$-*b*-PEO_{477} with iodomethane.[26] The higher encapsulation efficiency in this case can be explained by the higher degree quaternization of diblock copolymer $Q_{NH_2}PM2VP_{128}$-*b*-PEO_{477}. In addition, the micelles are not only formed by electrostatic attraction, but also by non-electrostatic attraction.

6.3.5. Salt stability of C3Ms observed with DLS and FCS

To investigate if core-crosslinking affects the stability of enzyme-containing C3Ms, C3Ms were prepared at the PMC, and the stability against salt was studied using DLS and FCS. The addition of salt in moderate to high concentrations could lead to the disintegration of enzyme-containing C3Ms, which is reflected as a decrease in light scattering intensity (observed by using DLS) and as an increase in the number of fluorescent particles detected in the confocal volume (N) (observed by using FCS).

In Figure 6.4A, the scattering intensity for the three different C3M samples is plotted against the salt concentration, normalized to their scattering intensity at zero added salt. The measurements were performed up to 200 mM NaCl in steps of 50 mM NaCl. The scattering intensities of all samples decreased with increasing salt concentration. For the untreated C3Ms, the intensity decreases faster upon titration with NaCl and is more significant than for C3Ms that are core-crosslinked. After the addition of 200 mM NaCl, the normalized scattering intensity of non-crosslinked C3Ms is less than 0.1, indicating total disintegration of the micelles and release of the enzymes. Salt ions screen the charged parts of the enzyme and of the diblock copolymer, thereby weakening the electrostatic interactions and decrease the entropy gain from counterion release. The core-crosslinked micelles are more resistant to salt addition, and their

light scattering intensity decreases more gradually. At NaCl concentrations as high as 200 mM, scattered intensities are still high (the normalized *I* remains at 0.52 and 0.71 for core-crosslinked C3M with 0.25 and 0.5 eq. DTBP, respectively). Due to network formation between quaternized diblock copolymers and enzymes inside the core of the micelles, CotA is trapped and cannot dissociate from these complexes.[8,20,51,53,54] The slight decrease in scattering intensity could be due to some polymer chains and CotA molecules that were not properly connected via amidine bonds, diffusing out of the micelles. The stability of CotA-containing C3Ms after crosslinking was thus remarkably improved.

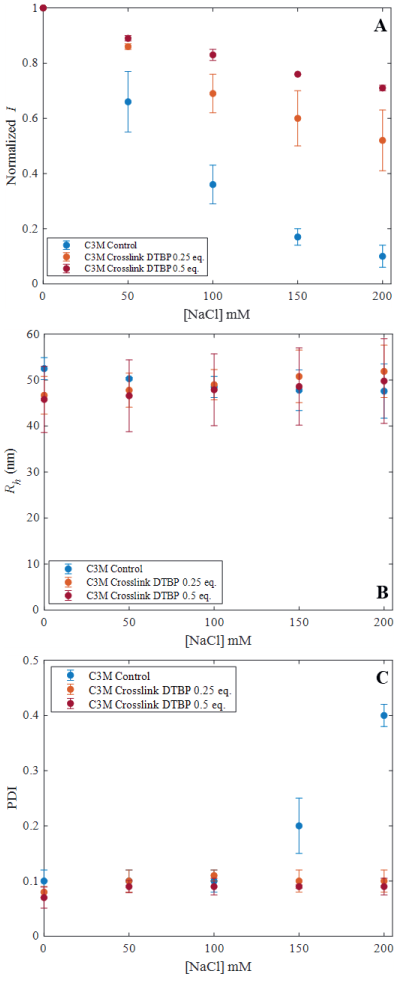

Figure 6.4. DLS stability measurements as a function of the salt concentration. (A) Normalized scattering intensity (*I*), (B) hydrodynamic radius (R_h), and (C) polydispersity index (PDI). C3Ms without crosslinks (blue), core-crosslinked C3Ms with 0.25 eq. DTBP (orange), core-crosslinked C3Ms with 0.5 eq. DTBP (red).

Increasing the NaCl concentration caused the R_h to decrease and PDI to increase in the non-crosslinked C3M control sample (Figures 6.4B and 6.4C). Adding 200 mM NaCl produced highly polydisperse particles: the PDI value reached values higher than 0.4.[45] In C3Ms with core-crosslinking, on the other hand, both the R_h and PDI are relatively constant, indicating that the micelles remained intact.

FCS was also used to monitor the salt stability of CotA-containing C3Ms. This was done by quantifying the total number of fluorescent particles in the confocal volume (N) as a function of the NaCl concentration. This number was then normalized to the initial N of free CotA in a low salt buffer. In Figure 6.5, it is shown that the normalized N increases with increasing salt concentration for all three samples, which indicates the release of CotA from the micelle cores.[26] However, CotA is released at a lower salt concentration and faster from the non-crosslinked C3Ms than from the core-crosslinked C3Ms. After adding 200 mM NaCl to the CotA-containing C3M control sample, the normalized N reached values close to 1.0, indicating that the micelles were completely disintegrated. For core-crosslinked micelles, N increased less significantly and more gradually; these C3Ms do not disintegrate even after the addition of 200 mM NaCl. Figure 6.5 also shows that the more crosslinker is added to the C3Ms, the better the resistance of the C3Ms against salt. This is expected since denser networks within the core of the C3Ms are formed, which will entrap CotA and prevent it from dissociation.

Figure 6.5B demonstrates that the R_h of non-crosslinked C3Ms decreases significantly with increasing NaCl concentration. After the addition of 200 mM NaCl, the size of the micelles was reduced by about 50 %. However, for the core-crosslinked C3Ms, the R_h remained relatively constant. FCS measurements confirmed the DLS results where core-crosslinking was found to improve the salt stability. Besides that, the salt stability of C3Ms could be further improved by adding a larger amount of crosslinking agents.

Core-crosslinking of C3Ms with DTBP allows cleaving the network in the micelle core by breaking the internal disulfide bonds (S-S) of DTBP using a reducing agent such as DTT. As DTT is expected to reduce the disulfide bonds within the DTBP crosslinker, this would lead to CotA being released after adding salt. However, when working at a pH above the pK_a of thiols (pK_a = 8.8-9.1), deprotonation would result in a thiolate anion that becomes susceptible to oxidation.[55] Even though DTT can still be used effectively at a pH of 6.5-9.0, its optimal pH range is between 7.1 and 8.0. Since the formation of CotA-containing C3Ms was done at pH 10.8, the formation of disulfide bonds is promoted, and cleavage of the crosslinks cannot happen. Liu et al. reported that cleaved disulfide bonds on DTBP could be repaired under oxidative conditions, including the presence of oxygen,[56] and can be simply reformed by

exposure to air.[21] Decreasing the pH to around pH 9 by adding 0.1 M HCl before adding 10 mM DTT helped to cleave the disulfide bond within the DTBP crosslinker,[23,57] and when followed by the addition of salt resulted in the release of CotA (Figure S6.5. Supplementary information).

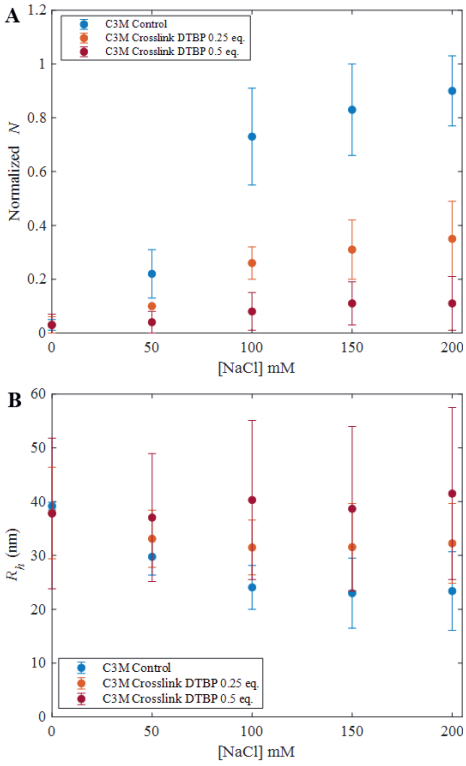

Figure 6.5. FCS analysis of salt-titrated C3Ms: without crosslinks (blue), core-crosslinked C3Ms with 0.25 eq. DTBP (orange), and core-crosslinked C3Ms with 0.5 eq. DTBP (red). (A) Normalized *N*, and (B) hydrodynamic radius (R_h).

6.3.6. Activity of enzyme-containing C3Ms

To determine the effect of core-crosslinking on the catalytic activity of CotA, enzyme activity measurements were performed using ABTS as substrate. In this assay, CotA takes an electron from ABTS, which results in a free radical on $ABTS^{\bullet+}$. This product has a green color and can be detected using ultraviolet/ visible (UV/ vis) spectroscopy. Figure 6.6 shows the relative enzymatic activities of free CotA and several C3M samples. The activity of free CotA in solution is set to 100 %, and for the C3M samples, the relative activities are 102 ± 5 %, 85 ± 1 %, and 87 ± 2 % for C3Ms without crosslink (control), C3Ms with 0.25 eq. DTBP, and C3Ms

with 0.5 eq. DTBP, respectively. Thus, the control sample has a very similar activity compared to the free enzyme sample. However, it should be noted that at the pH of the ABTS assay (pH 4.4), the micelles fall apart, and the enzyme is free in the solution again (Supplementary information, Figure S6.3). Core-crosslinking of the C3Ms resulted in a slight decrease in the activity of CotA laccase. This decrease in activity presumably occurs because the formed network hinders substrate binding to the catalytic site of CotA.[49] Moreover, an enzyme is a dynamic structure; core-crosslinking might reduce the flexibility of CotA or restrict its dynamics, thereby decreasing the affinity of the substrate to the enzyme.

We also measured the effect of adding reducing agents such as DTT. Following the addition of DTT to the samples and spin filtering to remove the excess DTT, it was found that the activity of the encapsulated enzyme was decreased significantly to only 16 ± 1, 26 ± 2, 20 ± 1 % for C3Ms without crosslinks, core-crosslinked C3Ms with 0.25 eq. DTBP, and core-crosslinked C3Ms with 0.5 eq. DTBP, respectively. Reducing agents such as DTT interfere with a substrate's oxidation reaction by modifying amino acid residues, thereby decreasing its activity.[58,59,64] Additionally, some remaining DTT could reduce the product $ABTS^{\bullet+}$ back to ABTS as well.[60,61]

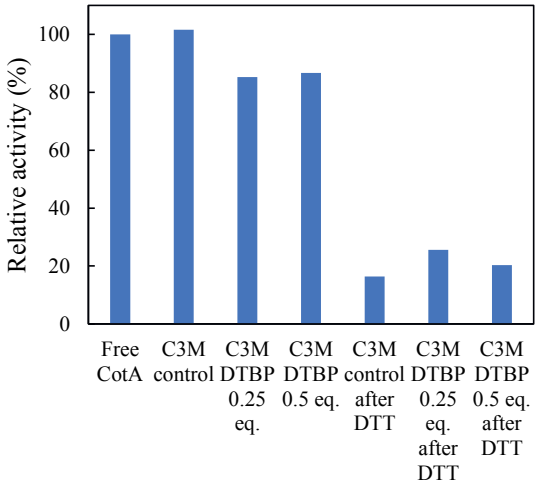

Figure 6.6. Activity measurement using ABTS as the substrate on free CotA and its C3Ms, both without crosslinks and with crosslinks (0.25 eq. and 0.5 eq. DTBP).

6.4. Conclusions

In this study, we functionalized a P2VP-*b*-PEO diblock copolymer by quaternization using *N*-(2-bromoethyl) phthalimide and iodomethane, resulting in both permanent positive charges and primary amine functionalities. The two-step quaternization reaction was done to increase the enzyme encapsulation efficiency and to provide the diblock copolymer functional groups for crosslinking. Enzyme-containing C3Ms were generated by mixing CotA with the amine-functionalized cationic-neutral hydrophilic diblock copolymer. C3M formation was confirmed by using DLS and FCS. DLS revealed that the PMC of the C3Ms was not at the expected value of charge balance between the negatively charged enzyme and positively charged diblock copolymer, which can be explained by the influence of other types of interactions such as hydrophobic interactions. FCS analysis showed that about 85 - 90 % of CotA was encapsulated into C3Ms. Core-crosslinked micelles were formed by treating the C3Ms with the crosslinker DTBP. DLS and FCS showed that core-crosslinked micelles are more stable to salt than the non-crosslinked micelles. In addition, it was shown that the DTBP crosslinks are reversible at moderate pH. CotA in core-crosslinked C3Ms has a slightly lower activity due to network formation in the core that prevents the substrate ABTS from binding to CotA. This study demonstrates that core-crosslinking significantly improves the salt stability of enzyme-containing C3Ms and is a promising strategy for improving C3Ms' ability to function as enzyme delivery systems.

References

1. Bronich, T. K., Kabanov, A. V and Kabanov, V. A. Soluble Complexes from Poly (ethylene oxide) - block -polymethacrylate Anions and N -Alkylpyridinium Cations. *Macromolecules* **30**, 3519–3525 (1997).
2. Harada, A. and Kataoka, K. Formation of Polyion Complex Micelles in an Aqueous Milieu from a Pair of Oppositely-Charged Block Copolymers with Poly(ethylene glycol) Segments. *Macromolecules* **28**, 5294–5299 (1995).
3. Topel, Ö., Çakir, B. A., Budama, L. and Hoda, N. Determination of critical micelle concentration of polybutadiene-block- poly(ethyleneoxide) diblock copolymer by fluorescence spectroscopy and dynamic light scattering. *J. Mol. Liq.* **177**, 40–43 (2013).
4. Santos, M. S., Tavares, F. W. and Biscaia, E. C. Molecular thermodynamics of micellization: Micelle size distributions and geometry transitions. *Brazilian J. Chem. Eng.* **33**, 515–523 (2016).
5. Voets, I. K., de Keizer, A. and Cohen Stuart, M. A. Complex coacervate core micelles. *Adv. Colloid Interface Sci.* **147**–**148**, 300–318 (2009).
6. Cohen Stuart, M. A., Besseling, N. A. M. and Fokkink, R. G. Formation of micelles with complex coacervate cores. *Langmuir* **14**, 6846–6849 (1998).
7. Voets, I. K., van der Burgh, S., Farago, B., Fokkink, R., Kovacevic, D., Hellweg, T., de Keizer, A., and Cohen Stuart, M. A. Electrostatically driven coassembly of a diblock copolymer and an oppositely charged homopolymer in aqueous solutions. *Macromolecules* **40**, 8476–8482 (2007).
8. Bourouina, N., Cohen Stuart, M. A. and Mieke Kleijn, J. Complex coacervate core micelles as diffusional nanoprobes. *Soft Matter* **10**, 320–331 (2014).
9. Lindhoud, S., de Vries, R., Norde, W. and Cohen Stuart, M. A. Structure and stability of complex coacervate core micelles with lysozyme. *Biomacromolecules* **8**, 2219–2227 (2007).
10. Mills, C. E., Obermeyer, A., Dong, X., Walker, J. and Olsen, B. D. Complex Coacervate Core Micelles for the Dispersion and Stabilization of Organophosphate Hydrolase in Organic Solvents. *Langmuir* **32**, 13367–13376 (2016).
11. Jaturanpinyo, M., Harada, A., Yuan, X. and Kataoka, K. Preparation of Bionanoreactor Based on Core-Shell Structured Polyion Complex Micelles Entrapping Trypsin in the Core Cross-Linked with Glutaraldehyde. *Bioconjug. Chem.* **15**, 344–348 (2004).
12. Harada, A. and Kataoka, K. Polyion complex micelle formation from double-hydrophilic block copolymers composed of charged and non-charged segments in aqueous media. *Polym. J.* **50**, 95–100 (2018).
13. Blocher McTigue, W. C. and Perry, S. L. Protein Encapsulation Using Complex Coacervates: What Nature Has to Teach Us. *Small* **16**, 1–17 (2020).
14. Magana, J. R., Sproncken, C. C. M. and Voets, I. K. On complex coacervate core micelles: Structure-function perspectives. *Polymers (Basel)*. **12**, 1953–1990 (2020).
15. Sureka, H. V., Obermeyer, A. C., Flores, R. J. and Olsen, B. D. Catalytic Biosensors from Complex Coacervate Core Micelle (C3M) Thin Films. *ACS Appl. Mater. Interfaces* **11**, 32354–32365 (2019).
16. Nolles, A., Hooiveld, E., Westphal, A. H., Van Berkel, W. J.H., Kleijn, J. M., and Borst, J. W. FRET Reveals the Formation and Exchange Dynamics of Protein-Containing Complex Coacervate Core Micelles. *Langmuir* **34**, 12083–12092 (2018).
17. Kembaren, R., Fokkink, R., Westphal, A. H., Kamperman, M., Kleijn, J. M., and Borst, J. W. Balancing Enzyme Encapsulation Efficiency and Stability in Complex Coacervate Core Micelles. *Langmuir* **36**, 8494–8502 (2020).
18. Lindhoud, S., De Vries, R., Schweins, R., Cohen Stuart, M. A. and Norde, W. Salt-induced release of lipase from polyelectrolyte complex micelles. *Soft Matter* **5**, 242–250 (2009).
19. Lindhoud, S., Voorhaar, L., De Vries, R., Schweins, R., Cohen Stuart, M. A., and Norde, W. Salt-induced disintegration of lysozyme-containing polyelectrolyte complex micelles. *Langmuir* **25**, 11425–11430 (2009).
20. Kembaren, R., Kleijn, J. M., Borst, W., Hofman, A. H. and Kamperman, M. Enhanced stability of complex coacervate core micelles following different core-crosslinking strategies. *Soft Matter* **18**, 3052–3062 (2022).
21. Xu, X., Smith, A. E. and McCormick, C. L. Facile 'One-Pot' preparation of reversible, disulfide-containing shell cross-linked micelles from a RAFT-synthesized, pH-responsive triblock copolymer in water at room temperature. *Aust. J. Chem.* **62**, 1520–1527 (2009).
22. Ayyub, O. B., Ibrahim, M. B. and Kofinas, P. Synthesis and characterization of microphase separated primary amine functionalized polystyrene-b-poly(2-vinylpyridine). *Polymer* **55**, 6227–6231 (2014).
23. Oe, Y., Christie, R. J., Naito, M., Low, S.A., Fukushima, S., Toh, K., Miura, Y., Matsumoto, Y., Nishiyama, N., Miyata, K., and Kataoka, K. Actively-targeted polyion complex micelles stabilized by cholesterol and disulfide cross-linking for systemic delivery of siRNA to solid tumors. *Biomaterials* **35**,

7887–7895 (2014).
24. Kembaren, R., Kleijn, J. M., Borst, W., Kamperman, M., and Hofman, A. H. Enhanced stability of complex coacervate core micelles following different core-crosslinking strategies. *Soft matter* **18**, 3052 – 3062 (2022).
25. Nielsen, J. and Rasmussen, P. H. Implementation of a combinatorial cleavage and deprotection scheme. 1. Synthesis of phthalhydrazide libraries. *Tetrahedron Lett.* **37**, 3351–3354 (1996).
26. Kembaren, R., Westphal, A. H., Kamperman, M., Kleijn, J. M. and Borst, J. W. Charged Polypeptide Tail Boosts the Salt Resistance of Enzyme-Containing Complex Coacervate Micelles. *Biomacromolecules* **23**, 1195–1204 (2022).
27. Nolles, A., Westphal, A. H., de Hoop, J. A., Fokkink, R. G., Kleijn, J. M., van Berkel, W. J. H., and Borst, J. W. Encapsulation of GFP in complex coacervate core micelles. *Biomacromolecules* **16**, 1542–1549 (2015).
28. Nolles, A., Westphal, A. H., Kleijn, J. M., van Berkel, W. J. H. and Borst, J. W. Colorful packages: Encapsulation of fluorescent proteins in complex coacervate core micelles. *Int. J. Mol. Sci.* **18**, 1557–1576 (2017).
29. Nederveen-Schippers, L. M., Pathak, P., Keizer-Gunnink, I., Westphal, A. H., van Haastert, P. J. M.,,Borst, J. W.,Kortholt, A., and Skakun, V. Combined fcs and pch analysis to quantify protein dimerization in living cells. *Int. J. Mol. Sci.* **22**, 7300–7319 (2021).
30. Yu, L., Lei, Y., Ma, Y., Liu, M., Zheng, J., Dan, D, and Gao, P. A Comprehensive Review of Fluorescence Correlation Spectroscopy. *Front. Phys.* **9**, 1–21 (2021).
31. Dehghani-Firouzabadi, A. A. and Firouzmandi, S. Synthesis and characterization of a new unsymmetrical potentially pentadentate Schiff base ligand and related complexes with manganese(II), nickel(II), copper(II), zinc(II) and cadmium(II). *J. Braz. Chem. Soc.* **28**, 768–774 (2017).
32. Malkov, A. V., Stewart-Liddon, A. J. P., Teplý, F., Kobr, L., Muir, K. W., Haigh, D., and Kočovský, P. New pinene-derived pyridines as bidentate chiral ligands. *Tetrahedron* **64**, 4011–4025 (2008).
33. Chamoulaud, G. and Bélanger, D. Chemical modification of the surface of a sulfonated membrane by formation of a sulfonamide bond. *Langmuir* **20**, 4989–4995 (2004).
34. Sadman, K., Wang, Q., Chen, Y., Keshavarz, B., Jiang, Z. and Shull, K. R. Influence of Hydrophobicity on Polyelectrolyte Complexation. *Macromolecules* **50**, 9417–9426 (2017).
35. Nosov, R., Padnya, P., Shurpik, D. and Stoikov, I. Synthesis of water-soluble amino functionalized multithiacalix[4]arene via quaternization of tertiary amino groups. *Molecules* **23**, 1–11 (2018).
36. Attia, M. I., El-Emam, A. A., Al-Turkistani, A. A., Kansoh, A. L. and El-Brollosy, N. R. Synthesis of novel 2-(Substituted amino)alkylthiopyrimidin-4(3H)-ones as potential antimicrobial agents. *Molecules* **19**, 279–290 (2014).
37. McMaster, P. D., Byrnes, E. W., Block, A. J. and Tenthorey, P. A. New Antiarrhythmic Agents. 5. α-Aminoaceto-2,6-xylidides with Functionalized Amide Alkyl Substituents. *J. Med. Chem.* **24**, 53–58 (1981).
38. Dompé, M., Cedano-Serrano, F. J., Vahdati, M., van Westerveld, L., Hourdet, D., Creton, C., van der Gucht, J., Kodger, T., and Kamperman, M. Underwater Adhesion of Multiresponsive Complex Coacervates. *Adv. Mater. Interfaces* **7**, 1901785–1901792 (2020).
39. Kim, S. H., Tan, J. P.K., Nederberg, F., Fukushima, K., Colson, J., Yang, C., Nelson, A., Yang, Y. Y., and Hedrick, J. L. Hydrogen bonding-enhanced micelle assemblies for drug delivery. *Biomaterials* **31**, 8063–8071 (2010).
40. Heinzelmann, G. and Figueiredo, W. Confinement effects on micellar systems with a hydrogen-bonding solvent. *J. Chem. Phys.* **145**, 1–13 (2016).
41. Cheng, C. C., Sun, Y. T., Lee, A. W., Huang, S. Y., Fan, W. L., Chiao, Y. H., Chiu, C. W., Lai, J. Y. Hydrogen-bonded supramolecular micelle-mediated drug delivery enhances the efficacy and safety of cancer chemotherapy. *Polym. Chem.* **11**, 2791–2798 (2020).
42. Venkatesan, P., Cheng, Y. and Kahne, D. Hydrogen Bonding in Micelle Formation. *J. Am. Chem. Soc.* **116**, 6955–6956 (1994).
43. Hoogeveen, N. G., Cohen Stuart, M. A., Fleer, G. J. and Böhmer, M. R. Formation and stability of multilayers of polyelectrolytes. *Langmuir* **12**, 3675–3681 (1996).
44. Gucht, J. van der, Spruijt, E., Lemmers, M. and Cohen Stuart, M. A. Polyelectrolyte complexes: Bulk phases and colloidal systems. *J. Colloid Interface Sci.* **361**, 407–422 (2011).
45. Bhattacharjee, S. Review article DLS and zeta potential – What they are and what they are not ? *J. Control. Release* **235**, 337–351 (2016).
46. Mayes, A. M., Olvera, M. and Cruz, D. Micelle Formation in Block Copolymer/ Homopolymer. *Macromolecules* **21**, 2543–2547 (1988).
47. Fujii, S., Yamada, S., Matsumoto, S., Kubo, G., Yoshida, K., Tabata, E., Miyake, R., Sanada, Y., Akiba, I., Okobira, T., Yagi, N., Mylonas, E., Ohta, N., Sekiguchi, H., and Sakurai, K. Platonic micelles:

Monodisperse micelles with discrete aggregation numbers corresponding to regular polyhedra. *Sci. Rep.* **7**, 1–8 (2017).
48. Koniev, O. and Wagner, A. Developments and recent advancements in the field of endogenous amino acid selective bond forming reactions for bioconjugation. *Chem. Soc. Rev.* **44**, 5495–5551 (2015).
49. Migneault, I., Dartiguenave, C., Bertrand, Michel, J. and Waldron, K. C. Three-dimensional carbon-based architectures for oil remediation: from synthesis and modification to functionalization. *J. Mater. Chem. A* **4**, 18687–18705 (2016).
50. Mattson, G., Conklin, E., Desai, S., Nielander, G.,Savage, M. D., Mogensen, S. A pactical approach to crosslink. *Mol. Biol. Rep.* **17**, 167–183 (1993).
51. Oupickí, D., Carlisle, R. C. and Seymour, L. W. Triggered intracellular activation of disulfide crosslinked polyelectrolyte gene delivery complexes with extended systemic circulation in vivo. *Gene Ther.* **8**, 713–724 (2001).
52. Elson, E. L. Fluorescence correlation spectroscopy: Past, present, future. *Biophys. J.* **101**, 2855–2870 (2011).
53. Oupicky, D., Howard, K. A., Koňák, Č., Dash, P. R., Ulbrich, K., and Seymour, L. W. Steric stabilization of poly-L-lysine/DNA complexes by the covalent attachment of semitelechelic poly[N-(2-hydroxypropyl)methacrylamide]. *Bioconjug. Chem.* **11**, 492–501 (2000).
54. Van der Kooij, H. M., Spruijt, E., Voets, I. K., Fokkink, R., Cohen Stuart, M. A., and van der Gucht, J. On the stability and morphology of complex coacervate core micelles: From spherical to wormlike micelles. *Langmuir* **28**, 14180–14191 (2012).
55. Poole, L. B. The basics of thiols and cysteines in redox biology and chemistry. *Free Radic Biol Med.* **80**, 148–157 (2015).
56. Liu, H., Zhao, F., Koo, B., Luan, Y., Zhong, L, Yun, K., and Shin, Y. Dimethyl 3,3″-dithiobispropionimidate (DTBP) as a cleavable disulfide-based polymer to encapsulate nucleic acids in biological sample preparation. *Sensors Actuators, B Chem.* **288**, 225–231 (2019).
57. Tangsangasaksri, M., Takemoto, H., Naito, M., Maeda, Y., Sueyoshi, D., Kim, H. J., Miura, Y., Ahn, J., Azuma, R., Nishiyama, N., Miyata, K., and Kataoka, K. SiRNA-Loaded Polyion Complex Micelle Decorated with Charge-Conversional Polymer Tuned to Undergo Stepwise Response to Intra-Tumoral and Intra-Endosomal pHs for Exerting Enhanced RNAi Efficacy. *Biomacromolecules* **17**, 246–255 (2016).
58. Dwivedi, U. N., Singh, P., Pandey, V. P. and Kumar, A. Structure-function relationship among bacterial, fungal and plant laccases. *J. Mol. Catal. B Enzym.* **68**, 117–128 (2011).
59. Hildén, K., Hakala, T. K. and Lundell, T. Thermotolerant and thermostable laccases. *Biotechnol. Lett.* **31**, 1117–1128 (2009).
60. Johannes, C. and Majcherczyk, A. Laccase activity tests and laccase inhibitors. *J. Biotechnol.* **78**, 193–199 (2000).
61. Valles, M., Kamaruddin, A. F., Wong, L. S. and Blanford, C. F. Inhibition in multicopper oxidases: A critical review. *Catal. Sci. Technol.* **10**, 5386–5410 (2020).
62. Harada, A. and Kataoka, K. Chain Length Recognition: Core-Shell Supramolecular Assembly from Oppositely Charged Block Copolymers. *Science* **283**,65−67 (1999).
63. Harada, A. and Kataoka, K. Novel polyion complex micelles entrapping enzyme molecules in the core. 2. Characterization of the micelles prepared at nonstoichiometric mixing ratios. *Langmuir* **15**, 4208–4212 (1999).
64. Christopher, L. P., Yao, B. and Ji, Y. Lignin biodegradation with laccase-mediator systems. *Front. Energy Res.* **2**, 1–13 (2014).

Supplementary information

S6.1. Quaternization degree of the diblock copolymer P2VP$_{128}$-*b*-PEO$_{477}$ after quaternization using *N*-(2-bromoethyl)phthalimide

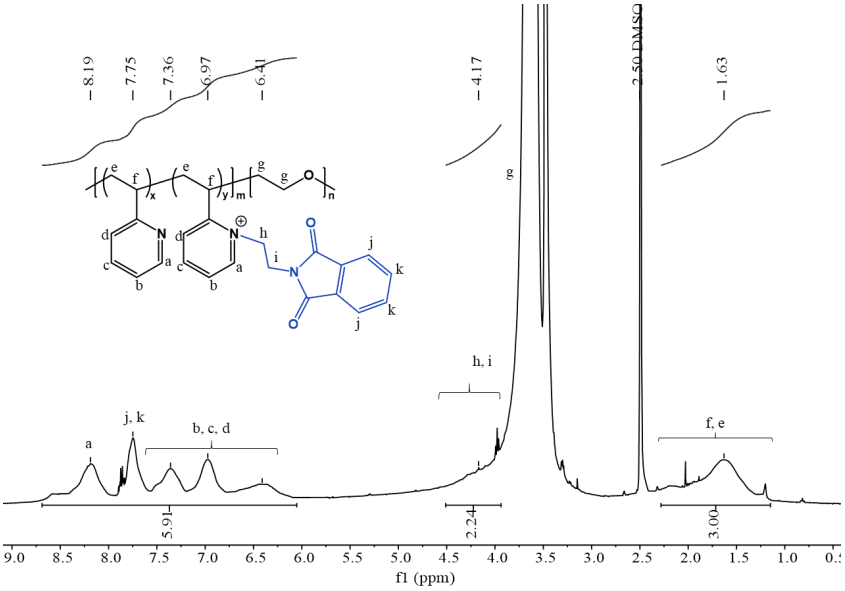

Figure S6.1. ^{1}H-NMR spectrum of the diblock copolymer P2VP$_{128}$-*b*-PEO$_{477}$ after quaternization using *N*-(2-bromoethyl)phthalimide. The spectrum was recorded in DMSO-d_6. The degree of quaternization (DQ) was calculated from the ratio of the integral area of the aromatic rings and the integral area of the methyl group.

DQ = (((5.91 – 4)/4) : (3/3)) * 100 % = 48 %.

S6.2. Quaternization degree of the diblock copolymer P2VP$_{128}$-*b*-PEO$_{477}$ after quaternization using *N*-(2-bromoethyl)phthalimide and iodomethane

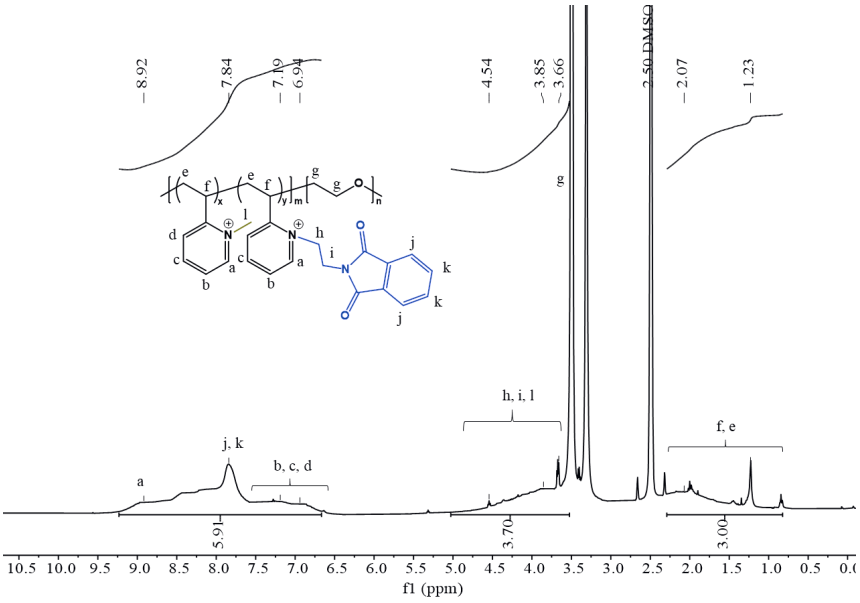

Figure S6.2. ^{1}H-NMR spectrum of the diblock copolymer P2VP$_{128}$-*b*-PEO$_{477}$ after quaternization using *N*-(2-bromoethyl)phthalimide and iodomethane. The spectrum was recorded in DMSO-d_6. The degree of quaternization (DQ) was calculated from the ratio of the integral area of the aromatic rings and the integral area of the methyl group.

DQ1 = ((5.91 - 4)/4 : (3:3) * 100 %) = 48 %

DQ2 = (3.7 - 2.24))/3 : (4/4)* 100 %) = 49 %

DQ total: ± 97 %

We assume full quaternization of the remaining 2VP groups after the second quaternization step.

S6.3. Normalized scattering intensity *I*, hydrodynamic radius R_h, and polydispersity index (PDI) for the three different C3Ms systems as a function of pH

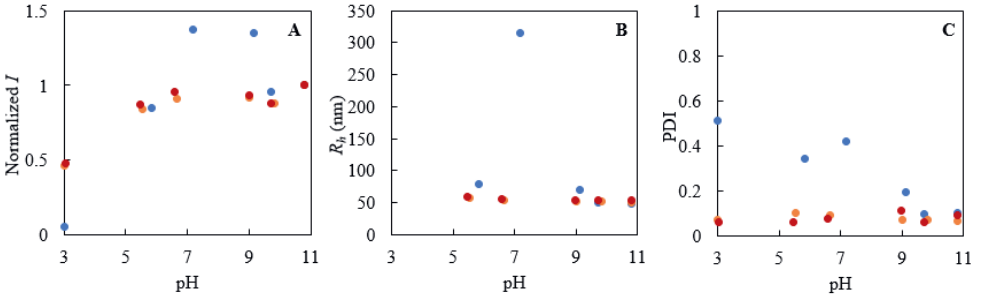

Figure S6.3. Stability measurements as a function of the pH (through the addition of 0.1 M HCl) as observed by using DLS. (A) Normalized scattering intensity (*I*), (B) hydrodynamic radius (R_h), and (C) polydispersity index (PDI). C3Ms without crosslinks (blue), C3Ms core-crosslinked with 0.25 eq. DTBP (orange), red (C3Ms core-crosslinked with 0.5 eq. DTBP (red).

S6.4. Multi-angle DLS for determining the micellar shape

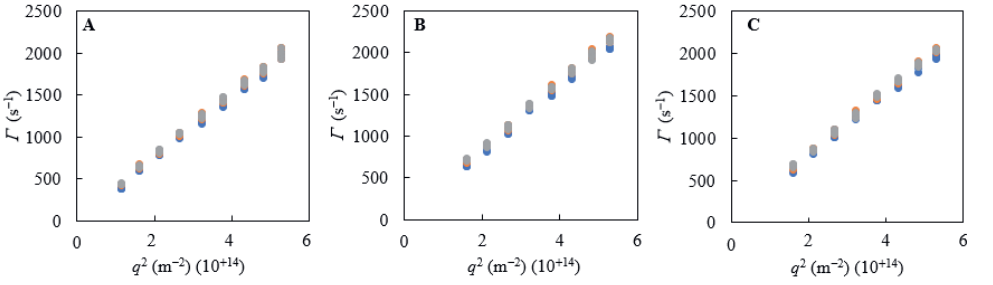

Figure S6.4. Multi-angle DLS data for three different C3Ms samples. (A) C3M control (without crosslinks), (B) core-crosslinked C3Ms with 0.25 eq. DTBP, and (C) core-crosslinked C3Ms with 0.5 eq. DTBP. The decay rate $\Gamma(q)$ was obtained from the DLS correlation curves by a first (blue), second (orange), and third (yellow) cumulant fit. Three overlapping straight lines indicate that the C3Ms are spherical.[62,63]

S6.5. Normalized number of fluorescent particles in the confocal volume *N* for the three different C3Ms samples against the salt concentration

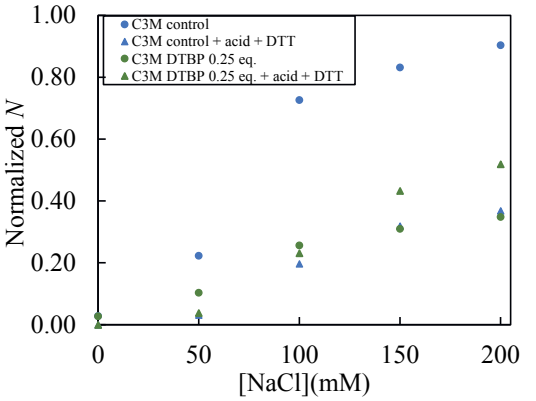

Figure S6.5. Stability measurements as a function of the salt concentration observed by FCS on C3Ms without crosslinks (blue), C3Ms core-crosslinked with 0.25 eq. DTBP (green). Spheres (○) represent samples without adding 0.1 M HCl and DTT, and triangles (Δ) represent C3M samples with added 0.1 M HCl to pH around 9 and DTT.

Chapter 7 :

Slowing down protein exchange between complex coacervate core micelles by increasing the protein net charge and by core-crosslinking

Manuscript in preparation as:

Kembaren, R., Hofman, A. H., Westphal A. H., Bos, I., Kamperman, M., Kleijn, J. M., and Borst, J. W. Slowing down protein exchange between complex coacervate core micelles by increasing the protein net charge and by core-crosslinking.

Abstract

Encapsulating proteins can be useful for many purposes, including preventing protein degradation and controlled delivery of functional or pharmaceutical proteins. An easy way to achieve protein encapsulation is by mixing a solution of charged proteins with an oppositely charged-neutral diblock copolymer solution, resulting in the formation of so-called complex coacervate core micelles (C3Ms). Previous studies revealed that adding charged domains to the protein or core-crosslinking of the micelles improve the stability of protein-containing C3Ms against salt-induced disintegration. However, whether these strategies also decrease the exchange rate of proteins between individual C3Ms is still unclear. This is important because the higher the exchange dynamics, the more the proteins are exposed to harmful effects of the surrounding solution. In this study, we used Förster resonance energy transfer (FRET) to observe the effect of increasing the net charge of the protein and crosslinking of the coacervate core on the protein exchange dynamics between C3Ms. To assess the effect of adding extra charges, we compared the exchange dynamics of C3Ms containing the enzyme CotA laccase and C3Ms containing genetically modified CotA laccase with 40 extra glutamic acid residues (CotA-E40). These proteins were fluorescently labeled with Alexa Fluor 488 (donor) and Alexa Fluor 568 (acceptor). The effect of core-crosslinking was determined by comparing the protein exchange rate between non-crosslinked and crosslinked C3Ms containing the fluorescent proteins mTurquoise2 (donor) and SYFP2 (acceptor). In all cases, fluorescence quenching was observed when diblock copolymer was added to the fluorescently labeled enzymes or the fluorescent proteins due to the formation of C3Ms. Fluorescence was restored when the micelles were disintegrated by adding salt. The protein exchange rate between C3Ms was higher when a low concentration of salt was present. With the addition of salt, the electrostatic attraction between protein and diblock copolymer is reduced. Fitting the FRET efficiency data with an analytical model shows that the exchange of CotA-E40 between micelles is only 1.2 times slower than that of native CotA. Core-crosslinking C3Ms is much more effective and slows the protein exchange rate between C3Ms by more than 80 times depending on the crosslinker concentration applied; for very high crosslinker concentrations protein exchange could even be completely inhibited. Therefore, core-crosslinking is a promising approach to generate protein-containing C3Ms that are stable at high ionic strength with a limited exchange of proteins between C3Ms.

7.1. Introduction

Encapsulation of proteins can be beneficial as a protection mechanism against protein degradation by, e.g., proteases[1] or against changing environmental conditions such as temperature, pH, and the presence of oxidizing agents.[2] A promising method to encapsulate proteins is by using complex coacervate core micelles (C3Ms), of which the formation is driven by electrostatic attraction between oppositely charged macromolecules and entropy gain from counterion release.[3,4] Proteins are biomacromolecules that can bear charges depending on the protein's pI and the pH of the solution. Upon mixing a protein solution with an oppositely charged-neutral diblock copolymer solution, small-soluble protein-polymer complexes (SCs) will be formed. At the right composition (charge ratio between protein and polymer around unity) and above the critical micelle concentration, these SCs will aggregate and form complex coacervate core micelles (C3Ms). The proteins are located in the water-rich environment of the micellar core, together with the charged part of the diblock, while the diblock copolymer's hydrophilic tails stick outwards into the aqueous solution. This hydrophilic corona prevents macroscopic phase separation of the coacervate cores and protects the micelles against aggregation by steric repulsion.[3–6] Formation of C3Ms does not require an organic solvent, heat, or specific chemical reagents[7] but is strongly influenced by concentrations (of both protein and polymer), pH, and ionic strength of the solution.[5,8,9]

C3Ms are in dynamic equilibrium with free protein and diblock copolymer in solution (and/ or with small soluble protein-polymer complexes).[5,10–14] This implies that there is still exchange of proteins between C3Ms and the solution and between C3Ms. This dynamic exchange can cause undesired protein exposure to the environment. Because of the low charge density of proteins compared to polyelectrolytes, protein-containing C3Ms are extremely sensitive to salt addition. Already at relatively low salt concentrations (in the range of 10 - 100 mM), the C3Ms disintegrate. In our previous work,[15,16] we investigated several strategies to improve the salt resistance of these C3Ms. We observed that increasing the protein's net charge (by bioconjugation or genetic engineering) and core-crosslinking enhances the salt stability of enzyme-containing C3Ms.[15] All strategies resulted in a shift to higher salt concentrations at which the C3Ms disintegrate. For practical applications, however, it is also needed to know the protein exchange dynamics between individual C3Ms and how these are affected by our strategies to increase the salt stability.

Förster resonance energy transfer (FRET) was used by Nolles et al.[5] to study the kinetics of C3M formation and protein exchange between C3Ms. They reported similar relaxation times

of 100 s for the formation of C3Ms and the exchange of proteins between C3Ms in low ionic strength solutions.[5] FRET was also used by Bos et al.[11] to measure molecular exchange in C3Ms formulated from homopolymers and diblock copolymers. They found that the exchange rate is largely independent of the micelle concentration but strongly dependent upon the salt concentration and the length of the charged blocks.[11]

The present study addresses the dynamic aspects of protein-containing C3Ms by monitoring protein exchange between these micelles using FRET as a read-out. We investigated the exchange rate in two model systems: 1) C3Ms containing native and genetically engineered (extra charged) CotA laccase, and 2) core-crosslinked C3Ms containing fluorescent proteins. To introduce additional negative charges to CotA, a sequence of 40 glutamic acids was genetically added to the C-terminus of CotA (CotA-E40).[15] The proteins were fluorescently labeled with Alexa Fluor 488 (as a FRET donor) and Alexa Fluor 568 (as a FRET acceptor). To study the effect of core-crosslinking, we used fluorescent proteins mTurquoise2 (donor) and SYFP2 (acceptor). C3Ms were prepared from the above-mentioned proteins with the quaternized diblock copolymer poly(*N*-methyl-2-vinyl-pyridinium)-*b*-poly(ethylene oxide) ($PM2VP_{128}$-*b*-PEO_{477}), or the amine-functionalized version of this diblock copolymer ($Q_{NH_2}PM2VP_{128}$-*b*-PEO_{477}), respectively. Protein exchange between C3Ms resulted in quenching of the donor emission and an increase in the acceptor photon emission upon the excitation at the donor channel.[5,10–12,17,18] We derived the micelle exchange rate constants from the rise in FRET efficiency over time, using a slightly modified analytical model developed by Bos et al.[11,14]

7.2. Experimental section

7.2.1. Materials

Alexa Fluor 488 C5 maleimide and Alexa Fluor 568 C5 maleimide were purchased from Thermo Fisher scientific. The diblock copolymer poly(2-vinylpyridine)$_{128}$-*block*-poly(ethylene oxide)$_{477}$ ($P2VP_{128}$-*b*-PEO_{477}) (M_n = 34.5 kg/ mol, M_w/ M_n = 1.1) was obtained from Polymer Source Inc. This diblock was quaternized either with iodomethane ($PM2VP_{128}$-*b*-PEO_{477}) or with a combination of *N*-(2-bromoethyl)phthalimide and iodomethane ($Q_{NH_2}PM2VP_{128}$-*b*-PEO_{477}) as described in our previous studies.[15,16,19] After quaternization following the procedures described before, the diblock copolymer had a degree of quaternization of about 70 % for $PM2VP_{128}$-*b*-PEO_{477} and 97 % for $Q_{NH_2}PM2VP_{128}$-*b*-PEO_{477}, measured with ^{1}H-NMR. The fluorescent proteins mTurquoise2 and SYFP2 are the same as used by Nolles et al.[20,21]

Dimethyl 3,3′-dithiopropionimidate dihydrochloride (DTBP) was purchased from Thermo Fisher Scientific.

7.2.2. CotA production and purification

The production and purification of native CotA and CotA-E40 were carried out as described in our earlier study.[15] In order to covalently bind the Alexa dyes to the native CotA and CotA-E40, a serine at position 313 in the amino acid sequence was replaced by a cysteine (CotA S313C and CotA-S313C-E40). In this way, the C5 maleimide and the cysteine could form a thioether bond. The CotA S313C and CotA-S313C-E40 genes were cloned into a pBAD vector and heterologously expressed in *E. coli* Rosetta cells. The induction of the CotA overexpression was done by adding 0.15 % L-arabinose at 25 ºC to the cell culture medium when the optical density of the cultured medium reached a value of 0.6–0.8.

The purification of CotA-S313C was performed using cation-exchange chromatography (cIEX using an SP-Sepharose FF column) and gel filtration chromatography (Superdex 200 column). CotA-S313C-E40 were purified using anion-exchange chromatography (aIEX using a Q-Sepharose FF column) followed by gel filtration chromatography (Superdex 200 column). The CotA and CotA-E40 proteins from the IEX were labeled with Alexa Fluor 488 and Alexa Fluor 568 C5 maleimide, respectively, with a molar ratio of 1:10 at 4 ºC by overnight incubation in the dark. The labeled protein was separated from the unreacted/ free fluorescent label with a Biogel-P6DG gel filtration column (BioRad). The fractions that were fluorescent under UV light and contained protein were pooled and concentrated by using an Amicon concentrator (cutoff of 10 kDa). The selected protein was then loaded into the gel filtration column (Superdex 200 column). The fractions that showed absorptions at 280 nm and 490 nm for CotA labeled with Alexa 488 dye, and 280 nm and 570 nm for CotA labeled with the Alexa 568 dye were collected and concentrated. The purity of labeled CotA was analyzed using SDS PAGE analysis.

7.2.3 C3M preparation

Encapsulation of CotA variants (native CotA and CotA-E40) was achieved by first diluting the fluorescently labeled enzymes in 10 mM sodium carbonate buffer at pH 10.8 (the final enzyme concentration was 2 μM), followed by the addition of diblock copolymer poly(*N*-methyl-2-vinyl-pyridinium)$_{128}$-*block*-poly(ethylene oxide)$_{477}$ (PM2PV$_{128}$-*b*-PEO$_{477}$) at the preferred mixing composition (PMC),[15] i.e., the ratio protein/ polymer at which the most C3Ms are formed.[15] After mixing, the samples were stored at room temperature before measurement.

Encapsulation of fluorescent protein (mTurquoise2 and SYFP2) was achieved by first diluting the fluorescently labeled enzymes in 10 mM borate buffer at pH 9 (the final enzyme concentration was 2 μM), followed by the addition of the amine-functionalized diblock copolymer Q_{NH_2}PM2VP$_{128}$-*b*-PEO$_{477}$ at their preferred mixing composition (Figure S7.5, Supplementary information). After mixing, the samples were stored at room temperature before measurement.

7.2.4. Core-crosslinking C3Ms

Core-crosslinking was performed on the fluorescent protein-containing C3Ms. After the formation of micelles, the crosslinker DTBP was added to the C3M solution with a concentration of one, two, and four times the total concentration of amine of the diblock copolymer.

7.2.5. Fluorescence emission spectra upon encapsulation

The emission spectra of the fluorescently labeled enzymes (native CotA and CotA-E40) were measured using a Cary Eclipse spectrofluorometer (Varian Inc.). The native CotA and CotA-E40 were dissolved in a 10 mM sodium carbonate buffer (pH 10.8). The samples were measured using 0.5 mL quartz cuvettes with a path length of 1 cm. Emission slits were set to bandwidths of 5 nm. The fluorescence emission spectra of 2 μM CotA-Alexa Fluor 488 and CotA-Alexa Fluor 568 were measured separately at excitation wavelengths of 490 and 578 nm, respectively. The emission spectra of the encapsulated enzymes were measured following the same procedure.

The emission of the fluorescent proteins mTurquoise2 and SYFP2 was measured using the same spectrofluorometer. The proteins were dissolved in a 10 mM borate buffer (pH 9.0), and emission slits were set to bandwidths of 5 nm. The samples were measured using 0.5 mL quartz cuvettes with a path length of 1 cm. The fluorescence emission spectra of 2 μM mTurquoise2 and SYFP2 were measured separately at excitation wavelengths of 440 and 490 nm, respectively. The emission spectra of the encapsulated proteins were measured following the same procedure.

7.2.6. Förster resonance energy transfer (FRET)

FRET is a photophysical phenomenon in which the excited-state energy from a donor molecule is transferred non-radiatively to an acceptor molecule. FRET can be used to study the

interactions between molecules. Three prerequisites should be fulfilled for FRET to occur: sufficient spectral overlap between donor emission and acceptor excitation, a favorable dipole-dipole orientation between donor and acceptor, and the donor and acceptor should be in close proximity to each other, since FRET only can occur if they are within 10 nm of each other.[5,11,22–27] FRET was used to study the kinetics of C3Ms formation and proteins exchange between micelles. FRET was quantified by recording the fluorescence emission of the fluorescently labeled enzymes (native CotA and CotA-E40) or the fluorescent proteins (mTurquoise2 and SYFP2) using a Cary Eclipse spectrofluorometer (Varian Inc.).

7.2.7. Kinetics of C3M formation

To study the kinetics of formation Cot A and CotA-E40 containing C3Ms, first buffer solutions (pH 10.8) of 2 μM free donor enzymes (labeled with Alexa 488) and 2 μM free acceptor enzymes (labeled with Alexa 568) with a volume ratio of 1:1 were mixed in a quartz cuvette. The emission was recorded over time at two wavelengths: 516 nm (donor emission channel) and 603 nm (acceptor emission channel) upon excitation of 490 nm (donor excitation channel). Then, diblock copolymer PM2PV$_{128}$-*b*-PEO$_{477}$ was added to the mixture at the PMC and quickly mixed. Immediately after mixing, the emission was recorded over time, again at 516 nm and 603 nm upon excitation of 490 nm.

For C3Ms composed of fluorescent protein (mTurquoise2 and SYFP2), a similar procedure was followed. Buffer solutions (pH 9.0) of 2 μM mTurquoise2 and 2 μM SYFP2 with a volume ratio of 1:1 were mixed in a quartz cuvette. The emission was recorded over time at two wavelengths: 475 nm (donor emission channel) and 527 nm (acceptor emission channel) upon excitation of 440 nm (donor excitation channel). Then, diblock copolymer Q_{NH_2}PM2VP$_{128}$-*b*-PEO$_{477}$ was added to the mixture at the PMC and quickly mixed. The emission was immediately recorded again over time at the same wavelengths upon excitation at 440 nm.

7.2.8. Protein exchange between preformed C3Ms

Protein exchange between donor and acceptor micelles was monitored by using FRET.[5] The FRET efficiency (E) was calculated as the relative fluorescence intensity of the donor in the presence (I_{DA}) and absence (I_D) of the acceptor, $E = 1 - I_{DA}/I_D$.[26,28]

C3Ms composed of native CotA with either the donor (labeled with Alexa Fluor 488) or the acceptor (labeled with Alexa Fluor 568) were made separately as described in the C3M

preparation section above. These two types of micelles were mixed rapidly at a 1:1 ratio. Immediately after mixing, the fluorescence emission of the C3Ms was recorded at 525 nm and 603 nm upon 490 nm excitation. This procedure was also applied for C3Ms composed of CotA-E40. To study the effect of salt on the exchange dynamics, different quantities of 20 mM NaCl were added to the C3Ms donor and C3Ms donor separately before the C3M mixing step.

C3Ms composed of mTurquoise2 (donor) and SYFP2 (acceptor) were made separately following the procedure described in the C3M preparation section above. These two different micelles were mixed rapidly at a 1:1 ratio; the fluorescence emission of the donor was recorded directly after mixing at 475 nm and 527 nm upon 440 nm excitation. This procedure was also done for core-crosslinked C3Ms.

7.2.9. Analytical model for protein exchange between C3Ms

In this study, we fit the exchange data (the FRET efficiency over time E (t)) with an analytical model for FRET-based exchange experiments based on the model developed by Bos et al.[11,14] As explicated by Nolles et al.[5] we assume that protein exchange between the complex coacervate core micelles happens via small soluble protein-polymer complexes (SCs) that dissociate from and associate with either donor or acceptor micelles (Scheme 7.1). This implies that we consider the exchange process as an expulsion/ insertion process and not as a fission/ fusion process (splitting of micelles into parts of substantial sizes, which subsequently merge again). The donors and acceptors also have the same exchange rate.

In the model, the measured FRET efficiency at a time t is regarded as the sum of the average FRET efficiency at a time t in the donor micelles $<E_D(t)>$ and the average FRET efficiency at a time t in the acceptor micelles $<E_A(t)>$. Donor and acceptor micelles are the micelles that had respectively only donor or acceptor fluorophores in their core at the start of the mixing experiments. We assume that the distribution of acceptors in the acceptor micelles and the distribution of donors in the donor micelles is the same. This results in the equation:

$$\frac{\langle E(t)\rangle}{E(\infty)} = \frac{1}{E(\infty)} \frac{f_D \langle n_D(t)\rangle \langle E_D(t)\rangle + (1-f_D) \langle m_D(t)\rangle \langle E_A(t)\rangle}{f_D N_D} \tag{7.1}$$

where $E(\infty)$ is the FRET efficiency of the completely mixed micelles, f_D is the fraction of donor micelles (in our study $f_D = 0.5$: the mixing ratio of donor and acceptor micelles is 1:1), N_D is the average number of donors in the donor micelles at the start of the experiment, n_D is the average number of donor molecules in the donor micelles at time t, and m_D is the average number of donors in the acceptor micelles at time t.

The expulsion and insertion rates of the SCs determine the time-dependent probability to find a certain number of acceptor molecules in the donor micelles and vice versa. In this way, $<E_D(t)>$ is related to the probability $P(n_A)$ to find n_A acceptor fluorophores in a donor micelle. The FRET efficiency in the donor micelles $<E_D(t)>$ is calculated using the equation:

$$\langle E_D(t)\rangle = \sum_{n_A} P(n_A, t)\frac{v\, n_A}{1+ v\, n_A} \tag{7.2}$$

where v is a geometrical constant, which includes the micellar core radius, the Förster radius of the donor-acceptor pair and the size of the fluorophores.[11] Simulations by Bos et al.[11] on C3M exchange dynamics show that this geometrical constant has a limited effect on $E(t)/ E(\infty)$. $P(n_A,t)$ is given by:

$$P(n_A, t) = e^{-\lambda(t)}\frac{\lambda(t)^{n_A}}{n_A!} \tag{7.3}$$

where $\lambda(t)$ is given by:

$$\lambda(t) = x_1.N_A.(1-f_D)(1-e^{-k_1.t}) + x_2.N_A.(1-f_D)(1-e^{-k_2.t}) \tag{7.4}$$

N_A is the average number of acceptors in acceptor micelles at the start of the mixing experiment. The parameters k_1 and k_2 are exchange rate constants, and x indicates the corresponding fraction of fluorophores that exchange with this exchange rate ($x_1 + x_2 = 1$). If all fluorophores are of the same type and exchange with the same rate, a single rate constant k would suffice to describe the exchange process. However, this is not the case in reality, and generally, more rate constants will be needed to fit the FRET efficiency curves. We have chosen to fit the results with two rate constants, as will be explained in the results and discussion section.

Similarly, the FRET efficiency in the acceptor micelles $<E_A(t)>$ is related to the probability of finding m_A acceptors in an acceptor micelle. $<E_A(t)>$ is calculated by using the equation:

$$\langle E_A(t)\rangle = \sum_{m_A} P(m_A, t)\frac{v\, m_A}{1+ v\, m_A} \tag{7.5}$$

where m_A is the number of acceptors in the acceptors micelles. $P(m_A, t)$ is the probability to find m_A acceptors in acceptor micelles at the time (t), is given by:

$$P(m_A, t) = e^{-\mu(t)}\frac{\mu(t)^{m_A}}{m_A!} \tag{7.6}$$

where $\mu\ (t)$ is given by:

$$\mu(t) = x_1.N_A.(1-f_D+f_D\, e^{-k_1 t}) + x_2.N_A.(1-f_D+f_D\, e^{-k_1 t}) \tag{7.7}$$

The average number of donors in donor micelles at a certain time t, $\langle n_D(t) \rangle$, can be calculated using the equation:

$$\langle n_D(t) \rangle = N_D.x_1.(f_D + (1 - f_D)e^{-k_1 t}) + N_D.x_2.(f_D + (1 - f_D)e^{-k_2 t}) \quad (7.8)$$

where N_D is the average number of donors in donor micelles at the start of the mixing experiment. Similarly, the average number of donors in acceptor micelles at a certain time t $\langle m_D(t) \rangle$ is given by:

$$\langle m_D(t) \rangle = N_D.f_D.x_1.(1 - e^{-k_1 t}) + N_D.f_D.x_2.(1 - e^{-k_2 t}) \quad (7.9)$$

Using Equations 7.2 to 7.9, Equation 7.1 can be fitted to the experimental results with the exchange rate constants k_1 and k_2 and the corresponding fractions x_1 and x_2 as fitting parameters.

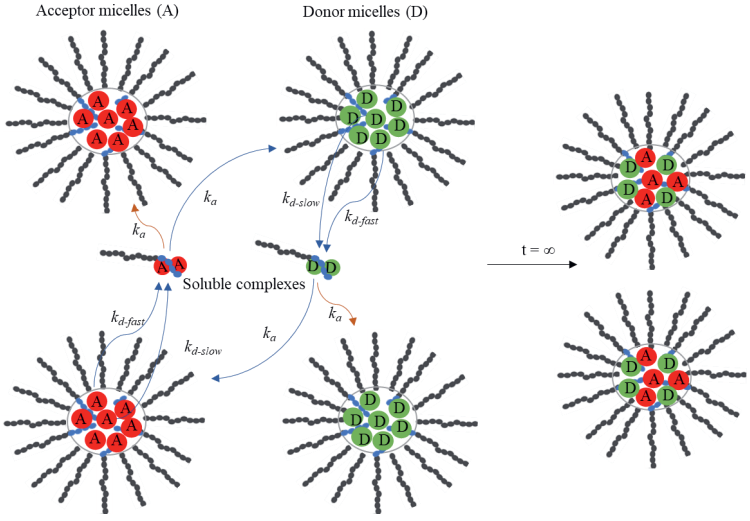

Scheme 7.1. Schematic representation of protein exchange between donor and acceptor micelles (expulsion/ insertion model) resulting in FRET. Association and dissociation rate constants are indicated as k_a and k_d.

7.3. Results and discussion

7.3.1. Fluorescence quenching upon encapsulation of native CotA and CotA-E40 into C3Ms

Encapsulating fluorescently labeled enzymes into complex coacervate core micelles results in fluorescence quenching. Figure 7.1 shows the normalized fluorescence emission spectra of native CotA and CotA-E40 labeled with Alexa Fluor 488 (donor) free in solution and encapsulated in C3Ms. Native CotA and CotA-E40 show similar spectra that upon

encapsulation decrease in intensity (Figure 7.1). This fluorescence quenching resulting from the formation of fluorescent protein-containing C3Ms has been observed earlier.[29–31]

In general, fluorescence quenching can happen because of various intermolecular processes such as excited-state reactions, molecular rearrangements, energy transfer, ground-state complex formation, and collisional quenching.[32,33] Close distance interaction between fluorophore and quencher is required for quenching, which can be dynamic or static quenching. Static quenching (also known as contact quenching) results from physical contact or the formation of a complex before excitation occurs (ground state complex).[33] On the other hand, dynamic quenching results from diffusive encounters during the lifetime of the excited state.[34] In the case of CotA labeled with Alexa Fluor 488, dynamic quenching takes place upon encapsulation, as a shortened fluorescence lifetime was observed (from 3.2 ± 0.1 ns to 2.0 ± 0.1 ns during encapsulation of native CotA, and from 3.4 ± 0.0 ns to 2.2 ± 0.2 ns during encapsulation of CotA-E40) (Figure S7.2., Supplementary information).

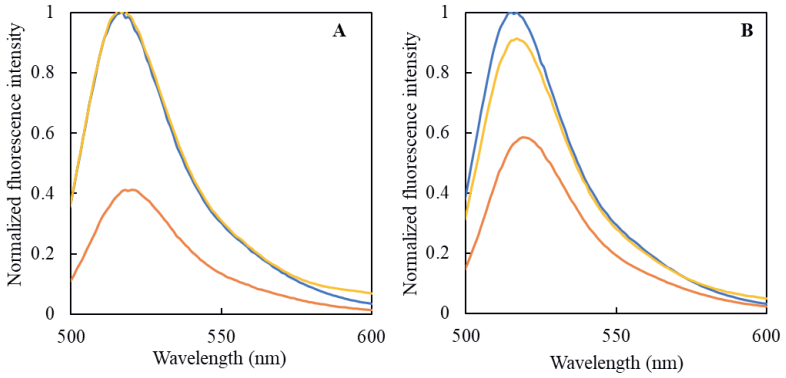

Figure 7.1. Normalized fluorescence spectra of Cot A labeled with Alexa Fluor 488, free in solution (blue), encapsulated in C3Ms (orange), and with the addition of 200 mM NaCl to the C3M solution (yellow). (A) native CotA and (B) CotA-E40. The emission was recorded upon excitation of 490 nm. The normalization was done by dividing the emission intensities by the maximum intensity of the free donor enzyme.

Figure 7.1A shows that the initial fluorescence intensity is completely restored after adding 200 mM NaCl to the C3Ms of native CotA. This indicates that these C3Ms disintegrated completely, and all enzymes were released. The increased salt concentration on the C3M solution weakens the electrostatic interactions between the protein and polymer and reduces the entropy gain from counterion release, which leads to the disassembly of the C3Ms[5,9,15,19,35–37]

Encapsulation of CotA-E40 also shows fluorescence quenching but to a slightly lesser extent than in the case of native CotA. It seems that the polyglutamic acid tails of CotA-E40 reduce the physical contact or diffusive encounters between Alexa 488 fluorophores on CotA-E40 and the polymer, leading to less quenching. Adding 200 mM NaCl to CotA-E40 micelles restored the fluorescence intensity up to 90 %, indicating that some micelles or small protein-polymer complexes are still present.

Micelle formation kinetics is associated with the formation of soluble complexes (SCs) between the enzyme and polymer and the aggregation of these soluble complexes into micelles. We used FRET to monitor this process. However, due to the fast formation (at a timescale of milliseconds to seconds), we could not monitor the formation of soluble complexes (SCs) and C3Ms over time using FRET measurements (Figure S7.1., Supplementary information). This suggests that the formation of SCs and C3Ms is a diffusion-controlled process.[5] Zhang et al. also observed that the complexation process between PEO-*b*-PQDMA and PEO-*b*-PSSNa was fast and could finish within seconds.[38]

7.3.2. FRET efficiency and exchange dynamics of native CotA and CotA-E40

In this study, we used FRET as a read-out for monitoring protein exchange between preformed C3Ms. We labeled CotA with Alexa 488 (donor) or Alexa 568 (acceptor) and recorded the fluorescence emission spectra. Before we measured the kinetics/ exchange dynamics, we determined the FRET efficiency of completely mixed micelles. We mixed free donor and acceptor enzymes at a ratio of 1:1 and subsequently the diblock copolymer was added. In comparison, we mixed donor C3Ms and acceptor C3Ms and recorded the emission spectra until the mixture was equilibrated. At a mixing ratio of 1:1, the highest final FRET efficiency (*E*) was obtained (Figure S7.3., Supplementary information). Excitation of the C3Ms mixture at the donor excitation wavelength results in non-radiative transfer of the excited-state energy from donor to acceptor molecules in the same micelle; the acceptor molecules emit a photon when returning to the ground state.[17,18] As a result, we observed quenching of the donor and an increase in the acceptor photon emission (Figure 7.2).

Based on the decrease in fluorescence intensity at 525 nm (donor quenching), FRET efficiency (*E*) of about 27 ± 6 % is determined for mixed donor/ acceptor native CotA micelles, while the mixed donor/ acceptor C3Ms composed of CotA-E40 had a FRET efficiency of about 13 ± 2 %. The lower FRET efficiency for the mixed donor-acceptor C3Ms of CotA-E40 can be explained by the lower number of enzyme molecules incorporated in these micelles than in the native CotA micelles.[8] FCS data revealed that native CotA-C3Ms contain about 55 enzyme

molecules per micelle. For C3Ms composed of CotA-E40 this number is about 28. A decrease in micelle aggregation number leads to a decrease in FRET efficiency. This is supported by the model of $E(t)$ and simulations.[11] Adding salt decreased the FRET efficiency, and at high salt concentrations, FRET did not even happen because the micelles had fallen apart. However, at 20 mM NaCl, most CotA was still present in the micelles, and E had not significantly decreased yet (Figure S7.4, Supplementary information).

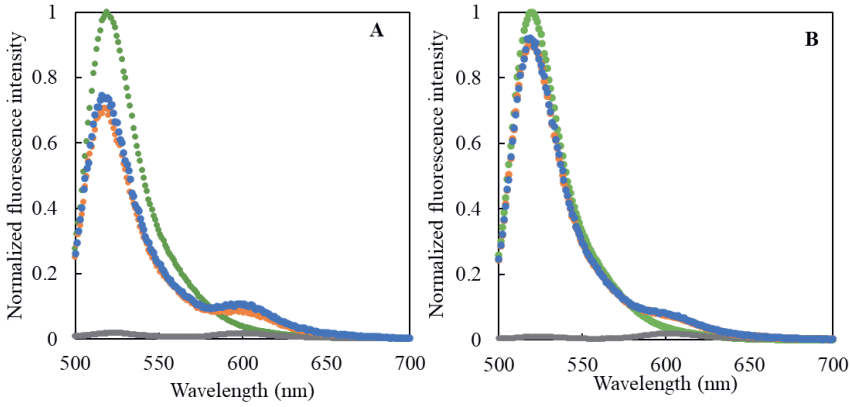

Figure 7.2. Normalized fluorescence emission spectra of C3Ms with CotA-Alexa Fluor 488 (donor only) (green), C3Ms with CotA-Alexa Fluor 568 (acceptor only) (grey), mixed donor C3Ms and acceptor C3Ms (orange), and C3Ms prepared from mixed free donor and acceptor (blue). (A) native CotA, and (B) CotA-E40. The normalization was done by dividing the emission intensities by the maximum intensity of the C3Ms with donor only. The emission was recorded upon excitation at 490 nm.

After determination of the FRET efficiencies for completely mixed donor/ acceptor micelles, we measured the protein exchange rate between C3Ms of native CotA and CotA-E40 without adding salt and with 20 mM NaCl. Donor C3Ms and acceptor C3Ms were prepared separately, mixed quickly, and the donor fluorescence intensity at 525 nm was recorded over time. Figure 7.3 shows the results. When we mixed the donor C3Ms and acceptor C3Ms, the FRET efficiency (E) increased quickly and became constant as the mixture reached equilibrium (Figure 7.3). The protein exchange rate between native CotA-C3Ms was slightly higher than between CotA-E40-C3Ms. Increasing the net charge of the enzyme results in a stronger electrostatic attraction between CotA and the polymer and slows down the exchange. Figure 7.3 also shows that the addition of only 20 mM NaCl strongly increased the exchange rate for both types of micelles. The FRET efficiency increased faster and reached the value of the

completely mixed micelles $E(\infty)$ earlier than without adding 20 mM NaCl. Salt ions screen the electrostatic interaction between protein and diblock copolymer, but at this low salt concentration, the C3Ms are still intact. However, the decrease in electrostatic attraction lowers the energy barrier of the activated expulsion process and therefore increases the exchange rate. Moreover, increasing the salt concentration reduces the interfacial tension between the coacervate core of the micelles and the aqueous solution, which favors the detachment of small complexes. This expulsion of SCs from the core is the rate-limiting step in the protein exchange between C3M.[11,39]

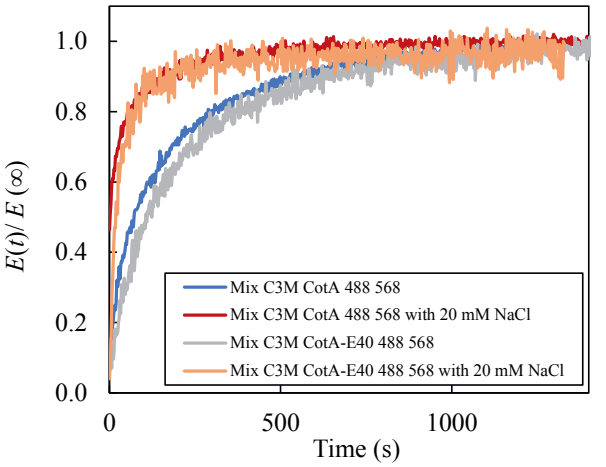

Figure 7.3. Normalized FRET efficiency as a function of time after mixing of donor C3Ms and acceptor C3Ms: native CotA-C3Ms (blue), CotA-E40-C3Ms (grey), native CotA-C3Ms with 20 mM NaCl (red), and CotA-E40-C3Ms with 20 mM NaCl (orange). The enzymes had been labeled with FRET pairs: Alexa Fluor 488 (donor) and Alexa Fluor 568 (acceptor).

To determine the exchange rate constants, we fitted the experimentally determined normalized FRET efficiency $E(t)/ E(\infty)$ to the analytical model described in the experimental section. From the fitting, we found two exchange rate constants: k_1 (slower rate) and k_2 (faster rate). Fitting with only one rate constant did not give satisfactory results, while fitting with more than two rate constants did not improve the fit quality. At low salt concentration, protein exchange is relatively slow, and the largest part of the protein exchange happens with the lowest rate constant (k_1). The fitting results are presented in Table 7.1; $1/k$ reflects the time scale of exchange. From the fitting, we found that about 80 % of the exchange took place at a time scale of about 500 s ($1/k_1 = 497 \pm 60$ s) for C3Ms composed of native CotA, and about 75 % of the exchange happened on a time scale of about 600 s ($1/k_1 = 616 \pm 88$ s) for C3Ms composed of

CotA-E40. Thus, the protein exchange between CotA-E40-C3Ms is slower by about 1.2 times compared to native CotA-C3Ms.

Because the rate constants differ significantly (k_1 is in the order of 10 times lower than k_2), it is unlikely that this is due to differences in the exchange rate of donor and acceptor (or donor and acceptor SCs). Instead, we assume that there is a small fraction of more loosely bound enzymes (or soluble enzyme-polymer complexes) at the outside of the micelles that can exchange relatively fast with the SCs and free protein in solution. To exchange the enzyme molecules that are in the center of the core, takes more time. These proteins have to diffuse through the core to the outside, and the electrostatic attraction with the charged block of the polymers does slow down this diffusion considerably. Also, the rearrangement, i.e., the evenly mixing of donors and acceptors in the cores of the micelles that leads to maximum FRET efficiency, is slow.

Table. 7.1. Fitting results on $E(t)/ E(\infty)$ for mixing donor and acceptor C3Ms containing native CotA or CotA-E40.

Sample	k_1 (s^{-1})	t_1 (s)	x_1	k_2 (s^{-1})	t_2 (s)	x_2
CotA WT	0.0020 ± 0.0003	497 ± 60	0.8 ± 0.02	0.05 ± 0.01	24 ± 9	0.2 ± 0.02
CotA-E40	0.0017 ± 0.0003	616 ± 88	0.75 ± 0.21	0.02 ± 0.01	54 ± 12	0.25 ± 0.21
CotAWT with 20 mM NaCl	0.0040 ± 0.0003	251 ± 18	0.62 ± 0.02	4.45 ± 0.68	0.2 ± 0.0 3	0.39 ± 0.02
CotA-E40 with 20 mM NaCl	0.0026 ± 0.0019	517 ± 268	0.45 ± 0.06	0.04 ± 0.01	29 ± 9	0.55 ± 0.06

* k_1, and k_2 are the exchange rate constants, respectively; x indicates the corresponding fraction exchanged with these rate constants ($x_1 + x_2 = 1$), t (= $1/k$) indicates the time scale of exchange. Error margins represent the standard deviation from three repetitions (n = 3). Fitting the data used parameters f_D = 0.5. N_D and N_A of C3Ms composed of native CotA = 55. N_D and N_A of C3Ms composed of CotA-E40 = 28.

Increasing the salt concentration affects the fractions exchanged at shorter and longer times. After adding 20 mM NaCl, the fraction that was exchanged with the higher rate constant (k_2) increased for both native CotA and CotA-E40. Apparently, it becomes easier for the proteins to diffuse and rearrange in the micelles when salt is added, and the electrostatic interactions in the core become lower. The exchange rate between C3Ms composed of CotA-E40 is still lower than between native CotA-C3Ms; however, the additional charge from the 40 glutamic acid residues on CotA-E40 is insufficient to significantly decrease the exchange

dynamics even though improved salt stability was observed (in more specific, approximately 50% of the fluorescently-tagged enzymes were released from the cores of the micelles upon addition of 80 mM NaCl and 150 mM NaCl for native CotA and CotA-E40, respectively).[15]

In contrast to our results, simulations and experiments by Bos et al.[11,14] showed a significant decrease in the exchange rate with the increasing number of charges on one of the two core species on C3Ms composed of synthetic polyelectrolytes or DNA.[11,14,40] The difference may be due to the fact that proteins have a lower charge density than polyelectrolytes or DNA, which might make the relaxation dynamics in the core different. In addition, for protein-containing C3Ms, the expulsion of SCs is likely the rate-determining step for exchange, and these small protein-diblock complexes have a low net charge. Therefore, it may not surprise that the exchange rates for native CotA-C3Ms and CotA-E40-C3Ms are on the same order of magnitude.

The fast exchange indicates that C3Ms are not very effective for protecting proteins against environmental effects: even if the concentration is far above the critical micelle concentration and without added salt, enzyme exchange between micelles takes place within a few minutes. Adding extra charges to the protein decreases the exchange rates only by a relatively small amount (~20 %). In the next section, core-crosslinking of fluorescent proteins will be tested as a tool to decrease the protein exchange dynamics of between C3Ms.

7.3.3. Fluorescence quenching upon encapsulation of fluorescent proteins into C3Ms and subsequent core-crosslinking

Another strategy to create salt-resistant micelles is crosslinking. Here, we core-crosslinked the C3Ms that were generated from fluorescent proteins and amine-functionalized diblock copolymer Q_{NH_2}PM2VP$_{128}$-*b*-PEO$_{477}$. Different concentrations of the diblock copolymer were added to a constant concentration of fluorescent protein. The formation of C3Ms was observed by using DLS. The mixing composition that had the highest scattering intensity (*I*) and lowest polydispersity index (PDI) was identified as the preferred micellar composition (PMC), resulting in the highest concentration and most well-defined micelles[3,16,19,41,42] (Figure S7.5., Supplementary information).

Figure 7.4 shows the fluorescence emission spectra of mTurquoise2 free in solution and encapsulated in micelles. The encapsulated protein shows a decrease in fluorescence intensity of around 35 % compared to the protein-free in solution. In earlier studies, fluorescence quenching of fluorescent proteins (FPs) upon encapsulation in C3Ms was also observed. [29,30,31] However, the polymer used in this study showed a more severe effect, possibly due to the

ethyleneamine on the pyridine ring promoting physical contact or diffusive encounters between chromophores of mTurquoise2 and the polymer, leading to more quenching. When the core was crosslinked by adding the core-crosslinker DTBP to the micelle solution, with a concentration of two times (DTBP 2X) or four times (DTBP 4X) of the concentration of amines in the diblock copolymer, the fluorescence intensity dropped even more. The addition of a crosslinker could affect the β-barrel of the fluorescent protein, and the addition of a crosslinker might result in a more compact/ tight core resulting in additional quenching.

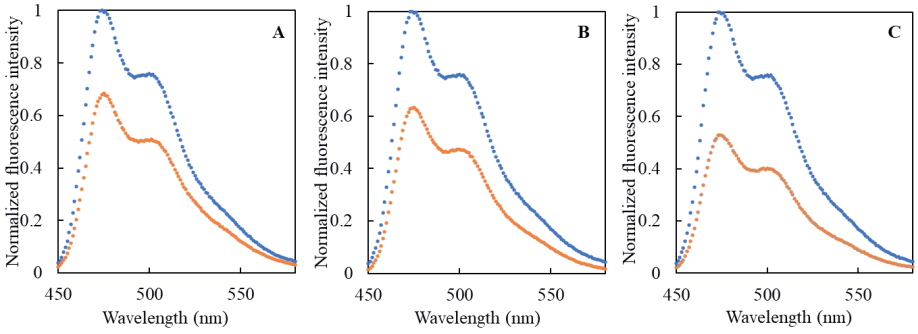

Figure 7.4. Normalized fluorescence emission spectra of free mTurquoise2 in solution (blue) and encapsulated in C3Ms (orange) for (A) non-crosslinked C3Ms, (B) core-crosslinked C3Ms DTBP 2X, and (C) core-crosslinked C3Ms DTBP 4X. The spectra were recorded upon excitation at 440 nm.

Like the formation of CotA-containing C3Ms, the formation of FP-containing C3Ms was found to happen so quickly that it was impossible to record this process in a FRET experiment (Figure S7.1., Supplementary information). In contrast to our results, experiments by Nolles et al. observed that the relaxation time of C3Ms composed of FP and PM2PV$_{128}$-*b*-PEO$_{477}$ was about 100 seconds.[5] Other equipment allowing faster measurement, such as a stopped-flow spectrofluorometer, could be used to monitor the formation of C3Ms.

7.3.4. FRET efficiency and exchange dynamics of non-crosslinked and crosslinked FP-containing C3Ms

Before we measured fluorescent proteins' exchange dynamics, we determined the FRET efficiency of mixed micelles. We used mTurquoise2 (donor) and SYFP2 (acceptor) in a ratio of 1:1 and recorded the fluorescence emission spectra. Figure 7.5 shows that mixing non-crosslinked donor and acceptor C3Ms and waiting for equilibrium gave a FRET efficiency of about 47 ± 5 %, and adding a crosslinker resulted in a FRET efficiency of about 44 ± 4 % and

8 ± 3 % for DTBP 2X and DTBP 4X, respectively. Meanwhile, when first free mTurquoise2 and SYFP2 were mixed, and then diblock was added, *E* was found to be about 51 ± 2 %; adding crosslinker resulted in *E* of about 51 ± 1 % for both DTBP 2X and DTBP 4X, respectively. Mixed C3Ms of donor-acceptor that have been crosslinked have lower FRET efficiency than non-crosslinked mixed C3Ms of donor-acceptor. The higher the crosslinker concentration added to the C3Ms, the lower the FRET efficiency, indicating the protein exchange between C3Ms decreased or no significant protein exchange between C3Ms occurs due to network forming in the core.

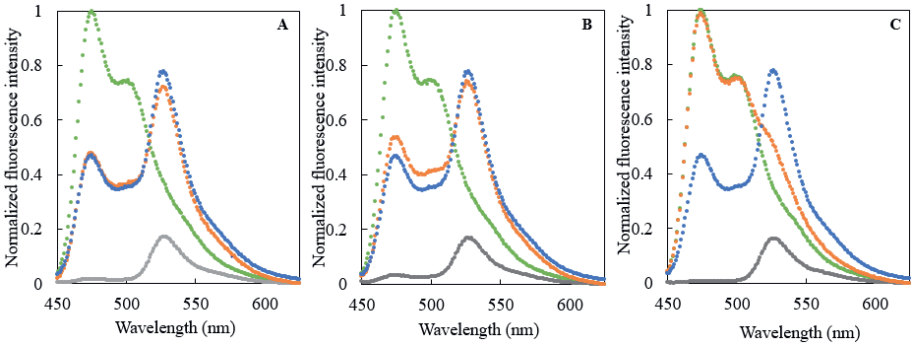

Figure 7.5. Normalized fluorescence emission spectra of C3Ms: donor only (green), C3M acceptor only (grey), mixed donor C3Ms and acceptor C3Ms (orange), and C3Ms prepared from mixed free donor and free acceptor (blue). (A) C3Ms without core-crosslinks, (B) core-crosslinked C3Ms DTBP 2X, and (C) core-crosslinked C3M DTBP 4X. The normalization was done by dividing the emission intensities by the maximum intensity of the C3M donor only. The emission was recorded upon excitation of 440 nm.

After measuring the maximum FRET efficiency, we performed exchange dynamics experiments on FP-containing C3Ms. We mixed C3Ms composed of mTurquoise2 (donor) with C3Ms composed of SYFP2 (acceptor) and monitored the donor fluorescence intensity at 475 nm upon 440 nm excitation over time. Figure 7.6 shows the normalized FRET efficiency $E(t)/E(\infty)$ after mixing donor C3Ms with acceptor C3Ms, without a core-crosslinker and in the presence of the core-crosslinker DTBP (DTBP 1X and DTBP 2X). Without crosslinker, the FRET efficiency quickly increased and reached the maximum value after several seconds, indicating that the exchange of the FPs between micelles is relatively rapid. The addition of crosslinker led to a slower increase of the FRET efficiency to the maximum FRET efficiency, pointing to a slower protein exchange between donor and acceptor micelles. When the micelle

solution was incubated with a four-fold excess of crosslinker (DTBP 4X), the FRET efficiency increased only a bit just after mixing, but then became constant and never reached the maximum FRET efficiency of completely mixed donor-acceptor micelles (Figure 7.6). Apparently, at this excess of crosslinker, the proteins are completely stuck in the core and cannot diffuse out, so no significant exchange takes place.

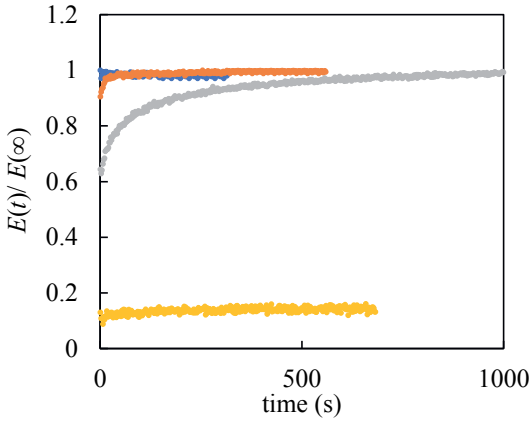

Figure 7.6. Normalized FRET efficiency $E(t)/ E(\infty)$ as a function of time after mixing donor C3Ms and acceptor C3Ms without crosslinker (blue), with crosslinker DTBP 1X (orange), with crosslinker DTBP 2X (grey), and with crosslinker DTBP 4X (yellow).

By fitting the experimental data to Equation 7.1, we can calculate the C3Ms exchange rate constants. For the fitting, we used 450 protein molecules within one micelle. This number of FPs per micelle has been determined by Nolles et al.[5,21] Since we have used FPs with the same charge (pH 9) and the same block copolymer with a comparable degree of quaternization, we assume $N = 450$ is a very good estimate. Again, we used two rate constants. The fits show that the exchange rate constant k_1 dominates the exchange process. By applying core-crosslinking, the value of k_1 decreased significantly, indicating the exchange rate C3Ms is getting slower. Table 7.2. summarizes the fitting results. Protein exchange on a timescale of about 30 s (x_1 = 72 %) was observed for FP containing micelles without crosslinker. However, with the addition of DTBP 1X, the fraction of slower exchange (x_1) increased to 91 % with an exchange on an increased timescale of about 80 s ($1/k_1$= 78.27 ± 10.96). Using core-crosslinking of DTBP 2X, x_1 even increased to 98 %, and the timescale went up to about 2600 s ($1/k_1$ = 2611.11 ± 673.58). The higher the concentration of crosslinker added to the solution of C3Ms, the lower k_1 and the

higher the corresponding fraction of slow protein exchange is. Clearly, the exchange slows down due to the more extensive and denser network of the crosslinked cores.

Core crosslinking of protein-containing micelles seems a promising strategy to limit the protein exchange rate between C3Ms as the proteins are kinetically trapped in the cores. This beneficials for protein protection applications. However, this is less favorable for delivery applications unless the crosslinks can be broken by a trigger (reversible crosslinks).

Table 7.2. Fitting results on $E(t)/E(\infty)$ for mixing donor and acceptor C3Ms containing mTurquoise and SYFP2, without and with crosslinker addition.

Sample	k_1 (s^{-1})	t_1 (s)	x_1	k_2 (s^{-1})	t_2 (s)	x_2
C3M mix mTurq2 SYFP2	0.04 ± 0.03	30.92 ± 21.45	0.72 ± 0.13	66.77 ± 34.92	0.02 ± 0.01	0.28 ± 0.13
C3M mix mTurq2 SYFP2 DTBP 1X	0.01 ± 0.002	78.27 ± 10.96	0.91 ± 0.03	82.07 ± 24.32	0.013 ± 0.005	0.09 ± 0.03
C3M mix mTurq2 SYFP2 DTBP 2X	0.0004 ± 0.0001	2611.11 ± 673.58	0.98 ± 0.0	144.4 ± 5.3	0.01 ± 0.0	0.02 ± 0.0

* k_1, and k_2 are the exchange rate constants, respectively, with x the corresponding fraction of exchange ($x_1 + x_2 = 1$); t (= $1/k$) indicates the time scale of exchange. Error margins represent the standard deviation from three repetitions ($n = 3$). Fitting the data used parameters $f_D = 0.5$. N_D of C3M composed of mTurquoise = 450. N_A of C3M composed of SYFP2= 450.

7.4. Conclusions

We studied the formation of protein-containing C3Ms and the dynamics of protein exchange between C3Ms using FRET. Fluorescence quenching occurs when the diblock copolymer is added to a solution of fluorescently labeled enzyme (CotA or CotA-E40) or fluorescent proteins (mTurquoise) due to the formation of C3Ms, and this quenching can be recovered by adding salt, indicating the salt-induced disintegration of the micelles. The rate of C3M formation was found to be too fast to determine the corresponding rate constants for all systems studied. Protein exchange between C3Ms took place on a longer timescale than C3M formation. The experimentally determined FRET efficiencies after mixing donor and acceptor micelles, as a function of time, could be fitted using an analytical model. For a good fit, two exchange rate constants were needed. Most likely, the higher exchange rate constant reflects the exchange via loosely bound proteins or small protein-polymer complexes at the outer part of the C3M core. The lower rate constant would then be related to the slower process of protein diffusion and rearrangement in the cores. Fitting the exchange data to the FRET-based exchange model showed that increasing the charge of CotA, by genetically adding a tail of 40 glutamic acid

residues (CotA-E40), slows down the exchange of the protein between C3Ms by a factor of 1.2. The addition of salt still boosts the exchange rate significantly. Salt ions screen the electrostatic interactions, lowering the energy barrier and increasing the expulsion of small complexes from the core, resulting in a faster exchange. Core-crosslinking fluorescent protein-containing C3Ms with DTBP (in excess of two times the amine concentration of the diblock copolymer) slows the protein exchange by more than 80 times compared to non-crosslinked C3Ms. Thus, the core-crosslinking strategy slowed down the protein exchange between C3Ms significantly better than providing extra charge to the proteins. This implies that core-crosslinking is the most promising of the two strategies to make C3Ms applicable for protecting proteins against a hostile environment. For protein delivery purposes, it will be necessary to make crosslinks in the C3Ms' core that are reversible and can be broken using a trigger.

References

1. Kaiser, M., Huber, R. and Ehrmann, M. Proteolysis. *Brenner's Encycl. Genet. Second Ed.* **5**, 501–503 (2013).
2. Ciulli, A. and Farnaby, W. Protein degradation for drug discovery Protein degradation for drug discovery. *Drug Discov. Today Technol.* **31**, 1–3 (2019).
3. Voets, I. K., de Keizer, A. and Cohen Stuart, M. A. Complex coacervate core micelles. *Adv. Colloid Interface Sci.* **147**–**148**, 300–318 (2009).
4. Cohen Stuart, M. A., Besseling, N. A. M. and Fokkink, R. G. Formation of micelles with complex coacervate cores. *Langmuir* **14**, 6846–6849 (1998).
5. Nolles, A., Hooiveld, E., Westphal, A. H., Van Berkel, W. J.H., Kleijn, J. M., and Borst, J. W. FRET Reveals the Formation and Exchange Dynamics of Protein-Containing Complex Coacervate Core Micelles. *Langmuir* **34**, 12083–12092 (2018).
6. Amann, M., Diget, J. S., Lyngsø, J., Pedersen, J. S., Narayanan, T., Lund, R. Kinetic Pathways for Polyelectrolyte Coacervate Micelle Formation Revealed by Time-Resolved Synchrotron SAXS. *Macromolecules* **52**, 8227–8237 (2019).
7. Zhao, M., and Zacharia, N. S. Protein encapsulation via polyelectrolyte complex coacervation : Protection against protein denaturation. *J. Chem. Phys.* **149**, 1–10 (2018).
8. Black, K. A., Priftis, D., Perry, S. L., Yip, J., Byun, W. Y., and Tirrell, M. Protein encapsulation via polypeptide complex coacervation. *ACS Macro Lett.* **3**, 1088–1091 (2014).
9. Blocher McTigue, W. C. and Perry, S. L. Protein Encapsulation Using Complex Coacervates: What Nature Has to Teach Us. *Small* **16**, 1–17 (2020).
10. Bos, I. and Sprakel, J. Langevin Dynamics Simulations of the Exchange of Complex Coacervate Core Micelles: The Role of Nonelectrostatic Attraction and Polyelectrolyte Length. *Macromolecules* **52**, 8923−8931 (2019).
11. Bos, I., Timmerman, M. and Sprakel, J. FRET-based determination of the exchange dynamics of complex coacervate core micelles. *Macromolecules* **54**, 398–411 (2021).
12. Heo, T. Y., Kim, S., Chen, L., Sokolova, A., Lee, S., and Choi, S. H. Molecular Exchange Kinetics in Complex Coacervate Core Micelles: Role of Associative Interaction. *ACS Macro Lett.* **10**, 1138–1144 (2021)
13. Spruncken, C. C. M., Magana, J. R. and Voets, I. K. 100th Anniversary of Macromolecular Science Viewpoint: Attractive Soft Matter: Association Kinetics, Dynamics, and Pathway Complexity in Electrostatically Coassembled Micelles. *ACS Macro Lett.* **10**, 167–179 (2021).
14. Bos, I., Brink, E., Michels, L. and Sprakel, J. DNA dynamics in complex coacervate droplets and micelles. *Soft Matter* **18**, 2012–2027 (2022).
15. Kembaren, R., Westphal, A. H., Kamperman, M., Kleijn, J. M. and Borst, J. W. Charged Polypeptide Tail Boosts the Salt Resistance of Enzyme-Containing Complex Coacervate Micelles. *Biomacromolecules* **23**, 1195–1204 (2022).
16. Kembaren, R., Kleijn, J. M., Borst, W., Kamperman, M., and Hofman, A. H. Enhanced stability of complex coacervate core micelles following different core-crosslinking strategies. *Langmuir* **36**, 8494–8502 (2020).
17. Jaffé, H. H. and Miller, A. L. The fates of electronic excitation energy. *J. Chem. Educ.* **43**, 469–473 (1966).
18. Heim, R. and Tsien, R. Y. Engineering green fluorescent protein for improved brightness, longer wavelengths and fluorescence resonance energy transfer. *Curr. Biol.* **6**, 178–182 (1996).
19. Kembaren, R., Fokkink, R., Westphal, A. H., Kamperman, M., Kleijn, J. M., and Borst, J.W. Balancing Enzyme Encapsulation Efficiency and Stability in Complex Coacervate Core Micelles. *Langmuir* **36**, 8494–8502 (2020).
20. Nolles, A., Westphal, A. H., Kleijn, J. M., van Berkel, W. J. H. and Borst, J. W. Colorful packages: Encapsulation of fluorescent proteins in complex coacervate core micelles. *Int. J. Mol. Sci.* **18**, 1557-1576 (2017).
21. Nolles, A., Westphal, A. H., Kleijn, J. M., van Berkel, W. J. H. and Borst, J. W. Encapsulation of GFP in complex coacervate core micelles. *Biomacromolecules* **16**, 1542–1549 (2015).
22. Ha, T. Single-Molecule FRET. *Single Mol.* **2**, 283–284 (2001).
23. Spriet, C., Trinel, D., Riquet, F., Vandenbunder, B., Usson, Y., and Heliot, L. Enhanced FRET contrast in lifetime imaging. *Cytom. Part A* **73**, 745–753 (2008).
24. Algar, W. R., Hildebrandt, N., Vogel, S. S. and Medintz, I. L. FRET as a biomolecular research tool — understanding its potential while avoiding pitfalls. *Nat. Methods* **16**, 815–829 (2019).
25. Vandenberk, N., Barth, A., Borrenberghs, D., Hofkens, J. and Hendrix, J. Evaluation of Blue and Far-Red Dye Pairs in Single-Molecule Förster Resonance Energy Transfer Experiments. *J. Phys. Chem. B* **122**, 4249–4266 (2018).

26. Berney, C. and Danuser, G. FRET or no FRET: A quantitative comparison. *Biophys. J.* **84**, 3992–4010 (2003).
27. Teunissen, A. J. P., Pérez-Medina, C., Meijerink, A. and Mulder, W. J. M. Investigating supramolecular systems using Förster resonance energy transfer. *Chem. Soc. Rev.* **47**, 7027–7044 (2018).
28. Wallrabe, H. and Periasamy, A. Imaging protein molecules using FRET and FLIM microscopy. *Curr. Opin. Biotechnol. 2005,* **16**, 19–27 (2005).
29. Van der Gucht, J., Spruijt, E., Lemmers, M. and Cohen Stuart, M. A. Polyelectrolyte complexes: Bulk phases and colloidal systems. *J. Colloid Interface Sci.* **361**, 407–422 (2011).
30. Kötz, J., Kosmella, S. and Beitz, T. Self-assembled polyelectrolyte systems. *Prog. Polym. Sci.* **26**, 1199–1232 (2001).
31. Ando, T. and Asai, H. Charge effects on the dynamic quenching of fluorescence of 1, N-ethenoadenosine oligophosphates by iodide, thallium (I) and acrylamide. *J. Biochem.* **88**, 255–264 (1980).
32. Hu, Y. J., Liu, Y., Pi, Z. B. and Qu, S. S. Interaction of cromolyn sodium with human serum albumin: A fluorescence quenching study. *Bioorganic Med. Chem.* **13**, 6609–6614 (2005).
33. Wang, Y. Q., Zhang, H. M., Zhang, G. C., Tao, W. H. and Tang, S. H. Interaction of the flavonoid hesperidin with bovine serum albumin: A fluorescence quenching study. *J. Lumin.* **126**, 211–218 (2007).
34. Eftink, M. R. and Ghiron, C. A. Fluorescence quenching studies with proteins. *Anal. Biochem.* **114**, 199–227 (1981).
35. Lindhoud, S. *Polyelectrolyte complex micelles as wrapping for enzymes*. (2009).
36. Lindhoud, S., De Vries, R., Schweins, R., Cohen Stuart, M. A. and Norde, W. Salt-induced release of lipase from polyelectrolyte complex micelles. *Soft Matter* **5**, 242–250 (2009).
37. Lindhoud, S., Voorhaar, L., De Vries, R., Schweins, R., Cohen Stuart, M. A. Salt-induced disintegration of lysozyme-containing polyelectrolyte complex micelles. *Langmuir* **25**, 11425–11430 (2009).
38. Zhang, J., Chen, S., Zhu, Z. and Liu, S. Stopped-flow kinetic studies of the formation and disintegration of polyion complex micelles in aqueous solution. *Phys. Chem. Chem. Phys.* **16**, 117–127 (2014).
39. Heo, T. Y., Kim, S., Chen, L., Sokolova, A., Lee, S., and Choi, S. H. Molecular Exchange Kinetics in Complex Coacervate Core Micelles: Role of Associative Interaction. *ACS Macro Lett.* **10**, 1138–1144 (2021).
40. Spruijt, E., Stuart, M. A. C. and Van der Gucht, J. Linear Viscoelasticity and Swelling of Polyelectrolyte Complex Coacervates. *Macromolecules* **46**, 1633−1641 (2013).
41. Mills, C. E., Obermeyer, A., Dong, X., Walker, J. and Olsen, B. D. Complex Coacervate Core Micelles for the Dispersion and Stabilization of Organophosphate Hydrolase in Organic Solvents. *Langmuir* **32**, 13367–13376 (2016).
42. Bourouina, N., Cohen Stuart, M. A. and Mieke Kleijn, J. Complex coacervate core micelles as diffusional nanoprobes. *Soft Matter* **10**, 320–331 (2014).

Supplementary information

S7.1. Kinetics of the formation of proteins-containing complex coacervate core micelles

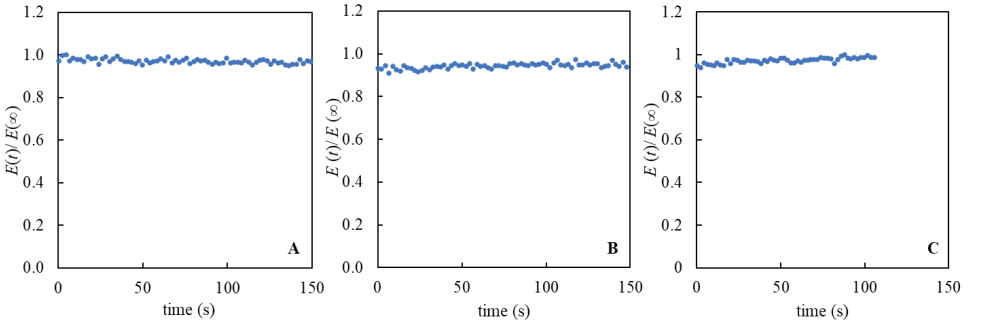

Figure S7.1. FRET C3M formation experiments on (A) native CotA, (B) CotA-E40, and (C) fluorescent proteins. The samples were prepared by mixing free donor and acceptor and then adding diblock copolymer (see 'Kinetics of C3M formation' in the experimental section for details). These data show that the formation of C3Ms is extremely fast and cannot be monitored using FRET.

S7.2. Fluorescence lifetime measurements on fluorescently labeled native CotA and CotA-E40

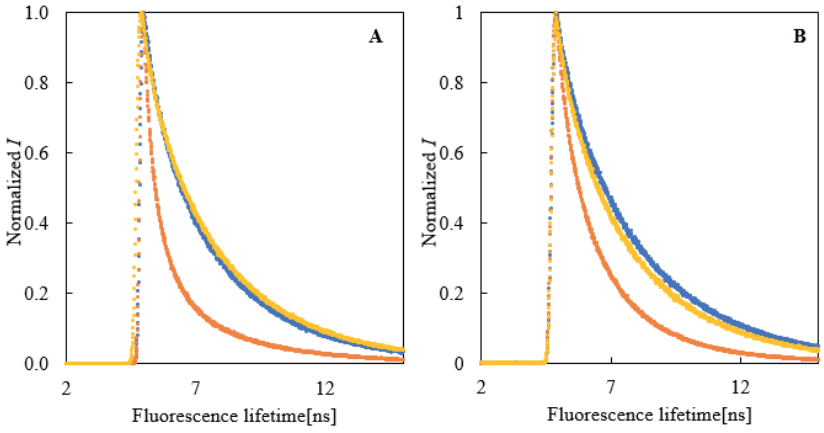

Figure S7.2. Lifetime measurements on (A) native CotA and (B) CotA-E40 as a free enzyme in solution (blue), encapsulated in C3Ms (orange), and after adding 200 mM NaCl into the enzyme-containing C3M samples (yellow). This shortened lifetime is evidence that the quenching that takes place in the micelles is dynamic.

Table S7.1. Fluorescence lifetime analysis

Samples	Average fluorescence lifetime (ns)
1. Free native CotA-Alexa 488	3.2 ± 0.1
2. C3M native CotA-Alexa 488	2.0 ± 0.1
3. Free CotA-E40-Alexa 488	3.4 ± 0.0
4. C3M CotA-E40-Alexa 488	2.2 ± 0.2

S7.3. FRET efficiency for native CotA-C3Ms with different mixing ratios of donors and acceptors

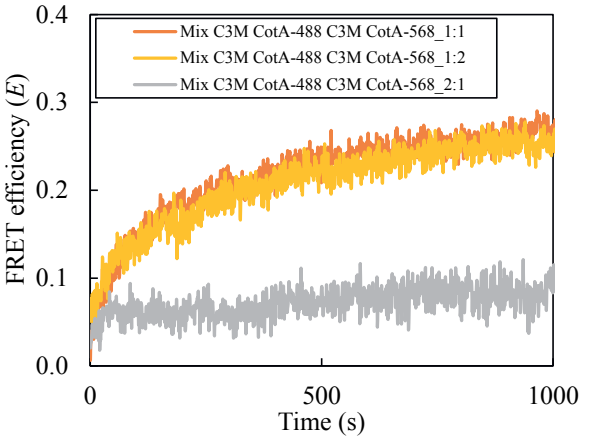

Figure S7.3. FRET efficiency (*E*) as a function of time for different mixing ratios of donor C3Ms and acceptor C3Ms.

S7.4. Normalized fluorescence emission for free enzymes and enzymes encapsulated in C3Ms

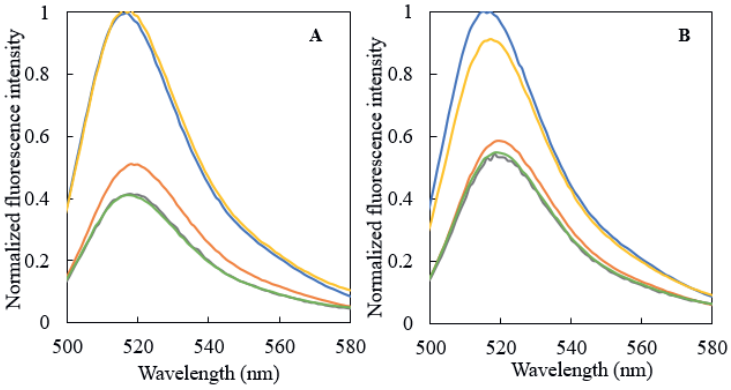

Figure S7.4. Normalized fluorescence spectra of free donor enzyme (blue), donor C3Ms (orange), mixed donor-acceptor C3Ms (grey), mixed donor-acceptor C3Ms with addition of 20 mM NaCl (green), and with addition of 200 mM NaCl (yellow). (A) native CotA, and (B) CotA-E40. The emission was recorded upon excitation of 490 nm.

S7.5. Encapsulation of fluorescent proteins into C3Ms using amine-functionalized diblock copolymer Q_{NH_2}PM2VP$_{128}$-*b*-PEO$_{477}$ observed by dynamic light scattering (DLS)

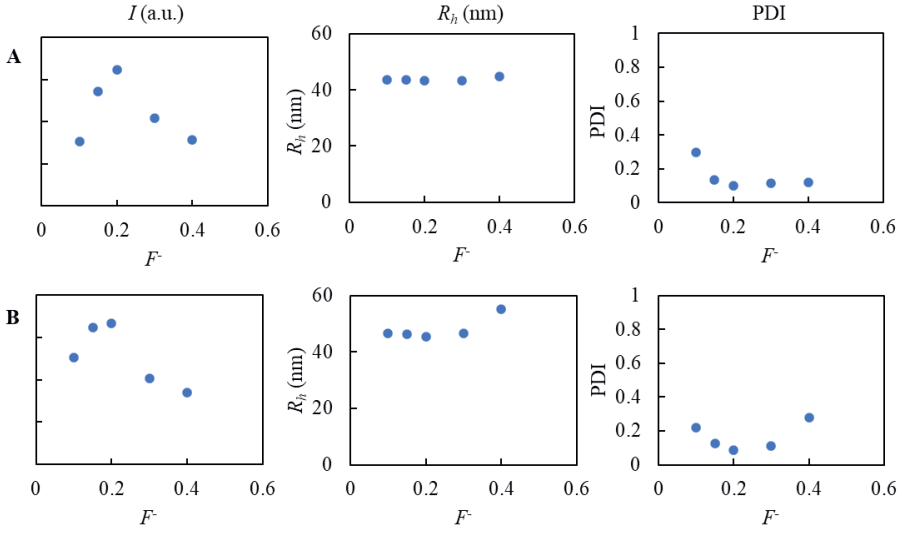

Figure S7.5. Light scattering intensity (I), hydrodynamic radius (R_h), and polydispersity index (PDI) for mixtures of (A) mTurquoise2, (B) SYFP2, and the diblock copolymer Q_{NH_2}PM2VP$_{128}$-*b*-PEO$_{477}$ at different mixing compositions (F^-) observed by using DLS.

The mixed ratio composition (F^-) is calculated by using the equation $F^- = \frac{[n^-]}{[n^+] + [n^-]}$. Where [$n$-] refers to the concentration of negative charge on the enzyme molecules, and [n^+] refers to the concentration of positive charge on the diblock copolymer. The preferred micellar composition (PMC) of the fluorescent proteins is found at a low value of F^- = 0.2. For charge neutrality, a value of F^- = 0.5 would be expected. This deviation of the PMC suggests that the C3M formation is not only driven by electrostatic attraction but also driven by other forces such as hydrophobic interaction.[20,21]

Chapter 8 :
General discussion

This final chapter highlights important findings and connections between the results of the various experimental chapters. In this chapter, I put my thesis in a broader scope and discuss the potential future of protein-complex coacervate core micelles (C3Ms). This thesis describes several strategies to improve salt stability and decrease the exchange dynamics of protein-containing C3Ms. The salt stability of C3Ms and their exchange dynamics determine the level of protection and controlled delivery offered by C3Ms as protein carriers. In this study, the focus was on the encapsulation of the enzyme CotA Laccase. In addition, as a proof of concept, the fluorescent proteins (mTurquoise2 and SYFP2) were used to study the exchange dynamics, next to fluorescently labeled CotA. To improve the salt stability of C3Ms, I have used the following strategies: addition of homopolymers (polyelectrolytes) of the same charge sign as the enzyme (three-component C3Ms), insertion of additional charges to the enzyme (by bioconjugation and by genetic engineering), and covalent core-crosslinking of the C3Ms.

8.1. Why encapsulate proteins into complex coacervate core micelles?

Proteins are valuable macromolecules that have been used for many applications such as pharmaceutical and food applications. For pharmaceutical applications, some proteins such as human growth hormone, factor VIII, insulin, monoclonal antibodies, and enzymes are often used as therapeutic proteins.[1–3] In contrast to low molecular weight drugs, proteins possess primary, secondary, tertiary, and, in some cases, quaternary structures. Disruption of these structures (by denaturation or degradation) can cause a loss of biological activity for many proteins.[4] Another problem encountered in the application of therapeutic proteins is their short half-life in blood circulation.[5] Encapsulating these proteins into C3Ms could extend their half-life in the blood circulation and protect the protein from shear forces inside the blood vessels.[6] Encapsulating proteins into C3Ms also provides the opportunity to control the release.[7–9] Due to the high loading efficiency of C3Ms, encapsulation of therapeutic proteins into C3Ms will make it possible to deliver many protein molecules from one micelle. The nanoscopic size of C3Ms aids cell intake/ absorption.[4] Another advantage over other methods to encapsulate proteins is that C3Ms are easy to prepare from just aqueous solutions (no organic solvents needed).

For food industry applications, enzymes such as α-amylase, protease, lactase, and glucose oxidase are often used to improve the taste and texture of food, and its nutritional properties, which offers substantial economic benefits to industries. It also benefits the consumer, who gets tastier and more nutritious food products.[10] Enzymes are commonly used ingredients by food industries, such as bakery, dairy, and beverages products. For food application, protein encapsulation into C3Ms is beneficial to protect the protein against environmental stresses and during manufacturing process operations where high temperatures can occur.

8.2. What did we find?

8.2.1. Formation, size, shape, and encapsulation efficiency of protein-containing C3Ms

This study focuses on the encapsulation of spore coat protein A (CotA) laccase into C3Ms. We have chosen CotA as a model protein because it is well-studied. The production and purification of CotA are also relatively easy. Moreover, using an active enzyme makes it possible to study the effect of encapsulation on enzyme activity. CotA has a strongly positively charged patch on its surface.[11,12] The charge of this patch (+15) is higher than the overall net charge of CotA at neutral pH (−10). The strong influence of the positive patch can be seen during the purification

of CotA laccase, in which this enzyme is still bound to the cation exchange column (SP-Sepharose column) using Tris HCl buffer pH 7.6, although it has a pI of 5.84.

Mixing positively charged diblock copolymer with negatively charged CotA laccase at neutral pH results in large aggregates and no C3Ms are formed probably due to the charged patches on the CotA surfaces. Additionally, there is no C3M formation at neutral pH because the electrostatic interaction between the enzyme and the diblock copolymer is too weak due to the insufficient negative charge of the enzyme. To reduce the effect of the positive patch and provide sufficient negative charge to the enzyme, the encapsulation of CotA was done at pH 10.8. CotA laccase is an alkaline-resistant enzyme. This pH does not affect the secondary structure of the protein and even improves the activity of CotA laccase.[13]

Encapsulation of protein was achieved by mixing protein solution with oppositely charged-neutral hydrophilic diblock copolymer solution of poly(2-methyl-vinyl-pyridinium)$_{128}$-*block*-poly(ethylene-oxide)$_{477}$ (PM2VP$_{128}$-*b*-PEO$_{477}$) (**Chapter 2, 3, 4, and 7**), or its amine-functionalized derivative (Q_{NH_2}PM2VP$_{128}$-*b*-PEO$_{477}$) (**Chapter 6 and 7**). The electrostatic interaction between the charged protein and the oppositely charged block of polymer, accompanied by entropy gain due to the release of counterions, drives the formation of complex coacervate core micelles. The neutral hydrophilic blocks of the polymers prevent macroscopic phase separation of the coacervate and aggregation of the micelles due to steric repulsion.[14–19] Furthermore, due to the hydrophobic character of some amino acid residues of the protein (resulting from, e.g., aromatic side chains of phenylalanine and tryptophan) and hydrophobic parts of the polyelectrolyte block of the polymers (such as vinyl backbone of PM2PV-*b*-PEO, the styrene group of PSS, and alkyl part of ethyleneamine), the formation of protein-containing C3Ms may also be promoted by hydrophobic interactions.[20–24]

To observe the formation of enzyme-containing C3Ms, we used dynamic light scattering (DLS) and fluorescence correlation spectroscopy (FCS). DLS allows the observation of the structural features of C3Ms based on the fluctuation of scattered light intensity due to the Brownian motions of particles. These scattered intensities can be auto-correlated to retrieve the diffusion coefficient of the particles in the solution. However, because DLS is only based on the scattering light intensity, it cannot give information about the fraction of enzyme incorporated in C3Ms (encapsulation efficiency). Similar to DLS, with FCS one can also observe the structural features of C3Ms based on the fluctuation of fluorescence intensity due to the Brownian motions of fluorescent particles moving in and out of the confocal volume. However, with FCS, we can also observe the fraction of enzyme encapsulated. To monitor the exchange dynamics of proteins between micelles, we used Förster resonance energy transfer

(FRET). We separately prepared C3Ms containing CotA labeled with a FRET donor (donor micelles) and C3Ms containing CotA labeled with a FRET acceptor (acceptor micelles). By mixing donor and acceptor micelles, the exchange of proteins leads to an increasing FRET efficiency as the two types of proteins become mixed in the same core of micelle, close enough to each other for FRET to occur and to be quantified. We also used fluorescent proteins to study protein exchange between C3Ms, which is more straightforward to perform using the fluorescence spectroscopy technique because no labeling step is needed.

We managed to observe the preferred micellar composition (PMC) by using DLS. On the PMC, the mixed ratio of protein and diblock copolymer resulted in the highest concentration and most well-defined micelles that observed as the highest scattering intensity and the lowest polydispersity index (PDI).[25–27] Our study shows that C3Ms composed of native CotA and genetically engineered CotA (**Chapter 2 and 4**) have a PMC at a mixing composition (F^-) of about 0.5. At $F^- = 0.5$, the concentrations of positive charges on the diblock and net negative charges on the enzyme are equal ([−]/[+] =1), and an electrically neutral core is expected to form.[19] However, for three-component C3Ms (**Chapter 2**) and C3Ms that are formed using the amine-functionalized diblock copolymer (**Chapter 5, 6 and 7**), the PMC deviates from the charge balance between negative and positive charges because of the contribution of other factors besides electrostatic interaction in the complex formation, such as hydrophobic interactions.

From the DLS and FCS data the diffusion coefficients were used to calculate the hydrodynamic radius (R_h) based on the Stokes-Einstein relation for spherical particles. DLS and FCS provided similar R_h values when the particle size distribution in the samples is relatively narrow (before the addition of salt). The R_h of C3Ms composed of native CotA and $PM2VP_{128}$-*b*-PEO_{477} at their PMC is 32-35 nm. However, C3Ms composed of bioconjugated CotA and genetic engineered CoA with the same diblock copolymer are smaller than C3Ms composed of native CotA. As the enzyme charge increases, the micellar size decreases because fewer enzyme molecules are required to neutralize the diblock copolymers; thus, fewer CotA molecules are incorporated into one micelle. On the other hand, the concentration of C3Ms composed of the higher charged CotA enzymes is higher than the concentration of C3Ms composed of native CotA, so that the encapsulation efficiency is approximately the same. Moreover, all micelles in this study have a spherical shape shown by multi-angle DLS.[6,18,28,29]

We used the cumulant method for analysis of particle size distribution and mean particle size from DLS measurement in this study. However, the cumulant method determines the particle size distribution based on the assumption that only one particle population exists and have a gaussian distribution around average particle size. After salt was added, the sample's polydispersity index (PDI) increased, and cumulant method provides less accurate R_h because the particle size distribution broadens, and multiple peaks are formed. In the case of polydisperse samples with bimodal or polymodal particle size distributions, other analysis methods such as the CONTIN or CORENN could be used.[62]

8.2.2. Enzyme activity and secondary structure

CotA oxidizes a wide range of substrates such as polyphenols, methoxy-substituted phenols, diamines, and even some inorganic compounds.[30,31] In this thesis, we measured the activity of CotA laccase using the non-phenolic substrate 2,2′-azino-bis(3-ethylbenzothiazoline-6-sulfonic acid) (ABTS) because the activity assay protocol using ABTS is well established, and the resulting green-colored product ($ABTS^{\bullet+}$) is easily detected by using an ultraviolet/ visible (UV/vis) spectrophotometer. The reduction of type I copper center (T1) on the laccase structure is the rate-limiting step in the reactions catalyzed by laccase. The pH dependence of the redox potential (E^o) for substrate and laccase lead to a larger difference in redox potential [$\Delta E^o = E^o_{\text{laccase,T1 Cu}} - E^o_{\text{substrate,single electron}}$] or driving force (for the electron transfer from substrate to T1 copper) at higher pH. The predominant effect of ΔE^o result in a higher substrate oxidation rate, in which the activity increases as the pH increases.[103,104] Some studies have shown that small halide anions such as chloride (Cl^-) and bromide (Br^-) can inhibit laccase activity due to interruption of the internal electron transfer of copper atoms that coordinate with these anions. Moreover, other inhibitors of laccases like EDTA affect the laccase activity by chelating copper atoms. The presence of reducing agents such as dithiothreitol (DTT) interferes with the reaction of substrate oxidation and by modifying amino acid residues.[32,105]

In this study, we cannot measure the activity of native CotA when it is inside micelles because the activity measurement using the ABTS assay is performed at pH 4.4, while C3Ms were generated at a pH of 10.8. Native CotA is released from the micelles at this low pH and then oxidizes the substrate ABTS. We found that the encapsulation of CotA in two-component and three-component C3Ms maintains its catalytic activity (**Chapter 2**). Moreover, genetically engineered CotA with short polyglutamic acid tails and bioconjugated CotA with short poly(acrylic acid) (PAA) tails showed improved CotA activity. A possible explanation for the

enhanced activity of these enzymes is due to the addition of these short, polar, and charged tails which improve the solubility of enzymes and the substrate can easily bind to the active site of CotA.[33–35] However, bioconjugation with longer polymer chains and the addition of core-crosslinkers to the C3Ms reduced the activity of CotA because such chains and the polymer network within the core hinder the binding of the substrate to the active site of CotA (**Chapter 3 and Chapter 6**). Circular dichroism (CD) shows that protein encapsulation into C3Ms maintains the secondary protein structure (**Chapter 2**). This supports the maintenance of CotA activity after encapsulation into C3Ms. The addition of a tag of amino acid residues by genetic engineering on the enzyme and bioconjugation of CotA with a short homopolymer did not alter the secondary structure of the protein either.

8.2.3. Combatting disintegration of encapsulated proteins

In this study, we observed a response of protein-containing C3Ms to the addition of salt, as salt affects the C3Ms formation and the C3Ms exchange dynamics.[15] Addition of salt weakens the electrostatic interaction by shielding the charges and decreases the entropy gain from the release of counterions.[36–38] Therefore, it opposes C3M formation. In addition, as the charge of a protein depends on the pH, the pH is also an important parameter for tuning the electrostatic interaction strength and the C3M stability.

We used both DLS and FCS to observe the salt stability of protein-containing C3Ms. Using DLS, we observed the dissociation of micelles as decreasing light scattering intensity (I). FCS showed dissociation of micelles as an increasing number of fluorescent particles detected in the confocal volume[37] as the fluorescent-labeled CotA is released from the core of micelles. This can be seen from the autocorrelation function, in which the intercept of the Y-axis equals $1+1/N$, where N is the average number of particles in the confocal volume. Moreover, the addition of salt broadens the distribution in micellar size, confirmed by the increasing PDI value observed by using DLS. The micellar aggregation number is hardly influenced at very low salt concentrations.[36,38] At medium salt concentration (below the critical salt concentration), the fraction of encapsulated protein decreases almost linearly with salt concentration. The C3Ms will be completely disintegrated after the addition of salt exceeds the critical salt concentration.

The critical salt concentration of complex coacervates generally depends on the type of salt used. Salt that is less hydrated and composed of highly polarizable ions (i.e., KSCN) is more effective in disturbing the electrostatic interactions in coacervate complexes than highly hydrated salts (i.e., NaCl).[39,40] Moreover, salts containing divalent ions such as Na_2SO_4 and

$CaCl_2$ are much more efficient in preventing coacervate formation than NaCl.[41] In this study, we observed the salt stability of protein-containing C3Ms using NaCl. The inert anion Cl^- takes a transitional position between kosmotropic and chaotropic salts and has little influence on polymer solubility and protein stability.[40] Moreover, NaCl is one of the most common salts used in food and pharmaceutical products and therefore is relevant for the application of C3Ms. For potential biomedical applications, the stability of micelles under physiological salt conditions is paramount. We used a range of salt concentrations around these physiological conditions (150 mM NaCl) to study the salt stability of enzyme-containing C3Ms.

In this thesis, we observed differences in salt stability by adding NaCl to different types of C3Ms with the same length of the diblock copolymer. For C3Ms composed of native CotA and diblock copolymer $PM2VP_{128}$-*b*-PEO_{477}, complete disintegration of C3M happens at salt concentrations above 100 mM NaCl (**Chapter 2, 3, 4**); however, for C3Ms composed of homopolymer PAA (weak polyelectrolyte) with amine-quaternized diblock copolymer ($Q_{NH_2}P2VP_{128}$-*b*-PEO_{477}), complete disintegration of C3M happens at salt concentrations above 400 mM NaCl (**Chapter 5**). For C3Ms composed of homopolymer PSS (strong polyelectrolyte) and $P2MVP_{128}$-*b*-PEO_{477}, complete disintegration of C3M only occurs at very high salt concentrations (far above 1 M NaCl) (**Chapter 2**).[39] From these findings, we can identify several trends in the salt stability of C3Ms. First, the charge density of the C3M components is important to the salt resistance of C3Ms since these charges determine the strength of interaction between the core components of the micelles. Polyelectrolytes with lower charge densities have lower critical salt concentrations. Secondly, a combination of polyelectrolytes with hydrophobic groups results in higher critical salt concentrations since the hydrophobic complexes are depleted of salt, and hydrophobic interactions promote the complex formation.[39]

Salt also accelerates the exchange dynamics of proteins between C3Ms. For our systems, exchange via an expulsion/ insertion mechanism of small soluble complexes (SCs) of proteins and polymer is most likely.[16,42] The SCs can be expelled from the micelle if they overcome the corresponding energy barrier. A decrease in electrostatic interactions by adding salt decreases this energy barrier and therefore increases the exchange rate.[42,43] Moreover, increasing the salt concentration reduces the interfacial tension between the coacervate core of the micelles and the aqueous solution, which favors the detachment of small complexes.[36,38,44–46] Protein exchange dynamics should be minimized to limit the undesired exposure of the protein to the environment and to protect and deliver the protein.

8.3. Do the offered strategies solve the challenges of C3M salt stability and exchange dynamics?

This thesis describes several potential strategies to improve salt stability and decrease the exchange dynamics of protein-containing complex coacervate core micelles. These strategies are adding a homopolymer of the same charge sign as the protein to the C3Ms (three-component micelles), adding extra charges to the protein by either bioconjugation or genetic engineering, and core-crosslinking of the micelles. Different applications have different stability requirements, so possibly also different strategies have to be followed. For example, therapeutic protein delivery requires stability under physiological salt conditions (150 mM NaCl and pH 7.4), for waste treatment or in seawater applications require stability at about 700 mM NaCl and pH 7.4–8.4,[47,48] and for food applications, C3Ms mostly require stability at acidic conditions (lower than pH 7). Below I discuss for each strategy the most significant results, providing comparable information to help to choose the best strategy for specific applications.

8.3.1. Three-component micelles strategy

For our first strategy, we observed the effect of adding a homopolymer with the same charge sign as the protein in the mixed solutions of enzyme and diblock copolymer to form three-component C3Ms. We used the anionic homopolymer poly(4-styrenesulfonate)$_{215}$ (PSS_{215}) as the third component, in addition to CotA and the diblock copolymer (**Chapter 2**). We chose this strategy because several previous studies reported a fairly high salt resistance of three-component coacervate phases and three-component C3Ms.[48,49] However, there is no clear explanation of how these three-component C3Ms improve the salt stability, so this needed further investigation of the three-component strategy for protein encapsulation.[50]

In three-component micelles, there are three types of interactions: first, the attraction between the negatively charged CotA and the positively charged diblock copolymer; second, the attraction between negatively charged PSS_{215} and positively charged diblock copolymer; and third, the repulsion between CotA and PSS_{215}. DLS showed that adding homopolymer indeed improves the salt stability of C3Ms, and the micelles were found to be stable even far above physiological salt concentration. The higher the concentration ratio of PSS over CotA, the better the salt stability of these micelles. However, FCS data showed that the enzyme already leaves the micellar core at lower salt concentrations than at which the two-component micelles disintegrate. The low charge density of the enzyme compared to the charge of the homopolymer results in the replacement of CotA laccase in the core by the homopolymer when

the salt concentration increases, amply before the micelles fall apart. The enhancement of salt stability in three-component micelles showed by DLS due to the attraction between negatively charged PSS_{215} and positively charged diblock copolymer. This study shows that three-component C3Ms are not suitable for achieving stable enzyme encapsulation.

8.3.2. Increasing the net charge of the protein (by bioconjugation or genetic engineering)

Due to the lower charge density of proteins in comparison to synthetic polyelectrolytes, protein-containing C3Ms disintegrate at lower salt concentrations than those composed of synthetic polyelectrolytes. The stability of C3Ms depends on the strength of the electrostatic interactions between the protein and polymer in the core. The oppositely charged groups of the two macromolecules in the core form ion pairs and hold the complex together. The more charges on the macromolecules capable of cooperative ionic interactions, the more salt is required to screen this attraction. Consequently, C3Ms are expected to be more stable when the protein's net charge increases. Increasing the net charge of protein can be done by bioconjugation and genetic engineering. Both approaches were investigated in this study.

Bioconjugation is the chemically coupling biomolecules with other biomolecules or synthetic polymers such as polyelectrolytes. Protein bioconjugation is generally used to study biological interactions in which protein binds with probe molecules or for biosensors in which proteins are attached to surfaces.[51] We chose the bioconjugation strategy because generally bioconjugation is a simple method to change the net charge of proteins. We coupled one or a few carboxyl groups from PAA to the primary amines of CotA using a combination of 1-ethyl-3-(3'-dimethylaminopropyl) carbodiimide hydrochloride (EDC) and *N*-hydroxysuccinimide (NHS) linker.[52,53] (**Chapter 3**). After bioconjugation, CotA has distribution in its charges due to the heterogeneity in the PAA attached: not all CotA molecules in a sample have the same amount of PAA chains attached, and one chain of PAA could be attached to more than one CotA; in addition, the PAA chains themselves are not monodisperse. To produce a bioconjugated enzyme fraction with a narrower net charge distribution, an extra purification step is required, such as size exclusion column chromatography or anion-exchange chromatography, to yield conjugates with precisely one or two PAA molecules chains per CotA molecule.[54]

DLS and FCS showed that native CotA-containing C3Ms fall apart below physiological salt concentration. However, C3Ms composed of CotA bioconjugated with long chains of PAA (PAA_{118}) and a high PAA to CotA ratio (5:1) have improved salt stability, and C3Ms are still

present at physiological salt concentration. The higher the molecular weight of PAA, the higher the critical salt concentrations of C3Ms due to the higher strength of the attraction between the negatively charged CotA-PAA and the positively charged diblock copolymer.[37] This result is different from what we found for three-component C3Ms. Bioconjugation of the homopolymer to the enzyme to make them one molecule hybrid is better than mixing them as two separate molecules in C3Ms: the enzyme cannot leave the C3Ms without the homopolymer, and there is no competition between the two.

We continued our study to increase the net negative charge of CotA by using genetic engineering. We modified CotA by adding chains of glutamic acids (10, 20, 30, or 40 glutamic acid residues) on its C-terminal (**Chapter 4**). This strategy resulted in a homogenous increase in the protein's net charge, and all protein samples had a precise composition. Genetic engineering has already been widely used to produce valuable products. A variety of recombinant therapeutic proteins for medical use have been created by genetic engineering, for example, to produce large amounts of insulin from yeast cells.[55,56] In our study, DLS and FCS showed improvement in the salt stability of genetically engineered CotA-containing C3Ms, and C3Ms were still present at physiological salt concentration. The more glutamic acid was tagged to CotA, the better the salt stability of these micelles.

This study shows that bioconjugation and genetic engineering are promising strategies for improving the salt stability of enzyme-containing C3Ms. The genetically engineered enzymes have a slightly higher encapsulation efficiency than the bioconjugated enzymes. Probably the broad distribution in the net charge of bioconjugated CotA results in protein competition during C3M self-assembly, resulting in slightly lower efficiency. Although C3Ms composed of higher charged CotA variants become more resistant to salt-induced disintegration, these C3Ms disintegrate at low pH values below their pI (which results in a positive net charge on the enzyme). This approach cannot improve the stability of the C3Ms against pH changes.

The effect of genetic engineering on the protein exchange dynamics between C3Ms was investigated using Förster resonance energy transfer (FRET). Native CotA and CotA-E40 were labeled with FRET pair probes: Alexa Fluor 488 and Alexa Fluor 568. Although genetic engineering with additional 40 glutamic acids enhances the salt stability of the enzyme-containing C3Ms, it does not significantly decrease the exchange rate. The fast exchanges indicate that C3Ms are not very effective at protecting proteins from environmental effects.

8.3.3. Core-crosslinking of C3Ms

We applied crosslinking between the diblock copolymers in the core to entrap the protein in the micelles without changing the protein, while maintaining the solubility of the micelles. For crosslinking, different functional groups (i.e., primary amine group, carboxylate, and sulfhydryl group) and crosslinkers (i.e., homobifunctional or heterobifunctional linker, cleavable or non-cleavable) can be used. In this thesis, we investigated the effect of crosslinking on salt stability for C3Ms consisting of poly(2-vinylpyridine)-*block*-poly(ethylene oxide) (QP2VP-*b*-PEO) and PAA (**Chapter 5**) and for CotA-containing C3Ms (with $Q_{NH_2}PM2VP_{128}$-*b*-PEO_{477} as the diblock) (**Chapter 6**). Thus, in both cases, the diblock copolymer was functionalized with an amine group.[57] We chose the amine functional group because this group can react with many different reactive groups (e.g., isothiocyanate, NHS ester, and imidoester), and will not interfere with the positive charge of the diblock copolymer. We have applied crosslinking between primary amines and carboxylate groups of the two different types of chains in the core (by using 1-ethyl-3-(3'-dimethylaminopropyl)carbodiimide hydrochloride (EDC) linker) (**Chapter 5**) and crosslinking between primary amines of the same type of polyelectrolyte chains (by using 3,3′-dithiopropionimidate dihydrochloride (DTBP) linker) (**Chapter 5 and 6**). Both approaches significantly improved the stability of the C3Ms against salt and pH changes. The crosslinked network in the core prevents these micelles from dissociating even at very high salt concentrations.[58–62] Moreover, reducing the disulfide bridges in the DTBP-crosslinked core at pH 7.4 almost completely restored the original C3M salt stability profile, thus enabling a reversible approach.

This study also showed that the core-crosslink strategy effectively decreases the protein exchange rate between micelles. The higher the crosslinker concentration added to the C3Ms, the slower the exchange occurs. The protein is trapped in the crosslinked network of the core, preventing it from diffusing out, and at sufficiently high crosslinker concentrations, protein exchange is completely inhibited. For protection protein application, kinetically trapped protein in the C3Ms is preferable; however, for delivery applications, reversible crosslinks (the network can be broken by using a trigger) are preferred since the protein need to be released.

8.4. What can be done to optimize the proposed strategies?

Instead of adding a homopolymer as the third component of C3Ms, we described that it is better to couple/ bioconjugate the charged homopolymer to the protein to improve the salt stability of enzyme-containing C3Ms. Increasing the net charge of CotA using bioconjugation with longer

polymers (PAA_{118}) increased the salt concentration above which the micelles completely disintegrated to about 400 mM NaCl. For applications that require C3Ms to stay well intact at above 400 mM, it is important to look at other polyelectrolyte tails for bioconjugation, such as poly(methacrylic acid) (PMAA). This polymer is an anionic, water-soluble, capable of reaction through carboxylates groups, and has hydrophobic features (the presence of the methyl group of PMAA), therefore could improve the salt stability of C3Ms.[39,63,64]

Bioconjugation using reactive side groups on naturally occurring amino acids (i.e., lysine, glutamic acid, and cysteine) leads to heterogeneities in the number and location of modifications. Site-specific protein bioconjugation could be achieved by adding unnatural amino acids (UAA) to the protein. Using unnatural amino acids such as 5-hydroxytryptophan allows chemoselective protein modification using the azo-coupling reaction.[65] A tRNA charged with the UAA of interest is engineered to recognize a stop codon, which then adds the UAA in the growing polypeptide chain during protein translation (commonly referred to as nonsense codon suppression mechanism).[66,67]

The salt stability enhancement of C3Ms using genetically engineered CotA with extra glutamic acids could still be improved by adding longer charged amino acid sequences. However, there is a maximum of amino acid residues that can be added to CotA above which the enzyme significantly changes its secondary structure or decreases its activity. In addition to adding a sequence of charged amino acids to the C-terminus of CotA, neutral amino acid residues on the surface of CotA can be replaced by charged amino acids. Genetic engineering could also reduce the positive patch effect on CotA laccase, in which lysine on the patch is mutated to the neutral or negatively charged amino acid residues. In addition, the genetically engineered protein could be transformed into a fusion protein with additional domains of charged and hydrophobic domains.[68] The fusion protein's charged and hydrophobic domains can interact electrostatically and hydrophobically with the oppositely charged diblock copolymer, potentially forming coacervate complexes with enhanced salt stability. Several other experimental studies have shown that hydrophobic amino acids such as isoleucine, phenylalanine, and tyrosine are well tolerated on the protein surface. These amino acids could be introduced to hydrophobic domains.[69] However, the effects on the secondary structure and enzyme activity need to be carefully examined.

The increase in net charge improved the stability of protein-containing C3M against salt; however, it did not improve the stability against pH changes. Other driving forces than electrostatic interactions, such as hydrophobic interactions, are also interesting for improving the stability of protein-containing C3Ms. Hydrophobized C3Ms components are expected to

prevent micelle dissociation due to the association of hydrophobic groups.[6] Additionally, temperature sensitivity polymers such as poly(*N*-isopropylacrylamide) (PNIPAM) can be incorporated as triblock copolymers to encapsulate protein.[27,70,71] Upon an increase in temperature, the presence of PNIPAM could provide additional attractive interactions, such as cation-π interaction, that stabilize the coacervate core of the micelles.[27,70,71]

Our results show that the core-crosslinking is the most effective strategy for increasing the salt stability of C3Ms and decreasing protein exchange dynamics. In the pH 7.4 (**Chapter 5**), disulfide bridges in the DTBP-crosslinked core can be reduced/ cleavage using a reducing agent such as DTT, and restore the original C3M salt stability (similar to non-crosslinked C3Ms), thus this reversible crosslink approach benefit for therapeutic protein delivery application. Core-crosslinking can be done using different crosslinkers and other active groups than amines and carboxylate, such as thiol, hydroxyl, or photoreactive groups.[72,73] Core-crosslinking with other cleavable crosslinker reagents besides cleavable disulfide-containing linkers also can be done, for example, by using a diazo-containing crosslinker. Crosslinking agents that contain diazo bonds within their structure can be cleaved using sodium dithionite.[65,74–77] Moreover, crosslinking agents containing an ester or thioester group within their structure can be cleaved under alkaline conditions using hydroxylamine. Core-crosslinking can also be performed using a cleavable photoreactive group that becomes reactive when exposed to UV or visible light. Linkers that use photolabile groups provide a tunable system for delivering and releasing proteins. A nitrobenzyl (NB) based linker is one of the most commonly used classes of photodegradable linkers. NB linkers are very popular because they react to cytocompatible light doses and their cleavage products are biocompatible. Irradiation with light at 365 nm results in complete cleavage of the nitrobenzyl linker.[78–81]

8.5. Application of protein-containing C3Ms with an improved salt stability

For future studies, it will be beneficial to encapsulate proteins that can be used for a specific application, such as controlled delivery of functional ingredients in food and pharmaceutical formulation. For industrial process application, the proteins should remain protected and encapsulated while performing their function. However, for therapeutic delivery application, the protein must be released locally in response to a specific trigger. Moreover, therapeutic protein delivery requires C3Ms that stable at physiological conditions and has low exchange dynamics. Moreover, the system must be non-toxic,[82,83,84] have small sizes (on the nanoscale), and should be easy to prepare. Our study used a diblock copolymer with PEO as its hydrophilic

neutral block, which is known for its low toxicity and immunogenicity.[85,86] The charged block of diblock copolymers should use biocompatible and biodegradable for encapsulations.[83,84] Some options for positively charged blocks that biocompatible and biodegradable are poly(L-lysine), poly(aminoalkyl aspartamide), and poly(aminoalkyl methacrylate).[87] Some options for negatively charged blocks are poly(aspartic acid),[88] hyaluronic acid,[89] and poly(methacrylic acid).[87] The size of protein-containing C3Ms is relatively small (< 100 nm), an ideal size for optimal uptake by the cell.[90] With disulfide-containing core-crosslinking, it is possible to release the proteins inside the cell with a high concentration of glutathione (e.g., cancer cells). For pharmaceutical applications, it is also important to test in vitro toxicity before doing in vivo study.

For delivery of (recombinant) therapeutic proteins encapsulated in C3Ms, the use of genetic engineering or reversible core-crosslinkers to enhance the salt stability of the micelles seems to be the best option since our bloodstream has a salt concentration of about 150 mM. On the other hand, for proteins that are obtained from nature (not recombinant), e.g., derived from animal and plant cells, the bioconjugation or reversible core-crosslinking strategy is suitable for improving the salt stability of the C3Ms in which they are incorporated. With crosslinking strategy, the micelles are kinetically stable. This strategy is suitable for encapsulation and delivery applications. For industrial process applications, it does not need to be a cleavable crosslink since within crosslinking; the protein can still perform its function/ activity. However, for therapeutic application, cleavable core-crosslink should be applied.

In this study, CotA and fluorescent proteins were encapsulated at basic pH, just to get the proper charge on the proteins for C3M formation. However, for the application of C3Ms for therapeutic protein delivery, C3Ms should be stable at physiological pH. The formation of well-defined CotA-containing C3Ms at neutral pH is possible to achieve by increasing the net charge of the CotA and reducing the charge patchiness (by mutation of lysine on the patch to glutamic acid or acetylation of lysine residues using acetic anhydride). Moreover, because each protein has its specific pI, it will be helpful to test several protein models that can be encapsulated at physiological pH. Here I would like to discuss the strategies implemented for specific applications such as therapeutic delivery for tumor/ cancer treatment, enzyme replacement therapy (ERT), vaccines, and nanobioreactors.

Drug delivery is an important aspect of cancer treatment. Human IgG and Chimeric IgG have been used for cancer treatment.[3] Many fast-growing tumors and inflammatory areas have underdeveloped blood micro-vessels with pores permeable to nano-sized particles, including polymeric micelles. At the same time, lymphatic drainage is constrained, resulting in the well-

known enhanced permeation and retention (EPR) impact of tumors and inflamed areas. This suggests that nanoparticles such as C3Ms can accumulate in tumors.[57,91–93]

Disulfide-containing core-crosslinking micelles are excellent candidates for the controlled release of anti-cancer therapeutics. In this type of core-crosslinking, undesired dissociation under physiological conditions can be prevented, and protein release can be realized by reducing the disulfide-containing linker.[91,92] The disulfide crosslinks can be cleaved using a thiol-disulfide exchange reaction. The concentrations of thiols in the plasma and cytosol of tumor tissues can be up to seven times higher than in normal tissue.[95,96] Crosslinked micelles are also expected to remain in the blood circulation for a long time, allowing accumulation in cancerous or inflamed tissues by the enhanced permeation and retention effect.[57,91–93,96–99] Moreover, the hydrophilic corona protects the core of C3Ms from the external environment and prevents protein recognition in vivo by the reticuloendothelial system (RES).[100] The hydrophilic polymer chains of the corona consequently have a steric stabilization effect, preventing the uptake of micelles by the macrophages.[61,101]

Another example of the application of enzyme-containing C3Ms for medical purposes is enzyme replacement therapy (ERT). ERT is a medical treatment in which enzyme replacement is given to patients who suffer from enzyme deficiency-related disease. In case of multiple enzyme deficiencies, several enzymes can be used for enzyme treatment therapy. Enzyme-containing C3Ms could be administrated intravenously into the bloodstream. Cleavable-crosslinking of the micelles is the best strategy for this medical purpose as it prevents the dissociation of C3Ms due to dilution below its critical micelle concentration in the bloodstream.

C3Ms also can be used for vaccination, such as Covid-19 vaccines. Protein-based vaccines are used to protect people from hepatitis, shingles, and many other viral infections. These injectables deliver proteins and immunity-stimulating adjuvants directly to a person's cells, contrary to RNA vaccines that deliver a fragment of genetic code that the cells must read to synthesize the proteins themselves to elicit a protective immune response. A way to formulate a protein-based vaccine is by encapsulating the proteins in C3Ms, thereby helping vaccine administration. For industrial applications, enzyme-containing C3Ms can be used as nanobioreactors that contain several enzymes for enzyme cascade that ensures faster substrate conversion.[102] In this nanobioreactors, crosslinking could be applied since this strategy results in kinetically trapped protein and could protect the protein in the core of micelles.

In this thesis, we showed the successful encapsulation of CotA laccase into C3Ms. These enzyme-containing C3Ms are not salt resistant and fully disintegrate already below

physiological salt concentration, which limits the application of this system. By applying genetic engineering and bioconjugation, the net charge of the enzyme can be increased, which improves the salt stability of C3Ms. However, increasing the net charge of the protein does not significantly decrease the protein exchange dynamics between C3Ms and also does not improve the stability against pH changes. Our results show that core-crosslinking is the most effective strategy for increasing salt stability, resistance to pH-changing, and decreasing exchange dynamics. Crosslinking can also prevent dissociation of C3Ms due to dilution when micelle formulations are injected into the blood for medical application. Reversible core-crosslinking of C3Ms containing enzymes or therapeutic proteins has excellent potential for pharmaceutical-controlled delivery applications.

References

1. Kirk, O., Borchert, T. V. and Fuglsang, C. C. Industrial enzyme applications. *Curr. Opin. Biotechnol.* **13**, 345–351 (2002).
2. Carter, P. J. Introduction to current and future protein therapeutics: A protein engineering perspective. *Exp. Cell Res.* **317**, 1261–1269 (2011).
3. Dimitrov, D. S. Chapter 1: Therapeutic proteins. *Methods Mol. Biol.* **899**, 1–26 (2012).
4. Putney, D. Encapsulation of proteins for improved delivery. *Curr. Opin. Chem. Biol. 1998,* **2**, 548–552 (1998).
5. Kamionka, M. Engineering of Therapeutic Proteins Production in Escherichia coli. *Curr. Pharm. Biotechnol.* **12**, 268–274 (2011).
6. Magana, J. R., Sproncken, C. C. M. and Voets, I. K. On complex coacervate core micelles: Structure-function perspectives. *Polymers.* **12**, 1953–1990 (2020).
7. Nguyen, H. H. and Kim, M. An Overview of Techniques in Enzyme Immobilization. *Appl. Sci. Converg. Technol.* **26**, 157–163 (2017).
8. Bilal, M., Iqbal, H.M.N., Guo, S., Hu, H., Wang, W., and Zhang, X. State-of-the-art protein engineering approaches using biological macromolecules: A review from immobilization to implementation view point. *Int. J. Biol. Macromol.* **108**, 893–901 (2018).
9. Thangaraj, B. and Solomon, P. R. Immobilization of Lipases – A Review. Part I: Enzyme Immobilization. *ChemBioEng Rev.* **6**, 157–166 (2019).
10. Raveendran, S., Parameswaran, B., Ummalyma, S. B., Abraham, A., Mathew, A. K., Madhavan, A., Rebello, S., and Pandey, A. Applications of microbial enzymes in food industry. *Food Technol. Biotechnol.* **56**, 16–30 (2018).
11. Enguita, F. J., Martins, L. O., Henriques, A. O. and Carrondo, M. A. Crystal structure of a bacterial endospore coat component: A laccase with enhanced thermostability properties. *J. Biol. Chem.* **278**, 19416–19425 (2003).
12. Liu, Z., Xie, T., Zhong, Q. and Wang, G. Crystal structure of CotA laccase complexed with 2,2-azinobis-(3-ethylbenzothiazoline-6-sulfonate) at a novel binding site. *Acta Crystallogr. Sect. Struct. Biol. Commun.* **72**, 328–335 (2016).
13. Kembaren, R., Fokkink, R., Westphal, A. H., Kamperman, M., Kleijn, J. M., and Borst, J. W. Balancing Enzyme Encapsulation Efficiency and Stability in Complex Coacervate Core Micelles. *Langmuir* **36**, 8494–8502 (2020).
14. Cohen Stuart, M. A., Besseling, N. A. M. and Fokkink, R. G. Formation of micelles with complex coacervate cores. *Langmuir* **14**, 6846–6849 (1998).
15. Voets, I. K., de Keizer, A. and Cohen Stuart, M. A. Complex coacervate core micelles. *Adv. Colloid Interface Sci.* **147**–**148**, 300–318 (2009).
16. Nolles, A., Hooiveld, E., Westphal, A. H., Van Berkel, W. J.H., Kleijn, J. M., and Borst, J. W. FRET Reveals the Formation and Exchange Dynamics of Protein-Containing Complex Coacervate Core Micelles. *Langmuir* **34**, 12083–12092 (2018).
17. Bos, I. and Sprakel, J. Langevin Dynamics Simulations of the Exchange of Complex Coacervate Core Micelles: The Role of Nonelectrostatic Attraction and Polyelectrolyte Length. *Macromolecules* **52**, 8923−8931 (2019).
18. Voets, I. K., De Vries, R., Fokkink, R., Sprakel, J., May, R. P., De Keizer, A., and Cohen Stuart, M. A. Towards a structural characterization of charge-driven polymer micelles. *Eur. Phys. J. E* **30**, 351–359 (2009).
19. Brzozowska, A. M., Keizer, A. De, Norde, W., Detrembleur, C. and Stuart, M. A. C. Grafted block complex coacervate core micelles and their effect on protein adsorption on silica and polystyrene. *Colloid Polym. Sci.* **288**, 1081–1095 (2010).
20. Mills, C. E., Obermeyer, A., Dong, X., Walker, J. and Olsen, B. D. Complex Coacervate Core Micelles for the Dispersion and Stabilization of Organophosphate Hydrolase in Organic Solvents. *Langmuir* **32**, 13367–13376 (2016).
21. Hofs, B., Voets, I. K., De Keizer, A. and Cohen Stuart, M. A. Comparison of complex coacervate core micelles from two diblock copolymers or a single diblock copolymer with a polyelectrolyte. *Phys. Chem. Chem. Phys.* **8**, 4242–4251 (2006).
22. Cooper, C. L., Dubin, P. L., Kayitmazer, A. B. and Turksen, S. Polyelectrolyte-protein complexes. *Curr. Opin. Colloid Interface Sci.* **10**, 52–78 (2005).
23. Sanson, N., Bouyer, F., Destarac, M., In, M. and Gérardin, C. Hybrid polyion complex micelles formed from double hydrophilic block copolymers and multivalent metal ions: Size control and nanostructure. *Langmuir* **28**, 3773–3782 (2012).
24. Kembaren, R., Westphal, A. H., Kamperman, M., Kleijn, J. M. and Borst, J. W. Charged Polypeptide Tail

Boosts the Salt Resistance of Enzyme-Containing Complex Coacervate Micelles. *Biomacromolecules* **23**, 1195–1204 (2022).
25. Burgh, S. Van Der, Fokkink, R., Keizer, A. De and Stuart, M. A. C. Complex coacervation core micelles as anti-fouling agents on silica and polystyrene surfaces. *Colloids Surfaces A Physicochem. Eng. Asp.* **242**, 167–174 (2004).
26. Voets, I. K., Van Der Burgh, S., Farago, B., Fokkink, R., Kovacevic, D., Hellweg, T., De Keizer, A., and Cohen Stuart, M. A. Electrostatically driven coassembly of a diblock copolymer and an oppositely charged homopolymer in aqueous solutions. *Macromolecules* **40**, 8476–8482 (2007).
27. Voets, I. K., Van Der Burgh, S., Farago, B., Fokkink, R., Kovacevic, D., Hellweg, T., De Keizer, A., and Cohen Stuart, M. A. Temperature responsive complex coacervate core micelles with a PEO and PNIPAAm corona. *J. Phys. Chem. B* **112**, 10833–10840 (2008).
28. Mayes, A. M., Olvera, M. and Cruz, D. Micelle Formation in Block Copolymer/ Homopolymer. *Macromolecules* **21**, 2543–2547 (1988).
29. Fujii, S., Yamada, S., Matsumoto, S., Kubo, G., Yoshida, K., Tabata, E., Miyake, R., Sanada, Y., Akiba, I., Okobira, T., Yagi, N., Mylonas, E., Ohta, N., Sekiguchi, H., and Sakurai, K. Platonic micelles: Monodisperse micelles with discrete aggregation numbers corresponding to regular polyhedra. *Sci. Rep.* **7**, 1–8 (2017).
30. Enguita, F. J., Marçal, D., Martins, L. O., Grenha, R., Henriques, A. O., Lindley, P. F., and Carrondo, M. A. Substrate and dioxygen binding to the endospore coat laccase from Bacillus subtilis. *J. Biol. Chem.* **279**, 23472–23476 (2004).
31. Singh, G., Bhalla, A., Kaur, P., Capalash, N. and Sharma, P. Laccase from prokaryotes: A new source for an old enzyme. *Rev. Environ. Sci. Biotechnol.* **10**, 309–326 (2011).
32. Dwivedi, U. N., Singh, P., Pandey, V. P. and Kumar, A. Structure-function relationship among bacterial, fungal and plant laccases. *J. Mol. Catal. B Enzym.* **68**, 117–128 (2011).
33. Han, X., Ning, W., Ma, X., Wang, X. and Zhou, K. Improving protein solubility and activity by introducing small peptide tags designed with machine learning models. *Metab. Eng. Commun.* **11**, 138-147 (2020).
34. Paraskevopoulou, V. and Falcone, F. H. Polyionic tags as enhancers of protein solubility in recombinant protein expression. *Microorganisms* **6**, 47-64 (2018).
35. Zhou, K., Zou, R., Stephanopoulos, G. and Too, H. P. Enhancing solubility of deoxyxylulose phosphate pathway enzymes for microbial isoprenoid production. *Microb. Cell Fact.* **11**, 1–8 (2012).
36. Yan, Y., De Keizer, A., Cohen Stuart, M. A., Drechsler, M. and Besseling, N. A. M. Stability of complex coacervate core micelles containing metal coordination polymer. *J. Phys. Chem. B* **112**, 10908–10914 (2008).
37. Chollakup, R., Beck, J. B., Dirnberger, K., Tirrell, M. and Eisenbach, C. D. Polyelectrolyte molecular weight and salt effects on the phase behavior and coacervation of aqueous solutions of poly(acrylic acid) sodium salt and poly(allylamine) hydrochloride. *Macromolecules* **46**, 2376–2390 (2013).
38. Wang, J., De Keizer, A., Fokkink, R., Yan, Y., Cohen Stuart, M. A., and Van der Gucht, J. Complex coacervate core micelles from iron-based coordination polymers. *J. Phys. Chem. B* **114**, 8313–8319 (2010).
39. Gucht, J. van der, Spruijt, E., Lemmers, M. and Cohen Stuart, M. A. Polyelectrolyte complexes: Bulk phases and colloidal systems. *J. Colloid Interface Sci.* **361**, 407–422 (2011).
40. Kang, B., Tang, H., Zhao, Z. and Song, S. Hofmeister Series: Insights of Ion Specificity from Amphiphilic Assembly and Interface Property. *ACS Omega* **5**, 6229–6239 (2020).
41. Perry, S. L., Li, Y., Priftis, D., Leon, L. and Tirrell, M. The effect of salt on the complex coacervation of vinyl polyelectrolytes. *Polymers* **6**, 1756–1772 (2014).
42. Bos, I., Timmerman, M. and Sprakel, J. FRET-based determination of the exchange dynamics of complex coacervate core micelles. *Macromolecules* **54**, 398–411 (2021).
43. Heo, T. Y., Kim, S., Chen, L., Sokolova, A., Lee, S., and Choi, S. H. Molecular Exchange Kinetics in Complex Coacervate Core Micelles: Role of Associative Interaction. *ACS Macro Lett.* **10**, 1138–1144 (2021).
44. Kim, J. M., Heo, T. Y. and Choi, S. H. Structure and Relaxation Dynamics for Complex Coacervate Hydrogels Formed by ABA Triblock Copolymers. *Macromolecules* **53**, 9234–9243 (2020).
45. Spruijt, E., Sprakel, J., Lemmers, M., Stuart, M. A. C. and Van Der Gucht, J. Relaxation dynamics at different time scales in electrostatic complexes: Time-salt superposition. *Phys. Rev. Lett.* **105**, 1–4 (2010).
46. Kramarenko, E. Y., Khokhlov, A. R. and Reineker, P. Stoichiometric polyelectrolyte complexes of ionic block copolymers and oppositely charged polyions. *J. Chem. Phys.* **125**, 194902-194910 (2006).
47. Almagor, M. and Cole, R. D. In physiological salt conditions the core proteins of the nucleosomes in large chromatin fragments denature at 73°C and the DNA unstacks at 85°C. *J. Biol. Chem.* **264**, 6515–6519 (1989).
48. Black, K. A., Priftis, D., Perry, S. L., Yip, J., Byun, W. Y., and Tirrell, M. Protein encapsulation via

polypeptide complex coacervation. *ACS Macro Lett.* **3**, 1088–1091 (2014).
49. Lindhoud, S., de Vries, R., Norde, W. and Cohen Stuart, M. A. Structure and stability of complex coacervate core micelles with lysozyme. *Biomacromolecules* **8**, 2219–2227 (2007).
50. Blocher, W. C. and Perry, S. L. Complex coacervate-based materials for biomedicine. *Wiley Interdiscip. Rev. Nanomedicine Nanobiotechnology* **9**, 76–78 (2017).
51. Kalia J. and Raines, R. T. Advances in Bioconjugation. *Curr Org Chem.* **14**, 138–147 (2010).
52. Riccardi, C. M., Mistri, D., Hart, O., Anuganti, M., Lin, Y., Kasi, R. M., and Kumar, C. V. Covalent interlocking of glucose oxidase and peroxidase in the voids of paper: Enzyme-polymer "spider webs. *Chem. Commun.* **52**, 2593–2596 (2016).
53. Zore, O. V., Kasi, R. M. and Kumar, C. V. Armored Enzyme–Nanohybrids and Their Catalytic Function Under Challenging Conditions. in *Methods in Enzymology* **590**, 169-192 (2017).
54. Morgenstern, J., Gil Alvaradejo, G., Bluthardt, N., Beloqui, A., Delaittre, G., and Hubbuch, J. Impact of Polymer Bioconjugation on Protein Stability and Activity Investigated with Discrete Conjugates: Alternatives to PEGylation. *Biomacromolecules* **19**, 4250–4262 (2018).
55. Nielsen, J. Production of biopharmaceutical proteins by yeast: Advances through metabolic engineering. *Bioengineered* **4**, 207–211 (2013).
56. Baeshen, N. A., Baeshen, M. N., Sheikh, A., Bora, R. S., Ahmed, M. M. M., Ramadan, H. A. I., Saini, K. S., and Redwan, E. M. Cell factories for insulin production. *Microb. Cell Fact.* **13**, 141–150 (2014).
57. Reddy, N., Reddy, R. and Jiang, Q. Crosslinking biopolymers for biomedical applications. *Trends Biotechnol.* **33**, 362–369 (2015).
58. Bourouina, N., Cohen Stuart, M. A. and Mieke Kleijn, J. Complex coacervate core micelles as diffusional nanoprobes. *Soft Matter* **10**, 320–331 (2014).
59. Oupický, D., Carlisle, R. C. and Seymour, L. W. Triggered intracellular activation of disulfide crosslinked polyelectrolyte gene delivery complexes with extended systemic circulation in vivo. *Gene Ther.* **8**, 713–724 (2001).
60. Kembaren, R., Kleijn, J. M., Borst, W., Hofman, A. H. and Kamperman, M. Enhanced stability of complex coacervate core micelles following different core-crosslinking strategies. *Soft Matter* **18**, 3052–3062 (2022).
61. Oupicky, D., Howard, K. A., Koňák, Č., Dash, P. R., Ulbrich, K., and Seymour, L.W. Steric stabilization of poly-L-lysine/DNA complexes by the covalent attachment of semitelechelic poly[N-(2-hydroxypropyl)methacrylamide]. *Bioconjug. Chem.* **11**, 492–501 (2000).
62. Van der Kooij, H. M., Spruijt, E., Voets, I. K., Fokkink, R., Cohen Stuart, M. A., and Van der Gucht, J. On the stability and morphology of complex coacervate core micelles: From spherical to wormlike micelles. *Langmuir* **28**, 14180–14191 (2012).
63. Burke, N. A. D., Mazumder, M. A. J., Hanna, M. and Stover, H. D. H. Polyelectrolyte Complexation Between Poly(methacrylic acid, sodium salt) and Poly(diallyldimethylammonium chloride) or Poly[2-(methacryloyloxyethyl) trimethylammonium chloride]. *J. Polym. Sci.* **45**, 4129–4143 (2007).
64. Oyama, H. T., Tang, W. T. and Frank, C. W. Effect of the Hydrophobic Interaction in the Poly(methacrylic acid)/Pyrene End-Labeled Poly(ethylene glycol) Complex. *Macromolecules* **20**, 1839–1847 (1987).
65. Addy, P. S., Erickson, S. B., Italia, J. S. and Chatterjee, A. A Chemoselective Rapid Azo-Coupling Reaction (CRACR) for "Unclickable" Bioconjugation. *J Am Chem Soc.* **139**, 11670–11673 (2017).
66. Lieser, R. M., Yur, D., Sullivan, M. O. and Chen, W. Site-Specific Bioconjugation Approaches for Enhanced Delivery of Protein Therapeutics and Protein Drug Carriers. *Bioconjug. Chem.* **31**, 2272–2282 (2020).
67. Smolskaya, S. and Andreev, Y. A. Site-specific incorporation of unnatural amino acids into escherichia coli recombinant protein: Methodology development and recent achievement. *Biomolecules* **9**, 255-272 (2019).
68. Dhar, P., Phiri, J., Szilvay, G. R., Westerholm-Parvinen, A., Maloney, T., and Laaksonen, P. Genetically engineered protein based nacre-like nanocomposites with superior mechanical and electrochemical performance. *J. Mater. Chem. A* **8**, 656–669 (2020).
69. Nisthal, A., Wang, C. Y., Ary, M. L. and Mayo, S. L. Protein stability engineering insights revealed by domain-wide comprehensive mutagenesis. *Proc. Natl. Acad. Sci. U. S. A.* **116**, 16367–16377 (2019).
70. Van Hees, I. A., Swinkels, P. J.M., Fokkink, R. G., Velders, A. H., Voets, I. K., Van Der Gucht, J., and Kamperman, M. Self-assembly of oppositely charged polyelectrolyte block copolymers containing short thermoresponsive blocks. *Polym. Chem.* **10**, 3127–3134 (2019).
71. Van Hees, I. A., Hofman, A. H., Dompé, M., van der Gucht, J. and Kamperman, M. Temperature-responsive polyelectrolyte complexes for bio-inspired underwater adhesives. *Eur. Polym. J.* **141**, 110034-110046 (2020).
72. Partis, M. D., Griffiths, D. G., Roberts, G. C. and Beechey, R. B. Cross-linking of protein by ω-maleimido alkanoyl N-hydroxysuccinimido esters. *J. Protein Chem.* **2**, 263–277 (1983).

73. Kim, J. O., Ramasamy, T., Yong, C., S., Nukolov, N. V., Bronich, T. K., and Kabanov, A.V. Cross-linked polymeric micelles based on block ionomer complexes. *Mendeleev Commun.* **23**, 179–186 (2013).
74. Denny, J. B. and Blobel, G. 125I-labeled crosslinking reagent that is hydrophilic, photoactivatable, and cleavable through an azo linkage. *Proc. Natl. Acad. Sci. U. S. A.* **81**, 5286–5290 (1984).
75. Leriche, G., Budin, G., Brino, L. and Wagner, A. Optimization of the azobenzene scaffold for reductive cleavage by dithionite; development of an azobenzene cleavable linker for proteomic applications. *European J. Org. Chem.* **2010**, 4360–4364 (2010).
76. Fonović, M., Verhelst, S. H. L., Sorum, M. T. and Bogyo, M. Proteomics evaluation of chemically cleavable activity-based probes. *Mol. Cell. Proteomics* **6**, 1761–1770 (2007).
77. Rabalski, A. J., Bogdan, A. R. and Baranczak, A. Evaluation of Chemically-Cleavable Linkers for Quantitative Mapping of Small Molecule-Cysteinome Reactivity. *ACS Chem. Biol.* **14**, 1940–1950 (2019).
78. Bai, X., Li, Z., Jockusch, S., Turro, N. J. and Ju, J. Photocleavage of a 2-nitrobenzyl linker bridging a fluorophore to the 5′ end of DNA. *Proc. Natl. Acad. Sci. U. S. A.* **100**, 409–413 (2003).
79. Levalley, P. J., Neelarapu, R., Sutherland, B. P., Dasgupta, S., Kloxin, C. J., and Kloxin, A. M. Photolabile Linkers: Exploiting Labile Bond Chemistry to Control Mode and Rate of Hydrogel Degradation and Protein Release. *J. Am. Chem. Soc.* **142**, 4671–4679 (2020).
80. Wegner, S. V., Sentürk, O. I. and Spatz, J. P. Photocleavable linker for the patterning of bioactive molecules. *Sci. Rep.* **5**, 1–7 (2015).
81. Sumranjit, J. and Chung, S. J. Recent Advances in Target Characterization and Identification by Photoaffinity Probes. *Molecules* **18**, 10425–10451 (2013).
82. Sharma, S., Parveen, R. and Chatterji, B. P. Toxicology of Nanoparticles in Drug Delivery. *Curr. Pathobiol. Rep.* **9**, 133–144 (2021).
83. Patra, J. K., Das, G., Fraceto, L. F., Campos, E. V. R., Rodriguez-Torres, M. D. P., Acosta-Torres, L. S., Diaz-Torres, L. A., Grillo, R., Swamy, M. K., Sharma, S., Habtemariam, S., and Shin, H. S. Nano based drug delivery systems: Recent developments and future prospects. *J. Nanobiotechnology* **16**, 1–33 (2018).
84. Sung, Y. K. and Kim, S. W. Recent advances in polymeric drug delivery systems. *Biomater. Res.* **24**, 1–12 (2020).
85. Bronich, T. K., Kabanov, A. V and Kabanov, V. A. Soluble Complexes from Poly (ethylene oxide) -block -polymethacrylate Anions and N -Alkylpyridinium Cations. *Macromolecules* **30**, 3519–3525 (1997).
86. Riess, G. Micellization of block copolymers. *Prog. Polym. Sci.* **28**, 1107–1170 (2003).
87. Lee, Y. and Kataoka, K. Biosignal-sensitive polyion complex micelles for the delivery of biopharmaceuticals. *Soft Matter* **5**, 3810–3817 (2009).
88. Adelnia, H., Tran, H. D. N., Little, P. J., Blakey, I. and Ta, H. T. Poly(aspartic acid) in Biomedical Applications: From Polymerization, Modification, Properties, Degradation, and Biocompatibility to Applications. *ACS Biomater. Sci. Eng.* **7**, 2083–2105 (2021).
89. Water, J. J., Schack, M. M., Velazquez-Campoy, A., Maltesen, M. J., Van De Weert, M., and Jorgensen, L. Complex coacervates of hyaluronic acid and lysozyme: Effect on protein structure and physical stability. *Eur. J. Pharm. Biopharm.* **88**, 325–331 (2014).
90. Ghezzi, M., Pescina, S., Padula, C., Santi, P., Del Favero, E., Cantù, L., and Nicoli, S. Polymeric micelles in drug delivery: An insight of the techniques for their characterization and assessment in biorelevant conditions. *J. Control. Release* **332**, 312–336 (2021).
91. Tangsangasaksri, M., Takemoto, H., Naito, M., Maeda, Y., Sueyoshi, D., Kim, H. J., Miura, Y., Ahn, J., Azuma, R., Nishiyama, N., Miyata, K., and Kataoka, K. SiRNA-Loaded Polyion Complex Micelle Decorated with Charge-Conversional Polymer Tuned to Undergo Stepwise Response to Intra-Tumoral and Intra-Endosomal pHs for Exerting Enhanced RNAi Efficacy. *Biomacromolecules* **17**, 246–255 (2016).
92. Paraiso, W. K. D., Takemoto, H., Naito, M., Maeda, Y., Sueyoshi, D., Kim, H. J., Miura, Y., Ahn, J., Nishiyama, N., Miyata, K., and Kataoka, K Poly-ion complex micelles effectively deliver CoA-conjugated CPT1A inhibitors to modulate lipid metabolism in brain cells. *Biomater. Sci.* **9**, 7076–7091 (2021).
93. Răileanu, M., Lonetti, B., Serpentini, C. L., Goudounèche, D., Gibot, L., and Bacalum, M. Encapsulation of a cationic antimicrobial peptide into self-assembled polyion complex nano-objects enhances its antitumor properties. *J. Mol. Struct.* **1249**, 131482-131490 (2022).
94. Gaucher, G., Dufresne, M. H., Sant, V. P., Kang, N., Maysinger, D., and Leroux, J. C. Block copolymer micelles: Preparation, characterization and application in drug delivery. *J. Control. Release* **109**, 169–188 (2005).
95. Xu, X., Smith, A. E. and McCormick, C. L. Facile 'One-Pot' preparation of reversible, disulfide-containing shell cross-linked micelles from a RAFT-synthesized, pH-responsive triblock copolymer in water at room temperature. *Aust. J. Chem.* **62**, 1520–1527 (2009).
96. Oe, Y., Christie, R. J., Naito, M., Low, S. A., Fukushima, S., Toh, K., Miura, Y., Matsumoto, Y., Nishiyama, N., Miyata, K., Kataoka, K. Actively-targeted polyion complex micelles stabilized by cholesterol and disulfide cross-linking for systemic delivery of siRNA to solid tumors. *Biomaterials* **35**,

7887–7895 (2014).
97. Van Nostrum, C. F. Covalently cross-linked amphiphilic block copolymer micelles. *Soft Matter* **7**, 3246–3259 (2011).
98. Liu, Y., Chen, F., Zhang, K., Wang, Q., Chen, Y., and Luo, X. pH-Responsive reversibly cross-linked micelles by phenol-yne click via curcumin as a drug delivery system in cancer chemotherapy. *J. Mater. Chem. B* **7**, 3884–3893 (2019).
99. Liu, H., Zhao, F., Koo, B., Luan, Y., Zhong, L., Yun, K., and Shin, Y. Dimethyl 3,3″-dithiobispropionimidate (DTBP) as a cleavable disulfide-based polymer to encapsulate nucleic acids in biological sample preparation. *Sensors Actuators, B Chem.* **288**, 225–231 (2019).
100. Kapare, H. S. and Metkar, S. R. Micellar drug delivery system: a review. *Pharm. Reson.* **2**, 21–26 (2020).
101. Fang, D., Pi, M., Pan, Z., Song, N., He, X., Li, J., Luo, F., Tan, H., and Li, Z. Stable, Bioresponsive, and Macrophage-Evading Polyurethane Micelles Containing an Anionic Tripeptide Chain Extender. *ACS Omega* **4**, 16551–16563 (2019).
102. Blocher McTigue, W. C. and Perry, S. L. Protein Encapsulation Using Complex Coacervates: What Nature Has to Teach Us. *Small* **16**, 1–17 (2020).
103. Yin, Q., Zhou, G., Peng, C., Zhang, Y., Kües, U., Liu, J., Xiao, Y., and Fang, Z. The first fungal laccase with an alkaline pH optimum obtained by directed evolution and its application in indigo dye decolorization. *AMB Express* **9**, 1–13 (2019).
104. Xu, F. Effects of redox potential and hydroxide inhibition on the pH activity profile of fungal laccases. *J. Biol. Chem.* **272**, 924–928 (1997).
105. Christopher, L. P., Yao, B. and Ji, Y. Lignin biodegradation with laccase-mediator systems. *Front. Energy Res.* **2**, 1–13 (2014).

Summary

This thesis describes the formation, salt stability, and exchange dynamics of enzyme/ protein-containing complex coacervate core micelles (C3Ms). The main aim of this research was the investigation of potential strategies to address the challenges that limit the implementation of protein-containing C3Ms for pharmaceutical and food applications: salt-induced disintegration and exchange dynamics. The salt stability of C3Ms and their exchange dynamics determine the level of protection and controlled delivery offered by C3Ms as protein carriers. The obtained results contribute to the development of C3M to encapsulate enzyme/ protein in which stability and dynamics can be adjusted to specific applications. In this research, CotA laccase and fluorescent proteins (mTurquoise2 and SYFP2) were used as protein models as they are easy to produce and purify. Dynamic light scattering (DLS) and fluorescence correlation spectroscopy (FCS) are the two main techniques used in this work to monitor the formation and stability of enzyme-containing C3Ms. To observe the protein exchange dynamics between micelles, we used Förster resonance energy transfer (FRET) as read out. Strategies that were explored to generate salt resistant C3Ms are the addition of homopolymers (polyelectrolytes) of the same charge sign as the enzyme (three-component C3Ms) (**Chapter 2**), introducing extra charges to the enzyme (using two approaches: chemical modification/ bioconjugation (**Chapter 3**) and genetic engineering (**Chapter 4**)), and covalent core-crosslinking of the C3Ms (**Chapter 6**). Application of core-crosslinking can be cleavable or non-cleavable (**Chapter 5**). We also examined the effect of the additional charges and core-crosslinking on the protein exchange between micelles (**Chapter 7**). Finally, in **Chapter 8**, we highlight important findings described in this thesis and discuss the different strategies to obtain stable micelles. We also discuss a broader scope and potential future applications of protein-complex coacervate core micelles and main findings are summarized below.

Complex coacervate core micelles (C3Ms) for protein encapsulation

In **Chapter 1**, a general introduction on protein encapsulation is provided as well as the research background, and the goals of this work. C3M is an excellent method to encapsulate active biomolecules such as proteins/ enzymes as it can preserve the enzyme's structure and activity and able to encapsulate many enzyme molecules in one micelle. However, the application of C3Ms also face some challenges. C3Ms can easily disintegrate when salt is added, and it is a dynamic system in which protein exchange between C3Ms happen continuously. The salt stability and protein exchange dynamics are related to the level of protection and delivery provided by C3Ms. In this chapter, we discuss several techniques to investigate the properties of C3Ms and the effect of encapsulation on the structure and activity of our model enzyme, the spore coat protein A (CotA) laccase.

Encapsulation of enzyme into two-component C3Ms and three-component C3Ms

In **Chapter 2**, the encapsulation of CotA laccase into C3Ms has been investigated. First the optimal pH for encapsulation was investigated as the charge of CotA is dependent on the pH. We found a pH of 10.8 was optimal for encapsulation purposes, preserving active CotA and the secondary structure of CotA was maintained. Two-component C3Ms were obtained by mixing aqueous solutions of CotA laccase with diblock copolymer poly(*N*-methyl-2-vinyl-pyridinium)$_{128}$-*block*-poly(ethylene oxide)$_{477}$ (P2MVP$_{128}$-*b*-PEO$_{477}$). Three-component C3Ms were achieved by mixing the enzyme with the negatively charged homopolymer poly(4-styrene sulfonate)$_{215}$ (PSS$_{215}$) before adding P2MVP$_{128}$-*b*-PEO$_{477}$. We used DLS and FCS to study how the addition of this homopolymer affects the encapsulation efficiency and salt stability of the micelles. Mixing composition (f^-) was calculated as the concentrations of negative charges on the enzyme divided by the total sum concentrations of charges on the system. The optimal mixing ratio between CotA and diblock copolymers results in the highest concentration of micelles, known as preferred micellar composition (PMC). C3Ms composed of native CotA have a PMC at a mixing composition (f^-) of about 0.5. For three-component C3Ms, a PMC at a mixing composition of f^- of about 0.6 was found which deviates from the charge balance between negative and positive charges because of the contribution of other driven forces complex formation besides electrostatic interaction, such as hydrophobic interactions. Three-component C3Ms appeared to have a smaller hydrodynamic radius (R_h) compared to two-component most likely because fewer enzymes are incorporated in C3Ms that was observed by using FCS. DLS results show an improvement in salt stability on the three-component C3M compared to the two-component C3M. The higher the concentration homopolymer added to the

system, the micelles become more salt resistant. However, further investigation on the three component C3M system using FCS showed that the release of CotA from these micelles occurred at a lower salt concentration and over a narrower concentration range than the two-component C3Ms. With the addition of the homopolymer to the C3Ms, the homopolymer acts as a competitor of the enzyme for encapsulation, thereby excluding CotA from the C3Ms already at low ionic strengths resulting in micelles composed of homopolymer and diblock copolymer which show higher salt stability. Utilization of three-component C3Ms is not a preferred strategy to generate salt resistant enzyme containing C3Ms.

Bioconjugation of PAA to CotA to improve the salt stability of CotA-containing C3Ms

From three-component C3Ms data, we know that the lower charge density of CotA compared to the homopolymer causes rapid release of CotA from this type of micelles. In **Chapter 3**, we increased the negative charge of CotA by couple the anionic homopolymer (poly(acrylic acid), PAA) to the lysine residues of this protein. We used a combination of 1-ethyl-3-(3'-dimethyl aminopropyl)carbodiimide hydrochloride (EDC) and *N*-hydroxy succinimide (NHS) linker to increase the bioconjugation efficiency. Native agarose gel electrophoresis and zeta potential experiments confirmed the increasing net charge of CotA-PAA. Furthermore, SDS-PAGE showed a higher molecular weight of bioconjugated enzymes due to the covalently bound PAA chains. However, the bands of CotA-PAA are more diffuse and smeared than the band of native CotA, that showed the heterogeneity in the PAA attached to CotA due to several lysines on CotA and several carboxylates on PAA. Bioconjugation did not affect the secondary structure of CotA laccase, but a decreased enzymatic activity was observed. The longer PAA (PAA_{118}) and the higher PAA concentrations incubated with CotA (5:1) decreased CotA activity about 60 %, possibly because PAA hinders the substrate from accessing the enzyme's catalytic site. CotA-PAA encapsulated with diblock copolymer $PM2VP_{128}$-*b*-PEO_{477} showed a slight decrease in the encapsulation efficiency due to the heterogeneity distribution of net enzyme charges. Both, DLS and FCS showed improved salt stability of CotA-PAA containing C3Ms. Coupling the enzyme with a homopolymer with the same charge sign as the enzyme is appropriate for improving the stability of enzyme-containing C3Ms in a high salt environment.

Improved salt stability of enzyme-containing C3Ms using genetically engineered CotA

In **Chapter 4**, we investigated whether a genetic engineering strategy is applicable to increase the net charge of the CotA and hereby generating more stable micelles. We generated CotA variants with the addition of 10, 20, 30, and 40 glutamic acids at the C-terminus of CotA.

Genetic engineering of CotA resulted in higher charged proteins with a precise composition. Enzyme-containing C3Ms were prepared by mixing the genetically modified CotA laccase with the diblock copolymer P2MVP$_{128}$-*b*-PEO$_{477}$, at pH 10.8. Native CotA and CotA variants resulted in a PMC with F^{-} of about 0.5 and the R_h of the micelles of approximately 31 nm, 27 nm, and 23 nm for native CotA, CotA-E20, and CotA-E40, respectively. Increasing the net charge of the enzyme resulted in more micelles with a smaller number of enzyme molecules per micelle. The encapsulation efficiency was not affected using enzymes with a polyglutamic acid tail (75 – 77 %). Addition of a polyglutamic acid tail to CotA improved the salt stability of enzyme-containing C3Ms.

Crosslinking as strategy to improve salt stability of C3Ms

In **Chapter 5**, we investigated covalent crosslinking as a method to achieve stable C3Ms between homopolymer and diblock copolymer. For this, the diblock copolymer needed to be quaternized with an amine-protected component (*N*-(2-bromoethyl)phthalimide). After a deprotected reaction using hydrazine hydrate, the diblock copolymer has positive charges and a primary amine functional group, which was established by ^{1}H-NMR, FTIR, and a ninhydrin assay. The C3Ms were prepared by mixing aqueous solutions of PAA with quaternized diblock copolymer at pH 7.4. DLS experiments showed that the PMC of the C3Ms was not found at the charge balance between negative charges on PAA and positive charges on the quaternized diblock copolymer, but at a lower ratio ([-]/ [+] = 0.39). This finding suggests that other types of interactions besides electrostatic attraction play a role in the formation of micelles, such as hydrophobic interactions. Next, crosslinking of the micellar core was performed by the use of two types of crosslinkers; 1-ethyl-3-(3'-dimethylaminopropyl)carbodiimide hydrochloride (EDC) and dimethyl 3,3′-dithiopropionimidate dihydrochloride (DTBP). EDC forms irreversible crosslinks between primary amine (of the diblock copolymer) and carboxylate group (of homopolymer PAA), while DTBP connects two amine groups (of the diblock copolymer). DTBP crosslinks contain disulfide bridges that can be broken again by adding a reducing agent. Core-crosslinking significantly improved the C3Ms' stability against high salt conditions and pH changes. The reduction of disulfide bridges in DTBP core-crosslinked micelles resulted in a largely restored salt stability similar to non-crosslinked C3Ms.

In **Chapter 6**, we continued our study on core-crosslink strategies on C3Ms, but encapsulated CotA laccase with the amine-functionalized diblock copolymer. Quaternization of the diblock copolymer was done by a two-step procedure using *N*-(2-bromoethyl)phthalimide and iodomethane. C3Ms were prepared by mixing an aqueous solution

of CotA laccase and amine-functionalized cationic-neutral diblock copolymer, poly(*N*-methyl-2-vinyl-pyridinium)$_{128}$-*block*-poly(ethylene oxide)$_{477}$ (Q_{NH_2}PM2VP$_{128}$-*b*-PEO$_{477}$) at pH 10.8. We used 1 dimethyl 3,3'-dithiobispropionimidate (DTBP) as a crosslinker. Core-crosslinked micelles showed higher stability against salt observed by DLS and FCS. However, core-crosslinking reduced the catalytic activity of CotA, probably due to network formation in the core, which prevents the substrate (ABTS) to bind to CotA. The formed micelles were treated with reducing agent to break disulfide bonds to destabilize the C3Ms. However, because the CotA-containing C3Ms were formed at pH 10.8, this basic pH promotes the formation of disulfide bonds, and therefore the disulfide bridge of DTBP cannot be cleaved. Decreasing the pH of the solution helps to cleave the disulfide bridge of DTBP. Core-crosslinking of enzyme-containing C3Ms improves the stability against high salt conditions.

Proteins exchange between C3Ms

In **Chapter 7**, we describe the effect of genetic engineering and core-crosslinking on the protein exchange dynamics between enzyme-containing C3Ms. To monitor this, we performed Förster resonance energy transfer (FRET) methodology as read-out. For genetic engineering strategy, CotA laccase with and without 40 glutamic acid residues was labeled with Alexa Fluor 488 (donor) and Alexa Fluor 568 (acceptor). For the core-crosslink strategy, we used the fluorescent proteins mTurquoise2 and SYFP2 as FRET pair and C3Ms were generated by mixing the fluorescent protein with quaternized diblock copolymer poly(*N*-methyl-2-vinyl-pyridinium)-*b*-poly(ethylene oxide) (PM2VP$_{128}$-*b*-PEO$_{477}$), and the amine-functionalized version of this diblock copolymer (Q_{NH_2}PM2VP$_{128}$-*b*-PEO$_{477}$), respectively. The micelles composed of donor and acceptor proteins were mixed, and the fluorescence emission of donor was recorded over time upon donor excitation. The exchange of donor and acceptor proteins in the confined micelle core will lead to a reduction of the donor intensity with respect to the initial donor intensity. The ratio of donor intensity quenched over the initial donor intensity is defined as the FRET efficiency. The exchange rate of protein molecules between C3Ms increased when salt was present in the buffer solution. Fitting the FRET efficiency data with an analytical model for FRET-based micelle exchange using two exchange rates (k_1 and k_2), we found that the exchange rate of C3Ms composed of CotA-E40 was 1.2 times slower than C3Ms composed of native CotA. Core-crosslinking of fluorescent protein containing C3Ms with DTBP 2X slows the protein exchange rate between C3Ms by more than 80 times compared to non-crosslinked C3Ms. Application of core-crosslink strategy decreases the exchange dynamics of proteins

between micelles significantly, making this approach the most effective to increase the salt stability and limited exchange between C3Ms.

In **Chapter 8**, a general discussion is provided where the most significant results of this thesis are summarized and critically reflected on which of the original aims was accomplished and what still needs to be done for encapsulation of proteins using diblock copolymers to form complex coacervate core micelles. This thesis demonstrates that via biochemical approaches (bioconjugation and genetic engineering), the stability of enzyme-containing C3Ms can be improved by the increase of the number of charges on the enzyme. Moreover, core-crosslink strategies can be used to improve the stability and to decrease the dynamic exchange of enzymes between micelles. This chapter also includes suggestions to optimize the proposed strategies described in this thesis and some options for future research. We conclude by considering potential applications for protein-containing C3Ms, such as therapeutic delivery for tumor/ cancer treatment.

List of publications

This thesis:

1. **Kembaren, R**., Fokkink, R., Westphal, A. H., Kamperman, M., Kleijn, J. M., and Borst, J. W. Balancing enzyme encapsulation efficiency and stability in complex coacervate core micelles. *Langmuir* **36**, 8494-8502 (2020). (Chapter 2)
2. **Kembaren**, **R**., Westphal A. H., Kamperman M., Kleijn, J. M., and Borst, J. W. Charged polypeptide tail boosts the salt resistance of enzyme-containing complex coacervate micelles. *Biomacromolecules* **23**, 1195–1204 (2022). (Chapter 4)
3. **Kembaren**, **R**., Kleijn, J. M., Borst, J. W, Kamperman, M., and Hofman, A. A. Enhanced stability of complex coacervate core micelles following different core-crosslinking strategies. *Soft matter* **18**, 3052 – 3062 (2022). (Chapter 5)

Other work

Li, M., **Kembaren, R**., Ni, Y., and Kleijn, J. M. Effect of enzymatic cross-linking of naringenin-loaded β-casein micelles on their release properties and fate in in vitro digestion. *Food Chem*. 352, 129400- 129407 (2021).

About the author

Riahna Kembaren was born on March, 23rd 1989 In Pekanbaru, Indonesia. In July 2007, she started a bachelor program in Biochemistry at Bogor Agricultural University. During her studies, she spent 10 months at Czech University of Life Science, Prague, as an Erasmus exchange student in 2011. During her bachelor thesis she worked on nanoencapsulation of carotenoid from palm pressed fiber waste. She obtained her BSc degree in 2012.
After finishing her bachelor study, she worked at a multinational company, Godrej Indonesia, for more than 3 years as Research and Development Executive. She developed the formulation for insecticide products.

In September 2016, she started a master program in Biochemical Engineering at University of Birmingham, the United Kingdom, funded by LPDP Scholarship. During her master thesis she worked on encapsulation of spearmint oil using complex coacervate method. She obtained her M.Sc. degree in December 2017.

In January 2018, she started her PhD on joint project of Physical Chemistry and Soft Matter Research Group and Biochemistry Laboratory at Wageningen University and Research Center, The Netherlands. She worked under supervision of Jan Willem Borst, Mieke Kleijn, and Marleen Kamperman.

Acknowledgements

It is more than 4 yours that I worked in two research groups: Physical Chemistry and Soft Matter (PCC), and Biochemistry (BIC). I would like to thank many people that help me and be with me through this journey.

Thank you for my supervisors, **Jan Willem Borst**, **Mieke Kleijn**, and **Marleen Kamperman**. Thank you for your kindness and patient to supervise me. I am very grateful that all of you give me the chance to work on this project and pursue my PhD. **JW**, thank you very much for your practical insight in the experiments. Thank you also for inviting me for BBQ and sailing with other lab members. I really love it. **Mieke**, thank you very much for your suggestion for the experiments and also for improving my writing, even after your retirement. Your dedication is really wonderful. **Marleen**, thank you very much for your help, suggestion, and care of me and always remind me to take care of myself including for taking holiday. I also want to thank my promotor, **Jasper**. Thank you for your help and support during this PhD journey. **Dolf**, thank you for your help. I remember how you safe me from getting lock in cold room in my first year of PhD, that is so kind of you. **Willem van Berkel**, Thank you for your insight and suggestion after the enzymology meeting.

I want to thank **Anton** for your kindness and help during our work together. Thank you for many practical insights for polymer synthesis and NMR data analysis. I also want to thank **Adrie** for your help and suggestion about genetic engineering. Thank you very much for **Remco**, **Diane**, **Raoul**, **Willy, Simon, Mark** and **Sjef** for your practical help and suggestions during my research. I cannot do it without all of your help. Thank **Mara**, **Leonie,** and **Laura** for your help to order the chemicals and other help about administration. **Lennart**, thank you for your kindness for helping me on training for teaching and arranging the practical. **Daan**, **Elwira**, and **Carlo**, thank you for your suggestion during enzymology and protein biophysics meetings in BIC.

Thank you for my "friends in crime": **Akankshya**, **Zohreh**, **Chandan**, **Jose**, **Vahid**, **Leonardo**, **Preeti**, **Sophie**, **Anastasia** and **Richard**. Thank you for our togetherness in the university and outside university live. For foods, drinks, party, games, shopping, travel, BBQ, laugh, support, and love-hate that we shared 😊. All of you make my time in the Netherlands become amazing. **Xiufeng**, **Akankshya**, **Zohreh, Anastasia, Ilja, Jing, and Raisa**, I am so grateful to share the office 7061 together with all of you. **Vahid** and **Leonardo**, thank you for being my paranymph and be there in one of the most important days in my life. Para mi mejores

amigos, **Jose** y **Leonardo**, muchas gracias por el tiempo que pasamos juntos, por nuestros almuerzos y por enseñarme algo de español. Espero poder hablar español con fluidez en el futuro con vosotros. Os extrañaré mis amigos. Besos.

Thank for other PCC friends **Riccardo**, **Nicolo**, **Jochem**, **Rob**, **Jesse**, **Martijn**, **Dana**, and **Huy** for the friendship that we shared. Thank you also for **Larry** for all of secret Santa office 7060-7062. Thank you for **Ralp** for our time together in the lab and with your "oil volcano" 😊. **Aljosha**, thank you for sending me the polymer list and other help. Thank you for **Inge**, **Lucile**, **Ellard**, **Ilse**, **Marco**, and **Mark** for our discussions and your help for my PhD project. **Hanne**, thank you for your kindness and help. Thank you for share the C3M figure to me.

Thank for BIC friends, **Bel**, **Pilar**, and **Ana**. I will miss the time when we compete to book AKTA in cold room 😊😊😊, thank you for all kindness and support. **Shubhajit**, thank you for your accompany in the lab and allow me to use your ice bucket😊😊😊. Good luck for finishing your PhD. **Cecilia**, thank you for your kindness during the lab cleaning/ lab tornado and beautiful smile that bright my day. Thank **Andre**, **Vera**, **Joao**, **Sumanth**, **Feras**, **Polet**, **Juriaan**, **Patrick**, **Mariska**, **Ping**, **Sjoerd**, **Lisa, Sergio**, and **Viren**, my working time in BIC become great with all your kindness and support. Thank you **Jente** for nice cake that you bake and shared with us, so lovely of you.

Thank you for my student: **Sinty**, **Walter**, and **Anne**. Thank you for your work together with me. I wish the best for your future study. Thank you for **Araceli** for your kindness and support. I hope you also will finish your PhD greatly. Thank for **Indonesian-PhD and PostDoc in Wageningen**. Thank you for all support that I have received. Thank you for **ICF Wageningen family** that support me during my study in the Netherlands. Thank you for "*Black Sweet*" prayer mate**: Lenny** and **Elvita**. Thank for all of your support and love. Thank you for **SHINee** and **EXO** for all songs that accompany me in the lab and in the office. All of your songs always bring good mood during my work.

Terimakasih untuk bapak ku, **Yahmin Sembiring**, dan mamak ku, **Maria br Tarigan**, untuk semua kasih sayang, doa dan dukungan nya. Semoga gelar PhD ini juga menjadi kebanggaan untuk bapak dan mamak. Ana sayang bapak dan mamak. Terimakasih juga untuk suami ku, **Alosius Des Afriando Sinuraya**. Terimakasih sayang untuk doa dan dukungan yang kam berikan. Dalam masa-masa kita jauh dan dekat selama study, kam terus menyemangati ana. Terimakasih untuk **keluarga besar sembiring** dan **tarigan mergana** untuk dukungan dan doanya. Semoga keberhasilan ini menjadi kebanggaan bagi keluarga besar juga.

Overview of completed training activities

Discipline specific activities

- Dutch Polymer Days, PTN, Lunteren, 2018.
- International Association of Colloid and Interface Scientists (IACIS), WUR and DELF University, Rotterdam, 2018.$^{+}$
- International Symposium on Polyelectrolytes, VLAG, Wageningen, 2018.
- Microscopy and Spectroscopy in Food and Plant Science, WUR, Wageningen, 2018.
- Dutch Polymer Days, PTN, Lunteren, 2019.*****
- Wageningen Indonesian Scientific Exposure (WISE), Indonesian WUR PhD, Wageningen, 2019.$^{+}$
- CHemistry As INnovating Sceince (CHAINS), NWO, online, 2020.*$^{+}$
- 13th International Symposium on Polyelectrolytes, East China University of Science and Technology, Online, 2021.*****
- 30th Dutch Soft Matter Meeting, TU Eindhoven, online, 2021.$^{+}$
- Bringing Chemical Biology to Cancer Research, Royal Society of Chemistry, online, 2021.*$^{+}$

*****oral presentation. $^{+}$poster presentation

General courses

- VLAG PhD week, VLAG, Baarlo, 2018.
- Supervising BSc and MSc thesis students, WGS, Bennekom, 2019.
- Scientific Publishing, WGS, Wageningen, 2019.
- Scientific Writing, WGS, Wageningen, 2020.
- Presenting with Impact 5, WGS, Wageningen, 2020.
- Career Perspectives, WGS, Online, 2021.
- Scientific Artwork, Data visualization and Infographics with Adobe Illustrator, WGS, Online, 2021.
- An Introduction to LaTeX, PE and RC, Online, 2021.
- Applied Enzymology, VLAG, Wageningen, 2022.

Optional activities

- Dairy Protein Biochemistry, VLAG, Wageningen, 2018.
- Thursday seminars Biochemistry, BIC, Wageningen, 2018-2022.
- Weekly meetings and seminars of the PCC group, PCC, Wageningen, 2018-2022.
- Journal club PCC, PCC, Wageningen, 2018-2022.
- Protein Biophysics, BIC, Wageningen, 2018-2022.
- Wageningen Indonesian Scientific Exposure (WISE) 2019 Organizing committee, PPI Wageningen, Wageningen, 2019.
- Wageningen Molecular Life Science Seminar Series, WUR, Wageningen, 2018-2020.
- Live Webinar Chromatography tools, tips and tricks, BIC and Cytiva, Wageningen, 2020.
- Live in Science, BIC, Wageningen, 2021-2022.
- Wet Adhesive group meeting, PCC, Wageningen, 2019.

The research described in this thesis was financially supported by Graduate School VLAG WUR

Cover design by Riahna Kembaren

Printed by ProefschriftMaken